THE UNIVERSITY OF SYDNEY

SYNTHESIS AND SELF-ASSEMBLY OF ASYMMETRIC BLOCK COPOLYMERS TOWARDS NANODISCS

Simran Davina Vinod Kerai

School of Chemistry, Faculty of Science

The University of Sydney

2026

A thesis submitted to fulfil the requirements for the degree of

Doctor of Philosophy (PhD)

Declaration

I hereby certify that the work presented in this Thesis was carried out by myself between March 2022 and September 2025 within the School of Chemistry at The University of Sydney, as part of the requirements for the degree of Doctor of Philosophy in Science. This Thesis has not been submitted for any degree or other purposes.

I certify that the intellectual content of this Thesis is the product of my own work and that all the assistance received in preparing this Thesis and sources have been acknowledged (refer to the *Statement of Contribution* section).

	23/09/2025
Simran Davina Vinod Kerai	Date

Thesis Abstract

Polymers have emerged as exciting candidates for self-assembly into nanomaterials. Advancements in polymer science have seen an increase in the design of complex, but well-defined systems unlocked by the evolvement of controlled and living polymerisation techniques. As such, architectures such as molecular polymer bottlebrushes (MPBs) that are considered synthetically complex, can be achieved as well-defined and uniform polymer building blocks. Additionally, their large scope for functionality provides opportunity for the synthesis of tailored building block materials, unlocking self-assembly pathways of morphologies and functional materials that have remained quite elusive to date. This thesis will explore the synthesis of MPB containing building blocks to better understand their bottom-up self-assembly behaviour towards polymeric discoidal nanoparticles.

The first research chapter shows the synthesis of poly(ethylene glycol)-*block*-(poly (2-(2-bromoisobutyryloxy)ethyl methacrylate)-*graft*-poly(benzyl methacrylate)) (PEG-*block*(pBIEM-*g*-pBzMA) MPB bottlebrush-linear 'tadpoles' synthesised by reversible-deactivation radical polymerisation (RDRP) techniques including reversible-addition-fragmentation chain-transfer (RAFT) polymerisation of a polymer backbone, and subsequent atom transfer radical polymerisation (ATRP) to graft polymeric side chains. The dimensions of the MPB component of these architectures was explored to determine their effect on self-assembled morphology.

The second research chapter explores the co-assembly of chemically different bottlebrush-linear architectures into discoidal particles. By co self-assembling two chemically distinct tadpoles, namely poly(ethylene glycol)-*block*-[poly(3-azido-2-hydroxypropyl methacrylate)-*graft*-poly(ethyl ethoxylate)] and poly(ethylene glycol)-*block*-[poly(2-(2-bromo

isobutyryloxy)ethyl methacrylate)-*graft*-poly(benzyl methacrylate) with tendency to self-assemble into discoidal particles, this chapter explores the relationship between concentration mixtures and nanoparticle morphologies. Furthermore, we investigate the effect of selectively disassembly one component in this mixture upon stimulus exposure in a proof-of-concept study.

The third research chapter extends the 'tadpole' architecture to a more complex bottlebrush-linear-bottlebrush 'dumbbell' architecture [(poly (2-(2-bromoisobutyryloxy)ethyl methacrylate)-*graft*-poly(benzyl methacrylate))-*block*-poly(ethylene glycol)-*block*-(poly (2-(2-bromoisobutyryloxy)ethyl methacrylate)-*graft*-poly(benzyl methacrylate))]. Whilst maintaining the required balance between corona-forming flexible blocks and rigid core-forming blocks, a range of brush dimensions are surveyed to assess their self-assembled morphologies. Extending their application, the co-assembly of these macromolecules with tadpole structures is investigated towards networks of nanoparticles.

Preface

The work described in this Thesis was performed in the School of Chemistry at The University of Sydney for the duration of the candidature. All results discussed herein are my original work except where specific reference to the work of others is made in the text.

This research is supported by various scholarships held at different times including an Australian Government Research Training Program (RTP) Scholarship, Research Scholarship in Polymer Chemistry, Postgraduate Research Supplementary Scholarship in Chemistry and Victor Cromack and Melba Alma Harris Cromack Scholarship.

Parts of the work detailed in this thesis have been published and/or presented in the following media:

Publications

1. **Kerai, S. D.;** Takano, S.; Zeng, P.; Müllner, M.: "Self-Assembly of Bottlebrush-Linear, Rod–Coil Copolymers into Discoidal Nanoparticles." *ACS Macro Letters* **2025**, *14*, 834-840.
2. Brisson, E.R.L.; Worthington M.J.H.; **Kerai, S**; Müllner, M.: "Nanoscale polymer discs, toroids and platelets: a survey of their syntheses and potential applications." *Chemical Society Reviews* **2024**, *53*, 1984–2021.

Presentations

1. **Kerai, S.D.**; Takano, S; Zeng. P; Müllner, M.: "Probing the Dimensions of Bottlebrush-Linear, Rod-Coil Copolymers Toward their Self-Assembly into Discoidal Nanoparticles" European Polymer Congress (EPF) 2025. Groningen, The Netherlands (June 2025) (Oral Presentation)

2. **Kerai, S.D.**; “Flatpack Nanomedicine: Some Assembly Required” University of Sydney, Faculty of Science 3 Minute Thesis - Runner’s Up and People’s Choice (July 2025) (Oral Presentation)
3. **Kerai S.D.**; “Flatpack Nanomedicine: Some Assembly Required” University of Sydney 3 Minute Thesis Finals. Sydney, Australia (August 2025) (Oral Presentation)
4. **Kerai S.D.**, Takano S, Zeng P, Müllner M.; “Probing the Dimensions of Bottlebrush-Linear, Rod-Coil Copolymers Toward their Self-Assembly into Discoidal Nanoparticles” Sydney Surfaces and Soft Stuff (Sassy) Meeting 2025. Sydney, Australia (May 2025) (Oral Presentation)
5. **Kerai S.D.**, Müllner M.; “The Self-Assembly of Molecular Polymer Brushes into Discoidal Nanoparticles” Sydney Surfaces and Soft Stuff (Sassy) Meeting 2023. Sydney, Australia (May 2023) (Poster Presentation)

Statement of Contribution

The results presented in this Thesis were obtained in collaboration with other researchers. This Thesis was proofread by A/Prof Markus Müllner. I acknowledge the use of generative AI tool Claude Sonnet 4, Anthropic https://claude.ai to generate referencing lists for input into Endnote Referencing Manager and for formatting advice toward ordering headings in a cohesive Chapter 1. Introduction. No generative AI tools were useThis statement clarifies the contribution of each collaborator to each chapter.

CHAPTER II: I developed the methodologies and performed all chemical syntheses, self-assembly studies, ^{1}H NMR characterisation, SEC characterisation, DLS characterisation, AFM characterisation, scheme and figure drawing, and writing. This work is presented in the following paper:

Kerai, S. D.; Takano, S.; Zeng, P.; Müllner, M.: "Self-Assembly of Bottlebrush-Linear, Rod–Coil Copolymers into Discoidal Nanoparticles." *ACS Macro Letters* **2025**, *14*, 834-840.

The TEM was performed mostly by Shin Takano, supplemented by Ping Zeng. A/Prof. Markus Müllner conceived the idea and supervised the research.

CHAPTER III: I developed the methodologies and conducted the self-assembly studies of the co-assembly systems. I synthesised the PBzMA polymers and performed the self-assembly studies. In these systems, I performed the ^{1}H NMR characterisation, SEC characterisation, DLS characterisation, and AFM characterisation. Ping Zeng performed the TEM characterisation. Ping Zeng performed the synthesis, self-assembly and disassembly characterisation for the PEE tadpole system only. A/Prof. Markus Müllner conceived the idea and supervised the research. I completed the scheme and figure drawing and writing of this chapter.

CHAPTER IV: I developed the methodologies and performed all chemical syntheses, self-assembly studies, ^{1}H NMR characterisation, SEC characterisation, DLS characterisation, AFM characterisation, scheme and figure drawing, and writing. Haoxiang Zeng performed the TEM characterisation. A/Prof. Markus Müllner conceived the idea and supervised the research. I completed the scheme and figure drawing and writing of this chapter.

I hereby certify that all contributions of the individuals have been accurately acknowledged.

23/09/2025

Simran Davina Vinod Kerai — Date

23/09/2025

A/Prof. Markus Müllner — Date

Acknowledgments

A PhD is a marathon that I would not have been able to see through without the support of many people in my life. Firstly, I'd like to thank my supervisor **A/Prof Markus Müllner.** I am very appreciative for your endless encouragement and support, especially in the many moments where I was ready to lay my lab coat down. Thank you for guiding my scientific thoughts and shaping me into the researcher I am today. You taught me that good science isn't about getting the results you want, but by understanding the narrative in front of you to ask better questions and see the bigger picture. Your door was always open, whether it be about project progress, presentations and writing, life in general, or to help me fight the regular Imposters Syndrome. Thank you for putting your trust in me and giving me the opportunity to return to Sydney, but also for putting me in positions to build my science network and launch into my career hereafter.

My gratitude extends to the entire **Polymer Nanostructures Group** in the many forms we have taken during my candidature. Thank you for the many chats in and out of the lab, for letting me drag you to restaurants in Newtown and beyond, and for enduring my 2000s RnB blasting in the lab. I have loved shared the highs and woes of polymer synthesis with you and will miss being in the PNG. A big thank you also to **Adrienne, Mala, Karun, Jennifer, Daniel, Chenyou, Samantha, Geosmin** and **Eleni.** Coffee and lunch breaks in your company saw me through some of my most testing moments of my PhD and I will be forever grateful. To **Duc, Vien, Alex, Isaac, Leo** and the entire **KCPC** – I have thoroughly enjoyed sharing lab and office spaces with you all, trying the treats you have brought back from your travels, and having a great bunch of people to learn from, chat and joke with. It has been a pleasure living in the trenches with you all. A PhD also goes beyond the lab and research. Some of my fondest memories in the School of Chemistry over the past four years have been whilst teaching and

demonstrating. Thank you to everyone that I've had the pleasure to work with. I always looked forward to my shifts with you, and the opportunities to continue to develop my skills and continue to pursue my passion for teaching chemistry.

To my first polymer world at MIPS, you are the reason I fell in love with polymers and research and then continued on this journey. Thank you to **Josh, Inin, Alex, May, Phuong, Ayaat, David & Nicole** for making my first research years fun and enlightening despite being amidst the weird world of Victorian lockdowns.

To all my friends who have been there to go to musicals, day trips, hidden restaurants and bars, waffle with, or be shoulders to lean on, and the entire extended family both, by blood and love, in the many corners of the world, if I wrote all your names out, I would need many more pages. A big appreciation to **Anay, Veeya, Tanika, Dasina, Ashish, Mama, Masi, Masa, Geeta Ba, Sanjay Bapa, Nani, Nana, Ba** & **Bapa** for never letting me feel alone on my academic journey and in life and showing me how proud you are. I count myself lucky to have so many of you cheering the loudest on the sidelines and having a genuine interest in the work that I do and the person that I am. Thank you for being my people.

Finally, to **Mum, Dad** and **Dillan** – even though the foreign world of science wasn't always easy to understand, your unconditional love and support is the driving force behind this thesis. Thanks for supporting my decision to be a 'poor uni student' a little while longer than most. Thank you for being my guinea pig audience for various iterations of work and presentations, not holding it against me when I bring my work frustrations home with me, and for supporting me through every dream I come up with, no matter where in the world it takes me. Your belief in me, even when mine had run out keeps me going.

This thesis is dedicated to all of you, as part of the wave that carried me through both my favourite memories and hardest lessons in life and chemistry thus far.

Glossary of Terms

δ	chemical shift
Đ	dispersity
χ	Flory-Huggins interaction parameter
γ	interfacial tension
μ	Maier–Saupe parameter
f	volume fraction
α-BiBB	α-bromoisobutyryl bromide
α-HDL	α-high-density lipoproteins
^{1}H NMR	proton nuclear magnetic resonance
2D	two-dimensional
3D	three-dimensional
AFM	atomic force microscopy
AIBN	2,2′-Azobis(2-methylpropionitrile)
Apo-A1	apolipoprotein-A1
ARGET	activators regenerated by electron transfer
ATRP	atom transfer radical polymerisation
BIEM	2-(2-bromoisobutyryloxy)ethyl methacrylate
BBCPs	bottlebrush block co-polymers
bpy	2,2’-Bipyridine
BzMA	benzyl methacrylate
$CDCl_3$	deuterated chloroform
CFLs	cerasome forming lipids
$CHCl_3$	chloroform

CDTPA	4-cyano-4-[(dodecylsulfanylthiocarbonyl)sulfanyl]pentanoic acid
CDSA	crystallisation-driven self-assembly
CPADB	4-cyano-4-(phenylcarbonothioylthio)pentanoic acid
CPP	critical packing parameter
CTA	chain transfer agent
CuBr	copper(I) bromide
CuCl	copper(I) chloride
DB	dumbbell
DCM	dichloromethane
DLS	dynamic light scattering
DMAc	*N,N*-dimethylacetamide
DMAP	*N,N*-dimethylaminopyridine
DMF	*N,N*-dimethylformamide
DP	degree of polymerisation
eATRP	electrochemical atom transfer radical polymerisation
EDC·HCl	*N*-ethyl-*N*′-(3- dimethylaminopropyl)carbodiimide hydrochloride
EDDA	ethylenediaminediacetic acid
EE	ethyl ethoxylate
EHMA	2-ethyl hexyl methacrylate
EISA	evaporation-induced self-assembly
EtOH	ethanol
Et_2O	diethyl ether
fd	feature diameter
ft	feature thickness
GC	gas chromatography

GE	grafting efficiency
GPC	gel permeation chromatography
HBs	hybrid bicelles
HDL	high-density lipoproteins
HEMA	2-hydroxyethyl methacrylate
HEMA-TMS	2-(trimethylsilyloxy)ethyl methacrylate
HMTETA	*1,1,4,7,10,10*-hexamethyltriethylenetetramine
HOVE	octadecyl vinyl ether-*block*-poly(2-hydroxyethyl vinyl ether)
ICAR	including continuous activator regeneration
iPrOH	isopropanol
k_a	rate of activation
k_d	rate of deactivation
k_p	rate of propagation
LAMs	less activated monomers
LC	liquid crystal
LiBr	lithium bromide
LNDs	lipid nanodiscs
MA	methyl acrylate
MAMs	more activated monomers
ME_6TREN	tris 2-(dimethylamino)ethyl amine
MEMA	2-*N*-morpholinoethyl methacrylate
MMA	methyl methacrylate
MeOD	methanol-d4
MeOH	methanol
$MgSO_4$	magnesium sulphate

MPBs	molecular polymer bottlebrushes
mPEG	poly(ethylene glycol) methyl ether
MWCO	molecular weight cutoff
NEt_3	triethylamine
NMP	nitroxide mediated polymerisation
NPs	nanoparticle
P2VP	poly(*2*-vinylpyridine)
P4VP	poly(*4*-vinylpyridine)
PAGE	poly(allyl glycidyl ether)
PB	poly(butadiene)
PBIEM	poly(2-(2-bromoisobutyryloxy)ethyl methacrylate)
PBzMA	poly(benzyl methacrylate)
PDMA	poly(N,N-dimethylacrylamide)
PHIC	poly(*n*-hexyl isocyanate)
PE	poly(ethylene)
PEE	poly(ethyl ethoxylate)
P(EE-*ran*-TP)	poly(ethoxyethyl glycidyl ether-*ran*-tetrahydropyranyl glycidyl ether)
PEG	poly(ethylene glycol)
PEGMA	poly(ethylene glycol) methyl ether methacrylate
PEtG	poly(ethyl glycoxylate)
PEP	poly(ethylenepropylene)
PHEMA	poly(2-hydroxyethyl methacrylate)
PISA	polymerisation induced self-assembly
PLA	poly(lactic acid)
PMBPS	poly[(+)-2,5-bis[4‘-((S)-2-methylbutoxy)phenyl]styrene]

PMA	poly(methyl acrylate)
PMDETA	*N,N,N',N'',N''*-pentamethyldiethylenetriamine
PMEMA	poly(2-*N*-morpholinoethyl methacrylate)
PMMA	poly(methyl methacrylate)
PNDs	polymer nanodiscs
PNMEP	poly(*N*-(2methacryloyloxyethyl)pyrrolidone
PPEGMA	poly(poly(ethylene glycol) methyl ether methacrylate)
PRINT	particle replication in nonwetting templates
PS	polystyrene
PTA	phosphotungstic acid
P*t*BA	poly(*tert*-butyl acrylate)
P*t*BMA	poly(*tert*-butyl methacrylate)
RAFT	reversible addition-fragmentation chain-transfer
RDRP	reversible deactivation radical polymerisation
RES	reticuloendothelial system
ROMP	ring-opening metathesis polymerisation
SANS	small-angle neutron scattering
SAXS	small-angle X-ray scattering
SCFT	self-consistent field theory
SEC	size exclusion chromatography
SEM	scanning electron microscopy
SET-LRP	single-electron transfer living radical polymerisation
SMALPs	styrene-maleic acid copolymer lipid particles
SSSR	superstrong segregation regime
TEM	transmission electron microscopy

T_g	glass transition temperature
THF	tetrahydrofuran
TP	tadpole
UA	uranyl acetate
UFLC	ultra-fast liquid chromatography
UV	ultraviolet
v/v	volume by volume
VIm	*N*-vinylimidazole
wt%	weight percentage

Table of Contents

Chapter I : Introduction

1. Designing Nanomaterials

Nanoparticles (NPs) remain influential across many industries as an exciting and effective means to improve the performance and specificity of functional materials.[1-3] Since Feynman's visionary lecture on the possibilities of nanomaterials in the 1950s,[4] the landscape of nanotechnology continues to evolve to find pathways to access elusive but attractive NP qualities with tuneable properties.[3, 5, 6] Being predominantly used in the biomedical field, NPs have been revolutionary in addressing issues concerning treatment, diagnosis, and theranostic applications.[6, 7] Other applications include agriculture, coatings, textiles, and electronics. To enhance their performance towards specific applications, the design of their size, surface chemistry, and shape is particularly important.[6]

1.1 Size

It is increasingly accepted that size influences the activity of NPs. In biomedicine, oral drug delivery requires passive transport across the lumen with particles with an average size of approximately 100 nm exhibit optimal absorption into enterocytes.[8] Size is also imperative to avoid clearance pathways such as renal clearance or the reticuloendothelial system (RES). NPs within the size range of 10 – 100 nm have been deemed to be optimal for intravenous administration.[9] Whilst certain physical biological barriers such as the BBB may have specific size cut-off ranges, studies have found that NPs between 40 – 50 nm experience optimal cellular uptake via passive transport.[10] In catalysis, smaller particles present a higher surface to volume ratio, making them more active for catalytic reactions.[11] Similarly, decreased sizes have improved performance of nanoparticle inks in three-dimensional (3D) printing for electronics.[12]

1.2 Surface Chemistry

One of the most influential NP properties for targeted application is surface chemistry. For biocompatible NPs, surfaces that carry a relatively neutral charge with hydrophilic character are particularly advantageous to avoid premature metabolism or excretion. Polymers that satisfy this criteria join a class of biocompatible polymers, with the current industry gold standard being poly(ethylene glycol) (PEG).[13] PEG recruits dysopsonin proteins within the protein corona of NPs that prevents recognition by immune systems thus prolonging circulation time.[14] The success of this stealth response is dependent on factors such as the molecular weight, density, and conformation of the PEG polymer.[15, 16] Alternative synthetic polymers have been investigated for their anti-fouling properties such as shape or chemically modified PEG derivates,[17] poly(2-oxazoline)s,[18, 19] poly(vinyl pyrrolidine),[20, 21] and poly(zwitterions).[22, 23] Surface chemistry has also been used for targeted therapies where surfaces are designed to resemble or interact with endogenous ligands specific to disease environments. This strategy has been used widely in the design of anti-cancer therapies,[9, 24-26] and inflammatory diseases,[27-29] because there are a plethora of characteristic receptors and endogenous molecules to choose from.

1.3 Shape

Additional to the parameter of size, it is now accepted that the shape does also significantly boost nanoparticle performance. In plasmonics and optics, the shape of particles can vastly change their properties. Asymmetric structures can alter the resonance frequency dependent on their aspect ratio,[30] allowing the wavelengths to be tuned across the spectrum.[31] Budy et al., showed that anisotropic morphologies exhibit higher sensitivity to the localised surface plasmon resonance, with relevance to sensing and light harvesting.[32] In addition, their non-Newtonian behaviour in fluid dynamics whereby nanofluids containing anisotropic nanoparticles can undergo shear thinning,[33] making them well-suited for applications such as

industrial lubricants and paints.[34] This behaviour is well explained in biological settings, where their higher aspect ratio facilitate preferential cellular interactions and fluid dynamics over spherical particles.[35] Ultimately, this elevates rates of margination towards endothelium within vasculature. Blanco and coworkers demonstrate this by comparing how spherical and anisotropic NPs respond to the stress from fluid dynamics of blood in vessels differently.[36] Spherical NPs continue in a laminar flow as they rotate in a uniform pattern, and therefore continue through vasculature in the cell-free layer, with minimal margination towards the vasculature wall (Figure 1.1). In contrast, the geometry of non-spherical NPs allows them to advance in a non-linear oscillation pattern. The randomness of this oscillation and greater particle surface area for fluid dynamics to act upon contributes to greater margination of NPs towards endothelial cells.[37] When at the vasculature wall, the difference in available surface area between spherical (Figure 1.1b) and disc-shaped NPs (Figure 1.1c) affects the potential contact area between cells and NPs, hence resulting in the latter experiencing greater likelihood of cellular uptake.[38, 39] This phenomenon is responsible for their preferential extravasation to smaller blood vessels and subsequently, NP accumulation in target tissues with reduced clearance.[40-42] In turn, nanodisc carriers are poised as optimal carriers for a plethora of biomedical applications such as for drug delivery.[43, 44] In a similar manner, the high aspect ratio and surface area are well-suited to catalytic applications, finding that octahedral nanocrystals have displayed better activity due to the multiple facets available for a range of reactions.[11, 45] In environmental applications, gas detection, heavy metal and contamination detection and water purification application also benefit from the increase in available active sites that high surface area in anisotropic particles affords.[46] Therefore, there is large interest in the fabrication of anisotropic NPs, with particular emphasis on discoidal NPs to advance current nanomaterials and models.

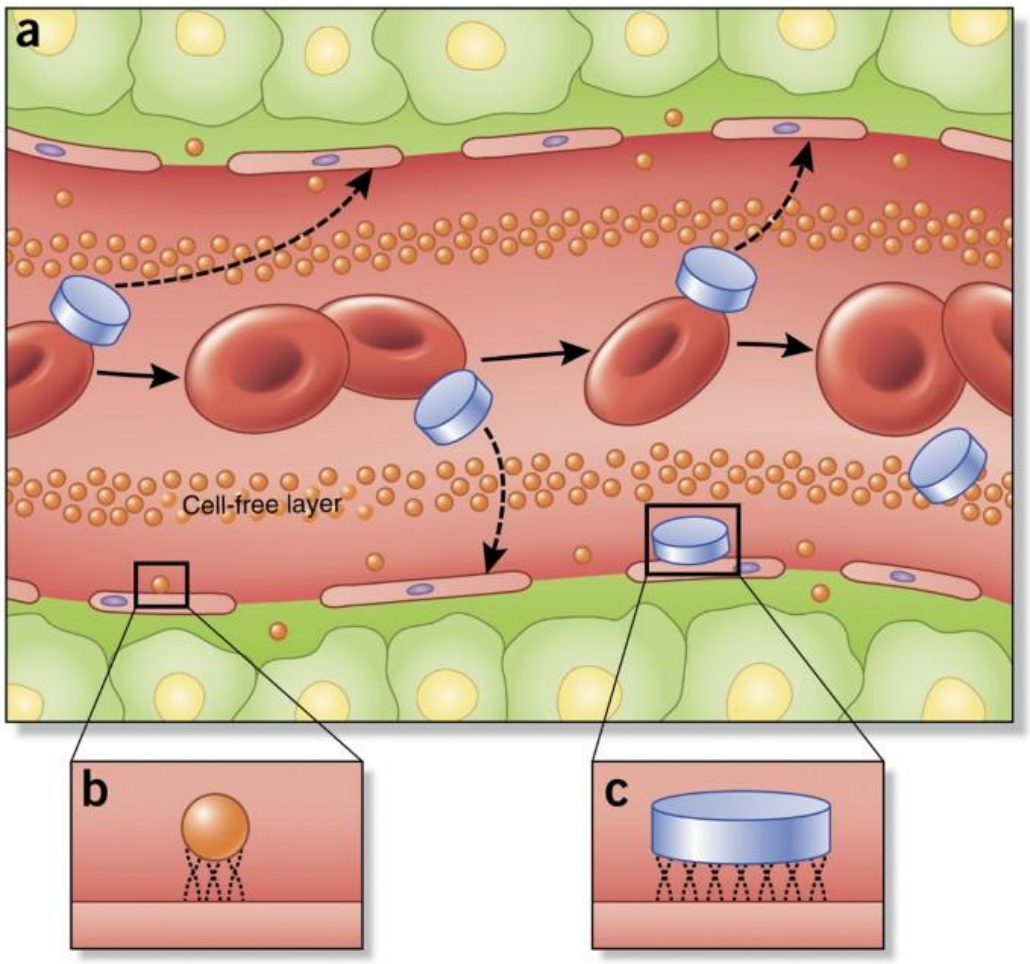

Figure 1.1. Spherical and anisotropic nanoparticle flow, localisation, and cellular interaction properties to demonstrate the importance of nanoparticle size and shape on biodistribution. **a)** localisation and interactions of spherical and anisotropic nanoparticles in vasculature **b)** cellular interactions of spherical nanoparticles with endothelial cells. **c)** cellular interactions with anisotropic nanoparticles with endothelial cells. Reproduced from Ferrari and coworkers.[36]

2. Current Nanodisc Models

Currently, the term nanodisc typically refers to four major classes of biologically relevant particles. These include lipid nanodiscs (LNDs), styrene-maleic acid copolymer lipid particles (SMALPs), polymer nanodiscs (PNDs) and hybrid bicelles (HBs). Typically, these models were intended as a membrane mimetic for biological studies. However, with increasing interest in anisotropic nanoparticles, some have been studied as drug delivery agents, particularly in oncology.

LNDs were the first type of nanodiscs to be reported.[47] Originally intended as reconstituted α-HDLs,[48, 49] they are comprised of a phospholipid bilayer that is then stabilised by lipoproteins such as apolipoprotein-A1 (Apo-A1).

SMALPs are similar in structure to LNDs, substituting the Apo-A1 that stabilise the structure with styrene-maleic acid copolymers.[50] Structural characterisation uncovered that the polymer assumes a 'bracelet' conformation around the lipid bilayer.[51] The styrene moieties afford the macromolecule greater stability, whilst the negative charge via the maleic acid moieties facilitates dispersion in aqueous environments. However, the applications of this model are also limited by a range of factors. Due to the charged nature of maleic acid units, this system is not applicable in acidic environments,[52] and incompatible with divalent metal ions.[53] To mitigate this, modifications to these polymers have been introduced.[54]

PNDs gain their name by the inclusion of polymeric amphiphiles that substitute the phospholipids that constitute the planar bilayer. Unlike SMALPs, they maintain the use of stabilising MSPs and therefore are not entirely polymeric in nature. In the presence of MSPs and detergent, these polymer amphiphiles can be directed to self-assemble into discs instead of spherical polymersomes.[55]

HBs differ entirely, comprised of cerasome forming lipids (CFLs) and shorter phospholipids,[56] that form the planar and curved edges of discoidal shapes respectively.[57] The CFLs assemble into a vesicular structure with the strength of a silicon-based shell. Comparisons between bicelle and liposomal drug carriers show the former exhibiting increased cellular uptake and drug efficacy,[58] attesting to the effects of NP shape presented in Section 1.3.

Whilst these models provide many biomedical advances, barriers preventing the wide-scale use in drug delivery involves cost, safety and stability. Arguably the largest challenge surrounds cost of production. Majority of these systems require stabilisation by MSPs, with Apo-A1 and

its derivatives being most commonly used. From a safety perspective, the use of endogenous components in nanodiscs with the intention of introducing these into other living organisms may induce immunogenic responses with overuse.[59] Whilst efforts towards synthetic Apo-A1 are evolving, barriers of immunogenicity and synthetic complexity remain.[59] Like all nanoparticles, the stability of nanodiscs is reliant on the free energy equilibrium of building blocks in response to their environment.[60] The involvement of detergents and complex synthetic strategies to achieve these models can affect the stability of some components.[61]

To overcome these limitations and make nanodiscs a versatile platform for all applications, inspiration has been taken from the extensive advantages that precise polymer design has to offer. Despite the inclusion of synthetic polymers in some of the aforementioned models, none of these are entirely polymeric in nature. Thus, there is large interest in achieving entirely synthetic discoidal NPs. We acknowledge that there are many reports of synthetic inorganic NPs such as silica,[62, 63] metallic,[64] or gold-based,[65] nanoparticles in nanomedicine.[66] However, to delicately balance the requirements of size, surface chemistry, and morphology with precision control, polymeric NPs are particularly advantageous. As a soft matter, synthetic polymers offer diverse chemical functionalities and tuneable physical properties, making them a versatile building block for self-assembly to suit any application.[67] In an amphiphile, having independent control over both the hydrophilic and hydrophobic segment,[68] polymer self-assembly remains an adaptable field of interest. By strategically designing the polymeric composition of building blocks, researchers can control the size, shape, and surface characteristics of the resulting nanoparticles, enabling precise tailoring for specific applications. To achieve such properties, many rely on reversible deactivation radical polymerisation (RDRP) techniques, particularly in applications where material precision and adaptability are paramount.

3. Reversible Deactivation Radical Polymerisation

RDRP techniques have been transformative in polymer chemistry, enabling the synthesis of well-defined polymers with precision in targeting molecular weights, narrow molecular weight distributions, and well-defined architectures. Therefore, these approaches are highly relevant in the synthesis of polymeric materials for nanoparticle fabrication. The three most widely used RDRP techniques are Atom Transfer Radical Polymerisation (ATRP), Reversible Addition-Fragmentation Chain Transfer (RAFT) Polymerisation, and Nitroxide Mediated Polymerisation (NMP). The process of NMP and its application has recently been reviewed.[69] With ATRP and RAFT being relevant to this project, these polymerisation techniques will be discussed further.

3.1 Reversible Addition-Fragmentation Chain Transfer (RAFT) Polymerisation

Since its development in the late 1990's,[70] RAFT polymerisation has become a standard technique in a polymer chemist's toolbox. This is largely due to its ease and versatility in affording even complex polymer architectures. The characteristic 'living' nature of this polymerisation technique is revolutionary in terms of RDRP approaches because it allows polymerisations to proceed to >99% monomer conversion whilst maintaining control, unlike other techniques which can facilitate a maximum of approximately 80% conversion.[71] This is because the equilibrium of dead and living chains in traditional RAFT is controlled by the number of available initiators. The RAFT process begins by radical initiation before an equilibrium is established between living and dormant chains facilitated by the chain transfer agent (CTA) and its interaction with propagating radicals.[71]

The CTA comprises of an R- and Z- group connected by a thiocarbonylthio (S=C-S) group. The R-group is known as the 'leaving group' due to its homolytic nature. Its main purpose is to control the reinitiation of the propagation of polymer chains by the strength of the connecting

C-S bond.[72] Alternatively, the functional Z-group acts to be reversibly transferred between living and dormant polymer chains in a degenerative transfer mechanism to facilitate their polymerisation before termination.[73] The Z-group is responsible for ensuring the stability of the RAFT intermediate, and in turn, controls the rate of propagation of polymer chains such that they exist over a narrow molecular-weight distribution throughout the entire process.[71] Figure 1.2 depicts the RAFT process. Whilst there are many subtypes of RAFT based on their radical initiator source, conventional RAFT typically uses azo-initiators. The initiator undergoes fragmentation, and the subsequent radicals can react with monomers to form and active propagating polymer chain (Pn·). In the pre-equilibrium, this propagating chain reacts with the CTA to form a RAFT intermediate. Via this intermediate, the radical can be exchanged from the active polymer chain to reinitiate other monomers and form another polymer chain (Pm·).

The RAFT equilibrium between the propagating radicals Pn· and Pm· and their transfer across the CTA is then established. The fragmentation of the chains controls the equilibrium between dormant chains attached to the CTA, and active chains until the monomers are consumed or termination is initiated. The controlled polymerisation that RAFT is known for relies on the fast rate of addition-fragmentation in comparison to the rate of monomer addition. This allows equal chance of monomer addition to the propagating radical chains, in turn narrowing the molecular weight distribution of resulting polymers. Additional to CTA choice, the kinetics of the addition and fragmentation steps of RAFT can be optimised experimentally by controlling radical concentration, initiator choice, and temperature.

One of the advantages of RAFT over other RDRP processes is its ability to polymerise a wide range of monomer types across a variety of reaction conditions. However, with different types of monomers exhibiting different reactivities, the RAFT CTA must be chosen appropriately to

ensure well-controlled and efficient polymerisations. Factors such as steric hindrance, polarity and electrophilicity of substituents can all influence the reactivity and kinetics of CTAs.[72]

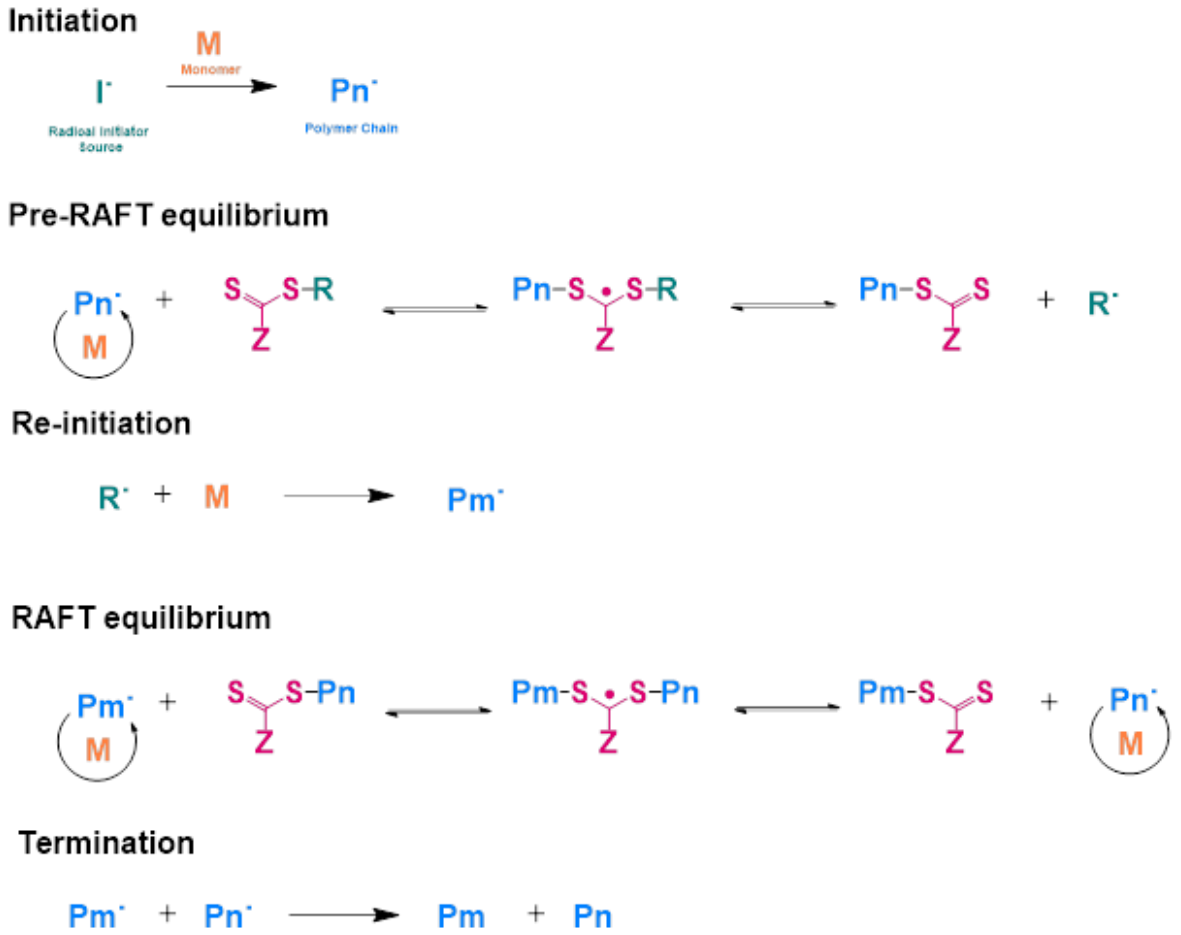

Figure 1.2. The mechanism of reversible addition-fragmentation chain transfer polymerisation across the initiation, propagating equilibriums, and termination steps.

Moad, Rizzardo, and Thang outlined the suitable Z- and R- groups of a CTA for the most efficient polymerisation of different monomers (Figure 1.3).[74] As expected, more activated monomers (MAMs) such as methacrylates, acrylates, styrenes, acrylamides and methacrylamides require a different combination of Z- and R-groups compared to less-activated monomers (LAMs) such as vinyl acetates. MAMs are distinguished by the presence of electron-donating groups adjacent to the vinyl bond, whilst LAMs have electron-withdrawing groups in this position.[75] Incompatibilities with RAFT agents based on their reactivity gave rise to universal or switchable CTA to allow copolymerisation of both monomer classes.[76]

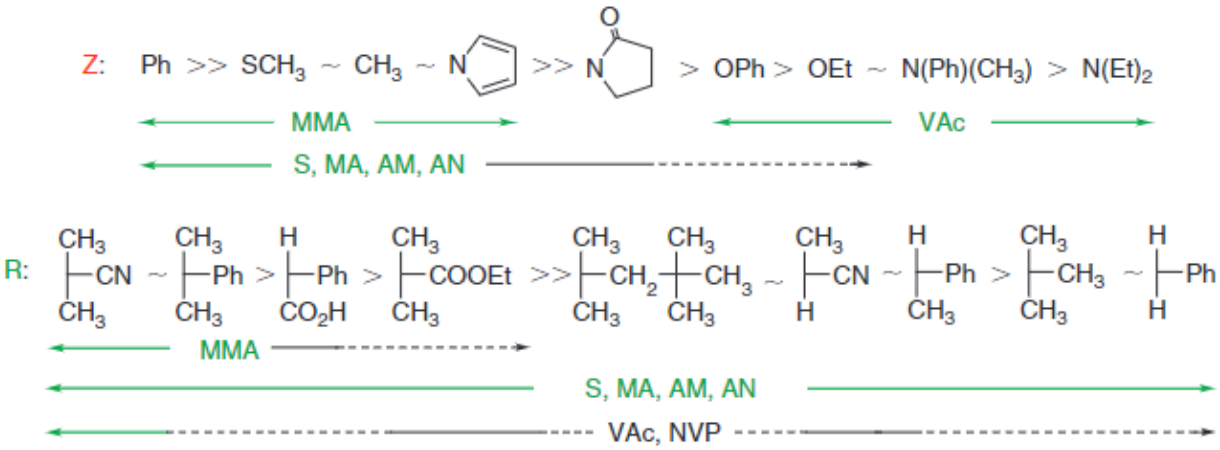

Figure 1.3. The compatibility of Z- and R- groups of a RAFT chain transfer agent with different monomers. Reproduced from Moad and coworkers.[74]

3.2 Atom Transfer Radical Polymerisation (ATRP)

Pioneered by Matyjaszewski and Sawamoto in 1995,[77, 78] ATRP is an extensively used RDRP strategy advantageous for synthesising polymers with narrow molecular weight distributions and diverse molecular architectures. The mechanism of conventional ATRP (Figure 1.4) involves an alkyl halide initiator (R-X) catalytically being activated by a donor ligand complexed with a transition metal (M_t^m/L), typically copper due to its low cost and predictable chemistry. The metal halide ligand is oxidised in this process, transitioning from lower oxidation state (M_t^m) that facilitates polymerisation activation, to the higher oxidation state (M_t^{m+1}) being the deactivating state. The active radical ($R^{\cdot}$) then reacts with free monomer to create a propagating chain at a constant rate of propagation (k_p). To ensure controlled polymerisation, the ATRP equilibrium must be balanced, maintaining a lower constant rate of activation (k_a) and concentration of activating molecules compared to the constant rate of deactivation (k_d) thereby allowing the polymerisation to proceed in a well-controlled manner and minimising the incidence of deactivating complexes and subsequent termination.[79]

Whilst this reaction is reversible between activation and deactivation of polymer propagation, chain termination reactions are still present, though negligible in occurrence, when two propagating radicals meet to form R-R dormant chains. Eventually, this contributes to the

equilibrium shift to favour chain activation and propagation resulting in greater concentration of deactivating complex ($X\text{-}M_t^{m+1}/L$), which slows the addition of monomers to propagating chains.

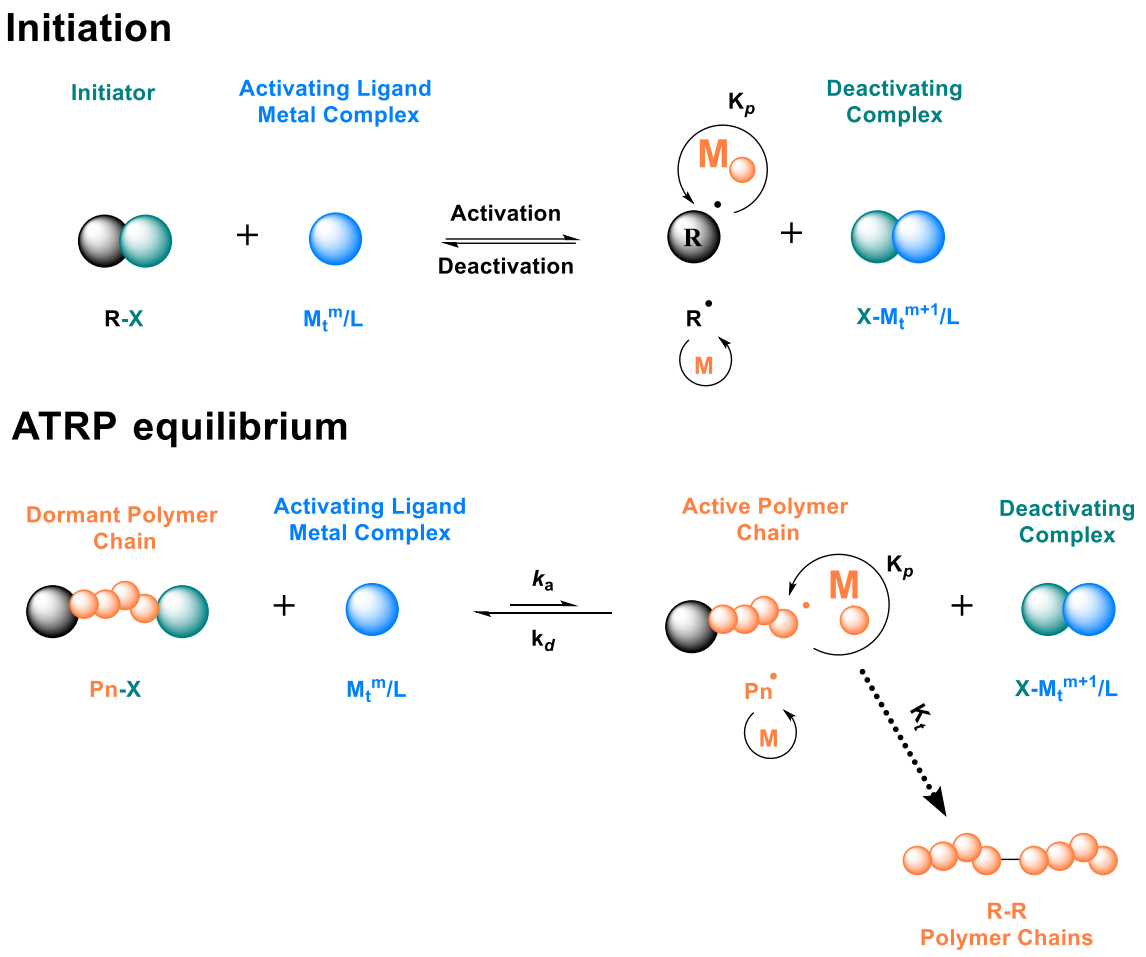

Figure 1.4. The mechanism of atomic transfer radical polymerisation in the initiation and equilibrium phases.

ATRP is an attractive polymerisation method due to its wide compatibility with not only a range of monomer classes, but also efficiency in both polar and non-polar solvents. To determine the optimal alkyl halide and ligand combination for a monomer class, thermodynamic and electrochemical properties must be considered to ensure optimal electron transfer.[80] Additional factors that must be considered include reaction temperature, solvent polarity, and pressure. As mentioned previously, whilst copper is most commonly used, the metal catalyst can also be

changed,[81] with reports on a range of metals being used including iron,[82, 83] ruthenium,[84, 85] cobalt,[86] and nickel.[87]

As the landscape of ATRP evolves, a series of ATRP subtypes have been uncovered. To reduce copper concentration to a few parts per million, including continuous activator regeneration (ICAR) ATRP,[88] single-electron transfer living radical polymerisation (SET-LRP),[89] photoinduced ATRP,[90] and electrochemical ATRP (eATRP)[91] are used. To limit copper concentration, these polymerisation types rely on reducing agents to reactivate active copper species. Methods that are more tolerant to oxygen compared to conventional ATRP have also been explored such as activators regenerated by electron transfer (ARGET) ATRP.[92, 93]

4. Polymer Self-Assembly

The self-assembly of polymeric materials into nanoparticles remains an extensively used strategy. The versatility of this approach is dependent on the differences in the properties and architectural design of the polymer starting material. The simplest of polymer structures available for self-assembly are linear in nature, usually existing in amphiphilic form, where monomers are either attached in distinct hydrophilic and hydrophobic blocks. The interplay of thermodynamic, geometric and kinetic factors largely govern morphological control of resulting nanoparticles. The incompatibility of these blocks in aqueous solution drives the thermodynamic process of their segregation into distinct phases, generally with a compact hydrophobic core, and relaxed hydrophilic shell. This is quantified by the Flory-Huggins interaction parameter (χ) which explains the incompatibility between polymer segments, and also between polymers and the solvent system.[94] When $\chi > 0.5$, the energy penalty drives self-assembly through phase separation and aggregation. Solvent selectivity determines the extent of block solvation,[95] which in turn, can also affect polymer packing and morphology. Entropically favourable morphologies for polymers include particles with a higher surface

curvature, namely micelles, cylinders and vesicles. The phase diagram that defines the realisation of these morphologies is defined by the volume fraction of amphiphiles (Figure 1.5). This phenomenon is denoted as the critical packing parameter (CPP) that compares the volume of the hydrophobic segment (V) to the surface area of the hydrophilic head (a_0) with respect to the length of the hydrophobic tail (l_c) (Figure 1.5). When CPP < 1, the molecular shape of the polymer building block is more tapered and lends towards shapes with more curved surfaces. When the CPP extends beyond 1, more lamellar phases are accessed before reaching inverse micelles. Whilst this model was initially developed to explain the behaviour of simple two segment surfactants and amphiphiles, the principles can be extended to multiblock copolymer systems towards hierarchical systems.

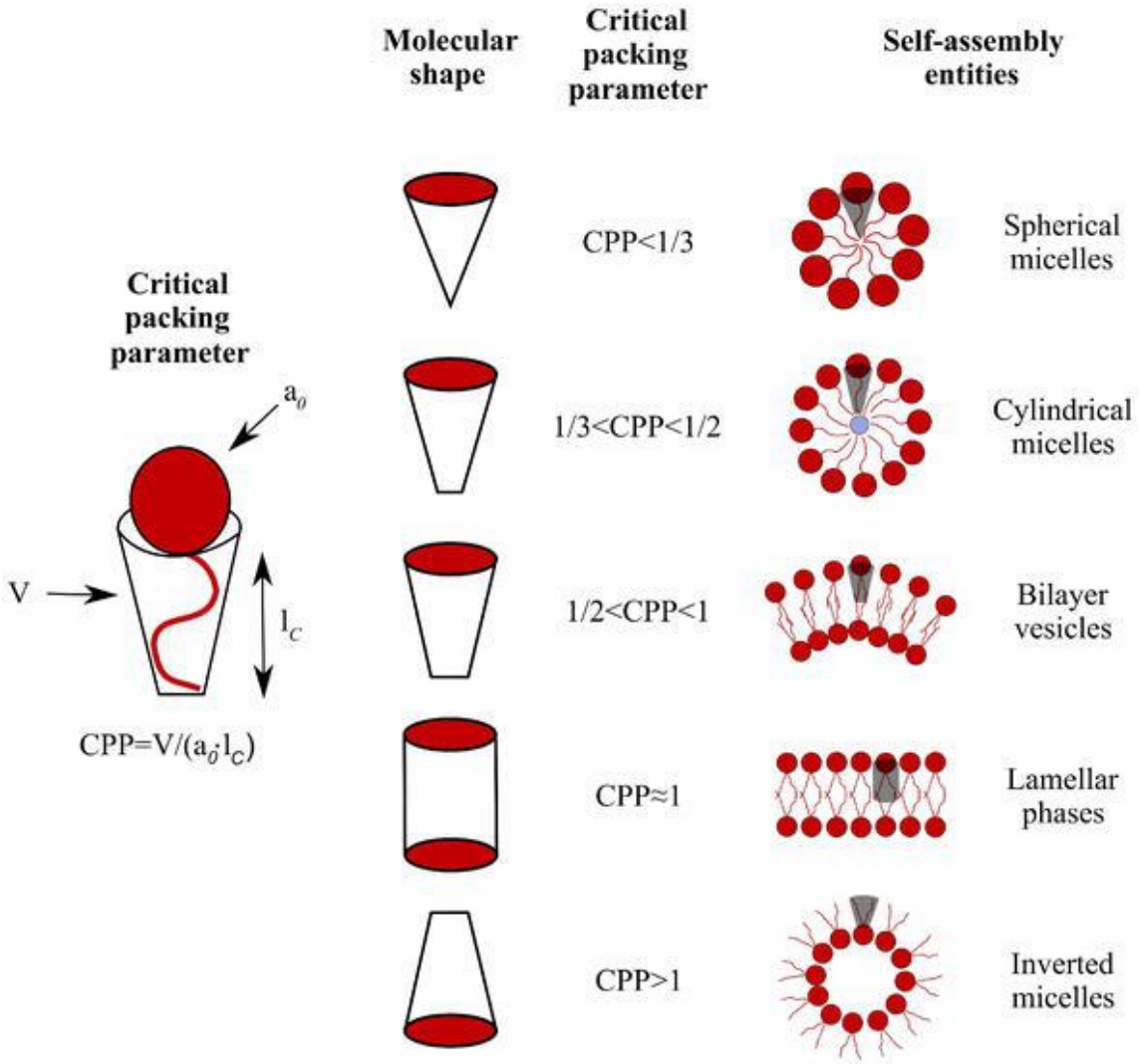

Figure 1.5. Critical packing parameter of amphiphilic building block that dictates the molecular shape and self-assembled entity. Reproduced from Dopazo et al.[96]

Self-assembly of such block copolymers has been reviewed extensively.[97, 98] The competition between interfacial tension (γ) and chain entropy also influences the particle core dimensions as the system tries to achieve equilibrium and minimise total free energy. The interactions between polymer chains can also affect their solution behaviour and influence interfacial tension, which has been theoretically investigated with self-consistent field theory (SCFT).[99] Depending on the chemical moieties present within these chains, hydrophobic, electrostatic, π-π interactions, and an interplay between these can also be manipulated to tune morphology.[100] With self-assembly behaviour being influenced by so many thermodynamic factors, strategies have looked to direct the process by altering solvent type, pH, concentration and ionic strength, making this process tuneable and diverse.[101] Despite this, morphologies existing beyond the traditional phase diagram defined by CPP such as discoidal nanoparticles have proven to be relatively difficult to achieve.

In some cases, kinetic factors can govern the self-assembly process, enabling access to kinetically 'frozen' intermediate morphologies.[102] This phenomenon gave rise to techniques such as polymerisation induced self-assembly (PISA) which will be discussed further. Kinetic trapping typically occurs when chain mobility is restricted by factors such as glass transition temperature (T_g).[103] When the self-assembly temperature is below the T_g of a polymer, it becomes glassy and brittle.[68, 104] In contrast, polymers with lower T_g maintain flexibility and can rearrange in response to environmental change towards thermodynamic equilibrium.

Whilst linear block copolymer self-assembly has been used extensively, another layer of complexity can be achieved by using cyclic polymers and branched structures to access higher-order morphologies.[105] Branched structures remain an interesting domain and range from sparsely branched architectures such as star and comb polymers, to densely branched structures in the form of network polymers and the hyper-branched molecular polymer brushes (MPBs). As an amphiphilic building block, bottlebrush block co-polymers (BBCPs) are advantageous

due to the wider capacity to include different physiochemical properties and greater stability in solution.[106, 107] To ensure that these polymer systems remain well-defined despite the complexity of their architectures, many synthesis routes rely on RDRP techniques discussed previously in Section 3. The synthesis routes for MPBs will be discussed further in Section 5. Common morphologies of particles reportedly achieved by the self-assembly of BBCPs include micelles[108-112] and vesicles.[108, 112-114]

4.1 Self-Assembly of Molecular Polymer Bottlebrushes

The complexity of MPB architectures offers a plethora of structural features that can be manipulated to induce morphological control in self-assembly. These include BBCP side chain and backbone lengths which can be manipulated to alter volume fraction of hydrophilic and hydrophobic blocks, as well as grafting density. The combination of these parameters results in interesting packing behaviour of bottlebrushes compared to linear polymer systems.[115, 116] Their influence on intrinsic flexibility and chain entropy dictates self-assembled morphologies based on the curvature of interfaces between hydrophilic and hydrophobic domains. Theoretical studies largely form our understanding of the independent effect of these parameters on MPB packing behaviour, with some work in bulk self-assembly. Solution-based self-assembly studies remain the least explored. Figure 1.6. highlights some experimental studies where these parameters have been explored in variations of bottlebrush block copolymer architectures.

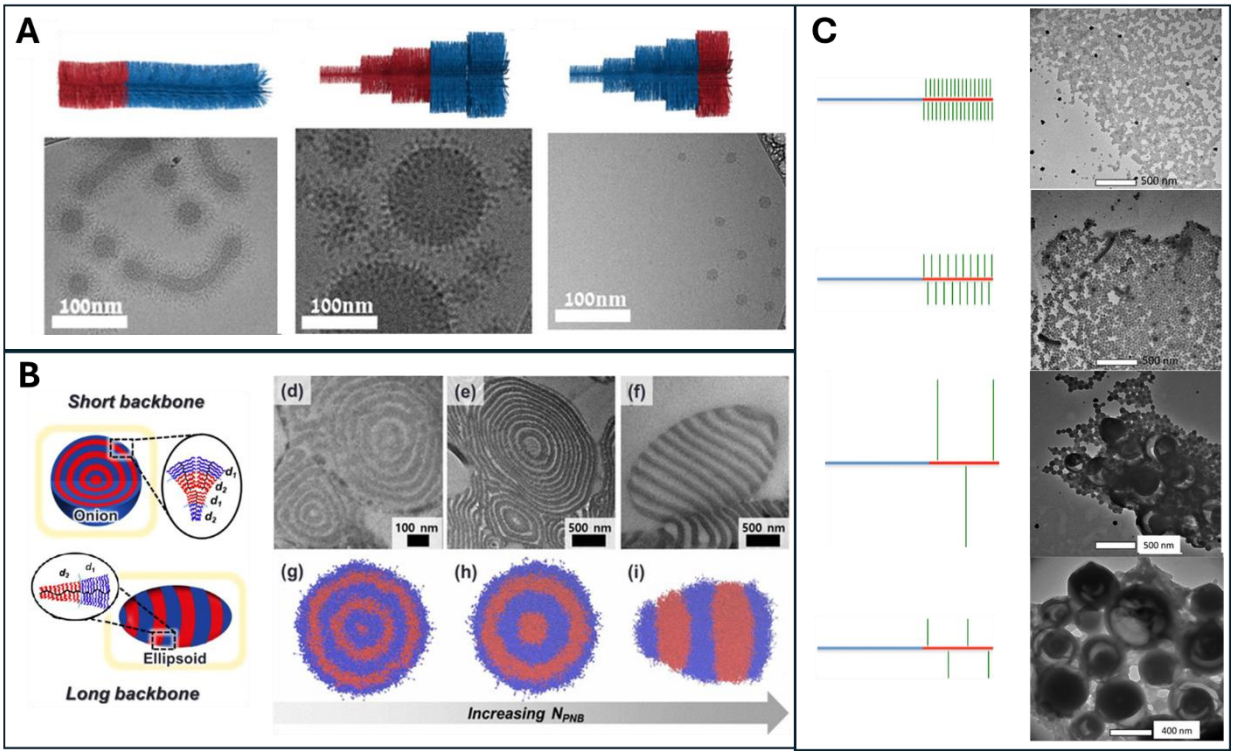

Figure 1.6. Schematic representations and corresponding TEM of systematic self-assembly studies altering key MPB structural parameters showing morphological evolution in response to changing packing in (A) asymmetric MPB copolymers with comparable hydrophobic wt% where tapered side chain lengths achieves greater particle surface curvature. Adapted from Matson et al.[112] (B) MPB block copolymers where increased backbone length decreases intrinsic flexibility, transitioning from onion-like to ellipsoid particles in emulsion droplets. Adapted from Kim et al. [120] (C) rod-coil 'toothbrush' block copolymers where increased grafting efficiency increases side chain stiffness, resulting in particles with less interfacial curvature. Adapted from Adamson et al.[123]

4.2 Polymer Side Chains

The side chains of MPBs have a large impact on steric and intermolecular interactions, thus affecting their packing arrangement.[117] A simple example of increasing the side chain length of an MPB containing amphiphile presented by Wooley and coworkers showed morphological transitions from spherical and cylindrical particles to bilayers.[118] The change in side chain simultaneously influenced the molar ratios between hydrophobic and hydrophilic segments, which is also expected to contribute to morphology changes. Isolating side chain length from

molecular weight changes, the Seo group opted to maintain amphiphile ratios in a Janus core-shell bottlebrush, instead creating asymmetry in side chain length on either side of a polymer backbone to influence self-assembled morphologies.[108] By increasing side chain asymmetry to favour a shorter core-forming section the backbone bending energy increases, disproportionally affecting nanoparticle curvature stability to favour less curved structures. In another approach, the Matson group incorporate macromolecular asymmetry between two blocks of a BBCP with conflicting chemistries by systematically shortening and lengthening the side chains of hydrophobic and hydrophilic blocks they were able to alter both volume fraction and polymer shape. Comparing systems of ~50 wt% hydrophobic fraction with differing shapes where the hydrophobic and hydrophilic side chains were either similar, tapered or invertedly tapered (Figure 1.6A), a progression from cylindrical to more spherical particles with greater surface curvature. The packing parameter is controlled by the shape of the bottlebrush, highlighting the role of building-block asymmetry in morphology control.[110, 119] Collectively, these examples show that side chain length proportionally increases MPB rigidity, resulting in morphologies with less interfacial curvature.

An interesting modelling tool used in self-assembly attesting to side chain induced rigidity is superstrong segregation regime (SSSR). SSSR was first introduced by Semenov, Khokhlov and coworkers modelled by block copolymers between highly incompatible blocks containing strongly interacting groups that consequently stretch to overcome any interfacial tension to lower free energy.[120, 121] As the incompatibility increases, micellar structures are no longer the stable conformation, and disc-like particles form. Whilst this has typically been explored with linear polymers, Vasilevskaya et al., proposed that it was easier to achieve with brush-like polymers, applying mathematical principles to predict SSR induction in systems.[122] They explain that increasing the length of side chains and grafting density can increase the stretching of the comb section, facilitating a crossover to SSSR when appropriately balanced with a

hydrophilic coil segment. Kim et al., experimentally confirm this model in micelles of polynorbornene-based fluorinated MPBs. Because of the additional steric hindrance that grafted side chains afford over linear polymers, interactions between incompatible short side chains and longer polymeric backbones facilitates backbone stretching.[123] Therefore, the radius of the core forming components increases. Whilst not accessing anisotropic particles themselves, they present this work as a scalable model to adjust the flexibility of polymer blocks, which can improve access to different morphologies.

4.3 Polymer Backbone

Alternatively, the conformational stretching of MPBs can be influenced via backbone design. Theoretical models by Zhulina, Sheiko, and Borisov,[124] have shown that extending the length of MPB backbones in solution lends to a stretched backbone conformation when side chains are of sufficient length. Therefore, polymer lengths, combined with environmental factors such as solvent quality have been controlled to access varied morphologies. Chremos et al. used molecular dynamic studies to correlate intrinsic stiffness of MPBs to morphological transition independent of side chain length and volume fraction.[125] They found that as backbone length increased, also increasing intrinsic MPB stiffness, the packing of the rod-like segments transitioned from favouring hexagonal cylinders to lamellar phases. Experimentally, Ishizu et al. designed an amphiphilic brush comprising of hydrophilic PEG, and poly(hydroxyethyl) methacrylate (PHEMA) as the hydrophobic component. With a shortened polymeric backbone, MPBs assumed a more ellipsoid conformation as opposed to typical cylindrical shapes. In turn, this affected their aggregation behaviour and self-assembly into higher-order morphologies such as compartmentalised onion-like nanoparticle with distinct domains visualised through electron microscopy techniques.[126] More recently, Kim and coworkers observe a similar phenomenon, where the confinement self-assembly of MPBs with longer backbones are driven by larger entropic bending penalty, as opposed to shorter backbones where surface energy is

the dominant factor in morphological control (Figure 1.6B). This facilitates a transition from ellipsoid to onion-like particles respectively.[127]

4.4 Grafting Density

Another factor on MPB conformation explored in SSSR theory,[124] and supported in other SCFT,[117] and molecular dynamic simulations,[105, 128] is grafting density. As grafting density increases, MPBs transition from linear to comb-like, to bottlebrush regimes.[129] Grubbs and coworkers explored the scaling effect of grafting density on backbone stiffness, identifying a critical threshold where chain conformation transitions become evident as a result of side chain repulsion induced rigidity.[129] While this study was conducted in solid phase, the general trends and observations are expected to correspond to similar systems in solution. In an architecturally relevant system to disc-forming building-blocks discussed further in Section 5.2, Martinez et al. investigated the effect of grafting density in a library of poly(styrene-*block*-(isoprene-*graft*-poly(ethylene oxide)) rod-coil polymers (Figure 1.6C). Reducing grafting density by approximately 90% evolved particles from spherical micelles to higher order structures.[130] This is attributed to the greater flexibility afforded to side chains as grafting density is reduced, due to the absences of inter side chain repulsion.

These systematic investigations highlight the large potential to direct MPB based architectures toward desired anisotropic morphologies through structural design.

5. Self-Assembly of Discoidal Nanoparticles

A notable anisotropic morphology lacking in self-assembly studies is discoidal particles. We recently reviewed self-assembly approaches resulting in discs,[67] noting that their difficulty to fabricate is reflected in the lack of reports in literature since their introduction in the 1990s.[131, 132] Herein, we focus on the self-assembly approaches toward discoidal particles as the motivation of this thesis. Readers are directed to relevant reviews and studies to achieve other

anisotropic nanoparticles such as platelets,[34, 67, 133] , worms,[133, 134] toroids,[34, 67, 135] and cylindrical nanorods.[34, 108, 111, 136]

A variety of polymer types and exotic self-assembly approaches have been employed in disc fabrication. The reported approaches have been distinguished into two groups, being top-down and bottom-up self-assembly. As their names suggest, top-down (Figure 1.7C) and bottom-up (Figure 1.7A & 1.7B) self-assembly methods are opposite in nature with the former starting from a bulk-material that is fashioned into nanoscale objects, and the latter assembling small molecules into NPs.

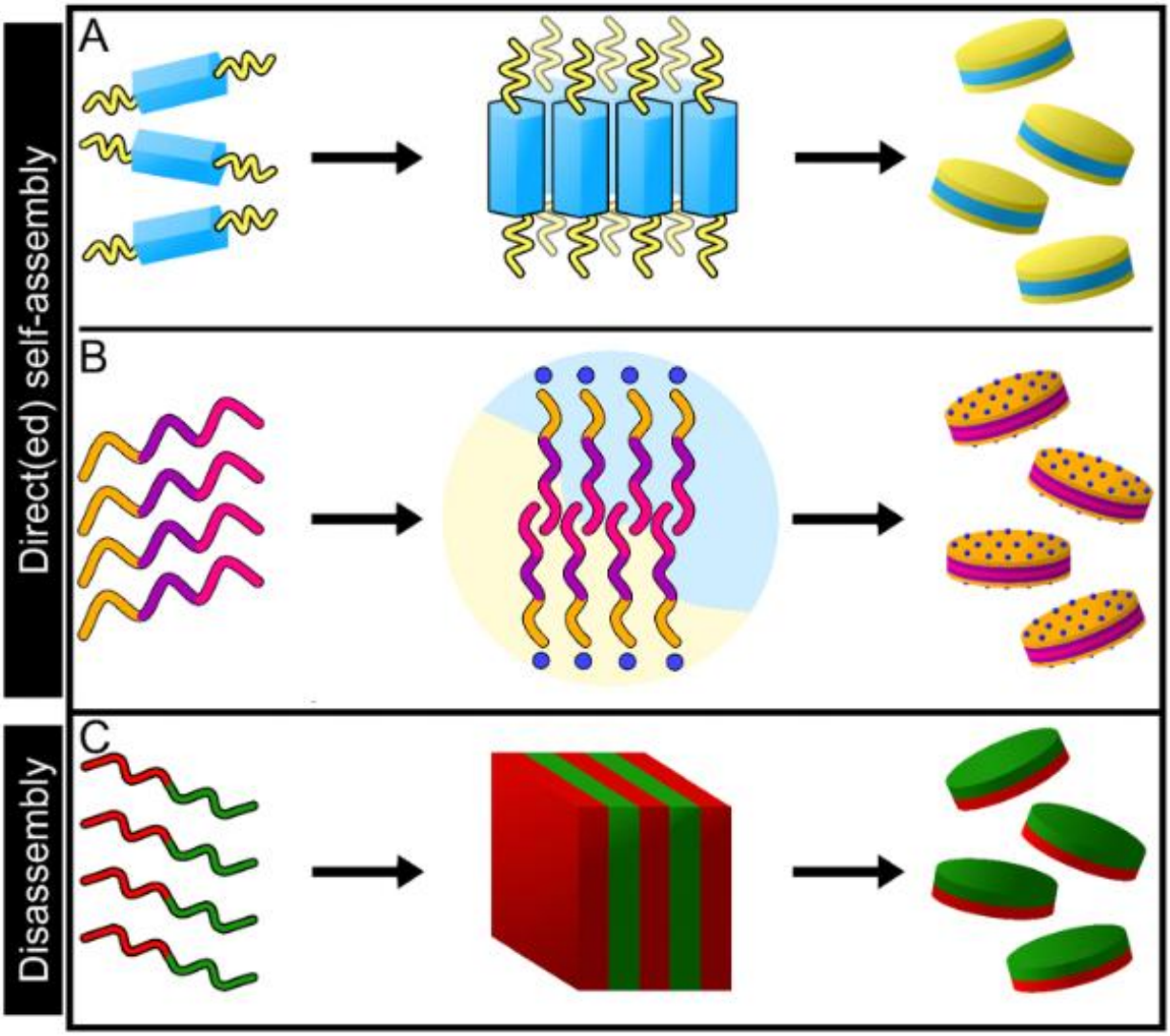

Figure 1.7. Schematic representation of self-assembly to achieve discoidal polymer nanoparticles by A) direct (B) directed, and (C) disassembly methods. Reproduced from Brisson et al.[67]

5.1 Top-Down Nanodisc Self-Assembly

To fabricate nanodiscs, the most common top-down self-assembly approach involves the disassembly of a superstructure. Large microparticles can be fabricated either in bulk thin film where solvent evaporation is involved,[98] or by confinement self-assembly within a droplet.[137] Choosing copolymer blocks with distinct chemistries affords phase separation within the microparticle that can then be modified later in the disassembly process. Figure 1.8 shows that while these approaches differ in their self-assembly approach, the mechanism of their disassembly into nanostructures is similar in that they both require post self-assembly modification steps.

Exploring the use of bulk thin films, Walther et al., use linear polystyrene-*block*-polybutadiene-*block*-poly(methyl methacrylate) (PSBM) amphiphilic polymers to assume lamellar-lamellar sheets (Figure 1.8A).[138] Cross-linkage along the polystyrene phases and subsequent sonication afforded compartmentalised janus nanodiscs, amongst other janus particle morphologies such as cylindrical rods and spheres. Janus particles characteristically have chemically distinctly domains, and derive their name from the Roman god known for two faces representing beginnings and endings.[139]

The Gröschel group have contributed greatly to the research landscape concerning evaporation-induced self-assembly (EISA) within oil in water emulsions. With linear polymers, they showed the assembly of polystyrene-*block*-polybutadiene-*block*-poly(methyl methacrylate) (PSBM) triblock terpolymers and subsequent cross-linking of the polybutadiene (PB) phase provided stability to the nanostructures once the particles were redispersed. By varying the weight percentage (wt%) of each block, the morphologies could be tuned, with 40 wt% PB block resulting in Janus nanodiscs (Figure 1.8B).

The Hawker group demonstrated the phase-separation of polystyrene-*block*-poly(*2*-vinylpyridine) (PS-*b*-P2VP) in droplets facilitated by a mixed surfactant strategy to tune the

surface energy into elongated axially stacked microparticles.[140] A second step to cross-link the P2VP domain was required for their disassembly into discs with a hydrophobic core stabilised by the modified P2VP shell. Exchanging the P2VP domain for poly(*4*-vinylpyridine) (P4VP), Deng et al. highlight a similar approach to give janus discs.[141]

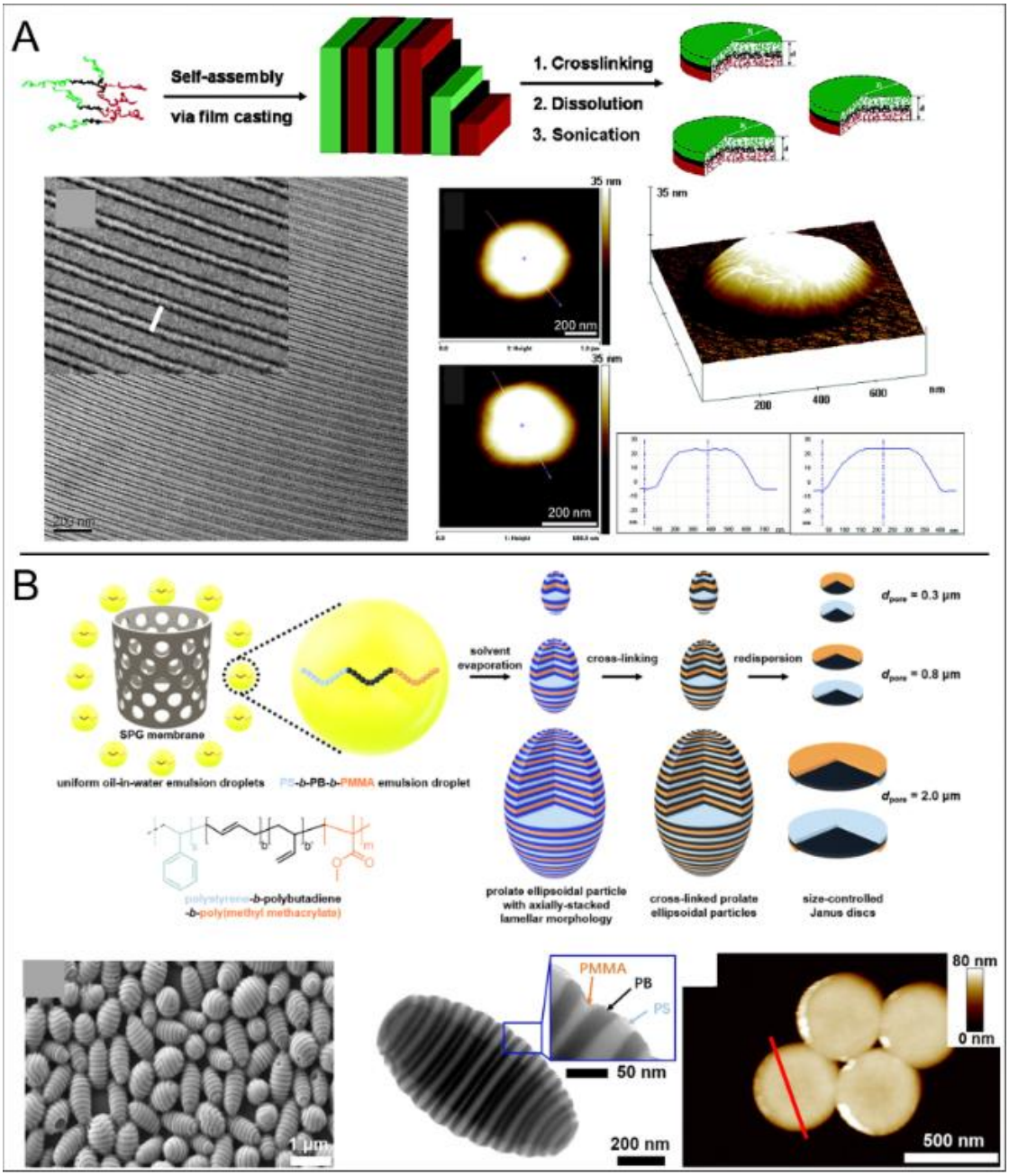

Figure 1.8. Hierarchal disassembly of microstructures into janus nanodiscs by different mechanisms. (A) Assembly of ABC terpolymer in bulk film to afford lamellar sheets and subsequent disassembly by sonication. (B) Self-Assembly of ABC terpolymer within confinement and disassembly by redispersion. Reproduced from Brisson et al.[67]

EISA has also been used with MPBs. AB diblock brush copolymers Extending their work on linear polymers with hyperbranched structures, Gröschel, Müllner and coworkers synthesised MPBs composed of poly[2-(2-bromoisobutyryloxy)ethyl methacrylate)-*graft*-polystyrene)-*block*-poly(2(trimethylsilyloxy)ethyl methacrylate-*graft*-poly(lactic acid)) (PBIEM$_{92}$-*g*-PS$_x$)-*b*-(PHEMA$_{104}$-*g*-PLA$_{33}$). The self-assembly into microparticles within an oil-in-water nano-emulsion.[142] With polymers predisposed to phase separation, this approach highlights the relevance of MPB architectures as kinetically favourable self-assembling material.

Whilst this technique facilitates good microphase separation that is essential for Janus particles, to achieve particles with dimensions on the nanoscale, post assembly processing steps such as cross-linking cannot be excluded from the fabrication process. Additionally, to take advantage of emulsion droplet confinement self-assembly, both components of the brush must be hydrophobic in nature so that they are contained within the droplet. Amphiphilic molecules will instead assemble at the emulsion interface displaying surfactant tendencies. To make them applicable for drug delivery and other biomedical applications, the properties of one phase must be switched to feature hydrophilic and biocompatible properties. This limits the monomers that can be applied by this process.

Another interesting approach presented by the Liu group employed swelling-induced phase separation as a means of compressing a discoidal structure within a micron-sized droplet.[143] Starting with a hydrophilically modified PS particle by introducing charged monomers along PS polymers, composite droplets were formed in the swelling polymerisation of 2-ethyl hexyl methacrylate (EHMA) in decane. Subsequent removal of the decane and soluble EHMA yielded micro-sized discs. By altering the composition of the polymeric NP surface by incorporating different percentages of hydrophilic monomer or changing their locality along the polymer chain, the shape and concavity of discs could be tuned. Whilst this example is

irrelevant based on particle size, the approach can be considered translatable to nano-sized objects.

Other top-down approaches that can achieve nanodiscs include lithography and particle replication in nonwetting templates (PRINT). Whilst these processes are not truly considered self-assembly because they use templates with pores for polymeric material to be moulded into desired shapes,[144] they have been used to access anisotropic particles that are otherwise difficult to achieve. The bulk material can then be removed from the template by washing to reveal the well-defined nanoparticles. PRINT is an extension of lithography that was developed to remove processing steps that are incompatible with organic material that are relevant for biocompatible nanoparticles.[145] This is achieved by introducing non-wetting polymers that do not leave excess bulk material behind. Both these approaches produce particles with precise shape and size based on the template. Enlow et al., demonstrate its use to assemble cylindrical NPs loaded with chemotherapeutics as a means of synthesising particles with greater control over tailored properties.[146] To further improve bioavailability of drug carriers, Rolland et al. applied this method to synthesise PEG based carriers of doxorubicin, achieving trapezoidal, conical, and cylindrical shaped NPs.[145] One downfall of lithography is the NP harvesting procedures. The simplest harvesting process involves the physical detachment of NPs from surfaces using a sharp tool with risk of mechanical damage to particles and moulds.

The development of bottom-up approaches provides alternatives to top-down methods that are attractive based on avoiding post-assembly processing steps and limiting the types of applicable polymer materials. The simplicity and ease of bottom-up self-assembly in comparison has seen a large increase in their study to realise polymer nanodiscs.

5.2 Bottom-Up Nanodisc Self-Assembly

Bottom-up self-assembly of amphiphilic block copolymers is favoured to achieve an extensive range of controlled polymeric nanostructures. An approach that has gained significant attention due to its ease in accessing anisotropic morphologies is Polymerisation-induced self-assembly (PISA). PISA is based on the principle of chain extending a solvophilic RAFT polymer with a solvophobic monomer. As the chain length of the second block increases, the polymer chains self-assemble into different morphologies *in situ*. Whilst this approach has been very successful in achieving cylindrical and worm-like micelles,[147, 148] planar structures such as disc-like micelles remain seldomly reported.[149] Focusing on bottom-up self-assembly approaches in solution resulting in disc-like micelle formation can be distinguished further into two categories, being directed self-assembly, and direct-self-assembly. The distinction is made on the governing factor that allows the energy penalty to compress or bend molecular assemblies into planar structures.

5.2.1 Directed Self-Assembly

Given the challenges associated with disc formation, directed self-assembly has provided an avenue for people to access desirable morphologies. This approach involves extrinsic factors such as templates, solvent mixtures or small molecule chaperones drive disc formation (Figure 1.7B).

The use of structure-guiding templates that facilitate the formation of particle morphologies has used to achieve uniform nanodiscs. Yang and co-workers exemplify this using a PEO-*block*-poly(3-triethoxysilylpropyl methacrylate)-*block*-PS triblock terpolymer.[150] By using paraffin droplets as templates in a paraffin-in-water emulsion, the terpolymers acted as a surfactant at the interface. Acidifying the system triggered a polycondensation of the triethoxysilypropyl component around the droplet, whilst the PEO and PS segments remained flexible. Upon dissolution of the droplets, Janus discs were retrieved that also had surfactant

capabilities in organic-aqueous solvent mixtures. Additional work substituted paraffin droplet as templating surfaces for silica particles adorned with imidazole domains.[151] Poly(acrylic acid)-*block*-PS interacted with these regions by electrostatic interactions. Subsequent cross-linking of the PAA region allowed well-defined discs of approximately 20 nm diameter to be retrieved.

Small molecules that can influence polymer interactions and their subsequent packing arrangements have also been explored to overcome energy bending penalties and access higher order morphologies. One small molecule used for this purpose is tartaric acid. PS-*b*-P2VP polymers in acetone were subject to slow addition of an aqueous tartaric acid solution.[152] In the aqueous anti-solvent, the polymers arranged themselves into spherical assemblies with a stacked lamellae phase induced by cross-linking of the P2VP domains by the tartaric acid. After exceeding a certain threshold of tartaric acid concentration, the P2VP became protonated in the acidic environment, which induced a morphological transition into polymer discs. This example crosses over between two strategies, involving both small molecule additives and the disassembly of a superstructure in a one-pot reaction.

Another example of small molecule additive avenues to disc formation was highlighted by Wooley and Pochan.[153] Their exotic approach involved the use of two PAA-*b*-PS diblock copolymers exhibiting different CPP to achieve an assembly with a planar domain and curved edges respectively. Without additives, these polymers self-assembled with those of their own CPP, affording a mixture of cylindrical micelles and bilayer structures. However, with the addition of ethylenediaminediacetic acid (EDDA), the two diblock copolymers could self-assemble into a hybrid structure to afford discs. The driving force of this hybrid self-assembly was credited to the electrostatic interactions of the PAA segment with the EDDA, as well as factors of blend ratios, and aqueous solvent addition.[154] The choice of diamine additive was

also investigated by the same group finding that multivalent and smaller sized diamines interacting with PAA segments favoured stable and uniform disc formation.[155]

5.2.2 Direct Self-Assembly

In contrast, direct self-assembly relies on the intrinsic chemical composition of the polymers, and their predominant interactions that lend to preferential packing into a flat structure (Figure 1.7C). Due to its simplicity, it is generally the most-preferred self-assembly route.

Direct approaches till date have relied heavily on crystallisable chemistry within core-forming polymer blocks as a means of instilling rigidity into building blocks. In the 1990s, two demonstrations of this approach were presented by Richter et al.,[131] and Nakano et al.,[132] with polyethylene-*block*-poly(ethylenepropylene) (PE-*b*-PEP) and octadecyl vinyl ether-*block*-poly(2-hydroxyethyl vinyl ether) (HOVE) respectively. The self-assembled micelles could be manipulated into a flattened structure by reducing the temperature below that of the crystallisable temperature for the core-forming PE and octadecyl containing blocks. Since then, many have exploited semicrystalline polymers, such as poly(*N,N*-dimethylacrylamide)-*block*-PE ($PDMA_{94}$-*b*-PE_{57}).[156] At elevated temperatures and pressure, spherical particles were observed, However, reducing the temperature below the melting point of the crystallisable PE segments forced a collapse of the core into discoidal particles (Figure 1.9). Other examples of crystalline core-forming blocks have involved polymers such as polymethylene[157], polyethylene,[158] and isotactic polystyrene,[159] as the driving force for disc formation. It is worth noting that control over polymer dimensions is still required with high degrees of polymerisation in either the hydrophilic corona or crystallisable core resulting in crowding and impeding the crystallising-driven mechanism.[132] Extending the use of crystallisable polymers, semi-crystalline materials have also been explored.

An intriguing crystalline material class also used in self-assembly are liquid crystal (LC) moieties. Venkataraman et al. synthesised an amphiphilic polymer with pendant cholesterol derivatives PEG-*block*-poly(2-(5-methyl-2-oxo-1,3-dioxane-5-carboxyloyloxy)ethyl carbamate)) (PEG-*b*-MTC-Chol).[160] Relying on the close packing of LC materials upon dialysis from DMF to water afforded well-defined discs. As the LC component of the building blocks increased, they also observed stacked discs into cylindrical microparticles by TEM.

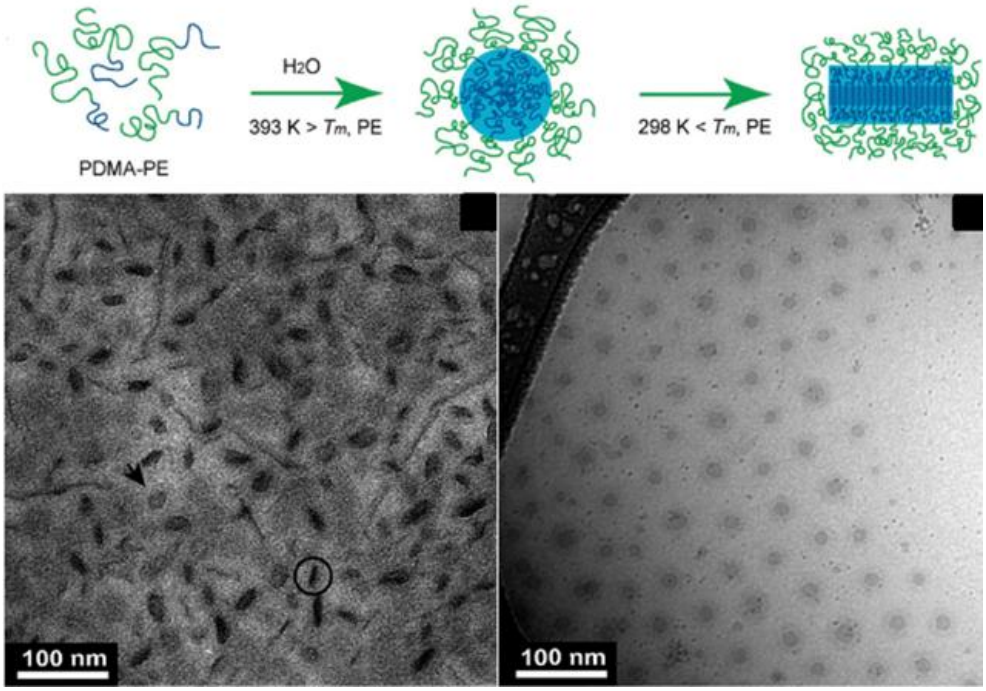

Figure 1.9. Direct self-assembly of crystalline polymers into micelles before temperature induced collapse into nanodiscs. Reproduced from Yin and Hillmyer.[156]

Opting for rod-like architectures, as means of achieving greater rigidity, Allen and coworkers modified a methoxy-PEG-*block*-poly(allyl glycidyl ether) (mPEG-*b*-PAGE) with different hydrocarbon chains to explore the driving force behind self-assembly in semi-crystalline polymers.[161] Using (mPEG-*b*-P(AGE-C_{16})$_{25}$ building blocks in both solvent-switch and solvent-evaporation self-assembly methods, mixtures of discs, toroids, worms and spheres were achieved. This indicated that the semi-crystalline properties of the polymer dictated the self-assembly process. However, altering the carbon tail grafts to C18 increased the polymer volume resulting in polymersomes. In contrast, reducing the chain to C12 produced rod-like

micelles, further confirming the importance of polymer dimensions to access discoidal morphologies.

An interesting approach that incorporates elements of direct and directed self-assembly with a crystallisable polymer was reported by Toebes and Wilson.[162] By manipulating the electrolyte levels and solvent environment of mPEG-*block*- *D,L*-lactide polymers in a solvent-switch method, they were able to access different morphologies including discs. Mixtures of THF and dioxane with a higher THF content seemingly favoured greater curvature in the packing, where cores were smaller than particle coronas. When dioxane content increased, disc formation was more prevalent likely due to polymer stretching. Salt addition was also seen to promote the stretching phenomenon.

Semi-crystalline polymers are also well documented in crystallisation-driven self-assembly (CDSA) approaches. Whilst the approaches presented above differ from this concept in that they force a collapse of crystallisable components in already formed morphologies, CDSA relies on intermediate crystalline 'seeds' that initiate epitaxial growth as unimers arrange themselves.[163] Liquid-CDSA, a process relying on liquid crystal properties of polymers has been recently introduced to achieve nanodiscs. In a seed solution poly(ethylene glycol)-*block*-poly(γ-benzyl *L*-glutamate) (PEG-*b*-PBLG) rod-coil polymers assumed smectic packing of the LC segments.[164] Further addition of PEG-*b*-PBLG unimers facilitated controlled two-dimensional (2D) growth of discs. This approach unlocks the potential of synthesising discs of tuneable dimensions simply by altering factors such as seed concentration and time. In the context of biomedicine however, a collapsed crystalline core phase impedes drug diffusion, which can hinder both drug loading and release. Studies have ascribed this to the lack of available space in the hydrophobic domain.[165, 166] Therefore, alternative chemistries continue to be explored.

Extending the idea of balancing a rigid segment with a flexible coil gave rise to polymers designed as rod-coil architectures. Reports of this architecture have typically seen rod segments involving conjugated, helical, or polypeptide-based materials. A novel demonstration of conjugated materials by Liu and coworkers used a polymerised camptothecin prodrug attached to a PEG chain (PEG-*b*-PCPTM) to achieve what they denote as poly(prodrug) amphiphiles. Combining the rod-coil architecture with non-specific steric and π-π interactions facilitated by the camptothecin achieved discs with diameters of ~300 nm.[167] Unfortunately this approach is not universal, relying heavily on the bulkiness of drug moieties.

Helical structures are inherently rigid due to their strong intermolecular forces positioning them as interesting self-assembly tools. Zhou and coworkers showed solvent-dependent self-assembly of PEG-*block*-poly[(+)-2,5-bis[4'-((S)-2-methylbutoxy)phenyl]styrene] (PEG-*b*-PMBPS) rod-coil polymers.[168] Transitioning from THF being a good solvent for both blocks, to aqueous environments, the rods packed in a nematic fashion while the PEG chains extended outward. However, when starting in dioxane being a bad solvent for the PEG, the strain on the linear chain lended toward spherical particles instead, highlighting the role of stabilising polymer conformations in morphologies of self-assembled particles. Wu et al. also ascribe nematic packing of the helical rods to disc formation in their demonstration with poly(*n*-hexyl isocyanate)-*block*-poly(ethylene glycol) (PHIC-*b*-PEG).[169] In toluene, the solubilised PHIC block maintains a stiff helical structure driving the planar self-assembly.

Another type of helical system self-assembled include polypeptides, with the most extensively used being PEG-*b*-PBLG. By increasing the DP of PBLG, Lin et al., showed a morphological transition from micelles, to disc-like structures with pores, to vesicles.[170] Polymers were first aggregated in THF solutions before self-assembly was induced by dropwise addition of water. The driving force of disc-formation in response to aqueous solvent was the helical rigidity from the PBLG, whilst the resulting pores were attributed to the inhomogeneous nature of the solvent

switch and potential for polymers to arrange at THF/water interfaces as bubbles. Interest in polypeptides is also focused on their LC properties at critical concentrations. The LC behaviour can be further influenced through temperature, to influence rod arrangements in self-assembling structures.[171]

More recently, researchers have looked to combining linear polymers with an MPB segment to achieve coil and rod blocks respectively. The unique interplay of side chain steric repulsion and conformational stretching of the polymer backbone chains lends to interesting physiochemical behaviour in different physical environments. In some cases, this affords MPB segments enough rigidity to overcome the bending energy penalty for disc formation. This, combined with their branched architecture contributes to the lower CMC of MPBs compared to linear polymers,[172] making them interesting candidates for self-assembly building blocks. Chen and coworkers presented a facile approach with an A*b*BA coil-rod-coil or brush-linear-brush architecture. With poly(*N*-(2methacryloyloxyethyl)pyrrolidone (PNMEP) coils and a poly(*tert*-butyl acrylate)-*block*-polystyrene (P*t*BA-*b*-PS) grafted MPB, discs ranging from 100 – 300 nm in width and ~ 30 nm in height were achieved in a coil-selective solvent.[173] With a PS containing MPB, staining by TEM uncovered a hexagonal pattern within the discs, providing insight into the 2D packing of the building blocks (Figure 1.10A). Employing rod-coil bottlebrush-linear MPBs, Zeng et al. self-assembled PEG-*block*-poly(ethyl glycoxylate) bottlebrush copolymers into discs ranging from 300 – 600 nm (Figure 1.10B).[174] Interestingly, the height of these discs persisted at ~7 nm which corresponds to the length of the rod-like MPB block instead of two rod segments assuming lamellar stacking to mimic a coil-rod-coil arrangement presented above. Furthering this work, demonstrations of pH-responsive disassembly of nanodiscs for controlled drug release were self-assembled with a similar disc height.[175]

Whilst these examples offer seemingly simplistic avenues to achieve discoidal self-assemblies, there are many factors of MPB design that can alter the volume fraction of designed amphiphiles, and therefore the self-assembled morphologies.

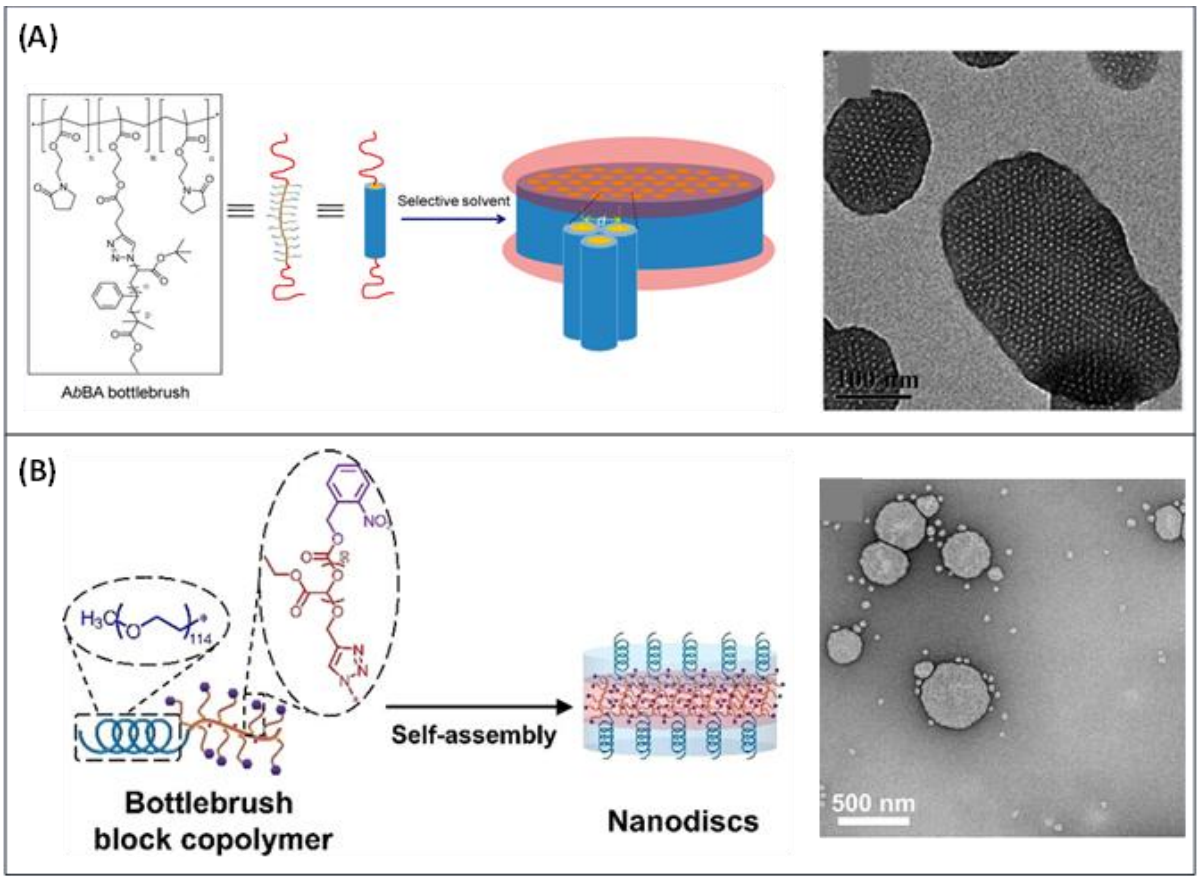

Figure 1.10. Discoidal nanoparticle self-assembly of molecular polymer brush based (A) ABA coil-rod-coil poly(N-(2methacryloyloxyethyl)pyrrolidone (PNMEP)-*block*-[poly(3-(methylamino) propylamine)-*graft*-poly(t-butyl acrylate)-*block*-polystyrene]-*block*-PNMEP, (Reproduced from Müllner and coworkers)[173] (B) AB coil-rod polyethylene glycol (PEG)-*block*-[poly(glycidal methacrylate)-graft-poly(ethyl glyoxylate)]. Reproduced from Chen and coworkers.[174]

6. Synthesis of Molecular Polymer Bottlebrushes

MPBs can be accessed by one of three synthetic pathways - grafting-to, grafting-from, and grafting-through methods (Figure 1.11).[172] The method of choice is heavily influenced by the desired MPB composition. The composition of MPBs that can be accessed depends on the number and type of side chains incorporated, as well as their locality along a backbone. The

simplest form is a homopolymer (Figure 1.11A) comprised entirely of one chemical environment. For self-assembly, MPBs require multiple chemical domains, which can be achieved by the introduction of two or more side chains. This can occur in multiple formats including block copolymer (Figure 1.11B), janus (Figure 1.11C) or core-shell (Figure 1.11F) structures. In these three cases, the MPB exhibits distinct chemical environments dictated by the locality of the side chains along the backbone in the case of block- and janus MPBs, and the order of polymer segments along each side chain in the case of core-shell brushes. Where differing chemical environments are not required but multiple chemistries are important, heteropolymer statistical (Figure 1.11D) and random (Figure 1.11E) MPBs can also be achieved.

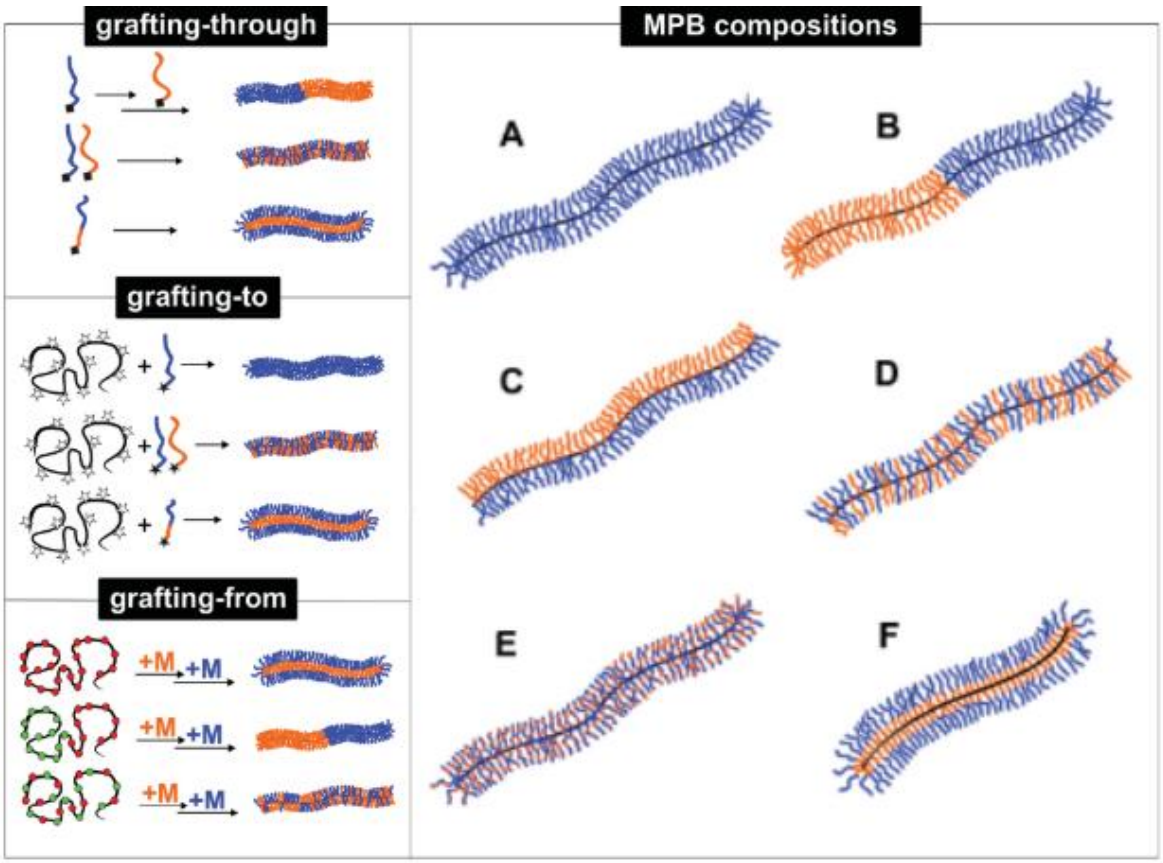

Figure 1.11. Synthetic approaches to assume polymer brushes of different compositions a) homopolymer, b) block copolymer c) janus, d) statistical copolymer, e) random copolymer and f) core-shell brushes. Reproduced from Müllner.[172]

6.1 Grafting-Through Method

The grafting-through method involves the synthesis of macromonomers that contain a terminal functionality that can undergo polymerisation (Figure 1.11). An important consideration in experimental designs is to ensure that the polymerisable moiety intended for 'grafting-through' must be chemically distinct from other functional groups present in the macromonomer to avoid interference in the polymerisation process. To achieve the graft-through synthesised macromonomers, polymerisation types that have been used for this approach include radical polymerisations such as conventional radical polymerisation,[176] ATRP[177-179] and RAFT polymerisation.[180-182] Because all macromonomers are installed with the same polymerisable group, grafting-through mechanisms proceed as a typical polymerisation. Grafting-through approaches are particularly useful to achieve MPB compositions such as block copolymers where side chain locality along a backbone must be controlled.

Whilst this strategy is adopted used for its simplicity and high grafting efficiency,[183] it is limited in the ability to synthesise ultra-long MPBs depending on the bulky nature of the synthesised macromonomers, with larger macromonomers also presenting as an issue for purification. However, the use of ROMP as an elegant polymerisation method overcomes barriers that previously prevented the polymerisation of complex and bulky macromonomers.[181] In order to utilise ROMP for the synthesis of MPBs, macromonomers must be installed with terminal cyclic olefin,[184] such as the commonly used norbornene. Because of its high ring-strain, along with the active ruthenium centre of Grubbs' catalysts,[185] ROMP reactions are typically very fast. However, these reactions are highly sensitive and require precise conditions to remain controlled.

6.2 Grafting-(on)To Method

The grafting-to method involves the synthesis of both a polymer backbone and linear polymer side chains individually, which are then connected via coupling reactions such as click

chemistry (Figure 1.11). Various brushes has been synthesised using a backbone with reactive groups such as alkyne functionalities on a poly(HEMA) backbone for click chemistry,[186, 187] or chloride groups along a poly(chloroethylvinyl ether)[188] backbone to then attach macromonomers via substitution reactions. This approach is highlighted for its precise control of grafting-density and grafting-position along a backbone depending on the availability of active grafting sites for side chains. Additionally, because the side chains can be synthesised and characterised individually, this approach can be advantageous where control over side chain chemistry is relevant. Conversely, the grafting density capability of this approach is limited by steric factors depending on side chain bulkiness.[183]

6.3 Grafting-From Method

Similar to the grafting-to method, grafting-from strategies also employ a polymer backbone with active grafting sites (Figure 1.11). The difference of this approach is that the backbone is installed with multiple polymerisation initiator sites instead of reactive coupling sites. The type of initiators installed dictate the polymerisation routes that can be chosen to graft side chains. Typically, side chain grafting is achieved by controlled and living-type polymerisations such as reversible-addition fragmentation chain-transfer (RAFT) by attachment of pendant CTA, or pendant bromine sites for atomic transfer radical polymerisation (ATRP).[189, 190] The grafting density of MPBs via this strategy can be tuned by co-polymerisation of the polyinitiator backbone to include spacer monomers in different patterns and in turn influencing steric hindrance. Thus, grafting-from method can be useful in targeting MPBs with long backbones and high molecular weight. A drawback of this method is that the side chains cannot easily be individually characterised without cleaving them off the backbone. Despite this, the degree of polymerisation, and consequent molecular weight can still be derived using simple characterisation techniques such as proton nuclear magnetic resonance (^{1}H NMR) and gas

permeation chromatography (GPC), to assume the composition of side chains with relative confidence.

Regardless of the chosen synthetic approach, all MPBs are unique as they can facilitate a variance between intramolecular chemical environments. This can be entirely within the side chain composition in the case of core-shell, block copolymer MPBs or Janus structures. MPB properties can be extended further by the inclusion of functional or stimuli-responsive moieties along polymer side chains and are therefore primed to provide greater scope for improving pharmacokinetic and pharmacodynamic profiles of therapeutics. By this approach, systems responsive to biologically relevant external stimuli such as temperature,[191-194] pH,[195-200] salt concentration,[200-203] and redox molecules[204, 205] have been reported. As a result, MPB based systems are positioned as interesting building-blocks to study their self-assembly into higher order morphologies.

Inspired by reports of how structural features in MPB architectures can be designed to tune morphological control discussed in Section 4.1, the motivation of this thesis is to develop structure property relationships directed towards the self-assembly of polymer nanodiscs. Building upon work where discs have been achieved using variations of linear-*block*-bottlebrush block copolymers, this work also aims to investigate this understudied architecture and understand their self-assembly behaviour in more detail.

7. Thesis Goals and Outlines

Linear-*block*-bottlebrush block copolymer variations represent an understudied building block in self-assembly. Their unique architecture and junctions between flexible and rigid segments afford them interesting packing behaviour which can lead to higher-order morphologies. This thesis aims to provide fundamental insight into how polymer architecture can be tuned to influence solution self-assembly outcomes.

Polymer nanodiscs are positioned as a lucrative system across a wide range of applications, owing to their enhanced fluid dynamics, aspect ratio, anisotropy and larger surface area for increased interactions. In addition, adding functional moieties can improve the specificity of these approaches. As it is generally accepted that a balance between flexible corona forming segments and a rigid core-forming block in a block copolymer amphiphile is required, linear-*block*-bottlebrush systems are positioned well to attempt to uncover discoidal fabrication avenues.

Whilst many planar objects are accessed using crystalline material that impedes functions such as cargo loading, or via directed routes that are complex in nature, it is the goal of this thesis to expand the use of arguably the simplest solution self-assembly route being 'direct self-assembly'. The aim of investigating underexplored linear-block-bottlebrush based architecture building blocks is to uncover more versatile and universal routes toward disc fabrication that relies on intrinsic thermodynamic principles instead of external or kinetic measures. To this effort, the dimensions of complex building blocks will be explored to find windows where planar packing occurs, and the potential application of these particles in proof-of-concept co-assembled stimuli-responsive systems will be investigated.

Currently, the use of linear-*block*-bottlebrush block copolymer variations towards amorphous nanodiscs remains limited to linear-*block*-bottlebrush and linear-*block*-bottlebrush-*block*-linear systems (Figure 1.10), but there is a lack of understanding regarding the building-block design rules that dictate planar packing.

The first research chapter explores the probing of a library of bottlebrush-linear polymer 'tadpoles' to investigate how their dimensions and composition influences self-assembled morphologies. By designing polymer tadpoles with changing backbone and side chain length of an MPB rod segment, we determined how the building block packing differed to yield

different morphologies. We also defined a window of dimensions where discs can be accessed, as a step towards improving general accessibility to discoidal morphologies for wider applications.

Extending the use of stimuli-responsive discs for applications where disassembly is an "all-or-nothing" response,[174, 175] the second research chapter explores how the co-assembly of chemically diverse tadpole structures can achieve continuous discs with distinct assembly and disassembly behaviour, and postulate how morphologies may be preserved upon exposure to a stimulus selective to a single component of a binary blend. This work also serves as a proof of concept towards more advanced multi stimuli-responsive materials where multiple building blocks can be incorporated into single particle, and responses can be tuned by chemical composition with opportunities for morphological preservation which is not considered viable in current reported systems.

In the third research chapter, the design of bottlebrush-linear block copolymers is extended by self-assembling underexplored bottlebrush-linear-bottlebrush 'dumbbell' polymer to explore morphological differences compared to self-assemblies from 'tadpole' structures. With their design informed by the tadpole structures previously investigated, this chapter explores how the change in flexibility of the linear corona-forming segment based on its locality in a block copolymer influences self-assembly outcomes. Furthermore, these macromolecules were investigated as physical cross-linkers towards connected anisotropic particles.

8. References

1. Pomerantseva, E.; Bonaccorso, F.; Feng, X.; Cui, Y.; Gogotsi, Y., Energy storage: The future enabled by nanomaterials. *Science* **2019,** *366* (6468), eaan8285.

2. Anselmo, A. C.; Mitragotri, S., Nanoparticles in the clinic: An update post <scp>COVID</scp> ‐ 19 vaccines. *Bioengineering & Translational Medicine* **2021,** *6* (3).

3. Sanchez, C.; Belleville, P.; Popall, M.; Nicole, L., Applications of advanced hybrid organic–inorganic nanomaterials: from laboratory to market. *Chemical Society Reviews* **2011,** *40* (2), 696-753.

4. Feynman, R., There's plenty of room at the bottom. In *Feynman and computation*, CRC Press: 2018; pp 63-76.

5. Baig, N.; Kammakakam, I.; Falath, W., Nanomaterials: a review of synthesis methods, properties, recent progress, and challenges. *Materials Advances* **2021,** *2* (6), 1821-1871.

6. Barreto, J. A.; O'Malley, W.; Kubeil, M.; Graham, B.; Stephan, H.; Spiccia, L., Nanomaterials: Applications in Cancer Imaging and Therapy. *Advanced Materials* **2011,** *23* (12), H18-H40.

7. Suhag, D.; Kaushik, S.; Taxak, V. B., Nanomaterials in Biomedicine. Springer Nature Singapore: 2024; pp 91-120.

8. Mitchell, M. J.; Billingsley, M. M.; Haley, R. M.; Wechsler, M. E.; Peppas, N. A.; Langer, R., Engineering precision nanoparticles for drug delivery. *Nature Reviews Drug Discovery* **2021,** *20* (2), 101-124.

9. Swami, A.; Shi, J.; Gadde, S.; Votruba, A. R.; Kolishetti, N.; Farokhzad, O. C., Nanoparticles for Targeted and Temporally Controlled Drug Delivery. Springer US: 2012; pp 9-29.

10. Kamaly, N.; Xiao, Z.; Valencia, P. M.; Radovic-Moreno, A. F.; Farokhzad, O. C., Targeted polymeric therapeutic nanoparticles: design, development and clinical translation. *Chem. Soc. Rev.* **2012,** *41* (7), 2971.

11. Astruc, D., Introduction: Nanoparticles in Catalysis. *Chem. Rev.* **2020,** *120* (2), 461-463.

12. Rao, C. H.; Avinash, K.; Varaprasad, B. K. S. V. L.; Goel, S., A Review on Printed Electronics with Digital 3D Printing: Fabrication Techniques, Materials, Challenges and Future Opportunities. *J. Electron. Mater.* **2022,** *51* (6), 2747-2765.

13. Knop, K.; Hoogenboom, R.; Fischer, D.; Schubert, U. S., Poly(ethylene glycol) in Drug Delivery: Pros and Cons as Well as Potential Alternatives. *Angew. Chem. Int. Ed.* **2010,** *49* (36), 6288-6308.

14. Li, M.; Jiang, S.; Simon, J.; Paßlick, D.; Frey, M.-L.; Wagner, M.; Mailänder, V.; Crespy, D.; Landfester, K., Brush Conformation of Polyethylene Glycol Determines the Stealth Effect of Nanocarriers in the Low Protein Adsorption Regime. *Nano Lett.* **2021,** *21* (4), 1591-1598.

15. Tenchov, R.; Sasso, J. M.; Zhou, Q. A., PEGylated Lipid Nanoparticle Formulations: Immunological Safety and Efficiency Perspective. *Bioconjugate Chemistry* **2023,** *34* (6), 941-960.

16. Shafaei, N.; Khorshidi, S.; Karkhaneh, A., The immune-stealth polymeric coating on drug delivery nanocarriers: In vitro engineering and in vivo fate. *Journal of Biomaterials Applications* **2023,** *38* (2), 159-178.

17. Liu, M.; Liu, S.; Xiu, J.; Zhang, J.; Deng, Y.; Zhao, X., "Y-type" PEG modified liposomes could eliminate the accelerated blood clearance (ABC) phenomenon and improved tumor therapy. *Applied Materials Today* **2023,** *32*, 101853.

18. Bludau, H.; Czapar, A. E.; Pitek, A. S.; Shukla, S.; Jordan, R.; Steinmetz, N. F., POxylation as an alternative stealth coating for biomedical applications. *Eur. Polym. J.* **2017,** *88*, 679-688.

19. Wilson, P.; Ke, P. C.; Davis, T. P.; Kempe, K., Poly(2-oxazoline)-based micro- and nanoparticles: A review. *Eur. Polym. J.* **2017,** *88*, 486-515.

20. Toussaint, F.; Lepeltier, E.; Franconi, F.; Pautu, V.; Jérôme, C.; Passirani, C.; Debuigne, A., Diversely substituted poly(N-vinyl amide) derivatives towards non-toxic, stealth and pH-responsive lipid nanocapsules. *Colloids and Surfaces B: Biointerfaces* **2024,** *235*, 113788.

21. Berger, M.; Toussaint, F.; Djemaa, S. B.; Laloy, J.; Pendeville, H.; Evrard, B.; Jerôme, C.; Lechanteur, A.; Mottet, D.; Debuigne, A.; Piel, G., Poly(vinyl pyrrolidone) derivatives as PEG alternatives for stealth, non-toxic and less immunogenic siRNA-containing lipoplex delivery. *Journal of Controlled Release* **2023,** *361*, 87-101.

22. Peng, S.; Ouyang, B.; Men, Y.; Du, Y.; Cao, Y.; Xie, R.; Pang, Z.; Shen, S.; Yang, W., Biodegradable zwitterionic polymer membrane coating endowing nanoparticles with ultra-long circulation and enhanced tumor photothermal therapy. *Biomaterials* **2020,** *231*, 119680.

23. Li, D.; Wei, Q.; Wu, C.; Zhang, X.; Xue, Q.; Zheng, T.; Cao, M., Superhydrophilicity and strong salt-affinity: Zwitterionic polymer grafted surfaces with significant potentials particularly in biological systems. *Advances in Colloid and Interface Science* **2020,** *278*, 102141.

24. Masood, F., Polymeric nanoparticles for targeted drug delivery system for cancer therapy. *Materials Science and Engineering: C* **2016,** *60*, 569-578.

25. Choudhury, H.; Gorain, B.; Pandey, M.; Khurana, R. K.; Kesharwani, P., Strategizing biodegradable polymeric nanoparticles to cross the biological barriers for cancer targeting. *International Journal of Pharmaceutics* **2019,** *565*, 509-522.

26. Hong, L.; Li, W.; Li, Y.; Yin, S., Nanoparticle-based drug delivery systems targeting cancer cell surfaces. *RSC Advances* **2023,** *13* (31), 21365-21382.

27. Escareño, N.; Hassan, N.; Kogan, M. J.; Juárez, J.; Topete, A.; Daneri-Navarro, A., Microfluidics-assisted conjugation of chitosan-coated polymeric nanoparticles with antibodies: Significance in drug release, uptake, and cytotoxicity in breast cancer cells. *Journal of Colloid and Interface Science* **2021,** *591*, 440-450.

28. Klemm, P.; Huschke, S.; Rodewald, M.; Ehteshamzad, N.; Behnke, M.; Wang, X.; Cinar, G.; Nischang, I.; Hoeppener, S.; Weber, C.; Press, A. T.; Höppener, C.; Meyer, T.; Deckert, V.; Schmitt, M.; Popp, J.; Bauer, M.; Schubert, S., Characterization of a library of vitamin A-functionalized polymethacrylate-based nanoparticles for siRNA delivery. *Polymer Chemistry* **2021,** *12* (6), 911-925.

29. Pu, Y.; Fan, X.; Zhang, Z.; Guo, Z.; Pan, Q.; Gao, W.; Luo, K.; He, B., Harnessing polymer-derived drug delivery systems for combating inflammatory bowel disease. *Journal of Controlled Release* **2023,** *354*, 1-18.

30. Peng, Y.; Xiong, B.; Peng, L.; Li, H.; He, Y.; Yeung, E. S., Recent Advances in Optical Imaging with Anisotropic Plasmonic Nanoparticles. *Anal. Chem.* **2015,** *87* (1), 200-215.

31. Liu, T.-M.; Yu, J.; Chang, C. A.; Chiou, A.; Chiang, H. K.; Chuang, Y.-C.; Wu, C.-H.; Hsu, C.-H.; Chen, P.-A.; Huang, C.-C., One-step shell polymerization of inorganic nanoparticles and their applications in SERS/nonlinear optical imaging, drug delivery and catalysis. *Sci. Rep.* **2014,** *4* (1).

32. Budy, S. M.; Hamilton, D. J.; Cai, Y.; Knowles, M. K.; Reed, S. M., Polymer mediated layer-by-layer assembly of different shaped gold nanoparticles. *J. Colloid Interface Sci.* **2017,** *487*, 336-347.

33. Sharma, A. K.; Tiwari, A. K.; Dixit, A. R., Rheological behaviour of nanofluids: A review. *Renewable and Sustainable Energy Reviews* **2016,** *53*, 779-791.

34. Pearce, A. K.; Wilks, T. R.; Arno, M. C.; O'Reilly, R. K., Synthesis and applications of anisotropic nanoparticles with precisely defined dimensions. *Nature Reviews Chemistry* **2020,** *5* (1), 21-45.

35. Doshi, N.; Prabhakarpandian, B.; Rea-Ramsey, A.; Pant, K.; Sundaram, S.; Mitragotri, S., Flow and adhesion of drug carriers in blood vessels depend on their shape: A study using model synthetic microvascular networks. *J. Control. Release* **2010,** *146* (2), 196-200.

36. Blanco, E.; Shen, H.; Ferrari, M., Principles of nanoparticle design for overcoming biological barriers to drug delivery. *Nat. Biotechnol.* **2015,** *33* (9), 941-951.

37. Decuzzi, P.; Pasqualini, R.; Arap, W.; Ferrari, M., Intravascular Delivery of Particulate Systems: Does Geometry Really Matter? *Pharmaceutical Research* **2009,** *26* (1), 235-243.

38. Yang, K.; Ma, Y.-Q., Computer simulation of the translocation of nanoparticles with different shapes across a lipid bilayer. *Nature Nanotechnology* **2010,** *5* (8), 579-583.

39. Florez, L.; Herrmann, C.; Cramer, J. M.; Hauser, C. P.; Koynov, K.; Landfester, K.; Crespy, D.; Mailänder, V., How Shape Influences Uptake: Interactions of Anisotropic Polymer Nanoparticles and Human Mesenchymal Stem Cells. *Small* **2012,** *8* (14), 2222-2230.

40. Muro, S.; Garnacho, C.; Champion, J. A.; Leferovich, J.; Gajewski, C.; Schuchman, E. H.; Mitragotri, S.; Muzykantov, V. R., Control of Endothelial Targeting and Intracellular Delivery of Therapeutic Enzymes by Modulating the Size and Shape of ICAM-1-targeted Carriers. *Molecular Therapy* **2008,** *16* (8), 1450-1458.

41. Ben-Akiva, E.; Meyer, R. A.; Yu, H.; Smith, J. T.; Pardoll, D. M.; Green, J. J., Biomimetic anisotropic polymeric nanoparticles coated with red blood cell membranes for enhanced circulation and toxin removal. *Science Advances* **2020,** *6* (16), eaay9035.

42. Decuzzi, P.; Godin, B.; Tanaka, T.; Lee, S. Y.; Chiappini, C.; Liu, X.; Ferrari, M., Size and shape effects in the biodistribution of intravascularly injected particles. *J. Control. Release* **2010,** *141* (3), 320-327.

43. Hinde, E.; Thammasiraphop, K.; Duong, H. T. T.; Yeow, J.; Karagoz, B.; Boyer, C.; Gooding, J. J.; Gaus, K., Pair correlation microscopy reveals the role of nanoparticle shape in intracellular transport and site of drug release. *Nature Nanotechnology* **2017,** *12* (1), 81-89.

44. Castoldi, A.; Empting, M.; De Rossi, C.; Mayr, K.; Dersch, P.; Hartmann, R.; Müller, R.; Gordon, S.; Lehr, C.-M., Aspherical and Spherical InvA497-Functionalized Nanocarriers for Intracellular Delivery of Anti-Infective Agents. *Pharmaceutical Research* **2019,** *36* (1).

45. Shen, L.; Wu, Z.; Zhao, J.; Wang, M.; Ni, J.; Liu, Y.; Zeng, J.; Chen, Q., Shape-controlled hydrogen evolution reaction of single Pd nanocrystals. *Chem. Commun.* **2025,** *61* (49), 8911-8914.

46. Unnathpadi, R.; Sunil, N.; Pullithadathil, B., Enhancing the Sensitivity of Contaminant Detection: Surface-Enhanced Raman Spectroscopy (SERS) with Carbon Nanomaterials. Springer Nature Switzerland: 2025; pp 189-207.

47. Bayburt, T. H.; Grinkova, Y. V.; Sligar, S. G., Self-Assembly of Discoidal Phospholipid Bilayer Nanoparticles with Membrane Scaffold Proteins. *Nano Letters* **2002,** *2* (8), 853-856.

48. Jonas, A.; Wald, J. H.; Toohill, K. L.; Krul, E. S.; Kézdy, K. E., Apolipoprotein A-I structure and lipid properties in homogeneous, reconstituted spherical and discoidal high density lipoproteins. *Journal of Biological Chemistry* **1990,** *265* (36), 22123-22129.

49. Jonas, A.; Kézdy, K. E.; Wald, J. H., Defined Apolipoprotein A-I Conformations in Reconstituted High Density Lipoprotein Discs. *Journal of Biological Chemistry* **1989,** *264* (9), 4818-4824.

50. Knowles, T. J.; Finka, R.; Smith, C.; Lin, Y.-P.; Dafforn, T.; Overduin, M., Membrane Proteins Solubilized Intact in Lipid Containing Nanoparticles Bounded by Styrene Maleic Acid Copolymer. *Journal of the American Chemical Society* **2009,** *131* (22), 7484-7485.

51. Jamshad, M.; Grimard, V.; Idini, I.; Knowles, T. J.; Dowle, M. R.; Schofield, N.; Sridhar, P.; Lin, Y.; Finka, R.; Wheatley, M.; Thomas, O. R. T.; Palmer, R. E.; Overduin, M.; Govaerts, C.; Ruysschaert, J.-M.; Edler, K. J.; Dafforn, T. R., Structural analysis of a nanoparticle containing a lipid bilayer used for detergent-free extraction of membrane proteins. *Nano Research* **2015,** *8* (3), 774-789.

52. Scheidelaar, S.; Martijn; Juan; Johannes; Breukink, E.; J, Molecular Model for the Solubilization of Membranes into Nanodisks by Styrene Maleic Acid Copolymers. *Biophysical Journal* **2015,** *108* (2), 279-290.

53. Ravula, T.; Hardin, N. Z.; Ramamoorthy, A., Polymer nanodiscs: Advantages and limitations. *Chem. Phys. Lipids* **2019,** *219*, 45-49.

54. Ravula, T.; Hardin, N. Z.; Ramadugu, S. K.; Ramamoorthy, A., pH Tunable and Divalent Metal Ion Tolerant Polymer Lipid Nanodiscs. *Langmuir* **2017,** *33* (40), 10655-10662.

55. Fiori, M. C.; Jiang, Y.; Zheng, W.; Anzaldua, M.; Borgnia, M. J.; Altenberg, G. A.; Liang, H., Polymer Nanodiscs: Discoidal Amphiphilic Block Copolymer Membranes as a New Platform for Membrane Proteins. *Scientific Reports* **2017,** *7* (1).

56. Gabriel, N. E.; Roberts, M. F., Spontaneous formation of stable unilamellar vesicles. *Biochemistry* **1984,** *23* (18), 4011-4015.

57. Amengual, J.; Notaro-Roberts, L.; Nieh, M.-P., Morphological control and modern applications of bicelles. *Biophysical Chemistry* **2023,** *302*, 107094.

58. Tahmasbi Rad, A.; Malik, S.; Yang, L.; Oberoi-Khanuja, T. K.; Nieh, M.-P.; Bahal, R., A universal discoidal nanoplatform for the intracellular delivery of PNAs. *Nanoscale* **2019,** *11* (26), 12517-12529.

59. Elzoghby, A. O.; Samir, O.; Soliman, A.; Solomevich, S.; Yu, M.; Schwendeman, A.; Nasr, M. L., Nanodiscs: Game changer nano-therapeutics and structural biology tools. *Nano Today* **2023,** *53*, 102026.

60. Bariwal, J.; Ma, H.; Altenberg, G. A.; Liang, H., Nanodiscs: a versatile nanocarrier platform for cancer diagnosis and treatment. *Chem. Soc. Rev.* **2022**.

61. Hardy, D.; Desuzinges Mandon, E.; Rothnie, A. J.; Jawhari, A., The yin and yang of solubilization and stabilization for wild-type and full-length membrane protein. *Methods* **2018,** *147*, 118-125.

62. Albayati, T. M.; Alardhi, S. M.; Khalbas, A. H.; Humdi, Z. J.; Ali, N. S.; Salih, I. K.; Saady, N. M. C.; Zendehboudi, S.; Abdulrahman, M. A., Comprehensive Review of Mesoporous Silica Nanoparticles: Drug Loading, Release, and Applications as Hemostatic Agents. *ChemistrySelect* **2024,** *9* (23).

63. Chen, L.; Zhang, S.; Duan, Y.; Song, X.; Chang, M.; Feng, W.; Chen, Y., Silicon-containing nanomedicine and biomaterials: materials chemistry, multi-dimensional design, and biomedical application. *Chemical Society Reviews* **2024,** *53* (3), 1167-1315.

64. Devi, L.; Ansari, T. M.; Alam, M. S.; Kumar, A.; Kushwaha, P., Metallic (Inorganic) Nanoparticles: Classification, Synthesis, Mechanism, and Scope. In *Metallic Nanoparticles for Health and the Environment*, CRC Press: 2024; pp 1-21.

65. Karnwal, A.; Kumar Sachan, R. S.; Devgon, I.; Devgon, J.; Pant, G.; Panchpuri, M.; Ahmad, A.; Alshammari, M. B.; Hossain, K.; Kumar, G., Gold Nanoparticles in Nanobiotechnology: From Synthesis to Biosensing Applications. *ACS Omega* **2024,** *9* (28), 29966-29982.

66. Fatima, S.; Qamar, F.; Quadri, S. N.; Abdin, M. Z.; Ahmad, F. J., Bioimaging Probes Using Functionalized Inorganic Nanoparticles. Springer Nature Switzerland: 2024; pp 135-158.

67. Brisson, E. R. L.; Worthington, M. J. H.; Kerai, S.; Müllner, M., Nanoscale polymer discs, toroids and platelets: a survey of their syntheses and potential applications. *Chemical Society Reviews* **2024,** *53* (4), 1984-2021.

68. Mai, Y.; Eisenberg, A., Self-assembly of block copolymers. *Chem. Soc. Rev.* **2012,** *41* (18), 5969-5985.

69. Lamontagne, H. R.; Lessard, B. H., Nitroxide-Mediated Polymerization: A Versatile Tool for the Engineering of Next Generation Materials. *ACS Applied Polymer Materials* **2020,** *2* (12), 5327-5344.

70. Tam Phuong, L. M., Ezio Rizzardo, San Hoa Thang Polymerization with living characteristics. WO9801478, 1998.

71. Perrier, S., 50th Anniversary Perspective: RAFT Polymerization—A User Guide. *Macromolecules* **2017,** *50* (19), 7433-7447.

72. Favier, A.; Charreyre, M. T., Experimental Requirements for an Efficient Control of Free‐Radical Polymerizations via the Reversible Addition‐Fragmentation Chain Transfer (RAFT) Process. *Macromolecular Rapid Communications* **2006,** *27* (9), 653-692.

73. Truong, N. P.; Jones, G. R.; Bradford, K. G. E.; Konkolewicz, D.; Anastasaki, A., A comparison of RAFT and ATRP methods for controlled radical polymerization. *Nature Reviews Chemistry* **2021,** *5* (12), 859-869.

74. Moad, G.; Rizzardo, E.; Thang, S. H., Living Radical Polymerization by the RAFT Process—A First Update. *Australian Journal of Chemistry* **2006,** *59* (10), 669.

75. Opiyo, G.; Jin, J., Recent progress in switchable RAFT agents: Design, synthesis and application. *European Polymer Journal* **2021,** *159*, 110713.

76. Moad, G., A Critical Survey of Dithiocarbamate Reversible Addition‐Fragmentation Chain Transfer (RAFT) Agents in Radical Polymerization. *Journal of Polymer Science Part A: Polymer Chemistry* **2019,** *57* (3), 216-227.

77. Wang, J.-S.; Matyjaszewski, K., Controlled/" living" radical polymerization. atom transfer radical polymerization in the presence of transition-metal complexes. *Journal of the American Chemical Society* **1995,** *117* (20), 5614-5615.

78. Kato, M.; Kamigaito, M.; Sawamoto, M.; Higashimura, T., Polymerization of Methyl Methacrylate with the Carbon Tetrachloride/Dichlorotris-(triphenylphosphine)ruthenium(II)/Methylaluminum Bis(2,6-di-tert-butylphenoxide) Initiating System: Possibility of Living Radical Polymerization. *Macromolecules* **1995,** *28* (5), 1721-1723.

79. Siegwart, D. J.; Oh, J. K.; Matyjaszewski, K., ATRP in the design of functional materials for biomedical applications. *Prog. Polym. Sci.* **2012,** *37* (1), 18-37.

80. Lin, C. Y.; Coote, M. L.; Gennaro, A.; Matyjaszewski, K., Ab Initio Evaluation of the Thermodynamic and Electrochemical Properties of Alkyl Halides and Radicals and Their Mechanistic Implications for Atom Transfer Radical Polymerization. *Journal of the American Chemical Society* **2008,** *130* (38), 12762-12774.

81. Matyjaszewski, K., Current status and outlook for ATRP. *European Polymer Journal* **2024,** *211*, 113001.

82. Gazzola, G.; Antonello, A.; Isse, A. A.; Fantin, M., Simple Iron Halides Enable Electrochemically Mediated ATRP in Nonpolar Media. *ACS Macro Letters* **2023,** *12* (12), 1602-1607.

83. Dadashi-Silab, S.; Matyjaszewski, K., Iron Catalysts in Atom Transfer Radical Polymerization. *Molecules* **2020,** *25* (7), 1648.

84. Afonso, M. B. A.; Cruz, T. R.; Silva, Y. F.; Pereira, J. C. A.; Machado, A. E. H.; Goi, B. E.; Lima-Neto, B. S.; Carvalho-Jr, V. P., Ruthenium(II) complexes of Schiff base derived from cycloalkylamines as pre-catalysts for ROMP of norbornene and ATRP of methyl methacrylate. *Journal of Organometallic Chemistry* **2017,** *851*, 225-234.

85. Bielawski, C. W.; Louie, J.; Grubbs, R. H., Tandem Catalysis: Three Mechanistically Distinct Reactions from a Single Ruthenium Complex. *Journal of the American Chemical Society* **2000,** *122* (51), 12872-12873.

86. Weiser, M. S.; Mülhaupt, R., Cobalt(II) octanoate and cobalt(II) perfluorooctanoate catalyzed atom transfer radical polymerization of styrene in toluene and fluorous media—A versatile route to catalyst recycling and oligomer formation. *Journal of Polymer Science Part A: Polymer Chemistry* **2005,** *43* (17), 3804-3813.

87. Duquesne, E.; Degée, P.; Habimana, J.; Dubois, P., Supported nickel bromide catalyst for Atom Transfer Radical Polymerization (ATRP) of methyl methacrylate. *Chem. Commun.* **2004,** (6), 640-641.

88. Faria, G. C. L.; Lyra, E. P., Exploring solution ICAR ATRP of methyl acrylate with AIBN as azo initiator: a kinetic modeling and simulation study. *Results in Materials* **2022,** *15*, 100313.

89. Gunter, K.; Sorci, M.; Belfort, G., A Simplified Predictive Tool for Design and Analysis of SET-LRP Reactions with Mechanistic Insight. *ACS Applied Polymer Materials* **2020,** *2* (11), 4924-4935.

90. Chen, G.; Guo, X.; Hu, B.; Lei, L., Heterogeneous Catalysts Catalyzed Photo‐Atom Transfer Radical Polymerization (Photo‐ATRP). *Macromolecular Chemistry and Physics* **2024**.

91. Chmielarz, P.; Fantin, M.; Park, S.; Isse, A. A.; Gennaro, A.; Magenau, A. J. D.; Sobkowiak, A.; Matyjaszewski, K., Electrochemically mediated atom transfer radical polymerization (eATRP). *Progress in Polymer Science* **2017,** *69*, 47-78.

92. Keating Iv, J. J.; Lee, A.; Belfort, G., Predictive Tool for Design and Analysis of ARGET ATRP Grafting Reactions. *Macromolecules* **2017,** *50* (20), 7930-7939.

93. Matyjaszewski, K.; Dong, H.; Jakubowski, W.; Pietrasik, J.; Kusumo, A., Grafting from Surfaces for "Everyone": ARGET ATRP in the Presence of Air. *Langmuir* **2007,** *23* (8), 4528-4531.

94. Tadros, T., Flory-Huggins Interaction Parameter. Springer Berlin Heidelberg: 2013; pp 523-524.

95. Van Leuken, S. H. M.; Van Benthem, R. A. T. M.; Tuinier, R.; Vis, M., Theoretically predicting the solubility of polydisperse polymers using Flory–Huggins theory. *Journal of Physics: Materials* **2024,** *7* (1), 015005.

96. Dopazo, G.; Martinez-Castillo, C.; Alonso-Ferrer, M.; Mejuto, J., Modeling the Behavior of Amphiphilic Aqueous Solutions. 2021.

97. Gröschel, A. H.; Müller, A. H. E., Self-assembly concepts for multicompartment nanostructures. *Nanoscale* **2015,** *7* (28), 11841-11876.

98. Wong, C. K.; Qiang, X.; Müller, A. H. E.; Gröschel, A. H., Self-Assembly of block copolymers into internally ordered microparticles. *Progress in Polymer Science* **2020,** *102*, 101211.

99. Liu, L.; Duan, C.; Wang, R., Theory of polymers in poor solvents: Inter-chain interaction, second virial coefficient, and Θ point. *Polymer* **2022,** *258*, 125312.

100. Li, J.; Fan, Y.; Gu, Q.; Zhou, X.; Sun, H.; Du, J., Homopolymer Self-Assembly: Principles, Driving Forces, and Applications. *Chem. Mater.* **2023,** *35* (24), 10348-10370.

101. Karayianni, M.; Pispas, S., Block copolymer solution self‐assembly: Recent advances, emerging trends, and applications. *Journal of Polymer Science* **2021,** *59* (17), 1874-1898.

102. Fielden, S. D. P., Kinetically Controlled and Nonequilibrium Assembly of Block Copolymers in Solution. *J. Am. Chem. Soc.* **2024,** *146* (28), 18781-18796.

103. Zeng, H.; Roberts, D. A., Recent Progress in Stimuli-Induced Morphology Transformations of Block Copolymer Assemblies. *Aust. J. Chem.* **2021,** *75* (2), 55-64.

104. Wright, D. B.; Patterson, J. P.; Gianneschi, N. C.; Chassenieux, C.; Colombani, O.; O'Reilly, R. K., Blending block copolymer micelles in solution; obstacles of blending. *Polymer Chemistry* **2016,** *7* (8), 1577-1583.

105. Wessels, M. G.; Jayaraman, A., Molecular dynamics simulation study of linear, bottlebrush, and star-like amphiphilic block polymer assembly in solution. *Soft Matter* **2019,** *15* (19), 3987-3998.

106. Müllner, M.; Müller, A. H. E., Cylindrical polymer brushes – Anisotropic building blocks, unimolecular templates and particulate nanocarriers. *Polymer* **2016,** *98*, 389-401.

107. Mao, J.; Gan, Z., Amphiphilic PEG‐co‐PGL‐g‐PCL Copolymer Brushes: Synthesis, Micellization and Controlled Drug Delivery. *Macromolecular Chemistry and Physics* **2009,** *210* (23), 2078-2086.

108. Nam, J.; Kim, Y.; Kim, J. G.; Seo, M., Self-Assembly of Monolayer Vesicles via Backbone-Shiftable Synthesis of Janus Core–Shell Bottlebrush Polymer. *Macromolecules* **2019,** *52* (24), 9484-9494.

109. Ahmed, E.; Womble, C. T.; Weck, M., Synthesis and Aqueous Self-Assembly of ABCD Bottlebrush Block Copolymers. *Macromolecules* **2020,** *53* (20), 9018-9025.

110. Alaboalirat, M.; Qi, L.; Arrington, K. J.; Qian, S.; Keum, J. K.; Mei, H.; Littrell, K. C.; Sumpter, B. G.; Carrillo, J.-M. Y.; Verduzco, R.; Matson, J. B., Amphiphilic Bottlebrush Block Copolymers: Analysis of Aqueous Self-Assembly by Small-Angle Neutron Scattering and Surface Tension Measurements. *Macromolecules* **2019,** *52* (2), 465-476.

111. Fenyves, R.; Schmutz, M.; Horner, I. J.; Bright, F. V.; Rzayev, J., Aqueous Self-Assembly of Giant Bottlebrush Block Copolymer Surfactants as Shape-Tunable Building Blocks. *J. Am. Chem. Soc.* **2014,** *136* (21), 7762-7770.

112. Su, L.; Heo, G. S.; Lin, Y. N.; Dong, M.; Zhang, S.; Chen, Y.; Sun, G.; Wooley, K. L., Syntheses of triblock bottlebrush polymers through sequential ROMPs: Expanding the functionalities of molecular brushes. *J. Polym. Sci., Part A: Polym. Chem.* **2017,** *55* (18), 2966-2970.

113. Hou, W.; Zhang, Z.; Shi, Y.; Chen, Y., Co-Assembly of Diblock Copolymers and Molecular Bottlebrushes. *Macromolecules* **2022,** *55* (15), 6364-6371.

114. Sunday, D. F.; Chang, A. B.; Liman, C. D.; Gann, E.; Delongchamp, D. M.; Thomsen, L.; Matsen, M. W.; Grubbs, R. H.; Soles, C. L., Self-Assembly of ABC Bottlebrush Triblock Terpolymers with Evidence for Looped Backbone Conformations. *Macromolecules* **2018,** *51* (18), 7178-7185.

115. Sakamoto, Y.; Nishimura, T., Recent advances in the self-assembly of sparsely grafted amphiphilic copolymers in aqueous solution. *Polymer Chemistry* **2022**.

116. Zhao, L.; Lin, Z., Self-assembly of non-linear polymers at the air/water interface: the effect of molecular architecture. *Soft Matter* **2011,** *7* (22), 10520.

117. Chen, Y.; Zhang, X.; Jiang, Y., The influence of side-chain conformations on the phase behavior of bottlebrush block polymers. *Soft Matter* **2020,** *16* (34), 8047-8056.

118. Dong, M.; Wessels, M. G.; Lee, J. Y.; Su, L.; Wang, H.; Letteri, R. A.; Song, Y.; Lin, Y.-N.; Chen, Y.; Li, R.; Pochan, D. J.; Jayaraman, A.; Wooley, K. L., Experiments and Simulations of Complex Sugar-Based Coil−Brush Block Polymer Nanoassemblies in Aqueous Solution. *ACS Nano* **2019,** *13* (5), 5147-5162.

119. Vu, C.; Abu Amara, N.; Alaboalirat, M.; Nativ‐Roth, E.; Zalk, R.; Leite, W.; Carrillo, J. M.; Bitton, R.; Matson, J. B., Aqueous Self‐Assembly of Cylindrical and Tapered Bottlebrush Block Copolymers. *Angewandte Chemie International Edition* **2025,** *64* (23).

120. Lodge, T. P.; Hillmyer, M. A.; Zhou, Z.; Talmon, Y., Access to the Superstrong Segregation Regime with Nonionic ABC Copolymers. *Macromolecules* **2004,** *37* (18), 6680-6682.

121. Semenov, A. N.; Nyrkova, I. A.; Khokhlov, A. R., Polymers with Strongly Interacting Groups: Theory for Nonspherical Multiplets. *Macromolecules* **1995,** *28* (22), 7491-7500.

122. Vasilevskaya, V. V.; Gusev, L. A.; Khokhlov, A. R.; Ikkala, O.; ten Brinke, G., Domains in Melts of Comb−Coil Diblock Copolymers: Superstrong Segregation Regime. *Macromolecules* **2001,** *34* (14), 5019-5022.

123. Kim, S.; Cho, Y.; Kim, J. H.; Song, S.; Lim, J.; Choi, S.-H.; Char, K., Structural Analysis of Bottlebrush Block Copolymer Micelles Using Small-Angle X-ray Scattering. *ACS Macro Letters* **2020,** *9* (9), 1261-1266.

124. Zhulina, E. B.; Sheiko, S. S.; Borisov, O. V., Theoretical advances in molecular bottlebrushes and comblike (co)polymers: solutions, gels, and self-assembly. *Soft Matter* **2022,** *18* (46), 8714-8732.

125. Chremos, A.; Theodorakis, P. E., Impact of intrinsic backbone chain stiffness on the morphologies of bottle-brush diblock copolymers. *Polymer* **2016,** *97*, 191-195.

126. Ishizu, K.; Satoh, J.; Toyoda, K.; Sogabe, A., Aggregation behaviors of AB-type brush-block-brush amphiphilic copolymers in aqueous media. *Journal of Materials Science* **2004,** *39* (13), 4295-4300.

127. Kim, E. J.; Shin, J. J.; Do, T.; Lee, G. S.; Park, J.; Thapar, V.; Choi, J.; Bang, J.; Yi, G.-R.; Hur, S.-M.; Kim, J. G.; Kim, B. J., Molecular Weight Dependent Morphological Transitions of Bottlebrush Block Copolymer Particles: Experiments and Simulations. *ACS Nano* **2021,** *15* (3), 5513-5522.

128. Sunday, D. F.; Burns, A. B.; Martin, T. B.; Chang, A. B.; Grubbs, R. H., Relationship between Graft Density and the Dilute Solution Structure of Bottlebrush Polymers: An Inter-chemistry Comparison and Scaling Analysis. *Macromolecules* **2023,** *56* (18), 7419-7431.

129. Lin, T.-P.; Chang, A. B.; Luo, S.-X. L.; Chen, H.-Y.; Lee, B.; Grubbs, R. H., Effects of Grafting Density on Block Polymer Self-Assembly: From Linear to Bottlebrush. *ACS Nano* **2017,** *11* (11), 11632-11641.

130. Martinez, A. P.; Cui, Z.; Hire, C.; Seery, T. A. P.; Adamson, D. H., Synthesis and Self-Assembly of Toothbrush-like Block Copolymers. *Macromolecules* **2015,** *48* (13), 4250-4255.

131. Richter, D.; Schneiders, D.; Monkenbusch, M.; Willner, L.; Fetters, L. J.; Huang, J. S.; Lin, M.; Mortensen, K.; Farago, B., Polymer Aggregates with Crystalline Cores: The System Polyethylene−Poly(ethylenepropylene). *Macromolecules* **1997,** *30* (4), 1053-1068.

132. Nakano, M.; Matsumoto, K.; Matsuoka, H.; Yamaoka, H., Characterization of Micellization Behavior of Amphiphilic Polymer Having Octadecyl Group by Small-Angle X-ray and Neutron Scattering. *Macromolecules* **1999,** *32* (12), 4023-4029.

133. Zhu, H.; Li, M.; Liu, B., Anisotropic Colloidal Particles by Molecular Self‐Assembly: Synthesis and Application. *ChemNanoMat* **2024,** *10* (3).

134. György, C.; Armes, S. P., Recent Advances in Polymerization‐Induced Self‐Assembly (PISA) Syntheses in Non‐Polar Media. *Angewandte Chemie* **2023,** *135* (42).

135. Xu, P.; Gao, L.; Cai, C.; Lin, J.; Wang, L.; Tian, X., Polymeric Toroidal Self‐Assemblies: Diverse Formation Mechanisms and Functions. *Advanced Functional Materials* **2022,** *32* (1), 2106036.

136. Li, Z.; Ma, J.; Lee, N. S.; Wooley, K. L., Dynamic Cylindrical Assembly of Triblock Copolymers by a Hierarchical Process of Covalent and Supramolecular Interactions. *J. Am. Chem. Soc.* **2011,** *133* (5), 1228-1231.

137. Yan, N.; Zhu, Y.; Jiang, W., Recent progress in the self-assembly of block copolymers confined in emulsion droplets. *Chemical Communications* **2018,** *54* (94), 13183-13195.

138. Walther, A.; André, X.; Drechsler, M.; Abetz, V.; Müller, A. H. E., Janus Discs. *J. Am. Chem. Soc.* **2007,** *129* (19), 6187-6198.

139. Walther, A.; Müller, A. H. E., Janus Particles: Synthesis, Self-Assembly, Physical Properties, and Applications. *Chem. Rev.* **2013,** *113* (7), 5194-5261.

140. Klinger, D.; Wang, C. X.; Connal, L. A.; Audus, D. J.; Jang, S. G.; Kraemer, S.; Killops, K. L.; Fredrickson, G. H.; Kramer, E. J.; Hawker, C. J., A Facile Synthesis of Dynamic, Shape‐Changing Polymer Particles. *Angewandte Chemie* **2014,** *126* (27), 7138-7142.

141. Deng, R.; Liang, F.; Zhou, P.; Zhang, C.; Qu, X.; Wang, Q.; Li, J.; Zhu, J.; Yang, Z., Janus Nanodisc of Diblock Copolymers. *Advanced Materials* **2014,** *26* (26), 4469-4472.

142. Steinhaus, A.; Pelras, T.; Chakroun, R.; Gröschel, A. H.; Müllner, M., Self‐Assembly of Diblock Molecular Polymer Brushes in the Spherical Confinement of Nanoemulsion Droplets. *Macromol. Rapid Commun.* **2018,** *39* (19), 1800177.

143. Qiao, S.; Li, S.; Song, Q.; Liu, B., Shape-Tunable Biconcave Disc-Like Polymer Particles by Swelling-Induced Phase Separation of Seeded Particles with Hydrophilic Shells. *Langmuir* **2023,** *39* (3), 1190-1197.

144. Tran, K. T. M.; Nguyen, T. D., Lithography-based methods to manufacture biomaterials at small scales. *Journal of Science: Advanced Materials and Devices* **2017,** *2* (1), 1-14.

145. Rolland, J. P.; Maynor, B. W.; Euliss, L. E.; Exner, A. E.; Denison, G. M.; Desimone, J. M., Direct Fabrication and Harvesting of Monodisperse, Shape-Specific Nanobiomaterials. *Journal of the American Chemical Society* **2005,** *127* (28), 10096-10100.

146. Enlow, E. M.; Luft, J. C.; Napier, M. E.; Desimone, J. M., Potent Engineered PLGA Nanoparticles by Virtue of Exceptionally High Chemotherapeutic Loadings. *Nano Letters* **2011,** *11* (2), 808-813.

147. Dorsman, I. R.; Derry, M. J.; Cunningham, V. J.; Brown, S. L.; Williams, C. N.; Armes, S. P., Tuning the vesicle-to-worm transition for thermoresponsive block copolymer vesicles prepared via polymerisation-induced self-assembly. *Polymer Chemistry* **2021,** *12* (9), 1224-1235.

148. Zhao, Z.; Lei, S.; Zeng, M.; Huo, M., Recent progress in polymerization‐induced self‐assembly: From the perspective of driving forces. *Aggregate* **2024,** *5* (1).

149. Hou, W.; Wu, J.; Li, Z.; Zhang, Z.; Shi, Y.; Chen, Y., Efficient Synthesis and PISA Behavior of Molecular Bottlebrush Block Copolymers via a Grafting-From Strategy through RAFT Dispersion Polymerization. *Macromolecules* **2023,** *56* (3), 824-832.

150. Jia, F.; Liang, F.; Yang, Z., Janus Mesoporous Nanodisc from Gelable Triblock Copolymer. *ACS Macro Letters* **2016,** *5* (12), 1344-1347.

151. Jiang, Z.; Bhaskaran, A.; Aitken, H. M.; Shackleford, I. C. G.; Connal, L. A., Using Synergistic Multiple Dynamic Bonds to Construct Polymers with Engineered Properties. *Macromolecular Rapid Communications* **2019,** *40* (10), 1900038.

152. Zhang, Q.; Fan, H.; Zhang, L.; Jin, Z., Nanodiscs Generated from the Solvent Exchange of a Block Copolymer. *Macromolecules* **2020,** *53* (16), 7025-7033.

153. Zhu, J.; Zhang, S.; Zhang, K.; Wang, X.; Mays, J. W.; Wooley, K. L.; Pochan, D. J., Disk-cylinder and disk-sphere nanoparticles via a block copolymer blend solution construction. *Nature Communications* **2013,** *4* (1).

154. Chen, Y.; Zhang, K.; Wang, X.; Zhang, F.; Zhu, J.; Mays, J. W.; Wooley, K. L.; Pochan, D. J., Multigeometry Nanoparticles: Hybrid Vesicle/Cylinder Nanoparticles Constructed with Block Copolymer Solution Assembly and Kinetic Control. *Macromolecules* **2015,** *48* (16), 5621-5631.

155. Li, Z.; Chen, Z.; Cui, H.; Hales, K.; Qi, K.; Wooley, K. L.; Pochan, D. J., Disk Morphology and Disk-to-Cylinder Tunability of Poly(Acrylic Acid)-b-Poly(Methyl Acrylate)-b-Polystyrene Triblock Copolymer Solution-State Assemblies. *Langmuir* **2005,** *21* (16), 7533-7539.

156. Yin, L.; Hillmyer, M. A., Disklike Micelles in Water from Polyethylene-Containing Diblock Copolymers. *Macromolecules* **2011,** *44* (8), 3021-3028.

157. Wang, H.; Wu, C.; Xia, G.; Ma, Z.; Mo, G.; Song, R., Semi-crystalline polymethylene-b-poly(acrylic acid) diblock copolymers: aggregation behavior, confined crystallization and controlled growth of semicrystalline micelles from dilute DMF solution. *Soft Matter* **2015,** *11* (9), 1778-1787.

158. Puig, J.; Zucchi, I. A.; Ceolín, M.; Schroeder, W. F.; Williams, R. J. J., Evolution of morphologies of a PE-b-PEO block copolymer in an epoxy solvent induced by polymerization followed by crystallization-driven self-assembly of PE blocks during cooling. *RSC Advances* **2016,** *6* (41), 34903-34912.

159. Li, Z.; Liu, R.; Mai, B.; Feng, S.; Wu, Q.; Liang, G.; Gao, H.; Zhu, F., Synthesis and self-assembly of isotactic polystyrene-block-poly(ethylene glycol). *Polym. Chem.* **2013,** *4* (4), 954-960.

160. Venkataraman, S.; Lee, A. L.; Maune, H. T.; Hedrick, J. L.; Prabhu, V. M.; Yang, Y. Y., Formation of Disk- and Stacked-Disk-like Self-Assembled Morphologies from Cholesterol-Functionalized Amphiphilic Polycarbonate Diblock Copolymers. *Macromolecules* **2013,** *46* (12), 4839-4846.

161. Le Devedec, F.; Won, A.; Oake, J.; Houdaihed, L.; Bohne, C.; Yip, C. M.; Allen, C., Postalkylation of a Common mPEG-b-PAGE Precursor to Produce Tunable Morphologies of Spheres, Filomicelles, Disks, and Polymersomes. *ACS Macro Letters* **2016,** *5* (1), 128-133.

162. Toebes, B. J.; Wilson, D. A., Membrane folding and shape transformation in biomimetic vesicles. *Soft Matter* **2021,** *17* (7), 1724-1730.

163. Macfarlane, L.; Zhao, C.; Cai, J.; Qiu, H.; Manners, I., Emerging applications for living crystallization-driven self-assembly. *Chemical Science* **2021,** *12* (13), 4661-4682.

164. Jin, X.; Zhang, C.; Lin, J.; Cai, C.; Chen, J.; Gao, L., Fusion Growth of Two-Dimensional Disklike Micelles via Liquid-Crystallization-Driven Self-Assembly. *Macromolecules* **2022,** *55* (10), 3831-3839.

165. Niyom, Y.; Phakkeeree, T.; Flood, A.; Crespy, D., Synergy between polymer crystallinity and nanoparticles size for payloads release. *Journal of Colloid and Interface Science* **2019,** *550*, 139-146.

166. Bikiaris, D.; Karavelidis; Karavas; Giliopoulos; Papadimitriou, Evaluating the effects of crystallinity in new biocompatible polyester nanocarriers on drug release behavior. *International Journal of Nanomedicine* **2011**, 3021.

167. Hu, X.; Hu, J.; Tian, J.; Ge, Z.; Zhang, G.; Luo, K.; Liu, S., Polyprodrug Amphiphiles: Hierarchical Assemblies for Shape-Regulated Cellular Internalization, Trafficking, and Drug Delivery. *Journal of the American Chemical Society* **2013,** *135* (46), 17617-17629.

168. Zhang, J.; Cao, H.; Wan, X.; Zhou, Q., Molecular Reorganization of Rod−Coil Diblock Copolymers at the Air−Water Interface. *Langmuir* **2006,** *22* (15), 6587-6592.

169. Wu, J.; Pearce, E. M.; Kwei, T. K.; Lefebvre, A. A.; Balsara, N. P., Micelle Formation of a Rod−Coil Diblock Copolymer in a Solvent Selective for the Rod Block. *Macromolecules* **2002,** *35* (5), 1791-1796.

170. Lin, X.; He, X.; Hu, C.; Chen, Y.; Mai, Y.; Lin, S., Disk-like micelles with cylindrical pores from amphiphilic polypeptide block copolymers. *Polymer Chemistry* **2016,** *7* (16), 2815-2820.

171. Uematsu, I.; Uematsu, Y., Polypeptide liquid crystals. Springer Berlin Heidelberg: 1984; pp 37-73.

172. Müllner, M., Molecular Polymer Brushes in Nanomedicine. *Macromol. Chem. Phys.* **2016,** *217* (20), 2209-2222.

173. Shi, Y.; Zhu, W.; Yao, D.; Long, M.; Peng, B.; Zhang, K.; Chen, Y., Disk-Like Micelles with a Highly Ordered Pattern from Molecular Bottlebrushes. *ACS Macro Lett.* **2014,** *3* (1), 70-73.

174. Zeng, H.; Liang, X.; Roberts, D. A.; Gillies, E. R.; Müllner, M., Self‐Assembly of Rod‐Coil Bottlebrush Copolymers into Degradable Nanodiscs with a UV‐Triggered Self‐Immolation Process. *Angewandte Chemie International Edition* **2024,** *63* (13).

175. Zeng, H.; Zeng, P.; Baek, J.; Kim, B. S.; Müllner, M., Self‐Assembly of Amorphous 2D Polymer Nanodiscs with Tuneable Size, pH‐Responsive Degradation and Controlled Drug Release. *Angewandte Chemie International Edition* **2025**.

176. Zhu, H.; Deng, G.; Chen, Y., Amphiphilic polymer brushes with alternating PCL and PEO grafts through radical copolymerization of styrenic and maleimidic macromonomers. *Polymer* **2008,** *49* (2), 405-411.

177. Cho, H. Y.; Krys, P.; Szcześniak, K.; Schroeder, H.; Park, S.; Jurga, S.; Buback, M.; Matyjaszewski, K., Synthesis of Poly(OEOMA) Using Macromonomers via "Grafting-Through" ATRP. *Macromolecules* **2015,** *48* (18), 6385-6395.

178. Ohno, S.; Matyjaszewski, K., Controlling grafting density and side chain length in poly(n-butyl acrylate) by ATRP copolymerization of macromonomers. *Journal of Polymer Science Part A: Polymer Chemistry* **2006,** *44* (19), 5454-5467.

179. Hobbs, C. E.; Vasireddy, M., Combining ATRP and ROMP with Thio‐Bromo, Copper‐Catalyzed, and Strain‐Promoted Click Reactions for Brush Copolymer Synthesis Starting from a Single Initiator/Monomer/Click Partner. *Macromol. Chem. Phys.* **2019,** *220* (7), 1800497.

180. Wang, M.-Q.; Zou, H.; Liu, W.-B.; Liu, N.; Wu, Z.-Q., Bottlebrush Polymers Based on RAFT and the "C1" Polymerization Method: Controlled Synthesis and Application in Anticancer Drug Delivery. *ACS Macro Letters* **2022,** *11* (2), 179-185.

181. Gegenhuber, T.; Müllner, M., Molecular Polymer Brushes Made via Ring‐Opening Metathesis Polymerization from Cleavable RAFT Macromonomers. *Macromol. Chem. Phys.* **2021,** *222* (13), 2100077.

182. Shen, Y.; Zhan, Y.; Tang, J.; Xu, P.; Johnson, P. A.; Radosz, M.; Van Kirk, E. A.; Murdoch, W. J., Multifunctioning pH-responsive nanoparticles from hierarchical self-assembly of polymer brush for cancer drug delivery. *AIChE Journal* **2008,** *54* (11), 2979-2989.

183. Sheiko, S. S.; Sumerlin, B. S.; Matyjaszewski, K., Cylindrical molecular brushes: Synthesis, characterization, and properties. *Progress in Polymer Science* **2008,** *33* (7), 759-785.

184. Wolf, W. J.; Lin, T.-P.; Grubbs, R. H., Examining the Effects of Monomer and Catalyst Structure on the Mechanism of Ruthenium-Catalyzed Ring-Opening Metathesis Polymerization. *Journal of the American Chemical Society* **2019,** *141* (44), 17796-17808.

185. Sanford, M. S.; Love, J. A.; Grubbs, R. H., Mechanism and Activity of Ruthenium Olefin Metathesis Catalysts. *Journal of the American Chemical Society* **2001,** *123* (27), 6543-6554.

186. Gao, H.; Matyjaszewski, K., Synthesis of Molecular Brushes by "Grafting onto" Method: Combination of ATRP and Click Reactions. *Journal of the American Chemical Society* **2007,** *129* (20), 6633-6639.

187. Gan, W.; Shi, Y.; Jing, B.; Cao, X.; Zhu, Y.; Gao, H., Produce Molecular Brushes with Ultrahigh Grafting Density Using Accelerated CuAAC Grafting-Onto Strategy. *Macromolecules* **2017,** *50* (1), 215-222.

188. Lanson, D.; Ariura, F.; Schappacher, M.; Borsali, R.; Deffieux, A., Application of living ionic polymerizations to the design of AB-type comb-like copolymers of various topologies and organizations. *Macromolecular Research* **2007,** *15* (2), 173-177.

189. Börner, H. G.; Beers, K.; Matyjaszewski, K.; Sheiko, S. S.; Möller, M., Synthesis of Molecular Brushes with Block Copolymer Side Chains Using Atom Transfer Radical Polymerization. *Macromolecules* **2001,** *34* (13), 4375-4383.

190. Banquy, X.; Burdyńska, J.; Lee, D. W.; Matyjaszewski, K.; Israelachvili, J., Bioinspired Bottle-Brush Polymer Exhibits Low Friction and Amontons-like Behavior. *Journal of the American Chemical Society* **2014,** *136* (17), 6199-6202.

191. Zhou, H.; Lu, Y.; Yu, Q.; Manners, I.; Winnik, M. A., Monitoring Collapse of Uniform Cylindrical Brushes with a Thermoresponsive Corona in Water. *ACS Macro Letters* **2018,** *7* (2), 166-171.

192. Chu, Y.; Li, H.; Huang, H.; Zhou, H.; Chen, Y.; Andreas, B.; Liu, L.; Chen, Y., Uni‐molecular nanoparticles of poly(2‐oxazoline) showing tunable thermoresponsive behaviors. *Journal of Polymer Science Part A: Polymer Chemistry* **2018,** *56* (2), 174-183.

193. Kazantsev, O. A.; Orekhov, D. V.; Simagin, A. S.; Kamorin, D. M.; Sivokhin, A. P.; Savinova, M. V.; Arifullin, I. R.; Kavtrova, V. D.; Lobayev, A. N., Oligo(ethylene glycol) methacrylate-based molecular bottlebrushes: Correlations between composition and phase transition temperatures in aqueous solutions. *European Polymer Journal* **2024,** *218*, 113340.

194. Li, X.; Shamsijazeyi, H.; Pesek, S. L.; Agrawal, A.; Hammouda, B.; Verduzco, R., Thermoresponsive PNIPAAM bottlebrush polymers with tailored side-chain length and end-group structure. *Soft Matter* **2014,** *10* (12), 2008.

195. Kelly, M. T.; Zhao, B., Worm-globule transition of amphiphilic pH-responsive heterografted bottlebrushes at air–water interface. *Soft Matter* **2024,** *20* (6), 1224-1235.

196. Zhang, T.; Wang, Y.; Ma, X.; Hou, C.; Lv, S.; Jia, D.; Lu, Y.; Xue, P.; Kang, Y.; Xu, Z., A bottlebrush-architectured dextran polyprodrug as an acidity-responsive vector for enhanced chemotherapy efficiency. *Biomaterials Science* **2020,** *8* (1), 473-484.

197. Jin, Z.; Seong, H. G.; Srivastava, S.; McGlasson, A.; Emrick, T.; Muthukumar, M.; Russell, T. P., 3D Printing of Aqueous Two‐Phase Systems with Linear and Bottlebrush Polyelectrolytes. *Angewandte Chemie* **2024,** *136* (25).

198. Arsenie, L. V.; Semsarilar, M.; Benkhaled, B. T.; Geneste, A.; Prélot, B.; Colombani, O.; Nicol, E.; Lacroix-Desmazes, P.; Ladmiral, V.; Catrouillet, S., Switchable pH-Responsive Morphologies of Coassembled Nucleobase Copolymers. *Biomacromolecules* **2024,** *25* (11), 7225-7236.

199. Nese, A.; Lebedeva, N. V.; Sherwood, G.; Averick, S.; Li, Y.; Gao, H.; Peteanu, L.; Sheiko, S. S.; Matyjaszewski, K., pH-Responsive Fluorescent Molecular Bottlebrushes Prepared by Atom Transfer Radical Polymerization. *Macromolecules* **2011,** *44* (15), 5905-5910.

200. Xu, Y.; Bolisetty, S.; Drechsler, M.; Fang, B.; Yuan, J.; Ballauff, M.; Müller, A. H. E., pH and salt responsive poly(N,N-dimethylaminoethyl methacrylate) cylindrical brushes and their quaternized derivatives. *Polymer* **2008,** *49* (18), 3957-3964.

201. Ishida, N.; Biggs, S., Salt-Induced Structural Behavior for Poly(N-isopropylacryamide) Grafted onto Solid Surface Observed Directly by AFM and QCM-D. *Macromolecules* **2007,** *40* (25), 9045-9052.

202. Yao, K.; Tang, C.; Zhang, J.; Bunyard, C., Degradable and salt-responsive random copolymers. *Polym. Chem.* **2013,** *4* (3), 528-535.

203. Basak, S.; Chatterjee, R.; Bandyopadhyay, A., Beyond Traditional Stimuli: Exploring Salt-Responsive Bottlebrush Polymers—Trends, Applications, and Perspectives. *ACS Omega* **2024,** *9* (31), 33365-33385.

204. Yang, C.; Huang, S.; Jia, T.; Peng, Y.; Wei, X.; Wang, M., Sub-10 nm Theranostic Unimolecular Micelles with High Tumor-Specific Accumulation, Retention, and Inhibitory Effect. *ACS Applied Bio Materials* **2019,** *2* (10), 4142-4153.

205. Guo, J.; Hong, H.; Chen, G.; Shi, S.; Nayak, T. R.; Theuer, C. P.; Barnhart, T. E.; Cai, W.; Gong, S., Theranostic Unimolecular Micelles Based on Brush-Shaped Amphiphilic Block Copolymers for Tumor-Targeted Drug Delivery and Positron Emission Tomography Imaging. *ACS Applied Materials & Interfaces* **2014,** *6* (24), 21769-21779.

Chapter II : Probing the Dimensions of Bottlebrush-Linear Block Copolymers Toward their Self-Assembly into Discoidal Nanoparticles

1. Abstract

Polymer building-blocks can be fundamentally designed to access specific morphologies by self-assembly. This chapter explores how tuning the architecture of a rod (bottlebrush)-coil (linear) copolymer system can induce morphological changes in self-assemblies. Employing both reversible addition-fragmentation chain transfer (RAFT) polymerisation and atomic transfer radical polymerisation (ATRP) to design a library of poly(ethylene glycol)-*block*-poly[2-(2-bromo isobutyryloxy)ethyl methacrylate]-*graft*-poly(benzyl methacrylate) [PEG-*b*-(PBIEM-*g*-PBzMA)] 'tadpole' copolymers we demonstrate how systematic and independent change of the backbone and side chain lengths of the core-forming rod segment can alter particle morphology. Observations of resulting morphologies ranging from polymersomes, dense spherical particles, and flattened monolayer discoidal particles, were rationalised in terms of packing behaviour, polymer crowding and interfacial energy in response to the bottlebrush-linear copolymer molar ratio. The findings establish a design framework for engineering shape-controlled nanostructures through bottom-up direct self-assembly and provide insights into how 'tadpole-like' molecular geometry can be harnessed to reliably access anisotropic discoidal morphologies relevant to biomedical delivery systems.

2. Introduction

The advancing field of nanotechnology has witnessed the positive impact of polymeric nanoparticles in many industries including biomedicine, electronics, and materials sciences. In particular, anisotropic particles, with their higher aspect ratio compared to their isotropic counterparts continue to garner significant attention.[1]

In the biomedical industry, discoidal nanoparticles have shown greater pharmacokinetic profiles compares to spherical systems. This is attributed to their higher surface area that facilitates enhanced opportunity for cellular interactions and subsequent biodistribution for drug delivery.[2-6] Additionally, their flat shape contributes to an atypical oscillation pattern in response to the fluid dynamics within the bloodstream, further promoting cell margination and uptake.[7] Therefore, discoidal nanoparticles are highly relevant for drug delivery and diagnostic applications.[7, 8] Inspiration from endogenous α-HDL has given rise to lipid nanodiscs, styrene-maleic acid lipid polymer nanodiscs (SMALPs), and polymer nanodiscs as discoidal drug deliver agents. Unfortunately, these suffer from barriers to their clinical translation surrounding cost, stability, and safety,[9, 10] largely due to the inclusion of scaffolding proteins and endogenous polypeptides. As an alternative, interest in polymeric nanoparticle systems continues to soar. Central to the development of such advanced nanostructures is the use of self-assembly techniques, particularly bottom-up approaches.

The bottom-up self-assembly approach offers several advantages. It allows for the precise and scalable fabrication of nanostructures, minimises the need for complex and expensive equipment, and leverages the inherent properties of the building blocks to drive their assembly. This method also enables the formation of highly uniform and monodisperse nanoparticles, which is critical for consistency in applications such as drug delivery and diagnostics. A large focus on polymerisation-induced self-assembly (PISA) has uncovered pathways to anisotropic

worm-like and cylindrical micelles.[11, 12] 2D nanomaterials that are planar in nature such as polymer nanodiscs are more difficult to fabricate, but are particularly exciting as a functional material. Despite first being explored in the late 1990s,[13, 14] literature on nanodisc fabrication remains limited, largely ascribed to the high demands of their self-assembly.

To overcome the bending energy penalty that favours morphologies with curved surfaces, many have relied on directed self-assembly processes involving assistance from external stimuli, [15-17] templates,[18] or small molecules,[19, 20] to achieve desired bending energies.[9] These methods typically involve meticulous control of various self-assembly parameters to access nanodiscs. The complexity of these approaches underscores the need to develop more generalised methodologies that can be applied across different polymer systems and application contexts.

Mechanisms relying on intrinsic polymer chemistries alone have favoured crystallisation-driven self-assembly (CDSA) as a means of producing uniform nanomaterials.[21, 22] The most common approach includes the use of semi-crystalline polymers, where the crystallinity of the core-forming segment can be exploited to drive disc formation,[23-26] while others have employed variations of liquid crystal material to access similar morphologies.[27, 28] However, crystalline chemistry in the core of nanoparticles limits their biomedical relevance as cargo carriers.

To mimic the favourable rigidity that crystallisable polymers offer in order to be energetically favourable to access discs,[29] strategies require precise control over polymer architecture. Tailored polymer building blocks require strong chain-chain interactions between polymer building-blocks to demonstrate favourable entropy. The simplest demonstrations of discoidal nanoparticles to date involve a combination of molecular polymer brush and linear polymer segments in an elegant building block. Akin to rod-coil copolymers before, the bottlebrush adopts the properties of a rigidifying rod-like segment, balanced by the flexibility of the corona forming linear polymer chain.

Chen and coworkers showed 2D self-assembly of discs using ABA coil-rod-coil, or linear-bottlebrush-linear block copolymers, using strong π-π stacking within the core-forming rods to achieve assemblies approximating ~400 nm in width and ~30 nm in height.[30] In an AB bottlebrush-linear system, our group recently demonstrated self-assembly of a functional linear-bottlebrush polymer 'tadpole' into discs ranging between 300 – 500 nm wide.[31] The modularity of this approach was further demonstrated by varying the hydrophobicity of the core-forming side chains, revealing that different side chains with low glass transition temperature (T_g) can be grafted without compromising the disc formation process.[32] To expand our understanding of disc-forming building blocks, we herein demonstrate that tadpole-like copolymers with a high T_g core can also form nanodiscs. We further show that a simpler "grafting-from approach" can be used to build a library of bottlebrush-linear bottlebrush copolymers, which we used to identify an optimal window in which nanodiscs can be realised.

3. Experimental Section

3.1 Materials

Poly(ethylene glycol) methyl ether 5000 (mPEG 5K), 4-cyano-4-(phenylcarbanothio) pentanoic acid (CPADB, 99 %), anhydrous dichloromethane (DCM, ≥99.8%), N-ethyl-N′-(3-dimethylaminopropyl)carbodiimide hydrochloride (EDC·HCl, 98%), 2-hydroxyethyl methacrylate (HEMA, 97%), α-bromoisobutyryl bromide (98%), N,N,N′,N″,N″-pentamethyldiethylenetriamine (PMDETA, 99%), 2,2′-Azobis(2-methylpropionitrile) (AIBN, 98%), anisole (99%), mesitylene (98%) and copper(I) bromide (CuBr, 98%) were purchased from Sigma-Aldrich. N,N-dimethylaminopyridine (DMAP, ≥99%), tetrahydrofuran (THF), petroleum benzine (b.p. 40-60 ℃), and diethyl ether were sourced from Merck. Pyridine (99%) and magnesium sulphate ($MgSO_4$) were purchased from Ajax. Dimethyl formamide (DMF, 99.8% by gas chromatography (GC)) was sourced from RCI LabScan. Benzyl methacrylate (BzMA, 98%) was sourced from Tokyo Chemical Industry Chemicals. AIBN was recrystallised from ethanol prior to use. Ethanol was dried with 4Å molecular sieves before use. HEMA and BzMA were filtered through a short basic aluminium oxide column to remove inhibitors. All other chemicals were used as received.

3.2 Experimental Procedure

Synthesis of PEG_{114}-CPADB (macro-RAFT agent)

In a typical procedure (Scheme 1), a dry round bottom flask (RBF) was charged with mPEG 5K (2.0 g, 0.4 mmol, 1.0 equiv.) and CPADB (167 mg, 0.7 mmol, 1.8 equiv.) in 10 mL anhydrous DCM. The RBF was then cooled with an ice bath and vigorously stirred. Subsequently, a solution of EDC·HCl (201 mg, 0.6 mmol, 1.8 equiv.) and DMAP (11.7 mg, 0.1 mmol, 0.24 equiv.) in 5 mL anhydrous DCM was added dropwise. The reaction was stirred over ice for a further 10 minutes, before being left to stir at room temperature overnight. The

macro-RAFT agents were recovered in cold diethyl ether three times over, redissolving in DCM. The recovered product was redissolved in DCM and washed three times over in deionised water. The organic layer was dried over $MgSO_4$ prior to filtration. The product was then concentrated under reduced pressure and lyophilised into a pink powder (1.6 g, 80% yield) and characterised by ^{1}H NMR spectroscopy (300 MHz, $CDCl_3$, δ 7.26 ppm) and SEC (DMAc/LiBr, 50 °C, PMMA). The macroCTA was stored at -20 ˚C in an airtight vial shielded from light.

Scheme S2.1 : Synthesis of PEG_{114}-CPADB macro-RAFT agent.

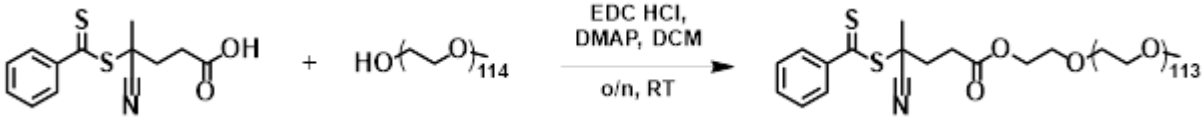

Synthesis of PHEMAx-*block*-PEG series

In a typical procedure, PEG-CPADB (150 mg, 28.5 μmol, 1 mol equiv.), HEMA, and AIBN (3.1 mg, 5.7 μmol, 0.2 mol equiv.) were charged to a vial in anhydrous EtOH with mesitylene (100 μL) as an internal standard. A time sample (t0) was taken and analysed by ^{1}H NMR spectroscopy. The vial was equipped with a stirrer bar and the solution bubbled with N2 to degas for 30 minutes before reacting at 70 ˚C for 5 hours. A further time sample (t5) was taken and analysed using ^{1}H NMR to determine the degree of polymerisation (DP) of the PHEMA block. The resulting polymer was recovered by precipitation in diethyl ether, redissolving in methanol three times over. The product was then lyophilised to give a pink powder. The final product was characterised by ^{1}H NMR spectroscopy (300 MHz, MeOD, δ 3.31 ppm) and SEC (DMAc/LiBr, 50 °C, PMMA).

Scheme S2.2. Synthesis of $PHEMA_n$-*block*-PEG_{114} via RAFT polymerisation

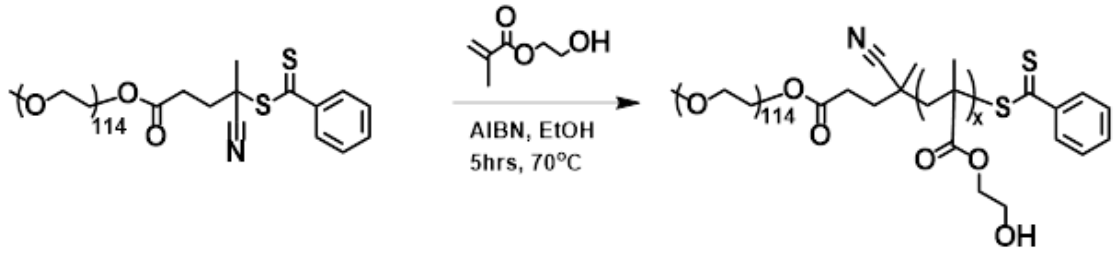

Synthesis of PBIEMx-*block*-PEG series

In a general procedure, PHEMA-*block*-PEG and pyridine (5 mol equiv. per -OH repeat unit) were dissolved in THF in a round-bottom flask and stirred on ice. α-BiBB (4 mol equiv. per -OH repeat unit) was added dropwise by syringe to the flask over 5 minutes. The reaction continued to stir over ice for 10 minutes, before reacting overnight at room temperature. The solution was subject to gravitational filtration to remove formed pyridinium salts and washed with THF before being concentrated by rotary evaporation. The resulting polymer was recovered by precipitation in hexane three times over, S4 redissolving in THF. Finally, the polymer was lyophilised to give a pale pink powder and characterised by ^{1}H NMR spectroscopy (300 MHz, $CDCl_3$, δ 7.26 ppm) and SEC (DMAc/LiBr, 50 °C, PMMA).

Scheme S2.3. Synthesis of $PBIEM_x$ -*block*-PEG_{114}

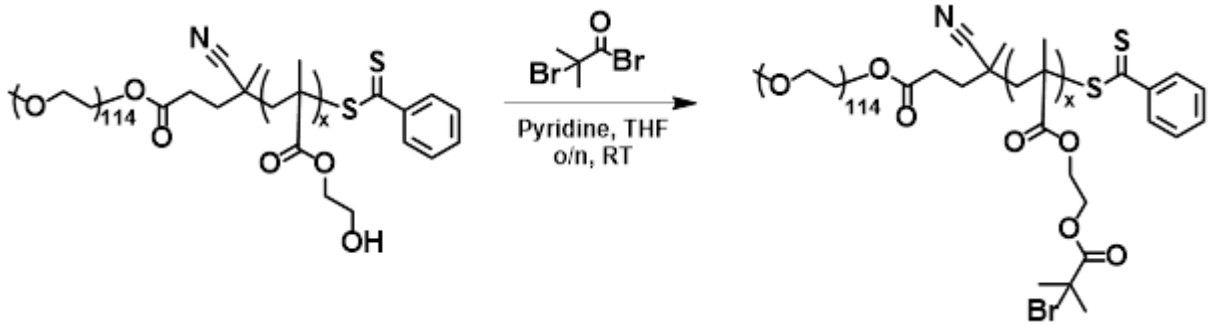

Synthesis of (PBIEMx-*graft*-PBzMAy)-block-PEG series

PBIEMx-*b*-PEG, BzMA, PMDETA (1.2 mol equiv. per -Br unit), and mesitylene (100 μL) as an internal standard were dissolved in anisole (80% v/v) in a Schlenk flask. After removal of an aliquot to monitor conversion, the vessel was subject to three freeze-pump-thaw cycles, with addition of CuBr (1.2 mol equiv. per -Br unit) prior to the last pump cycle. The flask was backfilled with nitrogen gas, and then reacted at 70 ̊C for 2.5 hrs. An aliquot was taken to

determine monomer conversion. The solution was run through a short neutral alumina column to remove copper catalyst, and anisole removed under nitrogen flow. The polymer was redissolved in DMF and purified by precipitation in diethyl ether three times. The resulting pellet was redissolved in DMF and solid content determined. Finally, the polymer was characterised by ^{1}H NMR spectroscopy (300 MHz, $CDCl_3$, δ 7.26 ppm) and SEC (DMAc/LiBr, 50 °C, PMMA).

Scheme S2.4. Synthesis of (PBIEM$_x$-*graft*-PBzMA$_y$)-*block*-PEG$_{114}$ using grafting-from approach with ATRP

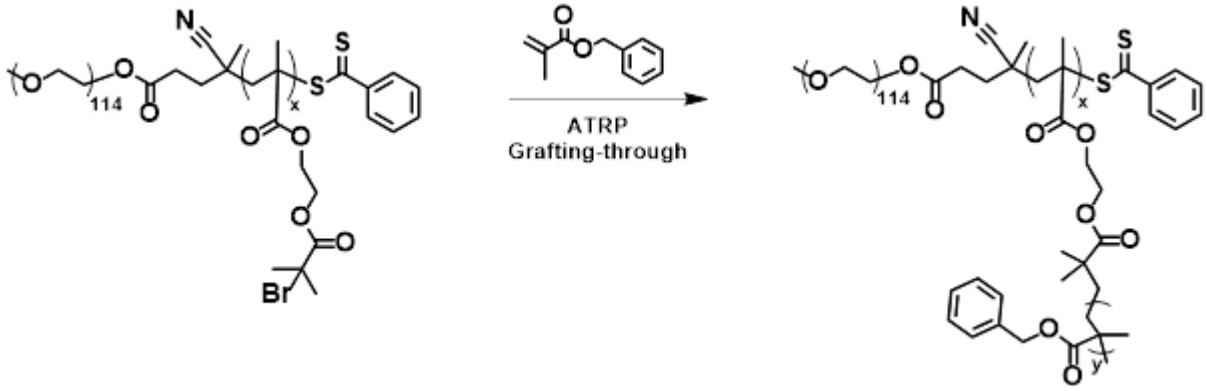

Self-Assembly of tadpoles

A 2mg/mL polymer solution in DMF (unless stated otherwise) was prepared and transferred into a vial capped with a dialysis membrane (MWCO 3500 Da). The solution was dialysed against DI water for 2 days, replacing the DI water twice a day. The resulting solution was collected and analysed by DLS and various microscopy techniques.

Kinetic monitoring of self-assembly

A 1 mL of a 2 mg/mL TP$_{15\text{-}75}$ solution in DMF was placed in a vial capped with a dialysis membrane (MWCO 3500 Da). The solution was dialysed against 600 mL deionised water. A 40 µL aliquot was taken and added to 80 µl mesitylene as a standard for ^{1}H NMR analysis in MeOD (ie. solvent switch rate of TP$_{15\text{-}75}$ comparing integral of (a) DMF using (b) mesitylene as a standard).

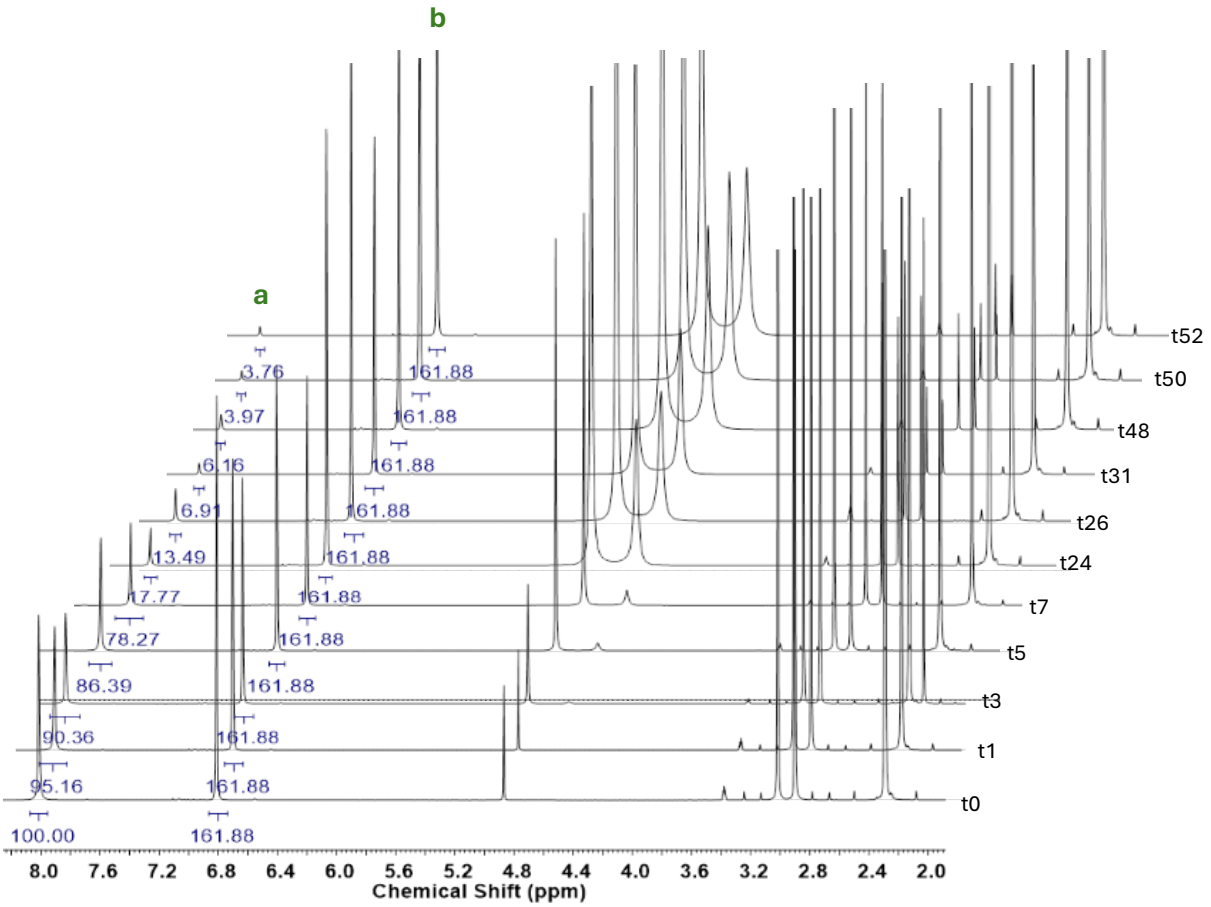

Figure S2.1. Kinetic monitoring of Self-Assembly by ^{1}H NMR of (a) DMF solvent peak against (b) mesitylene standard (300 MHz, MeOD, δ 3.31) across t0, t1, t3, t5, t7, t24, t26, t31, t48, t50, t52

Nuclear magnetic resonance (NMR) spectroscopy

NMR spectra were recorded at the University of Sydney using Bruker NEO 300 MHz NMR spectrometers. ^{1}H NMR measurements were carried out using a zg pulse program (90° pulse) with a recycle delay (D1) of 2-5 s. ^{1}H NMR spectra are referenced to the residual solvent peak for $CDCl_3$ (δ 7.26 ppm), or MeOD (δ 3.31 ppm) as appropriate. Deuterated solvents were obtained from Sigma Aldrich and used without any further purification.

Size exclusion chromatography (SEC)

SEC was performed using a Shimadzu Prominence UFLC (ultra-fast liquid chromatography) system fitted with a Shim-pack GPC-800DP guard column followed by two in-series Phenogel columns (5 μm, 104 Å and 105 Å). The system eluent was HPLC grade dimethyl acetamide

(DMAc) containing LiBr (0.03 wt%) and BHT (each at 0.05 wt%), eluting at a flow rate of 1 mL/min. The column assembly was incubated at 50 °C, and retention times were calibrated using narrow PMMA standards from PSS.

Atomic Force Microscopy (AFM)

AFM was performed in air using a Multimode 8 with NanoScope V controller (Bruker) in standard tapping-mode (Tap300Al-G cantilevers, 300 kHz, 30 Nm-1, Budget Sensors). Samples were prepared by depositing 10 μL of aqueous selfassembly dispersion onto a silicon wafer previously cleaned by CO_2 blast. The droplet was spin-coated by two 60 second cycles at 4000 rpm. Image analysis was performed on Bruker's Nanoscope Analysis software.

Dynamic light scattering (DLS)

DLS measurements were performed on a Malvern Zetasizer Ultra equipped with a He-Ne (633 nm) laser. The hydrodynamic diameters of polymer self-assembly samples were directly measured on DLS without any further treatment.

Transmission Electron Microscopy (TEM)

TEM observations were performed using the JEM-1400 (JEOL, Japan) with a beam acceleration of 120 kV. Sample solutions were adjusted to 0.5 g/L, and a 10 μL droplet placed on parafilm. A carbon-coated Cu grid (ProSciTech, Australia) was hydrophilised by GloQube Plus (Quorum), using a 25mA plasma current for 30 seconds. The hydrophilised grid was placed onto the sample droplet for 10 minutes prior to removal of excess solution with a filter paper. The sample was negatively stained with a 2wt% of phosphotungstic acid (PTA) solution adjusted to pH ~ 7 with excess solution removed with filter paper unless stated otherwise.

4. Results and Discussion

4.1 Synthesis of bottlebrush-linear polymer library

In this work we designed a "grafting-from" strategy to build a library of amphiphilic bottlebrush block copolymers (BBCPs) using a linear poly(ethylene glycol) (PEG) block (coil) and a poly(benzyl methacrylate) (PBzMA) bottlebrush block (rod) (Scheme 2.1). First, reversible addition-fragmentation chain-transfer (RAFT) polymerisation was used to synthesise a diblock copolymer by polymerising 2-hydroxyethyl methacrylate (HEMA) from a synthesised mPEG$_{114}$-CPADB macro-RAFT agent (Figure 2.1).

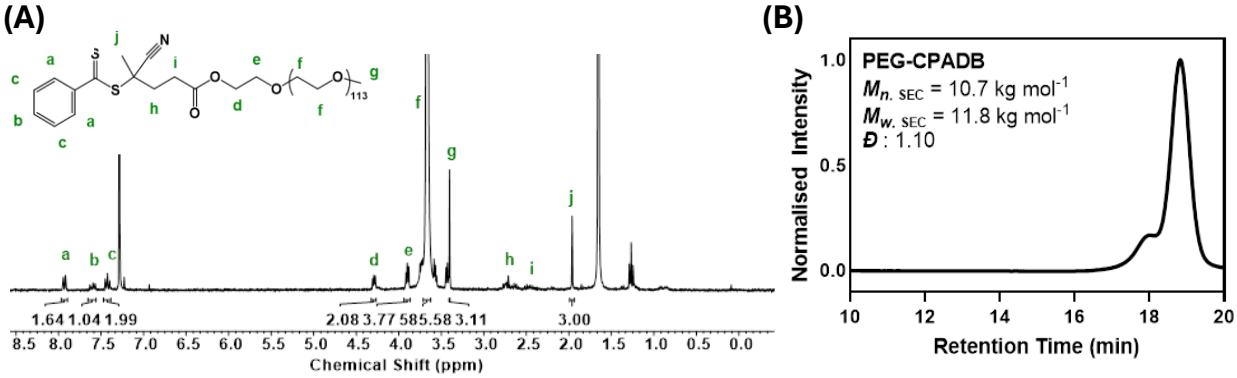

Figure 2.1. Characterisation data of mPEG$_{114}$-CPADB macroCTA agent (A) ^{1}H NMR (300 MHz, $CDCl_3$) δ 7.26 and B) SEC chromatograms in DMAc (50 °C and 1 mL min-1)

The PHEMA was subsequently esterified with α-bromoisobutyrate bromide to give a poly(ethylene glycol)$_{114}$-*block*-poly[2-(2-bromo isobutyryloxy)ethyl methacrylate]$_x$ (PEG$_{114}$-*b*-PBIEM$_x$) polyinitiator backbone. An exemplar ^{1}H NMR of PEG$_{114}$-*b*-PHEMA$_{15}$ is shown in Figure 2.2. A displaying integrated PHEMA peaks δ 4.06 (CH_2), 3.79 (CH_2), 2.01 (CH_2), 1.04 (CH_3) compared to the PEG peak at δ 3.66 (CH_2CH_2). Complete esterification to PEG$_{114}$-*b*-PBIEM$_{15}$ is evidenced by the shift of the CH_2 peaks to δ 4.40 and 4.23, along with the methyl group signal at 1.99 ppm. Additionally, a comparison of the size exclusion chromatography (SEC) chromatograms shows a slight shift toward a higher retention time because of the reduced apparent hydrodynamic size of PEG$_{114}$-*b*-PBIEM compared to PEG$_{114}$-*b*-PHEMA.

Characterisation data for further polymer backbones referenced in this research chapter can be found in supplementary material (Figure S2.2).

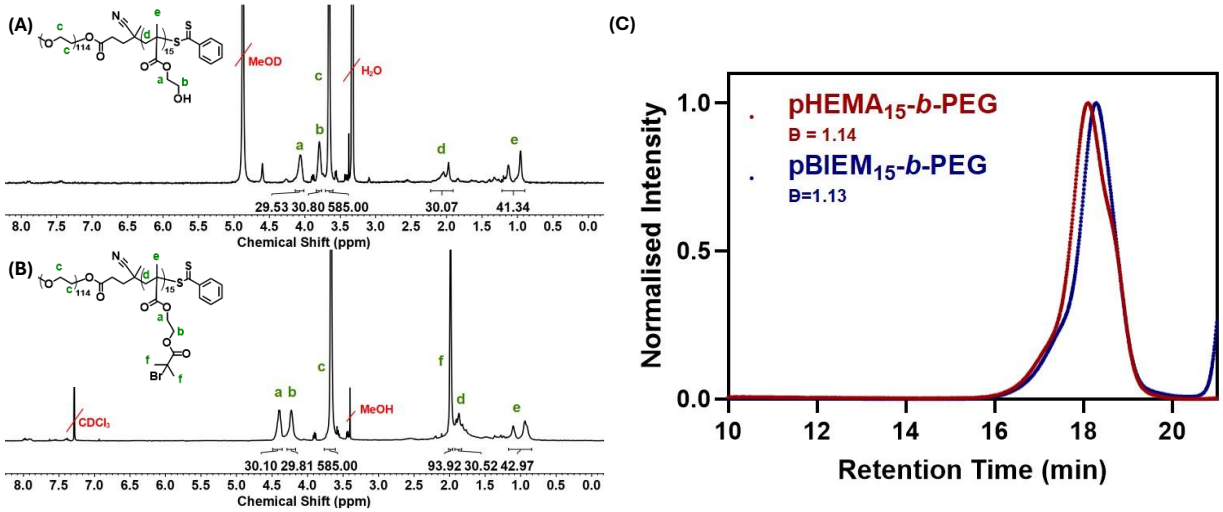

Figure 2.2. Representative characterisation data of polymer backbones (A) ^{1}H NMR of PEG_{114}-*b*-PHEMA (300 MHz, MeOD) δ 4.06 (a, CH_2), 3.79 (b, CH_2), 3.66 (c, CH_2CH_2), 2.01 (d, CH_2), 1.04 (e, CH_2). (B) ^{1}H NMR of PEG_{114}-*b*-PBIEM (300 MHz, $CDCl_3$) δ 4.40 (a, CH_2), 4.23 (b, CH_2), 3.66 (c, CH_2CH_2), 1.99 (f, CH_3), 1.88 (d, CH_2), 1.02 (e, CH_2). (C) SEC chromatograms comparison of PEG_{114}-*b*-PHEMA and PEG_{114}-*b*-PBIEM in DMAc (50 °C and 1 mL min^{-1})

The PBzMA brush segment was then synthesised using the grafting-from approach from the PBIEM moieties using atom transfer radical polymerisation (ATRP) to yield well-defined tadpole-like BBCPs macromolecules. By independently varying either the PHEMA block length of the copolymer or the PBzMA side chain length allowed for adjustment to the bottlebrush segment, and consequently the overall BBCP dimensions and hydrophilic-to-hydrophobic ratio (Table 2.1). As a first set, we used a PEG_{114}-*b*-$PBIEM_{15}$ backbone to generate a library of building blocks with constant backbone length, but variance in side chain lengths: PEG_{114}-*b*-($PBIEM_{15}$-*g*-$PBzMA_y$), with y = 6, 23, 51, 75, 144. Greater side chain length increased the overall hydrodynamic volume of the BBCPs, evident through a progressive shift towards shorter retention times in size exclusion chromatography (SEC) (Figure 2.5A). Side chain lengths were determined by ^{1}H NMR end group analysis, with comparison of the

integration of the CH_2 of the benzyl group at δ ~ 4.75 ppm to the repeating $(CH_2)_2$ PEG signal at δ ~ 3.55 ppm (Figures 2.3 & 2.4) under the assumption of 50% grafting efficiency.[33, 34]

Scheme 2.1. Synthesis of PEG-*b*-(PBIEM$_x$-*g*-PBzMA$_y$) (x = 9, 15, 31, 49) (y = 6, 23, 51, 75, 144) tadpole-like bottlebrush-linear bottlebrush copolymers.

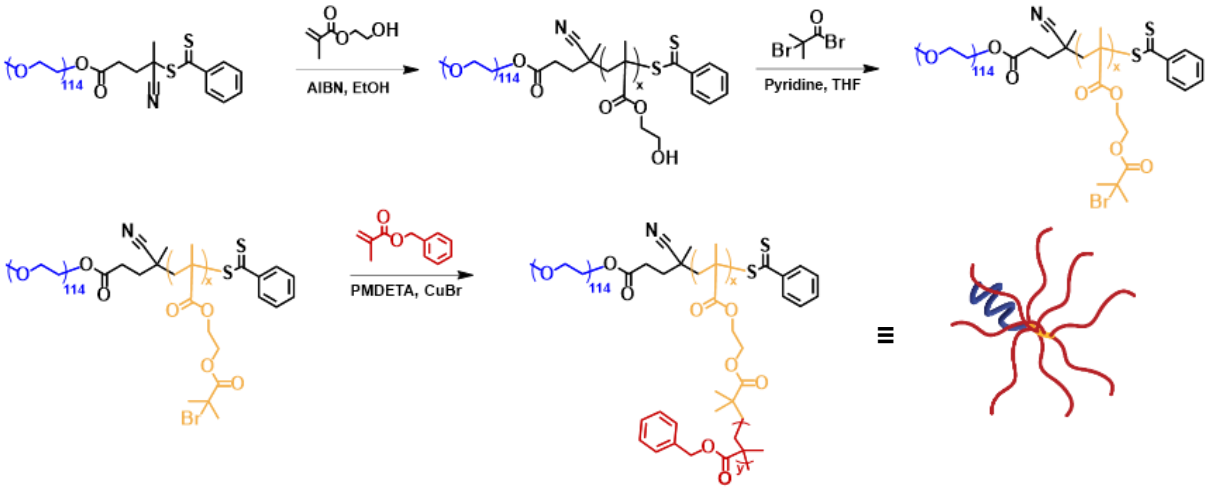

In addition, we synthesised a second BBCP set, maintaining a comparable side chain length (DP~ 76-79), instead changing the PBIEM backbone length (x = 9, 31, 49). Again, a shift in SEC retention time was attributed to the increasing hydrodynamic volume with increasing bottlebrush blocks (Figure 2.5B). A summary of the PEG$_{114}$-*b*-(PBIEM$_x$-*g*-PBzMA$_y$) BBCP libraries is shown in Table 2.1. From here on, we denote our materials as tadpoles (TP), encoding the DP of PBIEM backbone and the DP of the side chains, e.g. PEG$_{114}$-*b*-(PBIEM$_{15}$-*g*-PBzMA$_{75}$) becomes TP$_{15\text{-}75}$.

Table 2.1. Characterisation data of PEG$_{114}$-*b*-(PBIEM$_x$-*g*-PBzMA$_y$) polymer library

BBCPs	DP_{PEG}	DP_{PBIEM}	DP_{PBzMA}	[a]f_{BzMA}	[b]$M_{n,NMR}$	[c]$Đ_{SEC}$	Self-Assembly Morphology
TP$_{15\text{-}6}$	114	15	6	0.44	12 900	1.19	Polymersomes
TP$_{15\text{-}23}$	114	15	23	0.75	30 400	1.11	Dense Polymer Particles
TP$_{15\text{-}51}$	114	15	51	0.87	72 400	1.11	Dense Polymer Particles
TP$_{15\text{-}75}$	114	15	75	0.91	104 000	1.11	Discs
TP$_{15\text{-}144}$	114	15	144	0.95	195 000	1.11	Dense Polymer Particles
TP$_{9\text{-}79}$	114	9	79	0.86	67 600	1.16	Dense Polymer Particles
TP$_{30\text{-}76}$	114	31	76	0.95	207 000	1.12	Dense Polymer Particles
TP$_{45\text{-}79}$	114	49	79	0.97	346 000	1.15	Dense Polymer Particles

[a] Ratio of PEG:PBzMA repeat units, [b]Determined by ^{1}H NMR analysis, [c]Determined by SEC (M_w/M_n).

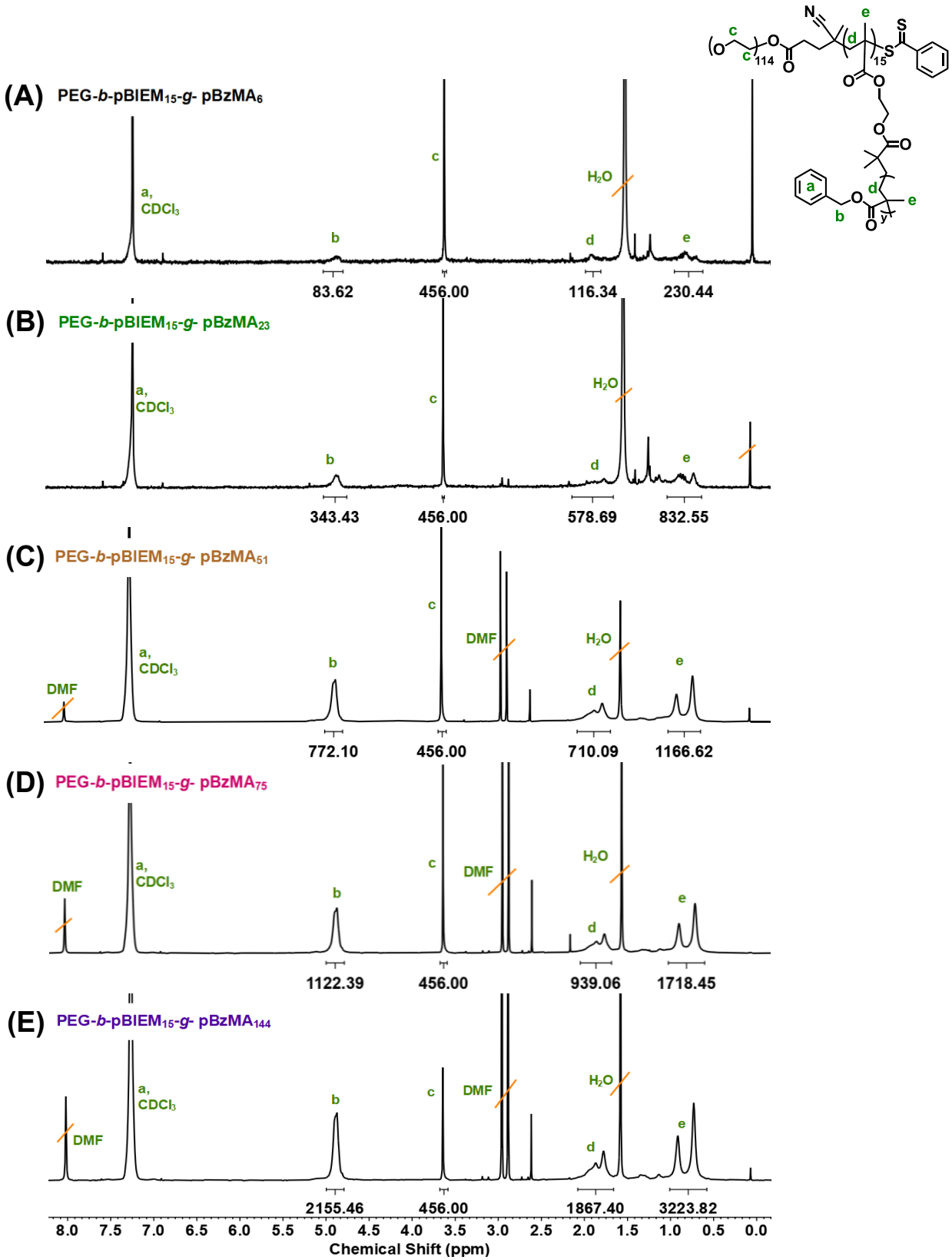

Figure 2.3. ^{1}H NMR of PEG_{114}-*b*-$BIEM_{15}$-*g*-$PBzMA_y$ (300 MHz, $CDCl_3$) δ 7.26 (a, Bzl), 4.87 (b, CH_2), 3.64 (c, CH_2CH_2), 1.82 (d, CH_2), 0.82 (e, CH_3) (A) $TP_{15\text{-}6}$, (B) $TP_{15\text{-}23}$, (C) $TP_{15\text{-}51}$, (D) $TP_{15\text{-}75}$, (E) $TP_{15\text{-}144}$

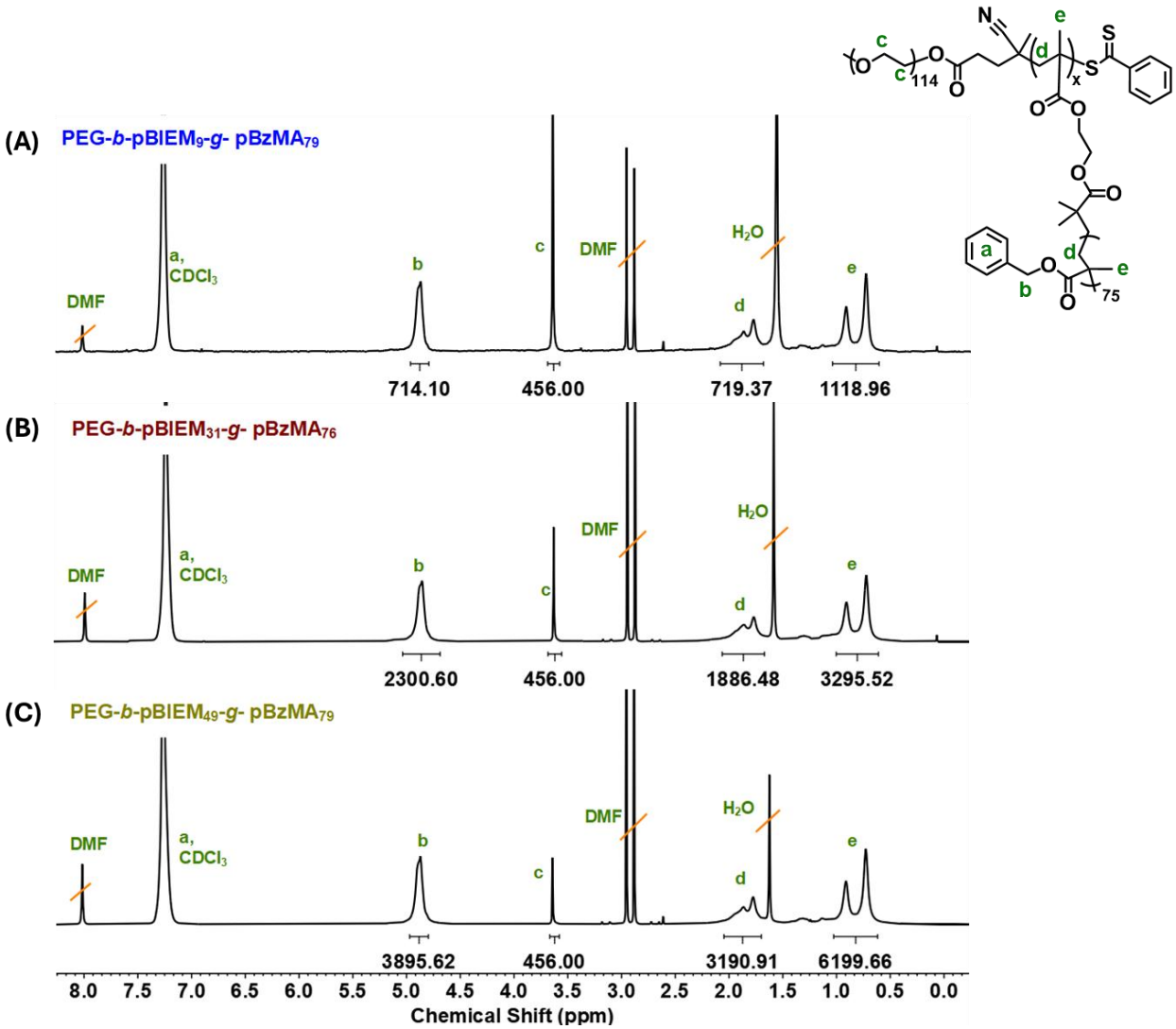

Figure 2.4. ^{1}H NMR of PEG_{114}-*b*-$BIEM_x$-*g*-$PBzMA_{75}$ (300 MHz, $CDCl_3$) δ 7.26 (a, Bzl), 4.87 (b, CH_2), 3.64 (c, CH_2CH_2), 1.82 (d, CH_2), 0.82 (e, CH_3) (A) $TP_{9\text{-}79}$, (B) $TP_{31\text{-}76}$, (C) $TP_{49\text{-}79}$

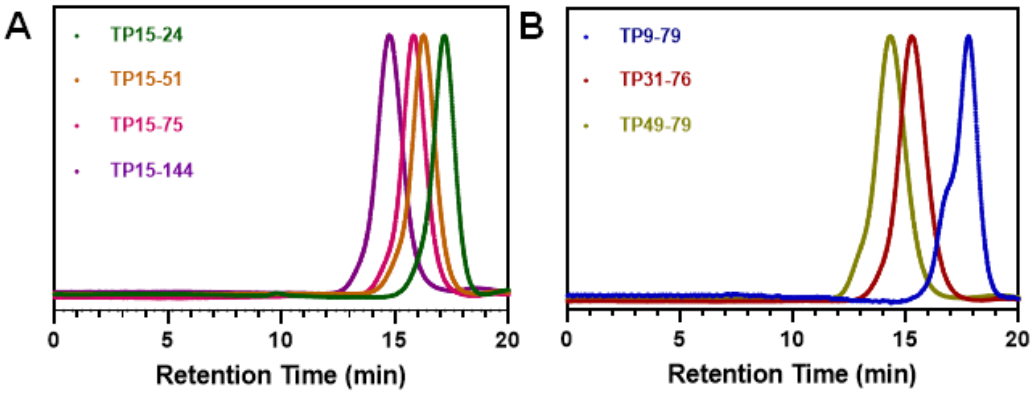

Figure 2.5. SEC traces in DMAc (50 °C and 1 mL min^{-1}) of (A) PEG_{114}-*b*-($PBIEM_{15}$-*g*-$PBzMA_y$) library with increasing side chain length (y = 6, 23, 51, 75, 144) and (B) PEG_{114}-*b*-($PBIEM_x$-*g*-$PBzMA_{75}$) library with varied backbone length (x = 9, 31, 79).

4.2 Effect of bottlebrush segment side chain length on self-assembly

Using the first set of BBCPs (constant PBIEM, but varying side chain length), we self-assembled the BBCPs via a solvent switch method, starting with a 2 mg/mL solution in DMF and their dialysis into deionised water. We used transmission electron microscopy (TEM) to survey the resulting assemblies (Figure 2.6) and dynamic light scattering (DLS) to estimate their hydrodynamic sizes (Figure S2.3A).

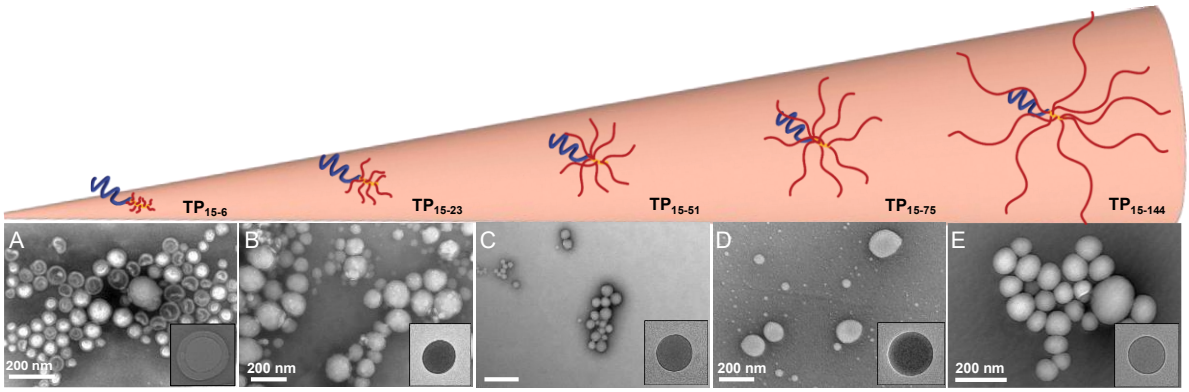

Figure 2.6. (top) Schematic representation of varying side chain lengths of BBCPs with TEM images of self-assemblies from (A) $TP_{15\text{-}6}$, (B) $TP_{15\text{-}23}$, (C) $TP_{15\text{-}51}$, (D) $TP_{15\text{-}75}$, (E) $TP_{15\text{-}144}$ (bottom) TEM micrographs of negatively-stained self-assembled BBCPs, with inset showing a representative unstained particle.

The self-assembly of $TP_{15\text{-}6}$ resulted in the formation of polymersomes, as verified by spherical structures with seemingly deflated membranes in TEM (Figure 2.6A). Particles with irregular topology were confirmed by atomic force microscopy (AFM) (Figure 2.7) with variance in deflated heights between the centres and boundaries of particles, further confirming vesicular morphologies (Figure 2.7B).

Increasing the side chain length twofold in $TP_{15\text{-}23}$ revealed spherical particles averaging 200 nm in hydrodynamic diameter (Figure S2.3A) and particles ranging from ~90-200 nm via TEM (Figure 2.6B). These particles are verified by AFM, with deflated heights of ~12-28 nm with monomodal and uniform height traces, indicating dense spherical particles (Figure 2.8).

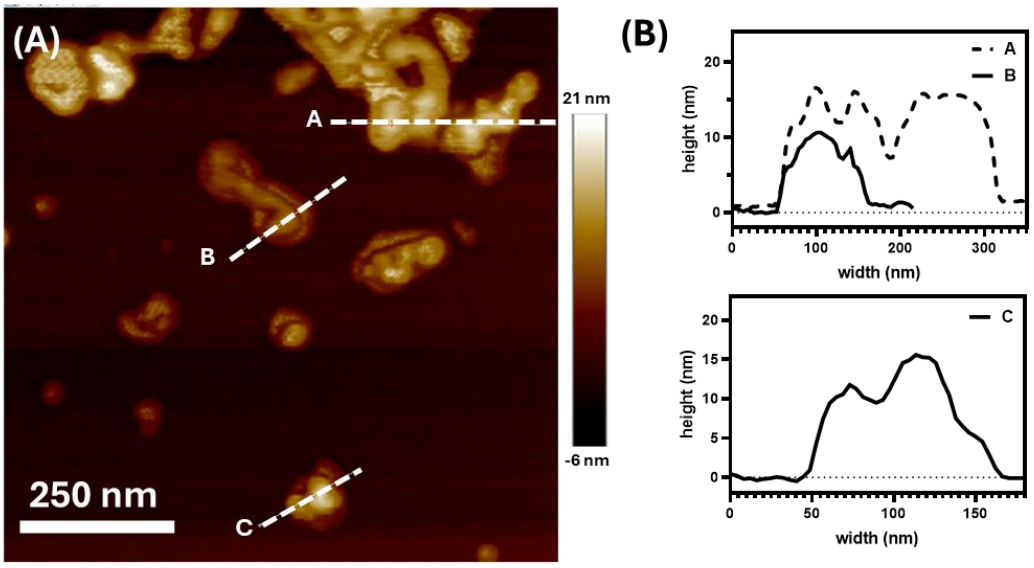

Figure 2.7. AFM of particles self-assembled from $TP_{15\text{-}6}$ (A) 2D Height map (B) Corresponding particle height

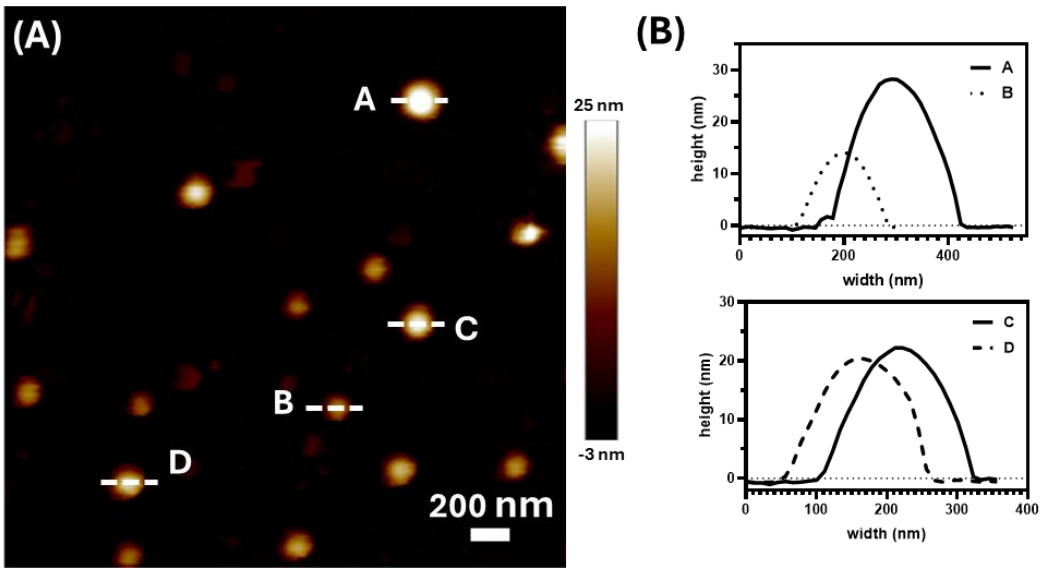

Figure 2.8. AFM of particles self-assembled from $TP_{15\text{-}23}$ **(A)** 2D Height map **(B)** Corresponding particle height plots

Doubling the side chain length again, $TP_{15\text{-}51}$ gave similar spherical morphologies, albeit with larger diameters (~80-300 nm) in TEM, AFM and DLS (Figure 2.6C, Figure 2.9, Figure S2.3A). Guided by the coexistence of seemingly different particles in TEM (Figure 2.9A), AFM was employed to establish that this sample also contained flat assemblies (height ~ 5 nm) that were dispersed amongst the larger particles (with deflated heights of ~20-30 nm) (Figure

2.9B-2.9D). The flat particles indicated the coexistence of another species, most likely discoidal assemblies.

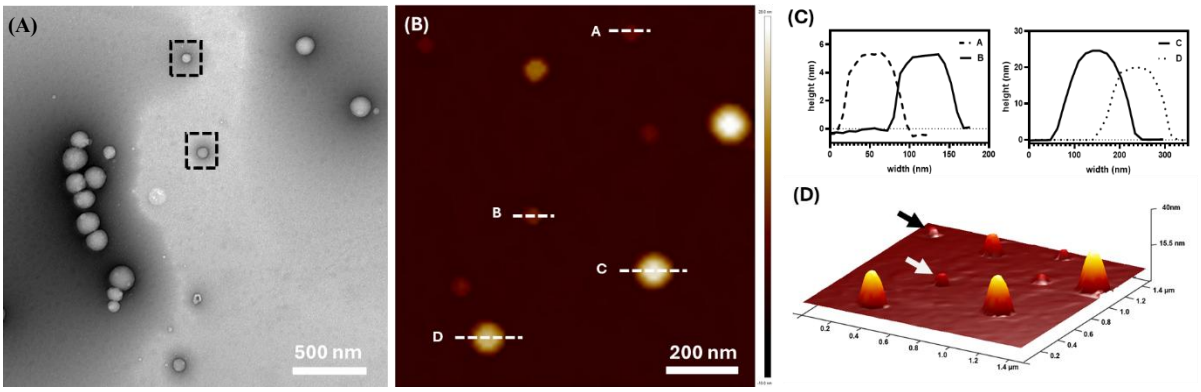

Figure 2.9. Characterisation of flat assemblies from $TP_{15\text{-}51}$ (A) TEM (B) 2D AFM height map (C) Corresponding particle height plots (D) 3D height map with arrows indicating stacked discs. Z-value -13 – +28nm.

Interestingly, when extending the side chains further, $TP_{15–75}$ self-assembled exclusively into nanodiscs with diameters ranging from ~50 to 160 nm. These flat particles were observed to be uniformly shaded in TEM (Figure 2.6D), which aligns with previous work.[29, 31, 32] The discoidal morphology was confirmed by AFM cross-section analyses (Figure 2.10), which occasionally revealed stacked discs (with doubled height) among single discs (Figure 2.10B & 2.10C) as an artifact of the sample preparation process. As the approximate carbon–carbon length in polymethacrylates correlates to ~0.25 nm,[35] a stretched bottlebrush backbone would measure ~4–5 nm in height, indicating the BBCPs should stack side-by-side rather than end-to-end. Further extension of the side chain length to $TP_{15\text{-}144}$ resulted in the formation of spherical particles with ~ 100-200 nm diameters with deflated heights between ~25-33nm (Figure 2.6E, Figure 2.12). Considering the ratio of hydrophilic PEG to hydrophobic PBzMA and their macromolecular topology, we postulate that the shortest PBzMA side chains (DP=6), combined with a reduced grafting density (ie. not 100% grafting efficiency) afford sufficient mobility of the bottlebrush segment to be stabilised sufficiently by the hydrophilic PEG block (f_{BzMA} = 0.44, Table 2.1), leading to polymer vesicles.

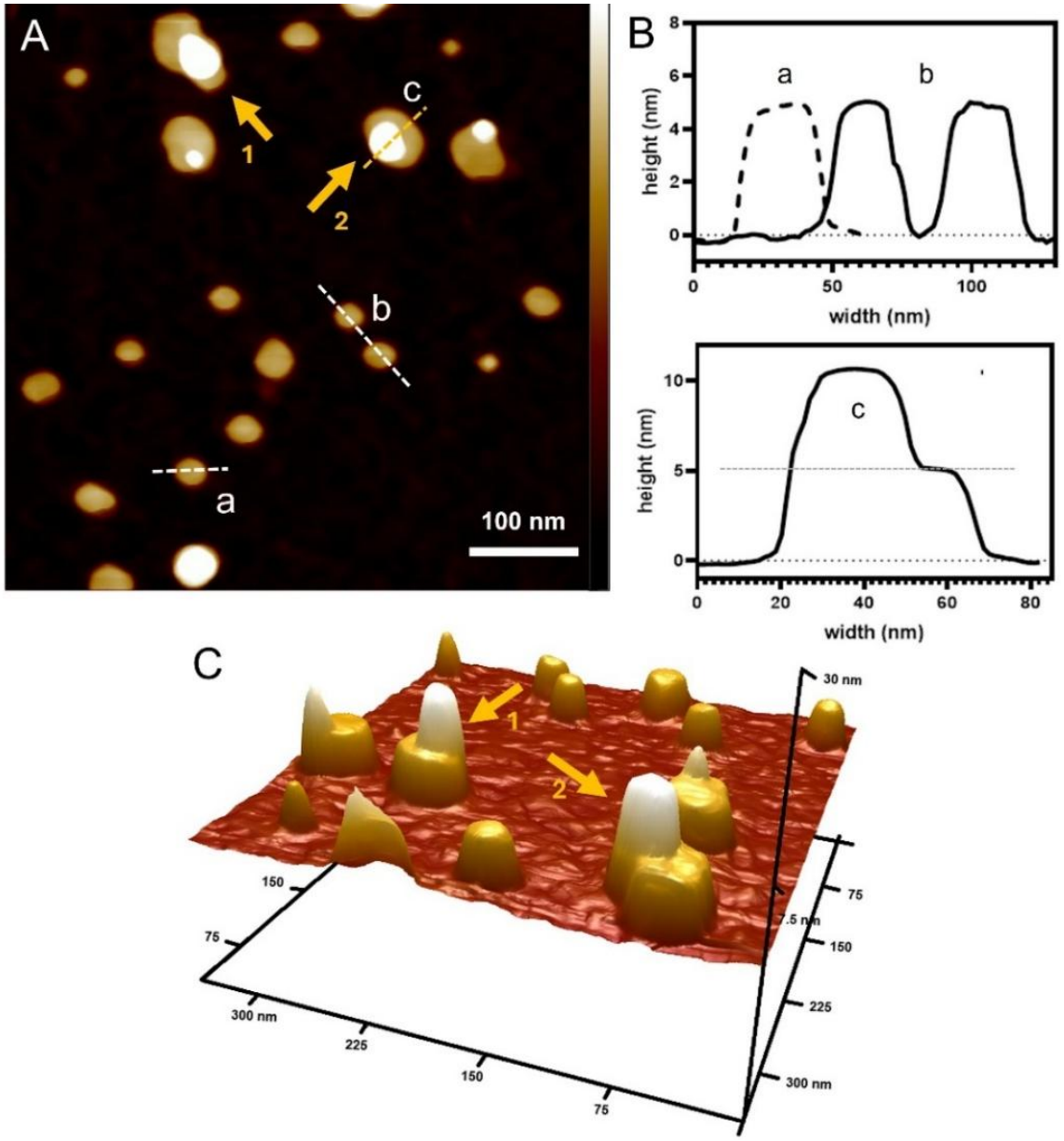

Figure 2.10. (A) AFM height image of self-assembled discs of $TP_{15\text{-}75}$ and its cross-sectional analysis (B). (C) 3D plot of the marked section in the height image, with arrows indicating stacked discs. Z-value -1 – +7nm.

With increasing side chain lengths, the hydrophobic component of the amphiphile increases, leading to architectural asymmetry. This translates to a less prominent flexible linear PEG, reducing its stabilisation of the self-assembly. This leads to the self-assembly of dense polymer particles (Figure 2.13B & C), as we have recently shown for a different system.[36] Further extension of side chain length with the grafting density remaining constant, increases crowding and steric repulsion in the bottlebrush segment, leading to segment stiffening.[37] This is further

supported by theoretical predictions.[38] In addition, a strong rigidity contrast of segments in rod–coil macromolecules can diminish the influence of volume fractions and dominate thermodynamic factors in the self-assembly of discrete nanostructures.[39] At $f_{BzMA} = 0.91$ found in $TP_{15–75}$, this steric repulsion affects the ability of the bottlebrush segment to bend and to adopt curvature during dialysis,[40] leading to planar, discoidal assemblies (Figure 2.13D). This segment stiffening is expected to be minimally affected by the nature of the solvent, provided the solvent is a good solvent for the bottlebrush. Using THF instead of DMF for the dialysis also exclusively yielded nanodiscs (Figure 2.11) indicating that the self-assembly depends more on the rod–coil structure than solvent effects. This aligns with molecular dynamic simulations, indicating that increasing side chain length leads to stiffening and an extension effect on bottlebrush backbones.[41] The stiffening role of the bottlebrush segment in the architecture is further supported through the comparison to self-assembly of linear block copolymer systems. Changes in volume fraction between hydrophilic and hydrophobic components is observed through the transition from spherical micelles toward bilayer and lamellar systems and finally inverted micelles as critical packing parameter (CPP) increases. Notably, discoidal particles are not well-defined in the CPP phase diagram largely because the flexibility in linear systems favours particles with surface curvature making them thermodynamically unfavourable.[42]

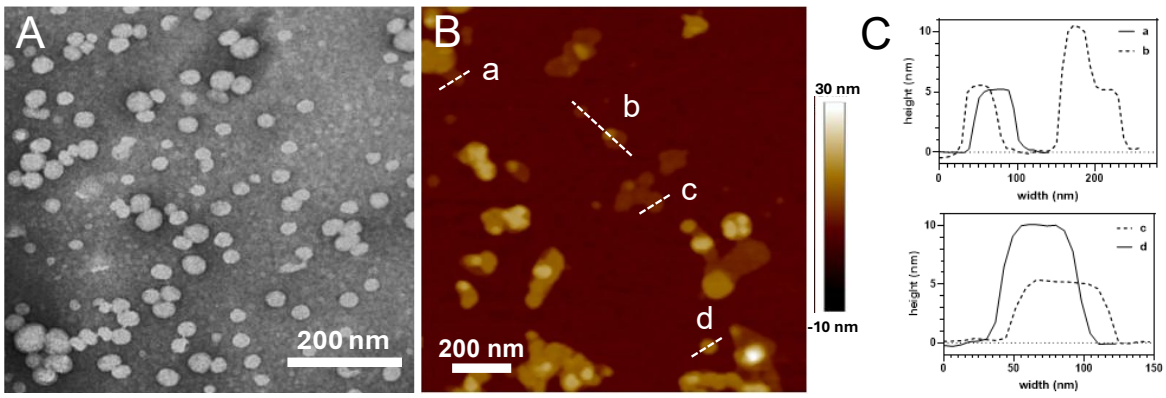

Figure 2.11. Characterisation of flat assemblies from TP_{15-75} from THF (A) TEM (B) 2D AFM height map (C) corresponding particle height plots

As the ratio of PEG to PBzMA diverts further, sufficient stabilisation of the self-assembled materials becomes problematic, leading to the formation of dense polymer particles (Figure 2.13E) (likely large compound micelles or nanoprecipitates)[43] with low colloidal stability. Scattering experiments indicate that the flexibility of bottlebrush backbones can be restored by excessive elongation of side chains as their mutual interaction and conformational entropy overwhelms steric effects.[44]

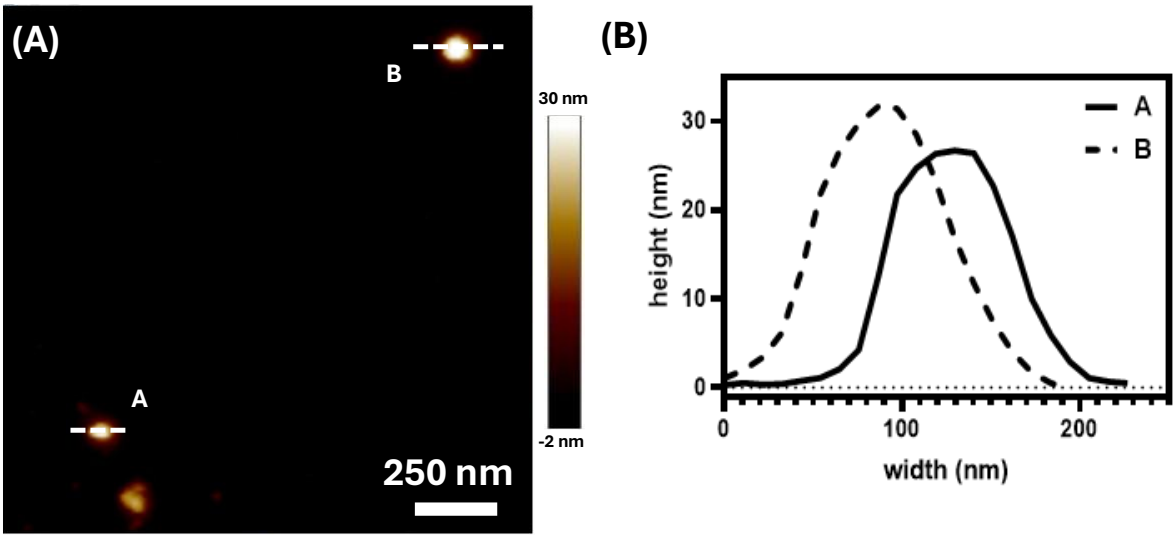

Figure 2.12. AFM of particles self-assembled from $TP_{15\text{-}144}$ **(A)** 2D Height map **(B)** Corresponding particle height plots

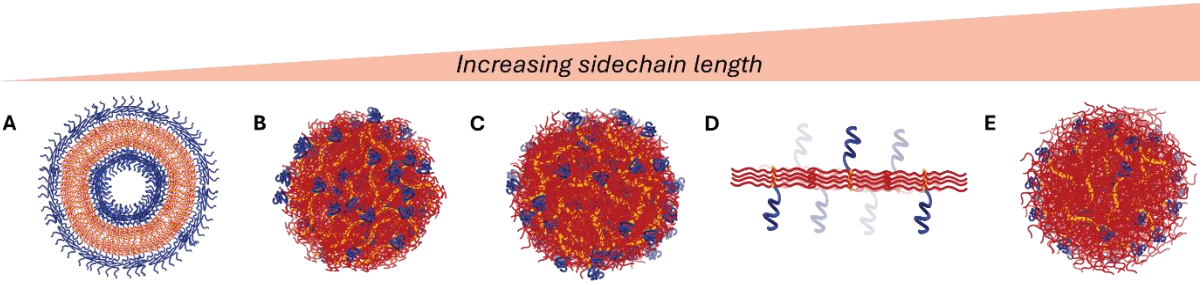

Figure 2.13. Schematic representation of self-assembled particle morphology with increasing side chain length from BBCPs (A) $TP_{15\text{-}6}$ (B) $TP_{15\text{-}23}$, (C) $TP_{15\text{-}51}$, (D) $TP_{15\text{-}75}$, (E) $TP_{15\text{-}144}$

4.3 Effect of molecular polymer brush segment backbone length on self-assembly

After finding that $TP_{15\text{-}75}$ yielded polymer nanodiscs, we then varied the bottlebrush backbone length as another parameter to alter both the molar ratio and dimensions of the hydrophobic segment. Whilst the grafting density across our systems remains constant as the synthetic procedure is identical, a very short backbone length (DP = 9) in $TP_{9\text{-}79}$ will allow for less

protruding side chains and a reduced steric hindrance between the side chains, mimicking systems with sparsely grafted side chains.[45] Thus, the corresponding self-assemblies of the highly asymmetric amphiphile $TP_{9\text{-}79}$ were also able to form polymersomes (Figure 2.14A, Figure 2.15). Despite maintaining a comparable PEG:PBzMA ratio (f_{BzMA} = 0.86) to $TP_{15\text{-}75}$, the curvature effect at the interface between the domains is influenced by the greater side chain flexibility and reduced persistent length of the backbone[46] lending to vesicular structures (Figure 2.18A).

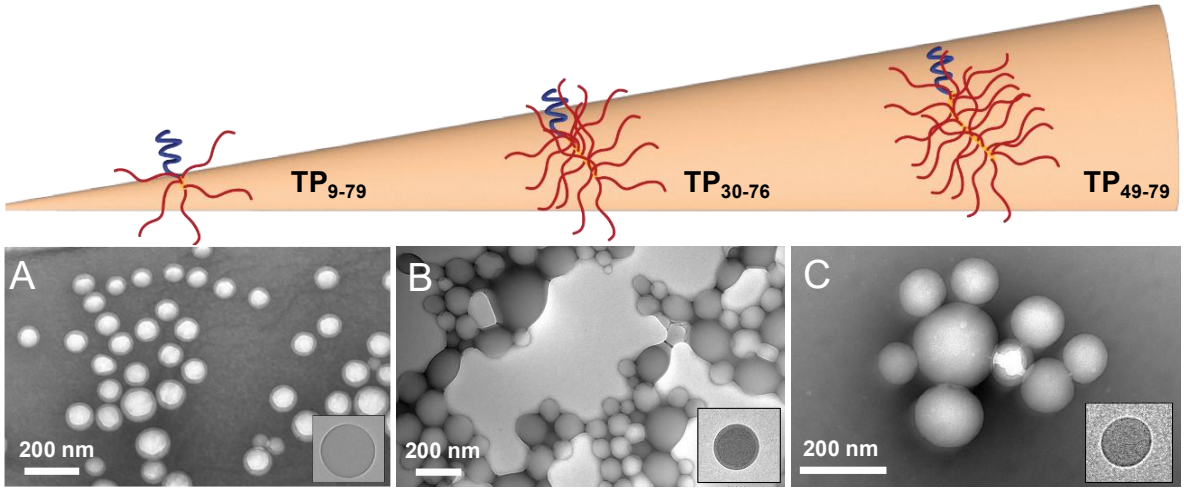

Figure 2.14. (top) Schematic representation of varying backbone lengths of BBCPs with TEM images of self-assemblies from (A) $TP_{9\text{-}79}$, (B) $TP_{30\text{-}76}$, (C) $TP_{49\text{-}79}$ (bottom) TEM micrographs of negatively-stained self-assembled BBCPs, with inset showing a representative unstained particle.

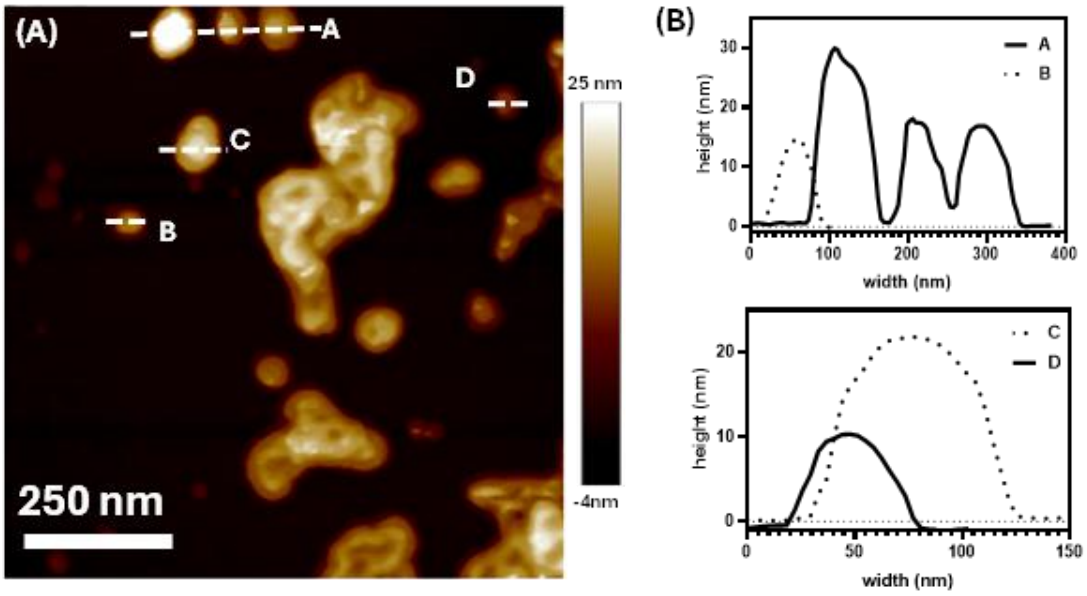

Figure 2.15. AFM of particles self-assembled from $TP_{9\text{-}79}$ (A) 2D Height map (B) Corresponding particle height plots

Increasing the backbone length in $TP_{30\text{-}76}$ and $TP_{49\text{-}79}$ meant that the hydrophobic bottlebrush segment increased dramatically in volume and was more likely to behave like a bottlebrush due to increased chain crowding and axial backbone stretching.[47] This resulted in spherical polymer self-assemblies (Figure 2.14B and 2.14C; Figure 2.16 & 2.17), produced by the collapse of the bottlebrush blocks, as described in earlier work.[36] Whilst the rigidity of the brush segments in these instances should satisfy the expected requirements of planar packing similar to $TP_{15\text{-}75}$ (Figure 2.18B), the decrease in PEG:PBzMA molar ratio leads to dense spherical morphologies (Figure 2.18C & D, further supporting the integral role molar ratio plays in designing disc-forming polymer building blocks.

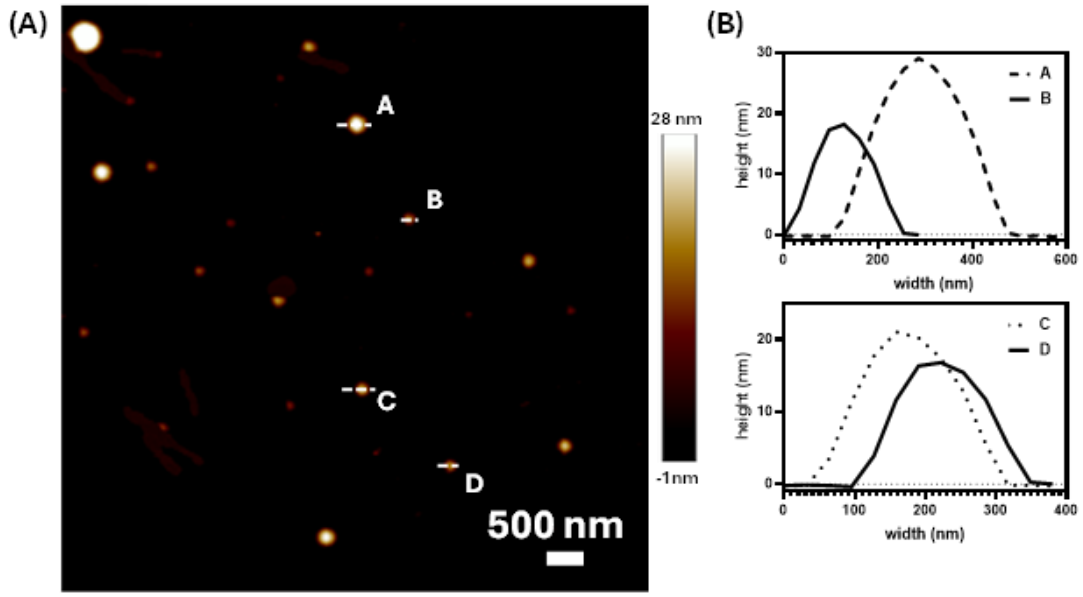

Figure 2.16. AFM of particles self-assembled from $TP_{31\text{-}76}$ (A) 2D Height map (B) Corresponding particle height plots

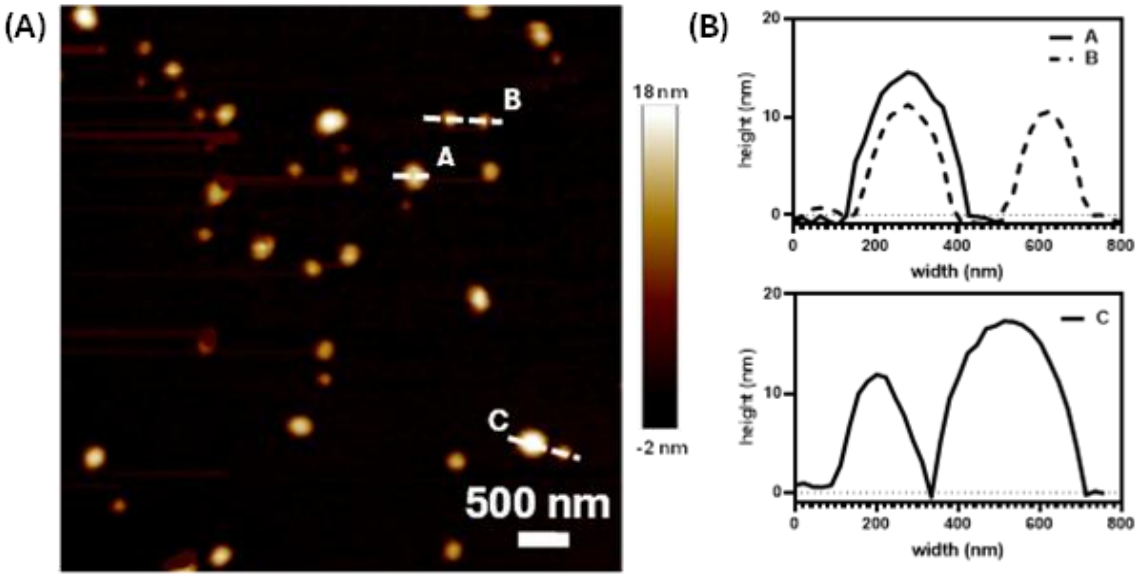

Figure 2.17. AFM of particles self-assembled from $TP_{49\text{-}79}$ (A) 2D Height map (B) Corresponding particle height plots

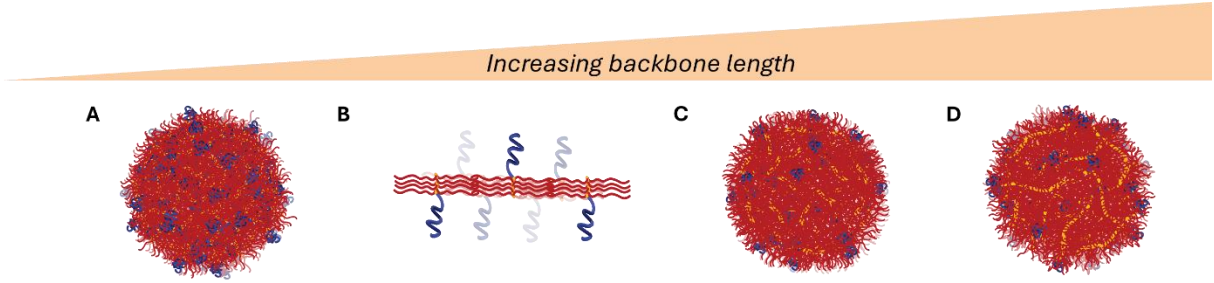

Figure 2.18. Schematic representation of self-assembled particle morphology with increasing backbone length from BBCPs (A) $TP_{9\text{-}79}$ (B) $TP_{15\text{-}75}$, (C) $TP_{31\text{-}76}$, (D) $TP_{49\text{-}79}$

To deduce the influencing parameter on disc formation, we compared the linear: bottlebrush molar ratios of $TP_{15\text{-}75}$ (Table 1) with that of previously reported "grafting-to" studies using poly(ethyl glycoxylate) (PEtG)[31] and poly(ethoxyethyl glycidyl ether-*ran*-tetrahydropyranyl glycidyl ether) P(EE-ran-TP)[32] side chains respectively. Both PEtG (DP PEG:PEtG ratio =9:59) (DP PEG:P(EE-ran-TP) = 9:33) exhibit molar ratios relatively similar to $TP_{15\text{-}75}$. However, when amphiphilicity was assessed based on mass ratios of hydrophilic and hydrophobic segments, we found that these tadpole models were not comparative. This suggests that the molar ratio between the hydrophilic coil to the hydrophobic rod segment plays an important role in the observed planar packing. At this ratio, we also expect that the backbone is appropriately extended by longer side chains that protrude radially in response to steric repulsion.[40, 48] This reduces flexibility within the core-forming segment, whilst enhancing the segregation strength between the domains of the amphiphile,[49, 50] both favourable for planar packing.

A notable difference between these systems, one that can also affect backbone conformation, is the grafting approach in the bottlebrush synthesis. Comparing the grafting efficiencies (GE) of the grafting-from approach utilised in this approach (GE = 50%) compared to the grafting-from approaches (GE = 75%), it is expected that increasing GE can introduce side chain overlapping and density,[51] in turn positively influencing persistent rigid conformations of backbones,[47, 52] which may account for deviations in required side chain length. Moreover, differences in side chain chemical compositions, particularly the glass transition temperature (T_g) may affect the bottlebrush conformational flexibility in the self-assembly process.[53] Comparing the high T_g PBzMA side chains of $TP_{15\text{-}75}$,[54] to low T_g PEtG,[55] and P(EE-ran-TP)[56] and the subsequent on side chain mobility may affect the mechanism of disc formation, and therefore, the observed diameter of particles.

5. Conclusion

In conclusion, this study revealed that a library of tadpole-like amphiphiles can be readily produced via a modular "grafting-from" approach. Depending on their composition, topology, and overall amphiphilic character, these amphiphiles self-assembled into either polymersomes, spherical polymer particles, or nanodiscs. The window to exclusively assemble these BBCPs into nanoscale polymer discs was narrow, but it demonstrated the opportunity of custom-designing building blocks with rod–coil character to produce pure polymer nanodiscs. In addition, we could demonstrate that BBCPs with a high T_g bottlebrush segment are able to form nanodiscs, just like their low T_g counterparts in previous studies. Insights from this study will aid the development of amorphous 2D nanoparticles and provide a route toward designing suitable building blocks for bottom-up fabrication of nanodiscs via solution self-assembly. While the complete mechanism of the disc formation remains unclear at this point, the above insights will aid future experiments to study the self-assembly process of rod–coil copolymers during dialysis. Previous work on rod–coil copolymers,[57] including our nanodiscs,[31] support a fusion driven self-assembly process involving intermediate assemblies. Simulation of this process will further provide an understanding of bottlebrush properties in a progressively changing solvent environment. More generally, architectural asymmetry in copolymers has become a growing focus in polymer self-assembly, both experimentally and theoretically,[58-64] to which this work will contribute.

6. References

1. Zhu, H.; Li, M.; Liu, B., Anisotropic Colloidal Particles by Molecular Self‐Assembly: Synthesis and Application. *ChemNanoMat* **2024,** *10* (3).

2. Doshi, N.; Prabhakarpandian, B.; Rea-Ramsey, A.; Pant, K.; Sundaram, S.; Mitragotri, S., Flow and adhesion of drug carriers in blood vessels depend on their shape: A study using model synthetic microvascular networks. *J. Control. Release* **2010,** *146* (2), 196-200.

3. Donahue, N. D.; Acar, H.; Wilhelm, S., Concepts of nanoparticle cellular uptake, intracellular trafficking, and kinetics in nanomedicine. *Advanced Drug Delivery Reviews* **2019,** *143*, 68-96.

4. Muro, S.; Garnacho, C.; Champion, J. A.; Leferovich, J.; Gajewski, C.; Schuchman, E. H.; Mitragotri, S.; Muzykantov, V. R., Control of Endothelial Targeting and Intracellular Delivery of Therapeutic Enzymes by Modulating the Size and Shape of ICAM-1-targeted Carriers. *Molecular Therapy* **2008,** *16* (8), 1450-1458.

5. Ben-Akiva, E.; Meyer, R. A.; Yu, H.; Smith, J. T.; Pardoll, D. M.; Green, J. J., Biomimetic anisotropic polymeric nanoparticles coated with red blood cell membranes for enhanced circulation and toxin removal. *Science Advances* **2020,** *6* (16), eaay9035.

6. Decuzzi, P.; Godin, B.; Tanaka, T.; Lee, S. Y.; Chiappini, C.; Liu, X.; Ferrari, M., Size and shape effects in the biodistribution of intravascularly injected particles. *J. Control. Release* **2010,** *141* (3), 320-327.

7. Blanco, E.; Shen, H.; Ferrari, M., Principles of nanoparticle design for overcoming biological barriers to drug delivery. *Nat. Biotechnol.* **2015,** *33* (9), 941-951.

8. Key, J.; Palange, A. L.; Gentile, F.; Aryal, S.; Stigliano, C.; Di Mascolo, D.; De Rosa, E.; Cho, M.; Lee, Y.; Singh, J.; Decuzzi, P., Soft Discoidal Polymeric Nanoconstructs Resist Macrophage Uptake and Enhance Vascular Targeting in Tumors. *ACS Nano* **2015,** *9* (12), 11628-11641.

9. Mu, Q.; Deng, H.; An, X.; Liu, G.; Liu, C., Designing nanodiscs as versatile platforms for on-demand therapy. *Nanoscale* **2024,** *16* (5), 2220-2234.

10. Elzoghby, A. O.; Samir, O.; Soliman, A.; Solomevich, S.; Yu, M.; Schwendeman, A.; Nasr, M. L., Nanodiscs: Game changer nano-therapeutics and structural biology tools. *Nano Today* **2023,** *53*, 102026.

11. Dorsman, I. R.; Derry, M. J.; Cunningham, V. J.; Brown, S. L.; Williams, C. N.; Armes, S. P., Tuning the vesicle-to-worm transition for thermoresponsive block copolymer vesicles prepared via polymerisation-induced self-assembly. *Polymer Chemistry* **2021,** *12* (9), 1224-1235.

12. Zhao, Z.; Lei, S.; Zeng, M.; Huo, M., Recent progress in polymerization‐induced self‐assembly: From the perspective of driving forces. *Aggregate* **2024,** *5* (1).

13. Richter, D.; Schneiders, D.; Monkenbusch, M.; Willner, L.; Fetters, L. J.; Huang, J. S.; Lin, M.; Mortensen, K.; Farago, B., Polymer Aggregates with Crystalline Cores: The System Polyethylene−Poly(ethylenepropylene). *Macromolecules* **1997,** *30* (4), 1053-1068.

14. Nakano, M.; Matsumoto, K.; Matsuoka, H.; Yamaoka, H., Characterization of Micellization Behavior of Amphiphilic Polymer Having Octadecyl Group by Small-Angle X-ray and Neutron Scattering. *Macromolecules* **1999,** *32* (12), 4023-4029.

15. Contini, C.; Pearson, R.; Wang, L.; Messager, L.; Gaitzsch, J.; Rizzello, L.; Ruiz-Perez, L.; Battaglia, G., Bottom-Up Evolution of Vesicles from Disks to High-Genus Polymersomes. *iScience* **2018,** *7*, 132-144.

16. Qiao, S.; Li, S.; Song, Q.; Liu, B., Shape-Tunable Biconcave Disc-Like Polymer Particles by Swelling-Induced Phase Separation of Seeded Particles with Hydrophilic Shells. *Langmuir* **2023,** *39* (3), 1190-1197.

17. Thiermann, R.; Bleul, R.; Maskos, M., Kinetic Control of Block Copolymer Self‐Assembly in a Micromixing Device – Mechanistical Insight into Vesicle Formation Process. *Macromolecular Chemistry and Physics* **2017,** *218* (2), 1600347.

18. Jia, F.; Liang, F.; Yang, Z., Janus Mesoporous Nanodisc from Gelable Triblock Copolymer. *ACS Macro Letters* **2016,** *5* (12), 1344-1347.

19. Li, Z.; Chen, Z.; Cui, H.; Hales, K.; Qi, K.; Wooley, K. L.; Pochan, D. J., Disk Morphology and Disk-to-Cylinder Tunability of Poly(Acrylic Acid)-b-Poly(Methyl Acrylate)-b-Polystyrene Triblock Copolymer Solution-State Assemblies. *Langmuir* **2005,** *21* (16), 7533-7539.

20. Zhu, J.; Zhang, S.; Zhang, K.; Wang, X.; Mays, J. W.; Wooley, K. L.; Pochan, D. J., Disk-cylinder and disk-sphere nanoparticles via a block copolymer blend solution construction. *Nature Communications* **2013,** *4* (1).

21. Shi, B.; Shen, D.; Li, W.; Wang, G., Self‐Assembly of Copolymers Containing Crystallizable Blocks: Strategies and Applications. *Macromolecular Rapid Communications* **2022,** *43* (14), 2200071.

22. Ganda, S.; Stenzel, M. H., Concepts, fabrication methods and applications of living crystallization-driven self-assembly of block copolymers. *Progress in Polymer Science* **2020,** *101*, 101195.

23. Yin, L.; Hillmyer, M. A., Disklike Micelles in Water from Polyethylene-Containing Diblock Copolymers. *Macromolecules* **2011,** *44* (8), 3021-3028.

24. Puig, J.; Zucchi, I. A.; Ceolín, M.; Schroeder, W. F.; Williams, R. J. J., Evolution of morphologies of a PE-b-PEO block copolymer in an epoxy solvent induced by polymerization followed by crystallization-driven self-assembly of PE blocks during cooling. *RSC Advances* **2016,** *6* (41), 34903-34912.

25. Wang, H.; Wu, C.; Xia, G.; Ma, Z.; Mo, G.; Song, R., Semi-crystalline polymethylene-b-poly(acrylic acid) diblock copolymers: aggregation behavior, confined crystallization and controlled growth of semicrystalline micelles from dilute DMF solution. *Soft Matter* **2015,** *11* (9), 1778-1787.

26. Li, Z.; Liu, R.; Mai, B.; Feng, S.; Wu, Q.; Liang, G.; Gao, H.; Zhu, F., Synthesis and self-assembly of isotactic polystyrene-block-poly(ethylene glycol). *Polym. Chem.* **2013,** *4* (4), 954-960.

27. Venkataraman, S.; Lee, A. L.; Maune, H. T.; Hedrick, J. L.; Prabhu, V. M.; Yang, Y. Y., Formation of Disk- and Stacked-Disk-like Self-Assembled Morphologies from Cholesterol-Functionalized Amphiphilic Polycarbonate Diblock Copolymers. *Macromolecules* **2013,** *46* (12), 4839-4846.

28. Jin, X.; Zhang, C.; Lin, J.; Cai, C.; Chen, J.; Gao, L., Fusion Growth of Two-Dimensional Disklike Micelles via Liquid-Crystallization-Driven Self-Assembly. *Macromolecules* **2022,** *55* (10), 3831-3839.

29. Brisson, E. R. L.; Worthington, M. J. H.; Kerai, S.; Müllner, M., Nanoscale polymer discs, toroids and platelets: a survey of their syntheses and potential applications. *Chemical Society Reviews* **2024,** *53* (4), 1984-2021.

30. Shi, Y.; Zhu, W.; Yao, D.; Long, M.; Peng, B.; Zhang, K.; Chen, Y., Disk-Like Micelles with a Highly Ordered Pattern from Molecular Bottlebrushes. *ACS Macro Lett.* **2014,** *3* (1), 70-73.

31. Zeng, H.; Liang, X.; Roberts, D. A.; Gillies, E. R.; Müllner, M., Self‐Assembly of Rod‐Coil Bottlebrush Copolymers into Degradable Nanodiscs with a UV‐Triggered Self‐Immolation Process. *Angewandte Chemie International Edition* **2024,** *63* (13).

32. Zeng, H.; Zeng, P.; Baek, J.; Kim, B. S.; Müllner, M., Self‐Assembly of Amorphous 2D Polymer Nanodiscs with Tuneable Size, pH‐Responsive Degradation and Controlled Drug Release. *Angewandte Chemie International Edition* **2025**.

33. Zheng, Z.; Müllner, M.; Ling, J.; Müller, A. H. E., Surface Interactions Surpass Carbon–Carbon Bond: Understanding and Control of the Scission Behavior of Core–Shell Polymer Brushes on Surfaces. *ACS Nano* **2013,** *7* (3), 2284-2291.

34. Neugebauer, D.; Sumerlin, B. S.; Matyjaszewski, K.; Goodhart, B.; Sheiko, S. S., How dense are cylindrical brushes grafted from a multifunctional macroinitiator? *Polymer* **2004,** *45* (24), 8173-8179.

35. Yoshikawa, C.; Sakakibara, K.; Nonsuwan, P.; Yamazaki, T.; Tsujii, Y., Nonbiofouling Coatings Using Bottlebrushes with Concentrated Polymer Brush Architecture. *Biomacromolecules* **2021,** *22* (6), 2505-2514.

36. Takano, S.; Nishimura, T.; Cheng, Y. T.; Müllner, M., Self-Assembly of Thioether-Based Diblock Copolymers: A Comparative Study of Linear and Bottlebrush Architectures. *Polymer Chemistry* **2025**.

37. Hou, W.; Wu, J.; Li, Z.; Zhang, Z.; Shi, Y.; Chen, Y., Efficient Synthesis and PISA Behavior of Molecular Bottlebrush Block Copolymers via a Grafting-From Strategy through RAFT Dispersion Polymerization. *Macromolecules* **2023,** *56* (3), 824-832.

38. Birshtein, T. M.; Borisov, O. V.; Zhulina, Y. B.; Khokhlov, A. R.; Yurasova, T. A., Conformations of comb-like macromolecules. *Polymer Science U.S.S.R.* **1987,** *29* (6), 1293-1300.

39. Stupp, S. I., Self-assembly of rodcoil molecules. *Current Opinion in Colloid & Interface Science* **1998,** *3* (1), 20-26.

40. Modica, K. J.; Martin, T. B.; Jayaraman, A., Effect of Polymer Architecture on the Structure and Interactions of Polymer Grafted Particles: Theory and Simulations. *Macromolecules* **2017,** *50* (12), 4854-4866.

41. Theodorakis, P. E.; Hsu, H.-P.; Paul, W.; Binder, K., Computer simulation of bottle-brush polymers with flexible backbone: Good solvent versus theta solvent conditions. *The Journal of Chemical Physics* **2011,** *135* (16), 164903.

42. Anachkov, S. E.; Kralchevsky, P. A.; Danov, K. D.; Georgieva, G. S.; Ananthapadmanabhan, K. P., Disclike vs. cylindrical micelles: Generalized model of micelle growth and data interpretation. *J. Colloid Interface Sci.* **2014,** *416*, 258-273.

43. Qi, M.; Zhou, Y., Multimicelle aggregate mechanism for spherical multimolecular micelles: from theories, characteristics and properties to applications. *Materials Chemistry Frontiers* **2019,** *3* (10), 1994-2009.

44. Bolisetty, S.; Airaud, C.; Xu, Y.; Müller, A. H. E.; Harnau, L.; Rosenfeldt, S.; Lindner, P.; Ballauff, M., Softening of the stiffness of bottle-brush polymers by mutual interaction. *Physical Review E* **2007,** *75* (4).

45. Lin, T.-P.; Chang, A. B.; Luo, S.-X. L.; Chen, H.-Y.; Lee, B.; Grubbs, R. H., Effects of Grafting Density on Block Polymer Self-Assembly: From Linear to Bottlebrush. *ACS Nano* **2017,** *11* (11), 11632-11641.

46. Zhang, H.; Diesendruck, C. E., Linear versus Helical Side Chains in Bottlebrush Polymers: Morphology and Mechanochemistry. *Macromolecules* **2024,** *57* (8), 3664-3670.

47. Sunday, D. F.; Burns, A. B.; Martin, T. B.; Chang, A. B.; Grubbs, R. H., Relationship between Graft Density and the Dilute Solution Structure of Bottlebrush Polymers: An Inter-chemistry Comparison and Scaling Analysis. *Macromolecules* **2023,** *56* (18), 7419-7431.

48. Zhulina, E. B.; Sheiko, S. S.; Borisov, O. V., Theoretical advances in molecular bottlebrushes and comblike (co)polymers: solutions, gels, and self-assembly. *Soft Matter* **2022,** *18* (46), 8714-8732.

49. Ulrich, H. F.; Gruschwitz, F. V.; Klein, T.; Ziegenbalg, N.; Anh, D. T. N.; Fujii, S.; Hoeppener, S.; Sakurai, K.; Brendel, J. C., Influence of Polymer Side Chain Size and Backbone Length on the Self‐Assembly of Supramolecular Polymer Bottlebrushes. *Chemistry – A European Journal* **2024,** *30* (26).

50. Panyukov, S.; Zhulina, E. B.; Sheiko, S. S.; Randall, G. C.; Brock, J.; Rubinstein, M., Tension Amplification in Molecular Brushes in Solutions and on Substrates. *The Journal of Physical Chemistry B* **2009,** *113* (12), 3750-3768.

51. Pan, X.; Ding, M.; Li, L., Experimental Validation on Average Conformation of a Comblike Polystyrene Library in Dilute Solutions: Universal Scaling Laws and Abnormal SEC Elution Behavior. *Macromolecules* **2021,** *54* (23), 11019-11031.

52. Xiao, L.; Li, J.; Peng, G.; Huang, G., The effect of grafting density and side chain length on the conformation of PEG grafted bottlebrush polymers. *Reactive and Functional Polymers* **2020,** *156*, 104736.

53. Christie, D.; Register, R. A.; Priestley, R. D., Direct Measurement of the Local Glass Transition in Self-Assembled Copolymers with Nanometer Resolution. *ACS Central Science* **2018,** *4* (4), 504-511.

54. Kaya, İ.; Pala, Ç. Y., Thermodynamics of poly(benzyl methacrylate)–probe interactions at different temperatures by using inverse gas chromatography. *Fluid Phase Equilibria* **2014,** *374*, 63-69.

55. Burel, F.; Rossignol, L.; Pontvianne, P.; Hartman, J.; Couesnon, N.; Bunel, C., Synthesis and characterization of poly(ethyl glyoxylate) – a new potentially biodegradable polymer. *e-Polymers* **2003,** *3* (1).

56. Song, J.; Hwang, E.; Lee, Y.; Palanikumar, L.; Choi, S.-H.; Ryu, J.-H.; Kim, B.-S., Tailorable degradation of pH-responsive all polyether micelles via copolymerisation with varying acetal groups. *Polymer Chemistry* **2019,** *10* (5), 582-592.

57. Zhuang, Z.; Cai, C.; Jiang, T.; Lin, J.; Yang, C., Self-assembly behavior of rod–coil–rod polypeptide block copolymers. *Polymer* **2014,** *55* (2), 602-610.

58. Lebedeva, I. O.; Zhulina, E. B.; Borisov, O. V., Self-Assembly of Bottlebrush Block Copolymers in Selective Solvent: Micellar Structures. *Polymers* **2021,** *13* (9), 1351.

59. Zhang, J.; Song, Q.; Peng, L.; Huang, X.; Li, W., Square Array of Cylinders Formed in Linear–Bottlebrush–Linear Triblock Copolymers. *Macromolecules* **2025,** *58* (8), 4112-4121.

60. Sánchez-Leija, R. J.; Mysona, J. A.; De Pablo, J. J.; Nealey, P. F., Phase Behavior and Conformational Asymmetry near the Comb-to-Bottlebrush Transition in Linear-Brush Block Copolymers. *Macromolecules* **2024,** *57* (5), 2019-2029.

61. Perales Rodriguez, C.; Mahanthappa, M. K.; Lodge, T. P., Lyotropic Phase Behavior of Coil-Bottlebrush Diblock Copolymers in Alkylimidazolium-Based Ionic Liquids. *Macromolecules* **2024,** *57* (7), 3081-3089.

62. Mikhailov, I. V.; Zhulina, E. B.; Borisov, O. V.; Nardin, C.; Darinskii, A. A., Architectural control over morphologies of bottlebrush block copolymer superstructures. *AIP Advances* **2023,** *13* (12).

63. Liberman, L.; Coughlin, M. L.; Weigand, S.; Edmund, J.; Bates, F. S.; Lodge, T. P., Impact of Side-Chain Length on the Self-Assembly of Linear-Bottlebrush Diblock Copolymers. *Macromolecules* **2022,** *55* (12), 4947-4955.

64. Vu, C.; Abu Amara, N.; Alaboalirat, M.; Nativ-Roth, E.; Zalk, R.; Leite, W.; Carrillo, J.-M.; Bitton, R.; Matson, J., Aqueous self-assembly of cylindrical and tapered bottlebrush block copolymers. American Chemical Society (ACS): 2025.

7. Supporting Information

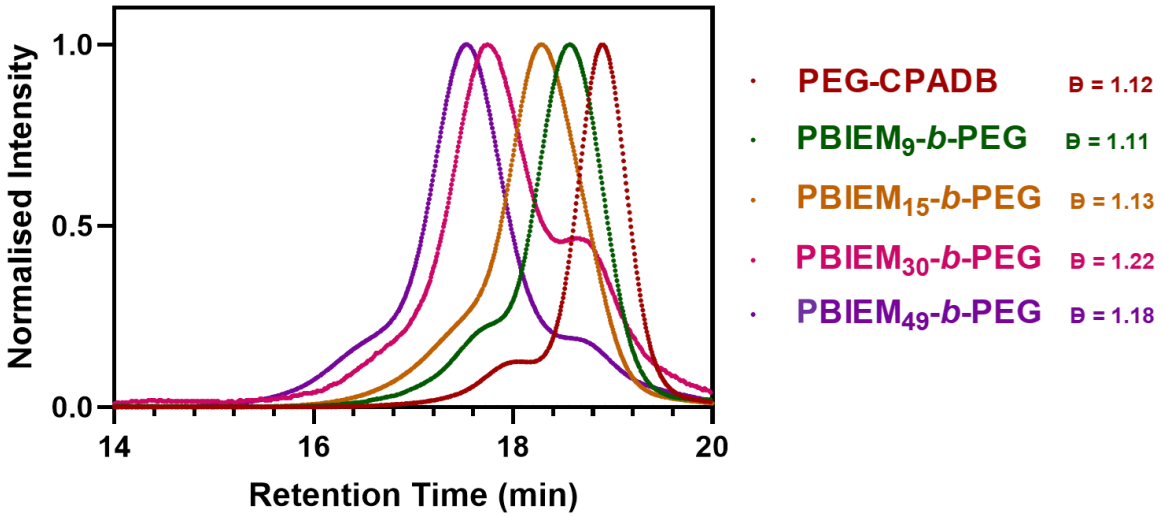

Figure S2.2. AFM of particles self-assembled from $TP_{49\text{-}79}$ (A) 2D Height map (B) Corresponding particle height plots.

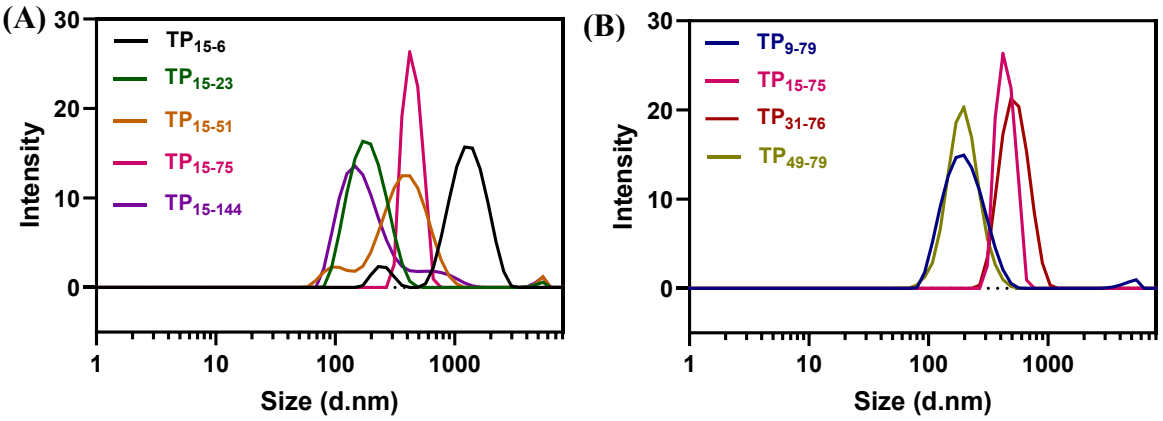

Figure S2.3. Overlapped hydrodynamic DLS intensity traces of **(A)** $TP_{15\text{-}Y}$, **(B)** $TP_{X\text{-}75}$.

Chapter III: Co Self-Assembly of Bottlebrush-Linear Block Copolymers into Stimuli-Responsive Discoidal Nanoparticles

1. Abstract

Co-assembly approaches of copolymer systems are gaining significant attention as a means of controlling particle morphology, size and stability, whilst simultaneously offering avenues to include multiple functionalities in single nanoparticles. However, these approaches are often limited by the incompatibility of competing polymer chemistries. Herein we employ two chemically distinct linear-bottlebrush block copolymer architectures, namely poly(ethylene glycol)-*block*-[poly(3-azido-2-hydroxypropyl methacrylate)-*graft*-poly(ethyl ethoxylate)] and poly(ethylene glycol)-*block*-[poly(2-(2-bromo isobutyryloxy)ethyl methacrylate)-*graft*-poly(benzyl methacrylate), that have previously been shown to self-assemble into discoidal nanoparticles. By comparing their co-assembly in binary blends of different compositions, we show that continuous phase discoidal particles can be achieved across the board. Furthermore, we show how their molecular reorganisation at acidic pH is dependent on their composition, postulating the ability of co-assembled materials to retain structure upon stimulus exposure. This work serves as a proof-of-concept study that bottlebrush-linear block copolymers can overcome limitations of block copolymer self-assembly towards advanced stimuli-responsive materials for wide applications.

2. Introduction

The incorporation of stimuli-responsiveness into 2D nanomaterials through functional polymer systems transforms these morphologies into sophisticated, dynamic platforms suitable for diverse applications.[1] While single-component block copolymer systems have been extensively explored across various morphologies, multi-component copolymer self-assembly remains underutilised despite its potential to expand self-assembled materials toward functional integration, property tuning, and responsive behaviour.

Stimuli-responsive polymers constitute powerful functional materials capable of rapid conformational changes upon alteration of environmental conditions including temperature,[2] pH,[3, 4] or ionic strength.[5, 6] These dynamic materials enable programmable responses and adaptive behaviour, establishing them as essential components in smart material systems. However, a fundamental limitation lies in their propensity toward structural instability upon activation. Functional systems induce disruption of intra- and intermolecular interactions, causing chain collapse or expansion, creating instability and subsequent morphology switching. These structural instabilities present critical challenges for applications requiring consistent morphological properties.

While such instabilities can occasionally be harnessed as functional features, many responsive polymers undergo complete structural reorganisation upon activation, representing conventional all-or-nothing systems that compromise morphological advantages.

Strategic integration of stimuli-responsive elements with morphologically stable components within co-assembled architectures offers a promising approach to overcome these structural limitations. Rather than relying solely on responsive polymers that compromise structural integrity, co-assembly approaches can introduce selective responsiveness while maintaining

overall morphological stability through structural elements that are not responsive to the same stimulus. The fundamental challenge in such multi-component co-assembly lies in achieving controlled integration while maintaining morphological precision.

Most current supramolecular co-assembly approaches employ systems with chemically similar polymers of different architectures to control morphology and size.[7] Alternatively, polymers are co-assembled with other materials such as nanoparticles, proteins or additives,[8] with potential to lower critical micelle concentrations and improve stability.[9] In some cases, linear diblock copolymers blends such as AB/AC or AB/CD have also been explored to determine their spatial arrangement in tuned morphologies.[10] The co-assembly of chemically distinct polymers, combining stimuli-responsive and non-responsive components, offers a compelling extension towards functional materials. This approach provides unique advantages through independent component optimisation, post-assembly modification capabilities, and dynamic reconfiguration in response to environmental factors. Despite the conceptual appeal and potential of multi-component co-assembly, significant fundamental questions remain regarding principles governing successful integration, factors controlling spatial organisation, and mechanisms of selective responsiveness. The complex interplay between enthalpic interactions, entropic effects, kinetic barriers, and external stimuli requires systematic investigation to establish predictive design frameworks essential for rational system design.

Polymer nanodiscs are highly sought after 2D nanomaterials with exceptional potential owing to their high surface-area-to-volume ratio, anisotropic properties, and tuneable functionality.[11] For discoidal nanostructures, maintaining the high surface-area to volume ratio and anisotropic properties during stimuli response becomes particularly challenging as polymer packing behaviour is disrupted. This chapter investigates the co-assembly of stimuli-responsive and non-responsive disc-forming block copolymers as a model system for understanding multi-

component assembly principles. As a proof-of-concept study, we demonstrate the viability and advantages of this approach through systematic investigation of pH-responsive and chemically inert polymer co-assembly. By varying component ratios, we establish the ability to create stable discoidal nanoparticles with tuneable responsive characteristics while maintaining morphological integrity.

Our approach reveals that controlled co-assembly preserves beneficial morphological characteristics while introducing selective functionality through strategic component integration. This work establishes fundamental principles for multi-component co-assembly while demonstrating practical strategies for creating nanostructures with spatially differentiated properties and programmable environmental responses. The findings transform the traditional trade-off between responsiveness and stability into a design opportunity, providing a foundation for next-generation smart materials that harness the benefits of both responsive and non-responsive components within unified, morphologically preserved nanostructures for applications such as triggered drug delivery, tissue engineering scaffolds, and theranostics.[12]

3. Experimental Section

3.1 Materials

Poly(ethylene glycol) methyl ether 5000 (mPEG 5K), 4-cyano-4-(phenylcarbanothio) pentanoic acid (CPADB, 99 %), anhydrous dichloromethane (DCM, ≥99.8%), N-ethyl-N′-(3-dimethylaminopropyl)carbodiimide hydrochloride (EDC·HCl, 98%), 2-hydroxyethyl methacrylate (HEMA, 97%), α-bromoisobutyryl bromide (98%), N,N,N′,N″,N″-pentamethyldiethylenetriamine (PMDETA, 99%), N,N'-azobis(isobutyronitrile) (AIBN, 98%), anisole (99%), mesitylene (98%) and copper(I) bromide (CuBr, 98%) were purchased from Sigma-Aldrich. N,N-dimethylaminopyridine (DMAP, ≥99%), tetrahydrofuran (THF), petroleum benzine (b.p. 40-60°C), and diethyl ether were sourced from Merck. Pyridine (99%) and magnesium sulphate ($MgSO_4$) were purchased from Ajax. Dimethyl formamide (DMF, 99.8% by gas chromatography (GC)) was sourced from RCI LabScan. Ethyl ethoxylate side chains were received from the Kim Group. PEE_{28} tadpole was synthesised by Ping Zeng. Benzyl methacrylate (BzMA, 98%) was sourced from Tokyo Chemical Industry Chemicals. AIBN was recrystallised from ethanol prior to use. Ethanol was dried with 4Å molecular sieves before use. HEMA and BzMA were filtered through a short basic aluminium oxide column to remove inhibitors. All other chemicals were used as received.

3.2 Methods

Synthesis of PEG-CPADB (macroCTA)

PEG5K (2g, 0.4mmol, 1 mol equiv.) and CPADB (167.6 mg, 0.6 mmol, 1.5 mol equiv.) were charged into a dry round bottom flask with anhydrous DCM (10mL) and stirred over ice. In a separate vial, DMAP (11.73 mg, 0.1 mmol, 0.24 mol equiv.) and EDC.HCl (11.5 mg, 0.6 mmol, 1.5 mol equiv.) were dissolved in anhydrous DCM (5mL). The contents of this vial was then added dropwise to the reaction vessel under vigorous stirring over ice. The reaction was stirred

on ice for a further 10 minutes, before reacting overnight at room temperature. The synthesised macroCTA was recovered by precipitation in cold diethyl ether three times, redissolving in DCM to remove unreacted small molecules. The crude product was then washed three times with DI water to remove unreacted PEG-OH. The pink organic solution was dried over anhydrous $MgSO_4$ before being concentrated under vacuum into a dark pink solid, and lypholised into a light pink powder. The macroCTA was stored at -20 ˚C in an airtight foiled vial.

Scheme S3.1: Synthesis of PEG_{114}-CPADB macro-RAFT agent.

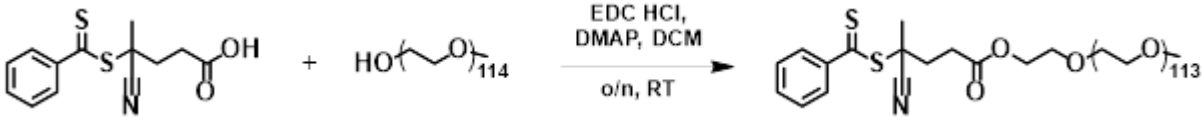

Synthesis of PEG-*block*-PHEMA$_{15}$

PEG-CPADB (500 mg, 0.95 mmol, 1 mol equiv.), HEMA (231.17 µL, 1.9 mmol, 20 mol equiv.), and AIBN (3.1 mg, 0.19 mmol, 0.2 mol equiv.) were charged to a vial in anhydrous EtOH (3.63 mL) with mesitylene (100 µL) as an internal standard. A time sample (t0) was taken and analysed by ^{1}H NMR. The vial was equipped with a stirrer bar and the solution bubbled with N_2 to degas for 30 minutes before reacting at 70℃ for 5 hours. A further time sample (t5) was taken and analysed using ^{1}H NMR to find the degree of polymerisation of the PHEMA block. The resulting polymer was recovered by precipitation in diethyl ether, redissolving in methanol three times over. The product was then lypholised to give a pink powder. The product was characterised by ^{1}H NMR (300 MHz, MeOD, δ, ppm) and SEC (DMAc/LiBr, 50 °C, PMMA).

Scheme S3.2. Synthesis of $PHEMA_{15}$-*block*-PEG_{114} via RAFT polymerisation

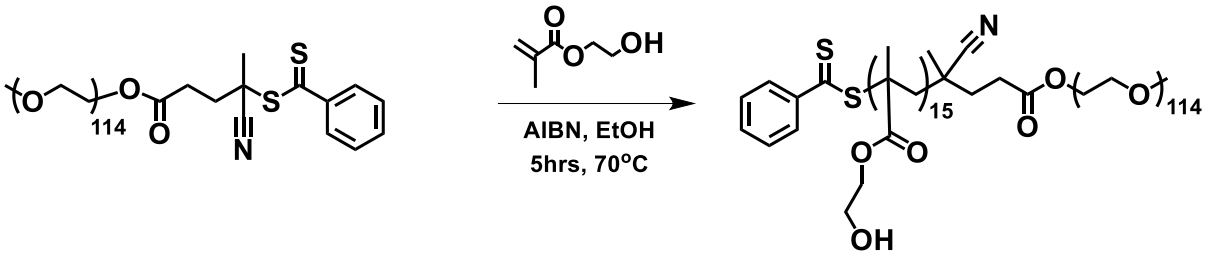

Synthesis of PEG-*block*-$PBIEM_{15}$

PEG-*block*-$PHEMA_{15}$ (140.6 mg, 8.12 mmol, 20 mol equiv. of -OH units) and Pyridine (306.7 µL, 3.81 mmol, 10 mol equiv. per -OH unit) were dissolved in anhydrous THF in a round-bottom flask and stirred on ice. α-BiBB (188.2 µL, 1.52 mmol, 4 mol equiv. per -OH unit) was added dropwise by syringe to the flask over 5 minutes. The reaction continued to stir over ice for 10 minutes, before reacting overnight at room temperature. The solution was passed through gravitational filtration to remove formed pyridinium salts and washed with THF before being concentrated by rotary evaporation. The resulting polymer was recovered by precipitation in hexane three times, redissolving in THF. Finally, the polymer was subject to dialysis in deionised water to remove residual pyridine for a few hours, and subsequently lypholised to give a pale pink powder. . The product was characterised by ^{1}H NMR (300 MHz, $CDCl_3$, δ, ppm) and SEC (DMAc/LiBr, 50 °C, PMMA).

Scheme S3.3. Synthesis of $PBIEM_{15}$ -*block*-PEG_{114}

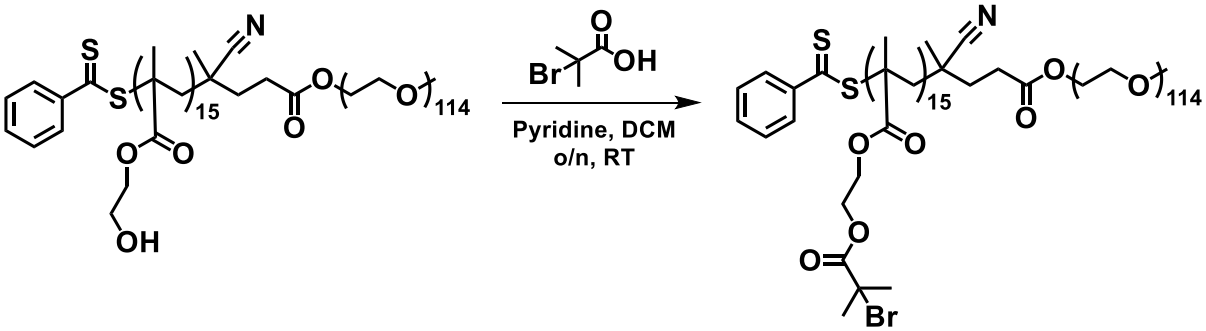

Synthesis of PEG-*block*-($PBIEM_{15}$-*graft*-($PBzMA_{75}$))

PBIEM-*block*-PEG (10 mg, 15.6 µmol, 15 mol equiv. of -Br units), BzMA (769 µL, 4.56 mmol, 120 mol equiv. per -Br unit), PMDETA (5.14 µL, 0.18 mmol, 5 mol equiv. per -Br unit), and mesitylene (100 µL) as an internal standard were dissolved in anisole (3.18 mL) in a Schlenk

flask. After removal of an aliquot to monitor conversion, the vessel was subject to three *freeze-pump-thaw* cycles, with addition of CuBr (6.19 mg, 62.6 μmol, 2 mol equiv. per -Br unit) prior to the last cycle. The flask was backfilled by bubbling nitrogen gas, and then reacted at 70 ℃ for 2.5 hrs. An aliquot was taken to determine monomer conversion. The solution was run through a short neutral alumina column to remove copper catalyst, and anisole removed under nitrogen flow. The polymer was redissolved in DMF and purified by precipitation in diethyl ether three times. The resulting pellet was redissolved in minimal DMF and solid content determined. The product was characterised by ^{1}H NMR (300 MHz, $CDCl_3$, δ, ppm) and SEC (DMAc/LiBr, 50 °C, PMMA).

Scheme S3.4. Synthesis of ($PBIEM_{15}$-*graft*-$PBzMA_{75}$)-*block*-PEG_{114} using grafting-from approach with ATRP

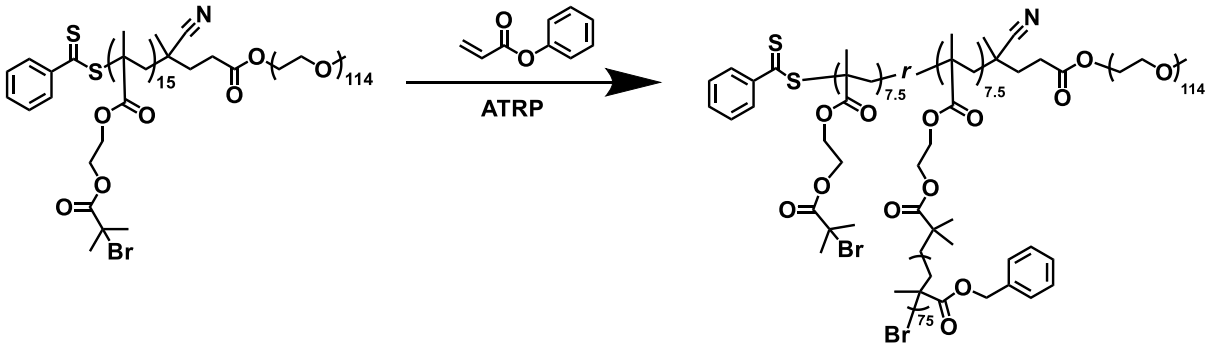

Self-Assembly of tadpoles

A 2mg/mL polymer solution in DMF (unless stated otherwise) was prepared and transferred into a vial capped with a dialysis membrane (MWCO 3500 Da). The solution was dialysed against DI water for 2 days, replacing the DI water twice a day. The resulting solution was collected and analysed by DLS and various microscopy techniques.

Disassembly of self-assembled particles

500 μL of self-assembled particle solution was transferred into a vial capped with a dialysis membrane (MWCO 3500 Da). The solution was dialysed against 0.1 M sodium acetate buffer

(pH ~3.6) for 1 day, replacing the buffer twice a day. The resulting solution was then charged with a stirrer bar and stirred at 300 rpm and analysed by DLS and various microscopy techniques on days recorded.

Nuclear magnetic resonance (NMR) spectroscopy

NMR spectra were recorded at the University of Sydney using Bruker NEO 300 MHz NMR spectrometers. ^{1}H NMR measurements were carried out using a zg pulse program (90° pulse) with a recycle delay (D1) of 2-5 s. ^{1}H NMR spectra are referenced to the residual solvent peak for $CDCl_3$ (δ 7.26 ppm), or MeOD (δ 3.31 ppm) as appropriate. Deuterated solvents were obtained from Sigma Aldrich and used without any further purification.

Size exclusion chromatography (SEC)

SEC was performed using a Shimadzu Prominence UFLC (ultra-fast liquid chromatography) system fitted with a Shim-pack GPC-800DP guard column followed by two in-series Phenogel columns (5 μm, 104 Å and 105 Å). The system eluent was HPLC grade dimethyl acetamide (DMAc) containing LiBr (0.03 wt%) and BHT (each at 0.05 wt%), eluting at a flow rate of 1 mL/min. The column assembly was incubated at 50 °C, and retention times were calibrated using narrow PMMA standards from PSS.

Atomic Force Microscopy (AFM)

AFM was performed in air using a Multimode 8 with NanoScope V controller (Bruker) in standard tapping-mode (Tap300Al-G cantilevers, 300 kHz, 30 Nm-1, Budget Sensors). Samples were prepared by drop-casting method, depositing 10 μL of aqueous self-assembly dispersion onto a tiled silicon wafer previously cleaned by CO_2 blast. The droplet was let to run for the length of the wafer before being dried under light nitrogen flow. Image analysis was performed on Bruker's Nanoscope Analysis software.

Dynamic light scattering (DLS)

DLS measurements were performed on a Malvern Zetasizer Ultra equipped with a He-Ne (633 nm) laser. The hydrodynamic diameters of polymer self-assembly samples were directly measured on DLS without any further treatment.

Transmission Electron Microscopy (TEM)

TEM observations were performed using the JEM-1400 (JEOL, Japan) with a beam acceleration of 120 kV. Sample solutions were adjusted to 0.5 g/L, and a 10 μL droplet placed on parafilm. A carbon-coated Cu grid (ProSciTech, Australia) was hydrophilised by GloQube Plus (Quorum), using a 25mA plasma current for 30 seconds. The hydrophilised grid was placed onto the sample droplet for 10 minutes prior to removal of excess solution with a filter paper. The samples were then stained using 10 μL of 2% uranyl acetate (UA) solution. First, UA solution was dropped on a parafilm to form a droplet. The grid was then stained for 30 seconds by inverting the grids on the droplet. After removing the UA solution with a filter paper, the grid was left to dry in the air.

4. Results and Discussion

4.1 Bottlebrush-Linear Block Copolymer Characterisation

Two bottlebrush-linear block copolymers were synthesised by varying approaches. Poly(ethylene glycol)$_{114}$-*block*-[poly(2-(2-bromo isobutyryloxy)ethyl methacrylate)$_{15}$-*graft*-poly(benzyl methacrylate)$_{75}$ (PEG$_{114}$-*b*-[PBIEM$_{15}$-*g*-PBzMA$_{75}$]) was synthesised using a grafting-from approach, whereby the high glass transition temperature (T_g) side chains were grown from a polyinitiator backbone bearing bromide units to undergo atom transfer radical polymerisation (ATRP). Side chain lengths were determined by ^{1}H NMR end group analysis, with comparison of the integration of the CH_2 of the benzyl group at $\delta \sim 4.75$ ppm to the repeating $(CH_2)_2$ PEG signal at $\delta \sim 3.55$ ppm (Figure 3.1B) under the assumption of 50% grafting efficiency.[13, 14]

Alternatively, poly(ethylene glycol)$_{114}$-*block*-[poly(3-azido-2-hydroxypropyl methacrylate)$_{20}$-*graft*-poly(ethyl ethoxylate)$_{28}$] (PEG$_{114}$-*b*-[PGMA-N3$_{20}$-*g*-PEE$_{28}$]) was received having been synthesised using a grafting-to approach of the low T_g PEE$_{28}$ side chains onto an amphiphilic backbone through CuAAC click chemistry. The grafting density was confirmed to be 75% by ^{1}H NMR analysis comparing pre- and post- side chain grafting. The ^{1}H NMR of the block copolymer is included in Figure 4.1B. Herein, these bottlebrush-linear block copolymers will be referred to as 'tadpoles' with the codes TP$_{BzMA}$ and TP$_{EE}$ respectively. These tadpole systems are summarised in Table 4.1.

Table 4.1. Characterisation data of PEG$_{114}$-*block*-bottlebrush block copolymer library

BBCPs	DP$_{PEG}$	DP$_{Backbone}$	DP$_{Side\ Chains}$	Grafting Density	[a]$f_{(hydrophobic)}$	[b]$M_{n,NMR}$	[c]$Đ_{SEC}$
TP$_{BzMA}$	114	15	75	0.5	0.91	99 100	1.11
TP$_{EE}$	114	20	28	0.75	0.86	55 400	1.22

[a] Ratio of PEG:Side Chain repeat units, [b]Determined by ^{1}H NMR analysis, [c]Determined by SEC (M_w/M_n).

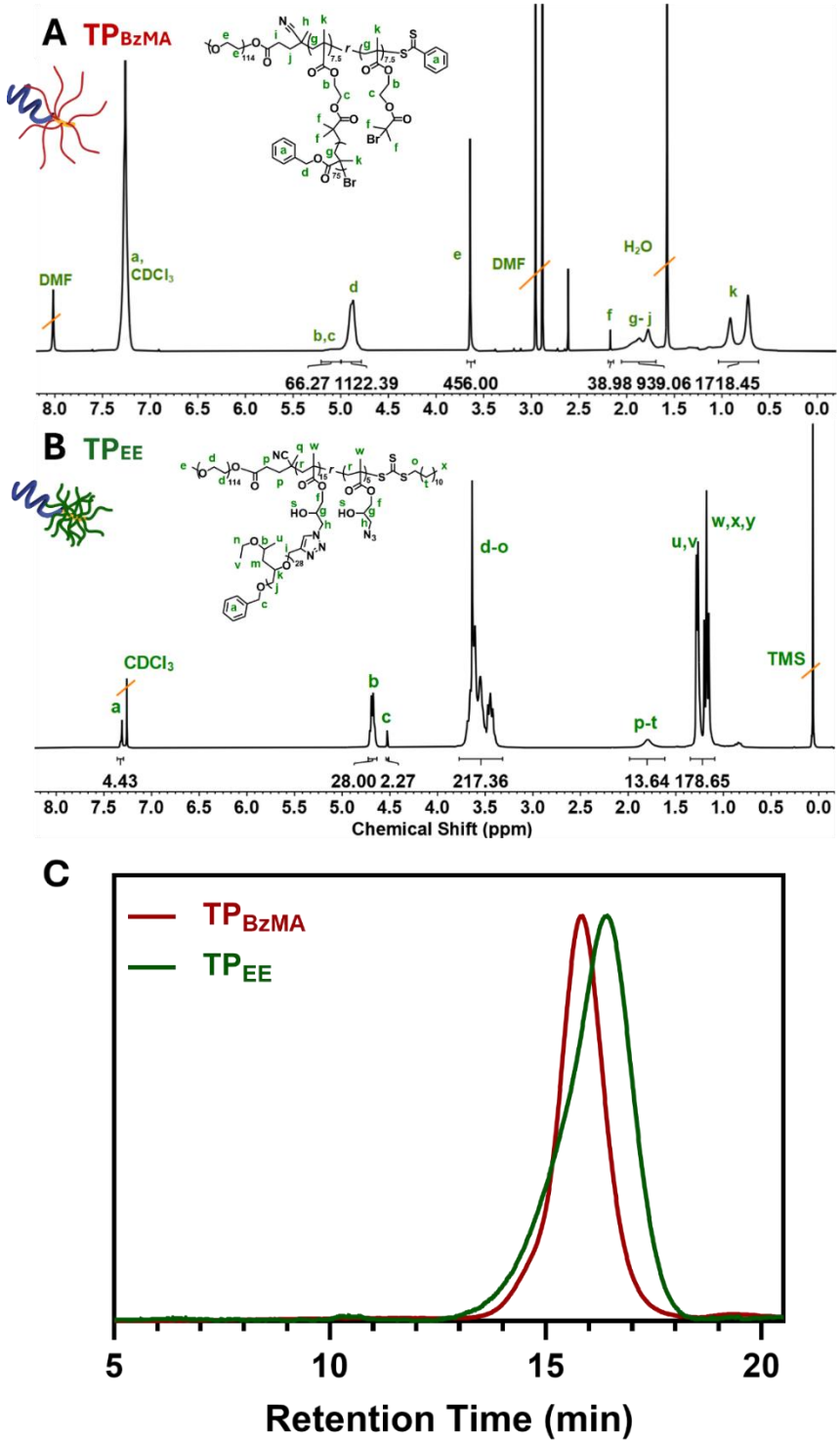

Figure 3.1. Characterisation data of block copolymers (A) ^{1}H NMR of PEG$_{114}$-*b*-[PBIEM$_{15}$-*g*-PBzMA$_{75}$] (300 MHz, $CDCl_3$)), (B) ^{1}H NMR of PEG$_{114}$-*b*-[PGMA-N3$_{20}$-*g*-PEE$_{28}$] (300 MHz, $CDCl_3$)), (C) SEC chromatogram of PEG$_{114}$-*b*-[PBIEM$_{15}$-*g*-PBzMA$_{75}$] (red) and PEG$_{114}$-*b*-[PGMA-N3$_{20}$-*g*-PEE$_{28}$] (green) in DMAc (50 °C and 1 mL min^{-1})

4.2 Bottlebrush-Linear Block Copolymer Co-Assembly & Disassembly

This study explores the co-assembly of different polymeric tadpole architectures. TP_{EE} analogues have previously been investigated as a pH-responsive material for drug delivery applications.[15] To investigate the generalisability of functional self-assembled systems and explore potential synergistic effects in mixed systems, this study examined the co-assembly of TP_{EE} with a chemically distinct core-forming block. TP_{BzMA} was selected as the co-assembly partner to provide maximum contrast in core properties with a significantly different glass transition temperature and absence of stimuli-responsiveness, whilst maintaining identical corona-forming blocks to isolate the effects of core chemistry on particle formation. Both TP_{EE} and TP_{BzMA} self-assemble into discoidal particles when individually processed using the solvent switch method, starting with polymer solutions in DMF being dialysed against deionised water at a total polymer concentration of 2 mg/mL. The individual systems form well-defined discoidal nanoparticles with deflated heights of ~7nm and ~5nm respectively by AFM (Figure 3.2). By diameter, these discoidal assemblies measure between ~200 – 300 nm and ~50 – 200 nm respectively by TEM (Figure 3.3A & 3.3E).

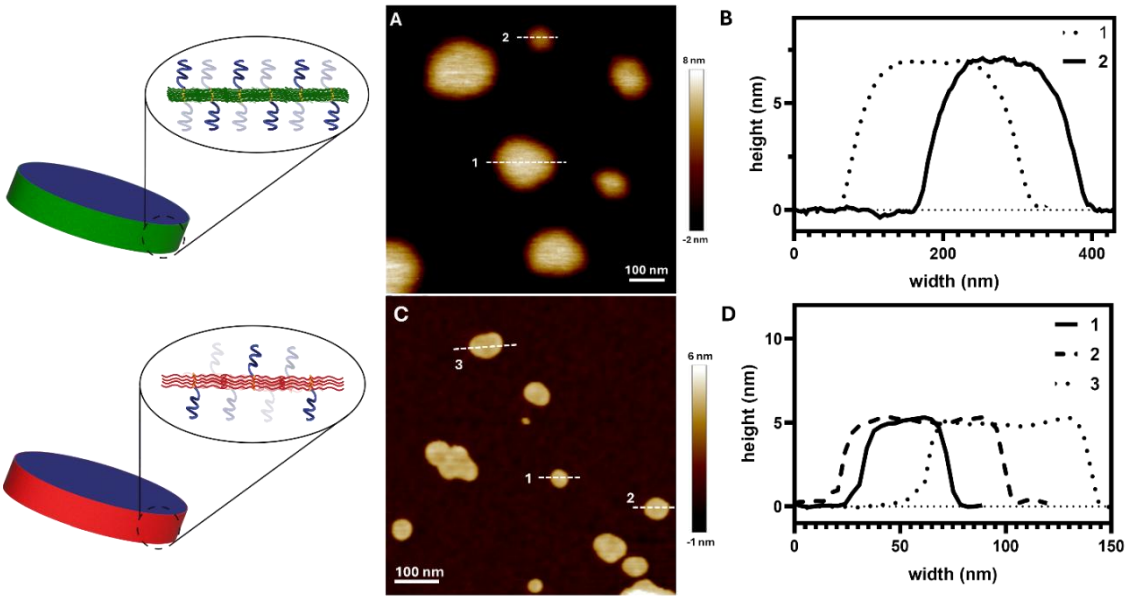

Figure 3.2. (left) Schematic representation of tadpole packing into self-assembled particles. (right) AFM micrographs of discoidal particles of (A) TP_{EE} and (C) TP_{BzMA} with (B) & (D) corresponding height maps respectively.

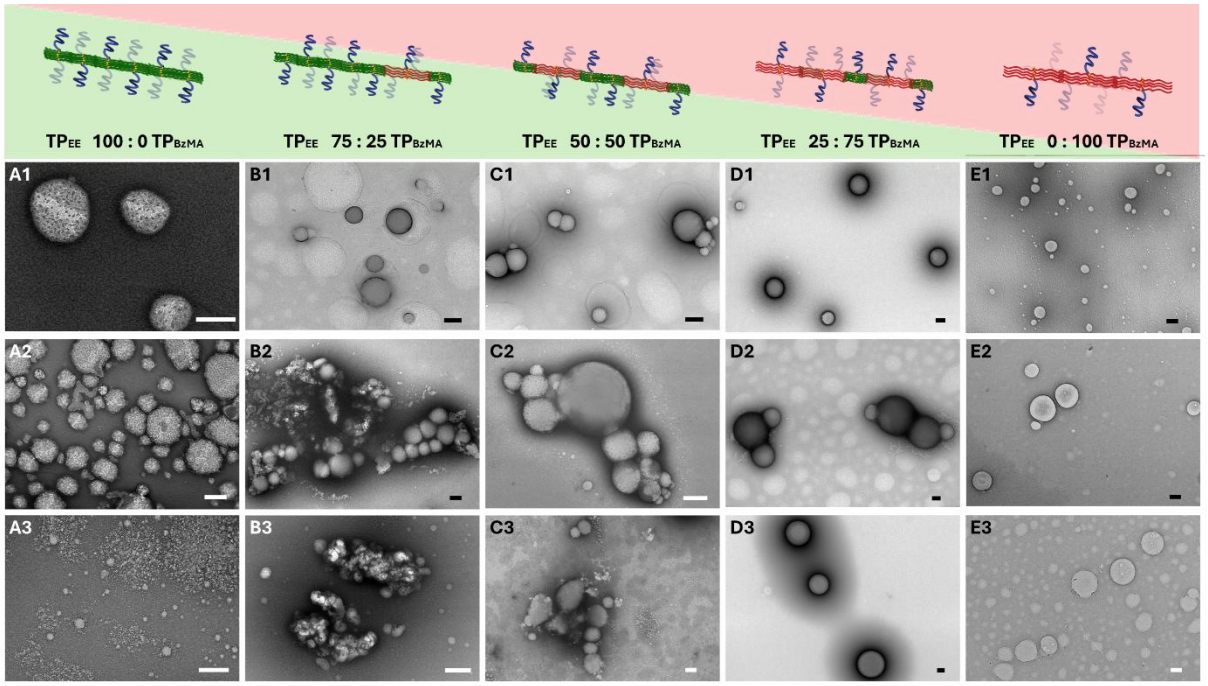

Figure 3.3. (top) Schematic representation of self-assembled particles from co-assembly of TP_{EE} (green) and TP_{BzMA} (red). (bottom)TEM micrographs of self-assembled and disassembled particles from the co-assembly of TP_{EE} : TP_{BzMA} in the ratios of (A) 100:0, (B) 25:75, (C) 50:50, (D) 25:75, (E) 0:100 and their treatment under acidic conditions for (A2,B2,C2,D2,E2) 5 days and (A3,B3,C3,D3,E3) 10 days. All scale bars for 200 nm.

The successful formation of discoidal particles by both tadpole structures has been previously attributed to the geometric constraints introduced by inter side chain repulsion that rigidifies the core-forming segments.[15, 16] Furthermore, both tadpoles maintain adequate lengths of hydrophilic linear PEG blocks to stabilise planar structures.[17] Despite their similar geometry, the appearance of these particles varies greatly. The distinct surface morphologies observed in AFM reflect the fundamental differences in glass transition temperatures between the core-forming polymers. The grainier phase appearance of TP_{EE} particles (Figure S3.1A) may correlate to the low T_g based off a similar system (T_g ~ -59 ℃)[18], where the assembly temperature at room temperature is well above the T_g, creating a more liquid-like core with higher chain mobility. In contrast, TP_{BzMA} particles exhibit smoother phase (Figure S3.1B). Because the assembly temperature is well below the T_g of BzMA side chains (T_g ~ 54 ℃),[19] creating a more rigid, glassy core with restricted chain dynamics,[20] similar to other high T_g systems.[21] By TEM this difference is observed as a 'dotty indented' surface that could stem from staining artefacts and a smooth surface respectively (Figure 3.3A & Figure 3.3B).

In an effort to extend the understanding of their self-assembly behaviour, we pursued the co-assembly of these chemically distinct tadpoles to determine their synergistic morphological effects. Upon co-assembly of TP_{EE} and TP_{BzMA} at different weight ratios while maintaining 2 mg/mL final polymer concentration, the apparent size by TEM and hydrodynamic diameter by DLS (Figure S3.2A) increase significantly compared to the individual components. The most pronounced size increase is observed in intermediate blend ratios, particularly evident in the 75:25 and 25:75 EE:BzMA compositions, consistent with mixed micelle systems where cooperative effects lead to larger aggregation numbers.[22, 23] Despite these size changes, discoidal morphology is maintained across all composition ratios as confirmed by TEM and AFM analysis. This is evidenced by seemingly flat, consistent phased particles by TEM (Figure 3.3). Additionally, all systems resulted in particles with deflated heights between 5-7 nm by

AFM (Figure 3.4A-B, 3.5A-B, 3.6A-B), consistent with the heights of discoidal particles from individual tadpole self-assembly (Figure 3.2). In some cases, a stacking effect can be observed (Figure 3.6), consistent with previous observations, where features of 10-12nm in height corresponding to two particles stacked in the drying process.[17] Where co-assembly strategies have previously shown that resulting particle geometries are a mix of the molecular geometry of the individual building blocks,[24-26] it is expected that the blends of these bottlebrush block copolymers (BBCPs) with sufficient packing parameter to achieve discs, will also result in discs.

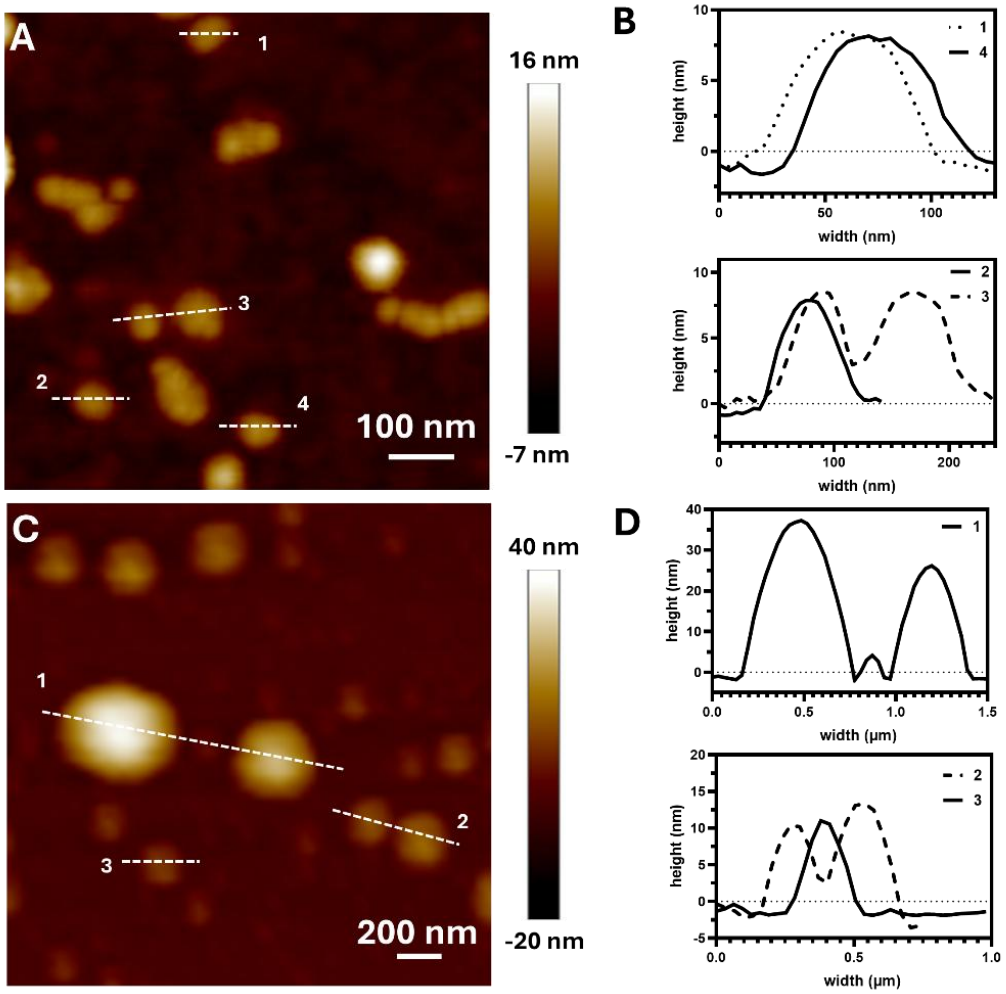

Figure 3.4. AFM micrographs of self-assembled particles from TP_{EE} 25:75 TP_{BzMA} with (B) corresponding height map and (C) after treatment at pH 3.6 with (D) corresponding height maps.

Interestingly, there is no evidence of phase separation into Janus-type particles or coexistence of two distinct morphologies in contrast to expectations for polymer blends with significant chemical incompatibility.[27] Instead, the co-assembled morphologies show evidence of continuous phase formation, indicating molecular-level integration rather than typical macroscopic phase separation.[28] Particles with greater composition of low T_g TP_{EE} appear grainier in AFM, and in TEM show dotted surfaces that reduce with TP_{EE} composition. In contrast, samples with higher TP_{BzMA} content appear less dotted by TEM and smoother (Figure 3.3). Another interesting observation is the increase in particle size in the co-assembled systems, similar to hierarchical structures from other mixed polymer systems.[29] This may speak to an interesting packing behaviour of the two incompatible core-forming blocks that can be investigated further through the inclusion of chromophores or fluorescent labelling in selective building blocks. Via this approach, compositional analysis of particles could also be investigated.

The mixed particle formation likely occurs through cooperative assembly mechanisms where both polymers contribute to the formation of hybrid structures. This is also supported by the absence of discrete particle populations. Wang et al. propose that the interactions of two block copolymers is dependent on both the intramolecular segregation of the hydrophilic and hydrophobic blocks, and the intermolecular repulsion between the different copolymers.[30] Given that this was described in a linear system, we postulate that the segregation degree of linear-brush tadpole architecture may play a large role in the mixing mechanism in the self-assembly process, altering the interplay of these contributing factors. To this effect, the identical PEG_{5000} corona blocks likely helps minimises interfacial energy penalties that typically drive phase separation in mixed micelle systems.[31] This design consideration creates a buffer that allows the chemically distinct core-forming segments to coexist within unified micellar structures. In addition, the mobility of bottlebrush segments in their collapsed state

would be significantly reduced, limiting opportunities to phase separate. Instead, the volume fraction of the BBCPs dictates the morphologies with both polymers co-existing in a connected network, as the entropic mixing gains provide a driving force for co-assembly that overcomes the enthalpic penalty from core block incompatibility.[32] Linear terpolymer systems maintaining the same corona-forming blocks with varying hydrophobic segments were also co-assembled by Cui et al. to assess their intermolecular mixing.[33] Whilst it must be noted that small molecule additives were involved to induce aggregation of one block and limit their mobility, the phenomena of two unlikely blocks co- existing in micelle cores is analogous to the system presented here. They postulate that this mixed micelle is in a non-equilibrium state, instead governed by kinetic factors.

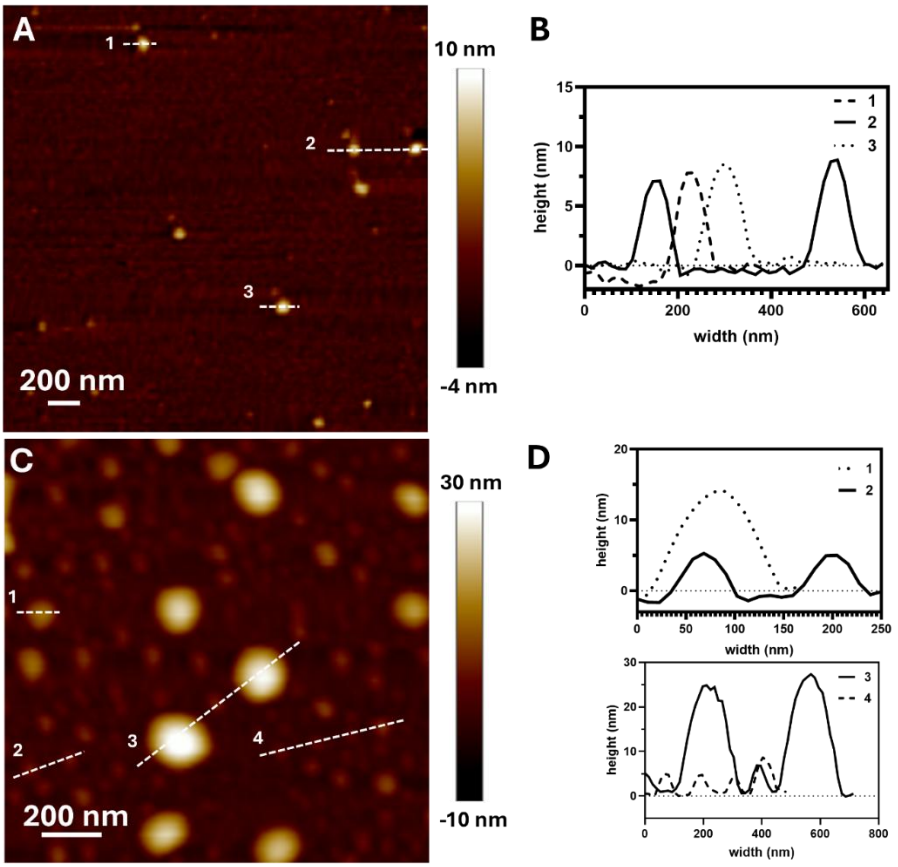

Figure 3.5. AFM micrographs of self-assembled particles from TP_{EE} 50:50 TP_{BzMA} with (B) corresponding height map and (C) after treatment at pH 3.6 with (D) corresponding height maps.

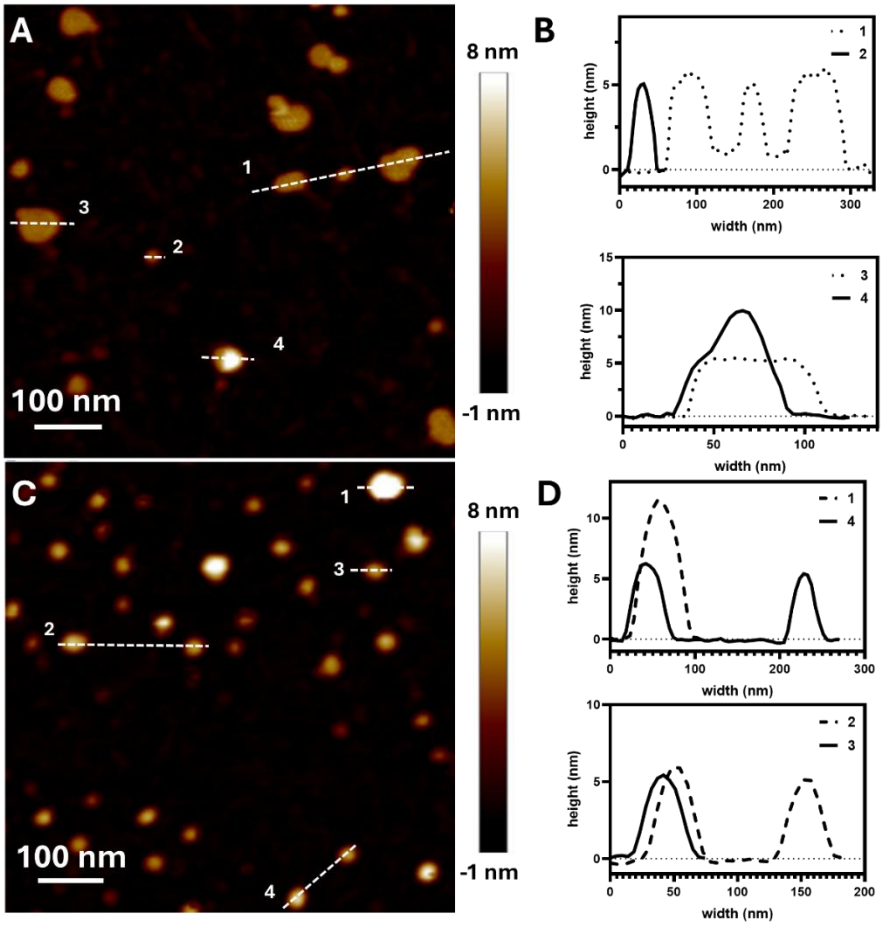

Figure 3.6. AFM micrographs of self-assembled particles from TP_{EE} 75:25 TP_{BzMA} with (B) corresponding height map and (C) after treatment at pH 3.6 with (D) corresponding height maps.

Upon exposure to acidic environments (pH~3.6) for 5-10 days, the co-assembled systems exhibit composition-dependent disassembly behaviour that differs markedly from conventional pH-responsive materials which typically show binary on/off responses rather than staged disassembly.[34, 35] While conventional pH-responsive polymers typically demonstrate predictable swelling or dissolution transitions, the present co-assembled systems display graded disassembly profiles that suggest multiple competing processes occurring simultaneously. The pure EE system establishes a baseline for pH-responsive behaviour, exhibiting complete disassembly within 10 days, with the disintegration of defined discoidal structures into small particulate debris, and a shift to smaller hydrodynamic size by DLS

(Figure S3.2C). This behaviour is consistent with the conversion of ethyl ethoxylate groups to glycidyl groups in the PEE side chains at pH ~ 5,[18] which causes them to lose the required amphiphilicity and rigidity to pack into defined particles.[36] However, by reducing the content of TP_{EE} in co-assembled systems, the apparent disassembly becomes less evident. Instead of complete disassembly, both networks of collapsed structures and discrete particles can be observed. As the PBzMA content is increased to be the majority component, defined circular particles are observed by TEM (Figure 3.3D). By AFM, these particles are observed to consistently maintain a deflated height of ~ 5nm, suggesting that they may be small discoidal particles (Figure 3.6C & D). Even relatively low concentrations of BzMA (25% in TP_{EE} 75:25 TP_{BzMA}) have demonstrated altered disassembly behaviour. Despite being composed primarily of pH-responsive components, the incomplete disassembly of these particles indicates that even small concentrations of stable components can alter disassembly profiles and prevent complete breakdown. Upon treatment with acidic pH for both 5- and 10-days results in an increase in hydrodynamic diameter for all co-assembled systems (Figure S3.2B). This is likely due to the network of particles observed by TEM from the incomplete disassembly of pH responsive tadpoles. However, at TP_{EE} 25:75 TP_{BzMA} this increase in size is less pronounced, in line with observations of particles retaining their structure at this ratio by TEM. In particles from the self-assembly of TP_{BzMA} alone, there is no change in size by TEM (Figure 3.3E) or hydrodynamic diameter by DLS (Figure S3.2C), further confirming that BzMA tadpoles are not affected by acidic environments.

This suggests cooperative effects where BzMA chains provide stabilisation beyond their stoichiometric contribution, possibly through formation of rigid domains that can either act through a ‘shielding’ effect towards neighbouring pH-responsive chains, or by their own molecular rearrangement in response to pH treatment. Given that the non-responsive TP_{BzMA} are expected to form kinetically frozen aggregates in the solvent switch as seen in other high

T_g systems due to limited side chain mobility,[37, 38] the former is more plausible. Shielding effects that prevent the complete disassembly of TP_{EE} segments may occur through various pathways.

One possibility involves kinetic trapping mechanisms where the high glass transition temperature of PBzMA components restricts molecular mobility necessary for typical pH responses.[39] Kinetic trapping in polymer assemblies occurs when the chain mobility does not match the thermodynamic stability of the system in response to a change in hydrophilicity.[40] In this scenario, pH-responsive PEE tadpoles may become physically constrained within the rigid high T_g TP_{BzMA} framework, unable to be accessed for protonation and subsequent hydrophilisation. This would suggest that only surface-accessible EE tadpoles, particularly those at assembly edges, can respond to pH changes while interior chains remain kinetically frozen. The effect of polymer nanoparticle T_g on the movement of small molecules has been modelled through drug release studies by Lappe et al. They found that at temperatures below the T_g of the nanoparticle system, drug release was largely impeded,[41] likely due to tight packing of the polymer chains and restricted motility. In a similar manner, there is also the possibility that acid penetration into the structures is limited, in turn reducing the hydrophilisation of PEE tadpoles.

Alternatively, the observed behaviour could result from trapped hydrolysis where PEE tadpoles can undergo protonation but remain physically entrapped within the assembly structure. In this scenario, chemical changes occur but are not accompanied by the expected dissolution due to physical constraints imposed by the rigid BzMA network. This has been observed in mixed micelle systems by Lo et al.,[42] where PEG-*block*-poly(lactic acid) (PEG-*b*-PLA) block copolymers were co-assembled with a dual-responsive amphiphilic polymer (mPEG-*b*-P[NnPAAm-co-VIm]). Upon protonation of pH-responsive *N*-vinylimidazole (VIm)

units in slightly acidic pH environments, the structures were retained, like our reported co-assemblies with higher TP_{BzMA} content. This was attributed to the PEG-*b*-PLA overbearing the repulsion forces from the protonation, thus restricting the copolymer movement within the structure. When the VIm units were able to be sufficiently protonated to be the stronger repulsive factor, the structures dissociated. In our system, this is analogous to copolymer blends where TP_{EE} is more prominent.

Another interesting observation is the temporal evolution of these co-assembled systems upon exposure to low pH environments. The evidence of smaller 'debris' near larger particles at Day 5 compared to Day 10 of acidic treatment (Figure 3.3) suggests a multi-step disassembly process involving slow hydrophilisation and partial disassembly, with subsequent reorganisation into new structural arrangements throughout this process, likely via one of the aforementioned mechanisms. The retention of flat 2D structures, particularly in high BzMA content systems, represents an intriguing display of this behaviour. AFM observations reveal persistent small circular features (Figure 3.6C) that likely represent majority PBzMA domains seemingly resistant to extensive morphological reorganisation. This structural persistence under acidic conditions further supports the theory of molecular mixing,[43] enabling the development of materials that maintain structural platforms while undergoing controlled functional changes. These observed behaviours extend existing knowledge in the field of stimuli-responsive polymers and co-assembled polymeric systems.

Several critical questions remain regarding the precise mechanisms governing these responses. The relative contributions of kinetic trapping versus chemical accessibility require further investigation through techniques that can probe molecular-level dynamics in real-time. Understanding how chain mobility varies spatially within the assemblies and how this correlates with observed disassembly patterns would provide crucial mechanistic insights.

Additionally, the role of interfacial effects between EE and BzMA domains in governing overall assembly stability warrants detailed examination.

The demonstration that 2D assemblies can be retained while exhibiting controlled disassembly responses establishes proof-of-concept for a new class of stimuli-responsive materials. Unlike conventional systems that rely on bulk property changes, these materials could support multiple functionalities through spatial organisation of responsive and stable components. To extend this further, the co-assembly of multiple systems that are responsive to distinct stimuli could be employed. This could enable sequential functionality where different payloads are released at predetermined timepoints, spatial functionality where surface properties remain constant while bulk properties evolve, or responsive stability where controlled changes occur whilst 2D structures can be maintained.[44]

The implications for developing multifunctional stimuli-responsive materials are significant. Current interest in controlled release systems emphasises the need for materials that can provide tuneable,[45] predictable responses to environmental stimuli. The ability to maintain 2D structural integrity while exhibiting graded functional responses represents a departure from traditional approaches where responsiveness and stability are considered mutually exclusive properties.[46]

5. Conclusion

This study has successfully demonstrated the co-assembly of chemically distinct tadpole-shaped bottlebrush copolymers into mixed discoidal nanoparticles with unique composition-dependent properties. All co-assembly ratios of two disc-forming building blocks preserved discoidal morphology with pronounced size increases compared to pure systems, likely due to cooperative assembly mechanisms, despite significant chemical differences between core-

forming blocks. This demonstrated the effectiveness of identical corona blocks in mediating incompatible core segments with the absence of phase separation and formation of continuous phases. This indicates that careful architectural design can overcome thermodynamic incompatibilities between chemically distinct polymer segments. Upon exposure to acidic pH expected to selectively protonate pH responsive TP_{EE} segments, composition-dependent pH-responsive disassembly that ranged from complete disassembly (pure TP_{EE}) to structural persistence with controlled modifications (high BzMA content) was observed. Notably, even minor amounts of pH-stable components (25% TP_{BzMA}) altered disassembly behaviour, suggesting cooperative stabilisation mechanisms that operate beyond simple stoichiometric contributions. The present system represents a significant step toward this goal by demonstrating that composition can be used as a design parameter to tune both the kinetics and extent of disassembly responses. The retention of structural platforms during disassembly opens new possibilities for applications requiring sustained functionality under changing environmental conditions. More work to establish the mechanism behind the molecular organisation in the self-assembly process, compositional analysis and the subsequent effect on stimuli-responsive morphological transition is needed through the inclusions of chromophores or fluorescent labelling with an expansion of microscopy techniques such as cryo-TEM. These findings establish a foundation for designing next-generation stimuli-responsive materials where structural integrity and functional responsiveness can be independently controlled through composition design, opening new avenues for applications in controlled drug delivery,[47] adaptive materials, and smart therapeutic systems.[48, 49]

6. References

1. Chang, D.; Ma, Y.; Xu, X.; Xie, J.; Ju, S., Stimuli-Responsive Polymeric Nanoplatforms for Cancer Therapy. *Frontiers in Bioengineering and Biotechnology* **2021,** *9*.

2. Nunziata, G.; Nava, M.; Lacroce, E.; Pizzetti, F.; Rossi, F., Thermo‐Responsive Polymer‐Based Nanoparticles: From Chemical Design to Advanced Applications. *Macromolecular Rapid Communications* **2025,** *46* (9).

3. Deirram, N.; Zhang, C.; Kermaniyan, S. S.; Johnston, A. P. R.; Such, G. K., pH‐Responsive Polymer Nanoparticles for Drug Delivery. *Macromolecular Rapid Communications* **2019,** *40* (10), 1800917.

4. Singh, J.; Nayak, P., <scp>pH</scp>‐responsive polymers for drug delivery: Trends and opportunities. *Journal of Polymer Science* **2023,** *61* (22), 2828-2850.

5. Shymborska, Y.; Budkowski, A.; Raczkowska, J.; Donchak, V.; Melnyk, Y.; Vasiichuk, V.; Stetsyshyn, Y., Switching it Up: The Promise of Stimuli‐Responsive Polymer Systems in Biomedical Science. *The Chemical Record* **2024,** *24* (2).

6. Beach, M. A.; Nayanathara, U.; Gao, Y.; Zhang, C.; Xiong, Y.; Wang, Y.; Such, G. K., Polymeric Nanoparticles for Drug Delivery. *Chemical Reviews* **2024,** *124* (9), 5505-5616.

7. Hou, W.; Zhang, Z.; Shi, Y.; Chen, Y., Co-Assembly of Diblock Copolymers and Molecular Bottlebrushes. *Macromolecules* **2022,** *55* (15), 6364-6371.

8. Fan, Y.; Ma, J.; Li, Y.; Huang, X.; Feng, S.; Chen, D., Co-assembly of Synthetic Particles with Heterogenous Components. *Chemistry of Materials* **2024,** *36* (9), 4011-4033.

9. Xu, H.; Yang, P.; Ma, H.; Yin, W.; Wu, X.; Wang, H.; Xu, D.; Zhang, X., Amphiphilic block copolymers-based mixed micelles for noninvasive drug delivery. *Drug Delivery* **2016,** *23* (8), 3063-3071.

10. Gröschel, A. H.; Müller, A. H. E., Self-assembly concepts for multicompartment nanostructures. *Nanoscale* **2015,** *7* (28), 11841-11876.

11. Brisson, E. R. L.; Worthington, M. J. H.; Kerai, S.; Müllner, M., Nanoscale polymer discs, toroids and platelets: a survey of their syntheses and potential applications. *Chemical Society Reviews* **2024,** *53* (4), 1984-2021.

12. Herdiana, Y.; Wathoni, N.; Shamsuddin, S.; Muchtaridi, M., Scale-up polymeric-based nanoparticles drug delivery systems: Development and challenges. *OpenNano* **2022,** *7*, 100048.

13. Zheng, Z.; Müllner, M.; Ling, J.; Müller, A. H. E., Surface Interactions Surpass Carbon–Carbon Bond: Understanding and Control of the Scission Behavior of Core–Shell Polymer Brushes on Surfaces. *ACS Nano* **2013,** *7* (3), 2284-2291.

14. Neugebauer, D.; Sumerlin, B. S.; Matyjaszewski, K.; Goodhart, B.; Sheiko, S. S., How dense are cylindrical brushes grafted from a multifunctional macroinitiator? *Polymer* **2004,** *45* (24), 8173-8179.

15. Zeng, H.; Zeng, P.; Baek, J.; Kim, B. S.; Müllner, M., Self‐Assembly of Amorphous 2D Polymer Nanodiscs with Tuneable Size, pH‐Responsive Degradation and Controlled Drug Release. *Angewandte Chemie International Edition* **2025**.

16. Zeng, H.; Liang, X.; Roberts, D. A.; Gillies, E. R.; Müllner, M., Self‐Assembly of Rod‐Coil Bottlebrush Copolymers into Degradable Nanodiscs with a UV‐Triggered Self‐Immolation Process. *Angewandte Chemie International Edition* **2024,** *63* (13).

17. Kerai, S. D.; Takano, S.; Zeng, P.; Müllner, M., Self-Assembly of Bottlebrush-Linear, Rod–Coil Copolymers into Discoidal Nanoparticles. *ACS Macro Letters* **2025**, 834-840.

18. Song, J.; Hwang, E.; Lee, Y.; Palanikumar, L.; Choi, S.-H.; Ryu, J.-H.; Kim, B.-S., Tailorable degradation of pH-responsive all polyether micelles via copolymerisation with varying acetal groups. *Polymer Chemistry* **2019,** *10* (5), 582-592.

19. Kaya, İ.; Pala, Ç. Y., Thermodynamics of poly(benzyl methacrylate)–probe interactions at different temperatures by using inverse gas chromatography. *Fluid Phase Equilibria* **2014,** *374*, 63-69.

20. Lodge, T. P., A unique platform for materials design. *Science* **2008,** *321* (5885), 50-51.

21. Bates, C. M.; Bates, F. S., 50th Anniversary Perspective: Block polymers—Pure potential. *Macromolecules* **2017,** *50* (1), 3-22.

22. Kelarakis, A.; Castelletto, V.; Krysmann, M. J.; Hamley, I. W., Nanoscale phase separation and mixing in a diblock copolymer/homopolymer blend. *Langmuir* **2008,** *24* (8), 3767-3772.

23. Moreno, S.; Rodriguez-Emmenegger, C.; Brynda, E., Morphological Transitions of Block Copolymer Micelles: Implications for Mesoporous Materials Ordering. *Macromol. Theory Simul.* **2024,** *33* (7), 2400046.

24. Zhu, J.; Zhang, S.; Zhang, K.; Wang, X.; Mays, J. W.; Wooley, K. L.; Pochan, D. J., Disk-cylinder and disk-sphere nanoparticles via a block copolymer blend solution construction. *Nature Communications* **2013,** *4* (1).

25. Yamaguchi, D.; Hashimoto, T., A Phase Diagram for the Binary Blends of Nearly Symmetric Diblock Copolymers. 1. Parameter Space of Molecular Weight Ratio and Blend Composition. *Macromolecules* **2001,** *34* (18), 6495-6505.

26. Miyake, G. M.; Piunova, V. A.; Weitekamp, R. A.; Grubbs, R. H., Precisely Tunable Photonic Crystals From Rapidly Self‐Assembling Brush Block Copolymer Blends. *Angewandte Chemie International Edition* **2012,** *51* (45), 11246-11248.

27. Moughton, A. O.; Hillmyer, M. A.; Lodge, T. P., Multicompartment Block Polymer Micelles. *Macromolecules* **2012,** *45* (1), 2-19.

28. Georgakis, S.; Kyriakos, K.; Pispas, S., Amphiphilic Block Copolymer Micelles in Selective Solvents: The Effect of Solvent Selectivity on Micelle Formation. *Polymers* **2019,** *11* (11), 1882.

29. Khandpur, A. K.; Foerster, S.; Bates, F. S.; Hamley, I. W.; Ryan, A. J.; Bras, W.; Almdal, K.; Mortensen, K., Polyisoprene-polystyrene diblock copolymer phase diagram near the order-disorder transition. *Macromolecules* **1995,** *28* (26), 8796-8806.

30. Wang, Z.; Sun, S.; Li, C.; Hu, S.; Faller, R., Controllable multicompartment morphologies from cooperative self-assembly of copolymer–copolymer blends. *Soft Matter* **2017,** *13* (35), 5877-5887.

31. Nagarajan, R., Molecular packing parameter and surfactant self-assembly: The neglected role of the surfactant tail. *Langmuir* **2002,** *18* (1), 31-38.

32. Flory, P. J., *Principles of Polymer Chemistry*. Cornell University Press: Ithaca, 1953.

33. Cui, H.; Chen, Z.; Zhong, S.; Wooley, K. L.; Pochan, D. J., Block Copolymer Assembly via Kinetic Control. *Science* **2007,** *317* (5838), 647-650.

34. Mura, S.; Nicolas, J.; Couvreur, P., Stimuli-responsive nanocarriers for drug delivery. *Nature Materials* **2013,** *12* (11), 991-1003.

35. Singh, A.; Sharma, S.; Singh, P., pH‐responsive polymers for drug delivery: Trends and opportunities. *Journal of Polymer Science* **2023,** *61* (17), 1702-1718.

36. Lee, E. S.; Gao, Z.; Bae, Y. H., Recent progress in tumor pH targeting nanotechnology. *J. Control. Release* **2008,** *132* (3), 164-170.

37. Mai, Y.; Eisenberg, A., Self-assembly of block copolymers. *Chem. Soc. Rev.* **2012,** *41* (18), 5969-5985.

38. Wright, D. B.; Patterson, J. P.; Gianneschi, N. C.; Chassenieux, C.; Colombani, O.; O'Reilly, R. K., Blending block copolymer micelles in solution; obstacles of blending. *Polymer Chemistry* **2016,** *7* (8), 1577-1583.

39. Debenedetti, P. G.; Stillinger, F. H., Supercooled liquids and the glass transition. *Nature* **2001,** *410* (6825), 259-267.

40. Fielden, S. D. P., Kinetically Controlled and Nonequilibrium Assembly of Block Copolymers in Solution. *J. Am. Chem. Soc.* **2024,** *146* (28), 18781-18796.

41. Lappe, S.; Mulac, D.; Langer, K., Polymeric nanoparticles – Influence of the glass transition temperature on drug release. *International Journal of Pharmaceutics* **2017,** *517* (1), 338-347.

42. Lo, C.-L.; Lin, S.-J.; Tsai, H.-C.; Chan, W.-H.; Tsai, C.-H.; Cheng, C.-H. D.; Hsiue, G.-H., Mixed micelle systems formed from critical micelle concentration and temperature-sensitive diblock copolymers for doxorubicin delivery. *Biomaterials* **2009,** *30* (23), 3961-3970.

43. von Burkersroda, F.; Schedl, L.; Göpferich, A., Why degradable polymers undergo surface erosion or bulk erosion. *Biomaterials* **2002,** *23* (21), 4221-4231.

44. Mousavi, S. M.; Low, F. W.; Hashemi, S. A.; Samsudin, N. A.; Shakeri, M.; Yusoff, Y.; Rahman, M. A.; Lai, C. W.; Babapoor, A.; Soroshnia, S., pH-responsive drug delivery systems as intelligent carriers for targeted drug therapy: Brief history, properties, synthesis, mechanism and application. *Eur. Polym. J.* **2022,** *162*, 110892.

45. Karimi, M.; Ghasemi, A.; Sahandi Zangabad, P.; Rahighi, R.; Moosavi Basri, S. M.; Mirshekari, H.; Amiri, M.; Shafaei Pishabad, Z.; Aslani, A.; Bozorgomid, M.; Ghosh, D.; Beyzavi, A.; Vaseghi, A.; Aref, A. R.; Haghani, L.; Bahrami, S.; Hamblin, M. R., Smart micro/nanoparticles in stimulus-responsive drug/gene delivery systems. *Chem. Soc. Rev.* **2016,** *45* (5), 1457-1501.

46. Matyjaszewski, K., Architecturally complex polymers with controlled heterogeneity. *Science* **2011,** *333* (6046), 1104-1105.

47. Aida, T.; Meijer, E. W.; Stupp, S. I., Functional supramolecular polymers. *Science* **2012,** *335* (6070), 813-817.

48. Hoffman, A. S., Stimuli-responsive polymers: Biomedical applications and challenges for clinical translation. *Adv. Drug Del. Rev.* **2013,** *65* (1), 10-16.

49. Alqosaibi, A. I., Nanocarriers for anticancer drugs: Challenges and perspectives. *Saudi Pharmaceutical Journal* **2022,** *30* (5), 622-634.

7. Supporting Information

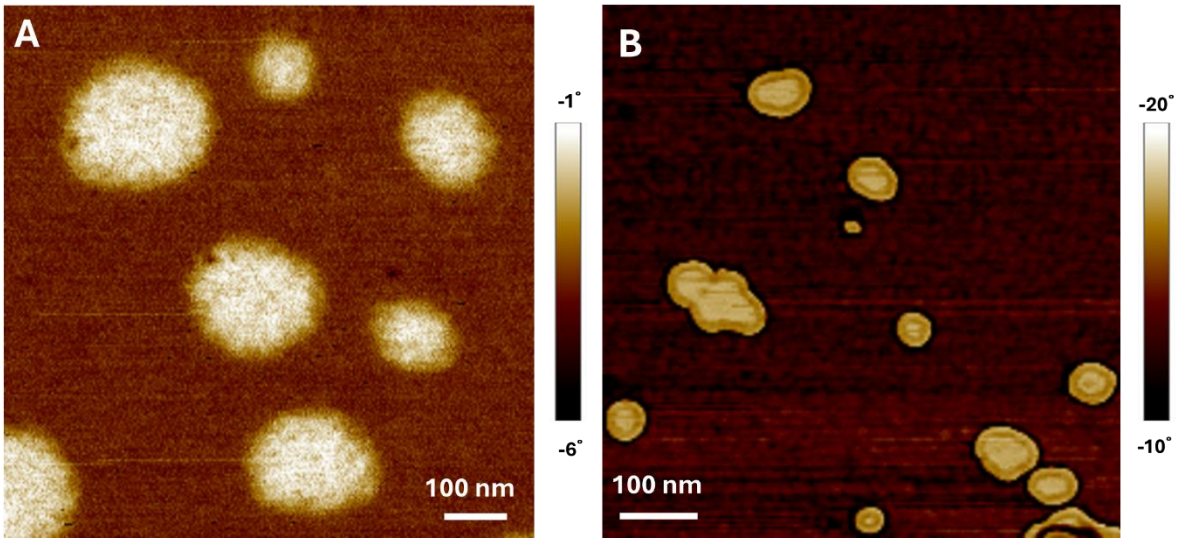

Figure S3.1. AFM phase micrographs of discoidal particles of (A) TP_{EE} and (B) TP_{BzMA}

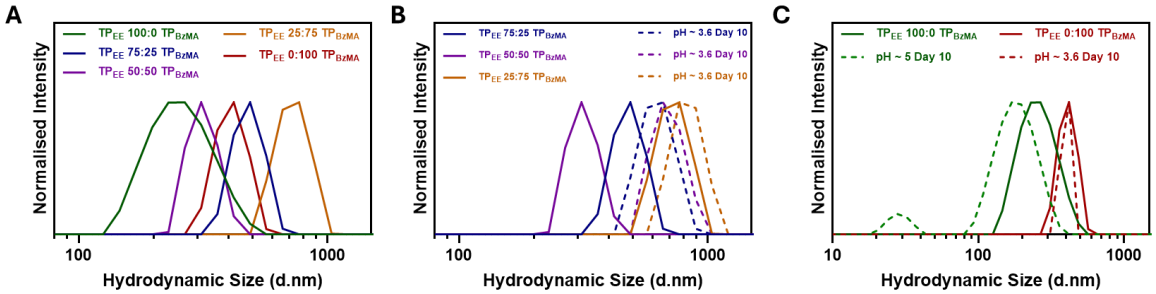

Figure S3.2. Hydrodynamic Size by Intensity normalised for (A) self-Assemblies and co-assemblies of TP_{EE} & TP_{BzMA} (B) co-assemblies of TP_{EE} & TP_{BzMA} after treatment at acidic pH (C) self-assemblies of TP_{EE} & TP_{BzMA} after treatment at acidic pH

Chapter IV : Self-Assembly of Bottlebrush-Linear-Bottlebrush Block Copolymer Architectures

1. Abstract

Bottlebrush-linear block copolymer architectures represent an interesting class of materials with unique self-assembly behaviour owing to their rigid flexible junctions between blocks. This chapter examines the self-assembly behaviour of rod-coil-rod or bottlebrush-linear-bottlebrush triblock copolymer architectures, specifically bottlebrush-linear-bottlebrush terpolymers as an extension of diblock copolymer systems for accessing advanced morphological regimes. By introducing rigid segments at both termini of a flexible central block, these architectures create bidirectional steric constraints that fundamentally alter the morphological landscape compared to simple bottlebrush-linear systems. The investigation reveals the morphological transition of self-assembled symmetrical bottlebrush-linear-bottlebrush architectures from multicomponent particles to dense precipitates and planar structures with respect to bottlebrush size. Furthermore, the use of these dumbbells in co-assembly approaches with bottlebrush-linear diblock copolymers shows potential for accessing networks of nanostructures. This work establishes design principles for predicting morphological outcomes in architecturally complex rigid-flexible block copolymer systems and demonstrates the potential of topological control as a pathway to control nanoparticle morphology.

2. Introduction

The architectural complexity of synthetic block copolymers has emerged as a defining factor in directing nanoscale self-assembly, offering unprecedented control over morphological outcomes through precise molecular design.[1, 2] While the self-assembly of the simplest linear block copolymer types primarily relies on incompatibility-driven phase separation defined by the Flory-Huggins (χ) parameter, the inclusion of rigid segments in alternating bottlebrush-linear block copolymer architectures introduces unique rigid-flexible junctions that fundamentally alter the driving forces for self-assembly.[3, 4] Additional to the increase in χ due to the stiffness asymmetry compared to linear systems, bottlebrush-linear block copolymer packing is also defined by factors such as Maier–Saupe parameter (μ) which describes rod-rod orientation interactions.[5] The competition between these forces influences the conformations of macromolecules in the self-assembly process,[6] leading to distinctive morphological phase diagrams characterised by highly anisotropic structures.[2, 7] The simplest iteration being a bottlebrush-linear diblock copolymer has been investigated with attention to the influence of the lengths and ratios of rigid and flexible segments on critical packing parameter and resulting assembly geometry.[8] Majority of these rigid segments include π-conjugated polymers, polypeptides, or liquid crystalline blocks.[7]

As a further development to linear rod-*alt*-coil block copolymers, bottlebrush block copolymers (BBCPs) introduce radial steric induced rigidity that are expected to alter self-assembly behaviour compared to conjugated systems.[9] The initial exploration of brush-*block*-linear architectures in this thesis established the establishing critical dimensions and volume fraction of hydrophilic and hydrophobic segments in a tadpole system to achieve discoidal nanoparticles.[10] The balance between brush rigidity introduced by inter-side chain repulsion and the entropic flexibility of the adjacent linear domain, highlighted the role of intramolecular

mechanical constraint in self-assembly toward flat anisotropic morphologies. Analogous coil-bottlebrush-coil block terpolymers have also been explored,[11] where the flexible coil blocks formed the corona of self-assembled materials, adhering to similar self-assembly principles as bottlebrush-linear block copolymers.

In contrast, block copolymers where the linear segments are positioned between rigid rod or bottlebrush blocks are expected to behave vastly different when self-assembled with steric constraints introduced along a polymer backbone. The rod-coil-rod, bottlebrush-linear-bottlebrush or 'dumbbell' BBCP architecture represents this next level of topological sophistication, comprising of two densely grafted brush blocks or rigid segments flanking a central linear or flexible segment. The transition from unilateral steric constraints in tadpole architectures to bilateral constraints in dumbbell systems fundamentally shifts the expected self-assembly outcomes. While tadpole systems experience asymmetric steric frustration from a single rigid block, dumbbell architectures must balance competing orientational preferences from two terminal rigid segments.[12] The hierarchical nanostructures that can emerge from these complex architectures have been shown to be dependent on interaction parameters between the rigid block components,[13] offering additional tunability in morphological outcomes.[14]

Despite the theoretical promise of dumbbell architectures, there remains a significant lack of experimental exploration into their self-assembly behaviour. Whilst some work has explored their self-assembly behaviour in brush selective solvents,[15, 16] self-assembly in coil-selective solvents is better positioned to access anisotropic particles and planar packing. This is because the rigidifying effect of brushes in poor solvents compared to linear blocks in poor solvents can vastly change their self-assembly behaviour.[17]

The investigation of dumbbell architectures in coil-selective solvents thus represents a natural extension of the foundational insights in understanding the self-assembly of tadpole structures,

and as a gateway to extend the understanding of architecturally complex block copolymer self-assembly. By systematically characterising how the transition from unilateral to bilateral steric frustration alters the self-assembly landscape, this work aims to establish design rules that predict morphological outcomes based on architectural parameters alone. This understanding will inform the development of next-generation architectures, with the potential to access previously inaccessible morphological regimes through further architectural elaboration.

3. Experimental Section

3.1 Materials

Poly(ethylene glycol) 4600 (PEG 4.6K), hydroxyethyl methacrylate (HEMA, 97%), α-bromoisobutyryl bromide (98%) (α-BiBB), 2,2'-Bipyridine (bpy, 99%), triethylamine (NEt_3, 99%) N,N,N′,N″,N″- pentamethyldiethylenetriamine (PMDETA, 99%), anisole (99%), mesitylene (98%), copper(I) bromide (CuBr, 98%) and deuterated solvents were purchased from Sigma-Aldrich. Tetrahydrofuran (THF), petroleum benzine (b.p. 40-60 ̊C), and diethyl ether were sourced from Merck. Pyridine (99%) and magnesium sulphate ($MgSO_4$) were purchased from Ajax. Dimethyl formamide (DMF, 99.8% by gas chromatography (GC)) was sourced from RCI LabScan. Benzyl methacrylate (BzMA, 98%) was sourced from Tokyo Chemical Industry Chemicals. CuBr was washed with glacial acetic acid prior to use. HEMA and BzMA were filtered through a short basic aluminium oxide column to remove inhibitors. All other chemicals were used as received.

3.2 Methods

Synthesis of Br-PEG-Br (Bifunctional Initiator)

A round bottom flask was charged with PEG 4.6K (2.0 g, 0.4 mmol, 1.0 equiv.), and Net_3 (0.35 g, 35 mmol, 8.0 equiv.) with DCM (20 mL). The vessel was sealed and stirred over ice for 10 minutes before α-BiBB (0.80 g, 35 mmol, 8.0 equiv.) was added dropwise. The solution was stirred on ice for a further 20 minutes before stirring at room temperature overnight. The solution was passed through gravitational filtration to remove formed pyridinium salts and washed with DCM. The synthesised bifunctional initiator was recovered by precipitation in cold ether once, redissolving in THF. Subsequently, the pellet was precipitated in n-hexane twice more, redissolving in THF to remove unreacted small molecules. The crude product was then washed three times with DI water to remove unreacted PEG. The organic solution was

dried over anhydrous $MgSO_4$ before being concentrated under vacuum into a white solid, and lyophilised into a pale white powder. The bifunctional initiator was stored at room temperature in an airtight vial shielded from light. The product was characterised by ^{1}H NMR (300 MHz, $CDCl_3$, δ 7.26 ppm, Figure 4.1A) and SEC (DMAc/LiBr, 50 °C, PMMA, Figure 4.1B).

Scheme S4.1. Synthesis of Br-PEG_{114}-Br bifunctional ATRP initiator

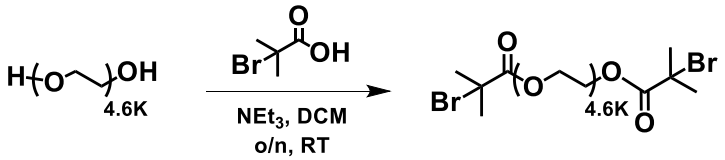

Synthesis of $PHEMA_{19}$-*block*-PEG-*block*-$PHEMA_{19}$

Bifunctional initiator (100 mg, 24 μmol, 1 mol equiv.), HEMA (408.8 μL, 3.36 mmol, 80 mol equiv.), and 2,2'-Bipyridine (13.1 mg, 8.4 μmol, 2 mol equiv.), and a 70:30 methanol/methyl ethyl ketone mixture (2 mL) were added to a schlenk flask equipped with a stirrer bar using mesitylene (100 μL) as an internal standard. A time sample (t0) was taken and analysed by ^{1}H NMR. The solution was subject to three freeze pump thaw cycles, with addition of CuCl (4.58 mg, 4.62 μmol, 1.1 mol equiv.) on the last freeze cycle. The flask was backfilled with N2 before reacting at 65 ℃ for 2.5 hours. A further time sample (t2.5) was taken and analysed using ^{1}H NMR to find the degree of polymerisation of the PHEMA block. The resulting polymer was recovered by precipitation in diethyl ether, redissolving in methanol three times over. The product was then lyophilised to give a white powder. The product was characterised by ^{1}H NMR (300 MHz, MeOD, δ 3.31 ppm, Figure 4.2A) and SEC (DMAc/LiBr, 50 °C, PMMA, Figure 4.2C).

Scheme S4.2. Synthesis of $PHEMA_{19}$-*block*-PEG-*block*-$PHEMA_{19}$

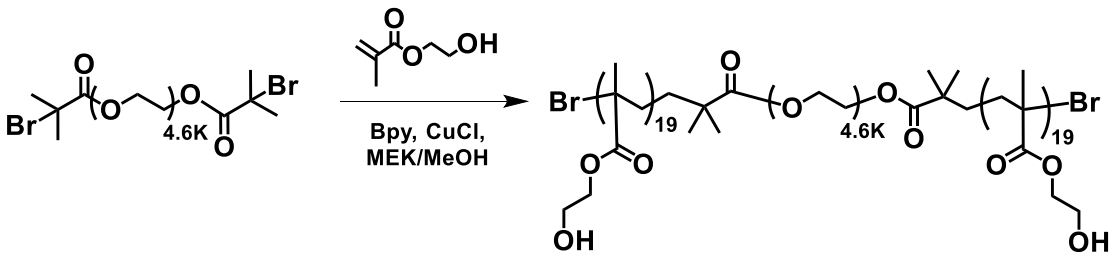

Synthesis of PBIEM$_{19}$-*block*-PEG-*block*-PBIEM$_{19}$

PHEMA$_{19}$-*block*-PEG-*block*-PHEMA$_{19}$ (80 mg, 8.2 μmol, 36 equiv. of -OH units) and Pyridine (119.5 μL, 1.19 mmol, 5 equiv. per -OH unit) were dissolved in THF (12 mL) in a round-bottom flask and stirred on ice. α-BiBB (146.7 μL, 1.19 mmol, 4 equiv. per -OH unit) was added dropwise by syringe to the flask over 5 minutes. The reaction continued to stir over ice for 10 minutes, before reacting overnight at room temperature. The solution was passed through gravitational filtration to remove formed pyridinium salts and washed with THF. The resulting polymer was recovered by precipitation in hexane three times, redissolving in THF. The product was dried of residual solvents under N_2 flow and subsequently lyophilised to give a pale white powder. The product was characterised by ^{1}H NMR (300 MHz, $CDCl_3$, δ 7.26 ppm, Figure 4.2B) and SEC (DMAc/LiBr, 50 °C, PMMA, Figure 4.2C).

Scheme S4.3. Synthesis of PBIEM$_{19}$-*block*-PEG-*block*-BIEM$_{19}$

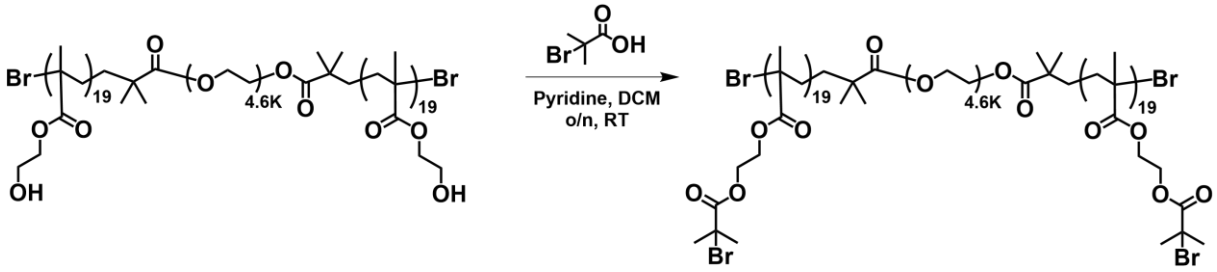

Synthesis of (PBIEM$_{19}$ -*graft*-PBzMA$_x$)-*block*-PEG-*block*-(PBIEM$_{19}$-*graft*-PBzMA$_x$)

PBIEM$_{19}$-*block*-PEG-*block*-PBIEM$_{19}$ (10 mg, 1.1 μmol, 32 mol equiv. of -Br units), BzMA, PMDETA (9.55 μL, 45.7 μmol, 1.1 mol equiv. per -Br unit), and mesitylene (100 μL) as an internal standard were dissolved in anisole (80% v/v) in a Schlenk flask. After removal of an aliquot to monitor conversion, the vessel was subject to three freeze-pump-thaw cycles, with addition of CuBr (6.19 mg, 62.6 μmol, 2 mol equiv. per -Br unit) prior to the last cycle. The flask was backfilled by bubbling nitrogen gas, and then reacted at 70 ℃ for 2.5 hrs. An aliquot was taken to determine monomer conversion. The solution was run through a short neutral alumina column to remove copper catalyst, and anisole removed under nitrogen flow. The polymer was redissolved in DMF and purified by precipitation in diethyl ether three times. The

resulting pellet was redissolved in minimal DMF and solid content determined. The product was characterised by ^{1}H NMR (300 MHz, $CDCl_3$, δ 7.26 ppm, Figure 4.4) and SEC (DMAc/LiBr, 50 °C, PMMA, Figure 4.3).

Scheme S4.4. Synthesis of (PBIEM$_{19}$-*g*-PBzMA$_x$)-*block*-PEG-*block*-(PBIEM$_{19}$-*g*-PBzMA$_x$)

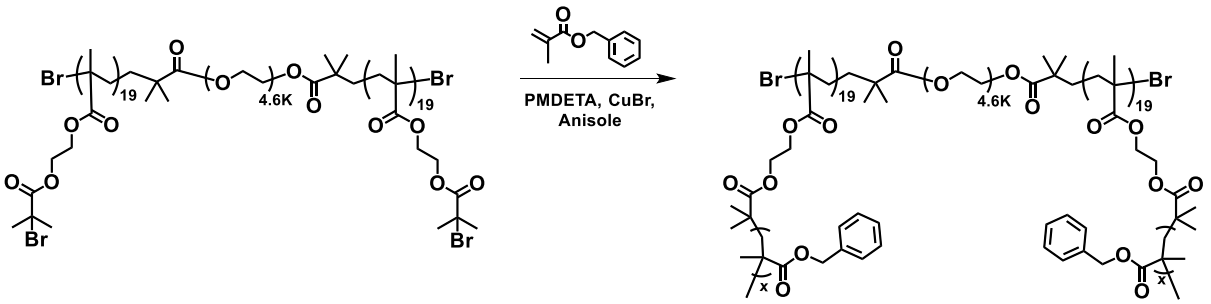

Nuclear magnetic resonance (NMR) spectroscopy

NMR spectra were recorded at the University of Sydney using Bruker NEO 300 MHz NMR spectrometers. ^{1}H NMR measurements were carried out using a zg pulse program (90° pulse) with a recycle delay (D1) of 2-5 s. ^{1}H NMR spectra are referenced to the residual solvent peak for $CDCl_3$ (δ 7.26 ppm), or MeOD (δ 3.31 ppm) as appropriate. Deuterated solvents were obtained from Sigma Aldrich and used without any further purification.

Size exclusion chromatography (SEC)

SEC was performed using a Shimadzu Prominence UFLC (ultra-fast liquid chromatography) system fitted with a Shim-pack GPC-800DP guard column followed by two in-series Phenogel columns (5 μm, 104 Å and 105 Å). The system eluent was HPLC grade dimethyl acetamide (DMAc) containing LiBr (0.03 wt%) and BHT (each at 0.05 wt%), eluting at a flow rate of 1 mL/min. The column assembly was incubated at 50 °C, and retention times were calibrated using narrow PMMA standards from PSS.

Self-Assembly of dumbbells

A 2mg/mL polymer solution in DMF was prepared and transferred into a vial capped with a dialysis membrane (MWCO 3500 Da). Where different polymers were co-assembled, polymers were transferred to a vial at prescribed wt% ratios to a achieve a final polymer

concentration of 2mg/mL. The solution was dialysed against DI water for 2 days, replacing the DI water twice a day. The resulting solution was collected and analysed by DLS and various microscopy techniques.

Dynamic light scattering (DLS)

DLS measurements were performed on a Malvern Zetasizer Ultra equipped with a He-Ne (633 nm) laser. The hydrodynamic diameters of polymer self-assembly samples were directly measured on DLS without any further treatment

Transmission Electron Microscopy (TEM)

TEM was performed on a JEM-2100CR instrument equipped with a 5k × 4k CMOS camera (EMSIS). Images were collected in bright-field mode with a spot size of 3 with diffraction contrast enhanced by using an objective lens with an aperture size of 20 μm, at an accelerating voltage of 200 kV. TEM samples were prepared by adding 4 μL of the polymer self-assembly solution onto a carbon-coated copper grid. After drying in air for 10 mins, the remained solution was removed by touching the edge of the grid with a filter paper. The samples were then stained using 10 μL of 2% uranyl acetate (UA) solution. First, UA solution was dropped on a parafilm to form a droplet. The grid was then stained for 30 seconds by inverting the grids on the droplet. After removing the UA solution with a filter paper, the grid was left to dry in the air.

Atomic Force Microscopy (AFM)

AFM was performed in air using a Multimode 8 with NanoScope V controller (Bruker) in standard tapping-mode (Tap300Al-G cantilevers, 300 kHz, 30 Nm-1, Budget Sensors). Samples were prepared by depositing 10 μL of aqueous self-assembly dispersion onto a silicon wafer previously cleaned by CO2 blast. The droplet was spin-coated by two 60 second cycles at 4000 rpm. Image analysis was performed on Bruker's Nanoscope Analysis software.

4. Results and Discussion

4.1 Synthesis of bottlebrush-linear-bottlebrush polymer library

To design a library of amphiphilic bottlebrush block copolymers (BBCPs) directly comparable to bottlebrush-linear BBCPs from Chapter II, we opted for a 'grafting-from' strategy. This library was designed to echo the dimensions of $TP_{15\text{-}75}$ from Chapter II, utilising a PEG coil for similar MW at 4600 mg/mol. From a synthesised poly(ethylene glycol) dibromide (Br-PEG-Br) (Figure 4.1), 2-hydroxyethyl methacrylate (HEMA) blocks were polymerised using atom transfer radical polymerisation (ATRP) (Scheme 4.1) to 19 repeat units long to maintain similar number of side chain grafts. The PHEMA was subsequently esterified with α-bromoisobutyrate bromide to give a poly[2-(2-bromo isobutyryloxy)ethyl methacrylate]$_{19}$-*block*-poly(ethylene glycol)$_{105}$-*block*-poly[2-(2-bromo isobutyryloxy)ethyl methacrylate]$_{19}$ ($PBIEM_{19}$-*b*-PEG_{105}-*b*-$PBIEM_{19}$) polyinitiator backbone (Figure 4.2) (Scheme 4.1).

Scheme 4.1. Synthesis of ($PBIEM_{19}$-*g*-$PBzMA_x$)-*b*-PEG_{105}-*b*-($PBIEM_{19}$-*g*-$PBzMA_x$) library, (where x = 5, 13, 29, 40 and 58) dumbbell-like bottlebrush-linear-bottlebrush block copolymers.

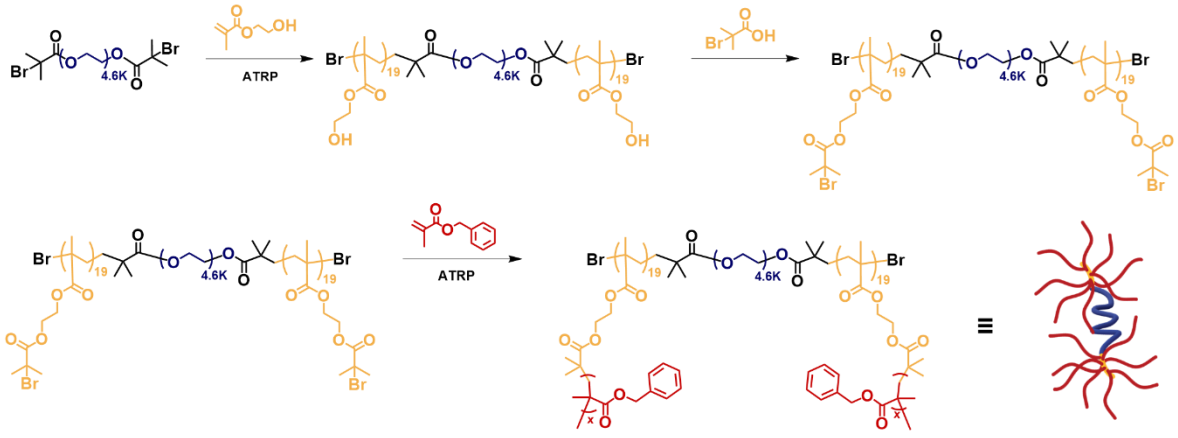

^{1}H NMR analysis of $PHEMA_{19}$ PEG_{105}-*b*-$PHEMA_{19}$ is shown in Figure 4.2.A displaying integrated PHEMA peaks δ 4.06 (CH_2), 3.79 (CH_2), 2.01 (CH_2), 1.04 (CH_3) compared to the PEG peak at δ 3.66 (CH_2CH_2). Complete esterification to $PBIEM_{19}$-*b*-PEG_{105}-*b*-$PBIEM_{19}$ is evidenced by the shift of the CH_2 peaks to δ 4.40 and 4.23, along with the methyl group signal

at 1.99 ppm (Figure 4.2.B). Additionally, a comparison of the size exclusion chromatography (SEC) chromatograms shows a slight shift toward a higher retention time because of the reduced apparent hydrodynamic size of PBIEM$_{19}$-*b*-PEG$_{105}$-*b*-PBIEM$_{19}$ compared to PHEMA$_{19}$-*b*-PEG$_{105}$-*b*-PHEMA$_{19}$ (Figure 4.2.C).

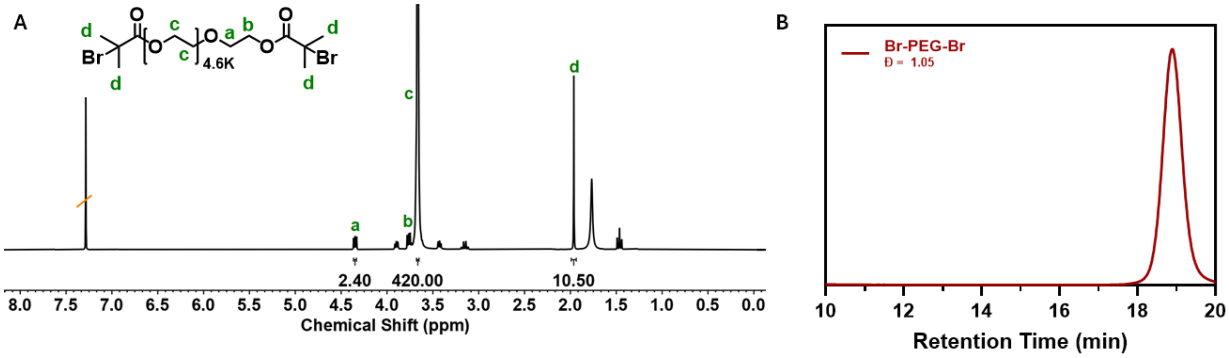

Figure 4.1. Characterisation data of PEG Dibromide Bifunctional ATRP initiator (Br-PEG-Br) (A) ^{1}H NMR (300 MHz, $CDCl_3$) δ 4.35 (a, CH_2), 3.76 (b, CH_2), 3.66 (c, CH_2CH_2), 1.95 (d, CH_3), (B) SEC chromatogram in DMAc (50 °C and 1 mL min^{-1})

The PBzMA brush segment was then synthesised using the grafting-from approach from the PBIEM moieties using ATRP to yield well-defined dumbbell-like BBCPs macromolecules (Scheme 4.1). By independently varying the PBzMA side chain length, adjustment to the bottlebrush segment directly influenced the overall BBCP dimensions and hydrophilic-to-hydrophobic ratio (Table 4.1). The generated BBCP library with varying side chain lengths includes PBIEM$_{19}$-*g*-PBzMA$_x$)-*b*- PEG$_{105}$-*b*-(PBIEM$_{19}$-*g*-PBzMA$_x$), where x = 5, 13, 29, 40 and 58. These side chain lengths were chosen to maintain comparable hydrophobic fraction ($f_{\text{hydrophobic}}$) and side chain lengths to tadpole BBCPs from Chapter II. In particular, DB$_{29}$ and DB$_{58}$ echo these parameters for TP$_{15\text{-}75}$. Greater side chain length increased the overall hydrodynamic volume of the BBCPs, evident through a progressive shift towards shorter retention times in SEC (Figure 4.3).

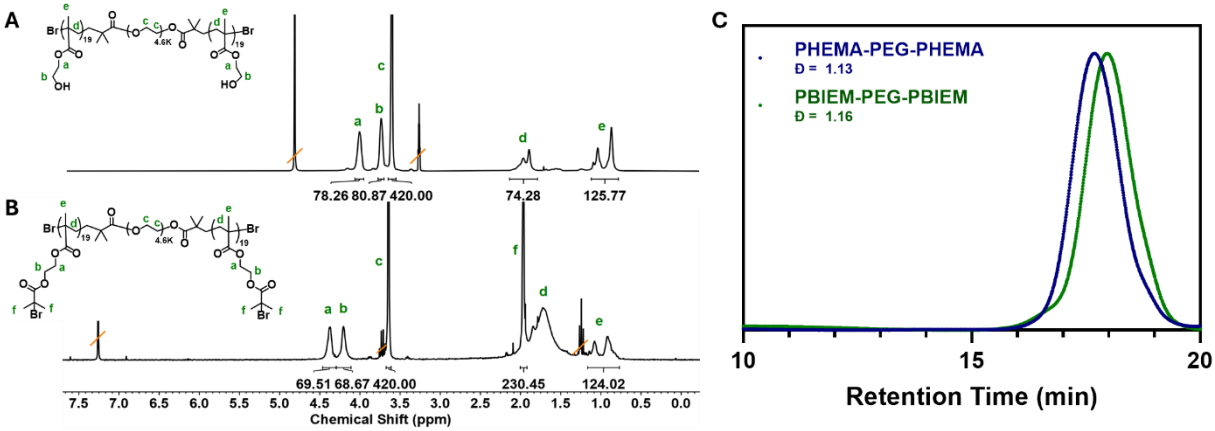

Figure 4.2. Characterisation data of polymer backbones (A) ^{1}H NMR of PHEMA$_{19}$-*b*-PEG-*b*-PHEMA$_{19}$ (300 MHz, MeOD) δ 4.06 (a, CH_2), 3.79 (b, CH_2), 3.66 (c, CH_2CH_2), 2.01 (d, CH_2), 1.04 (e, CH_2). (B) ^{1}H NMR of PBIEM$_{19}$ -*b*-PEG-*b*-PBIEM$_{19}$ (300 MHz, $CDCl_3$) δ 4.40 (a, CH_2), 4.23 (b, CH_2), 3.66 (c, CH_2CH_2), 1.99 (f, CH_3), 1.88 (d, CH_2), 1.02 (e, CH_2). (C) SEC chromatograms comparison of PHEMA-*b*-PEG$_{114}$-*b*-PHEMA and PBIEM-*b*-PEG$_{114}$-*b*-PBIEM in DMAc (50 °C and 1 mL min^{-1})

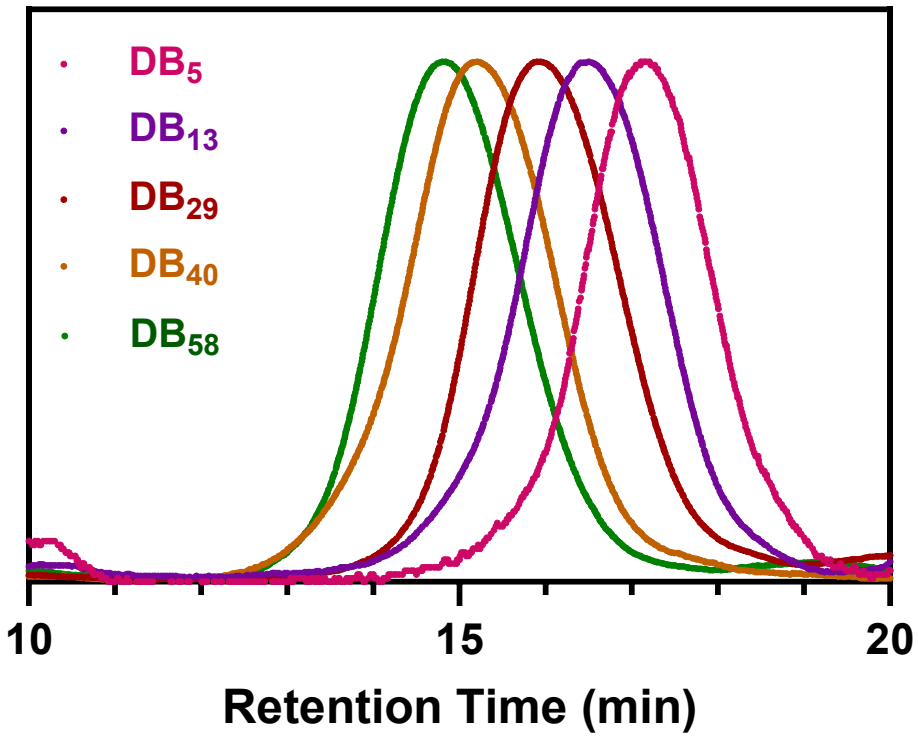

Figure 4.3. SEC traces in DMAc (50 °C and 1 mL min^{-1}) of (PBIEM$_{19}$-*g*-PBzMA$_x$)-*b*-PEG-*b*-(PBIEM$_{19}$ -*g*-PBzMA$_x$) library with increasing side chain length (y = 5, 13, 29, 40 and 58).

Side chain lengths were determined by ^{1}H NMR end group analysis, with comparison of the integration of the CH_2 of the benzyl group at δ ~ 4.75 ppm to the repeating $(CH_2)_2$ PEG signal at δ ~ 3.55 ppm (Figures 4.4) under the assumption of 50% grafting efficiency.[18, 19] These BBCPs are summarised in Table 4.1. From herein, we refer to the BBCP dumbbells (DB) encoded with their side chain length e.g. ($PBIEM_{19}$-*g*-$PBzMA_5$)-*b*-PEG_{105}-*b*-($PBIEM_{19}$-*g*-$PBzMA_5$) becomes DB_5.

Table 4.1. Characterisation data of ($PBIEM_{19}$ -*g*-PBzMAx)-*b*-PEG-*b*-($PBIEM_{19}$ -*g*-PBzMAx) polymer library

BBCPs	DP_{PEG}	DP_{PBIEM}	DP_{PBzMA}	[a]f_{BzMA}	[b]$M_{n,NMR}$	[c]$Đ_{SEC}$
DB_5	105	19,19	5	0.52	31 900	1.22
DB_{13}	105	19,19	13	0.74	58 700	1.23
DB_{29}	105	19,19	29	0.86	112 300	1.17
DB_{40}	105	19,19	40	0.90	149 100	1.21
DB_{58}	105	19,19	58	0.93	209 400	1.15

[a] Ratio of PEG:PBzMA repeat units, [b]Determined by ^{1}H NMR analysis, [c]Determined by SEC (M_w/M_n).

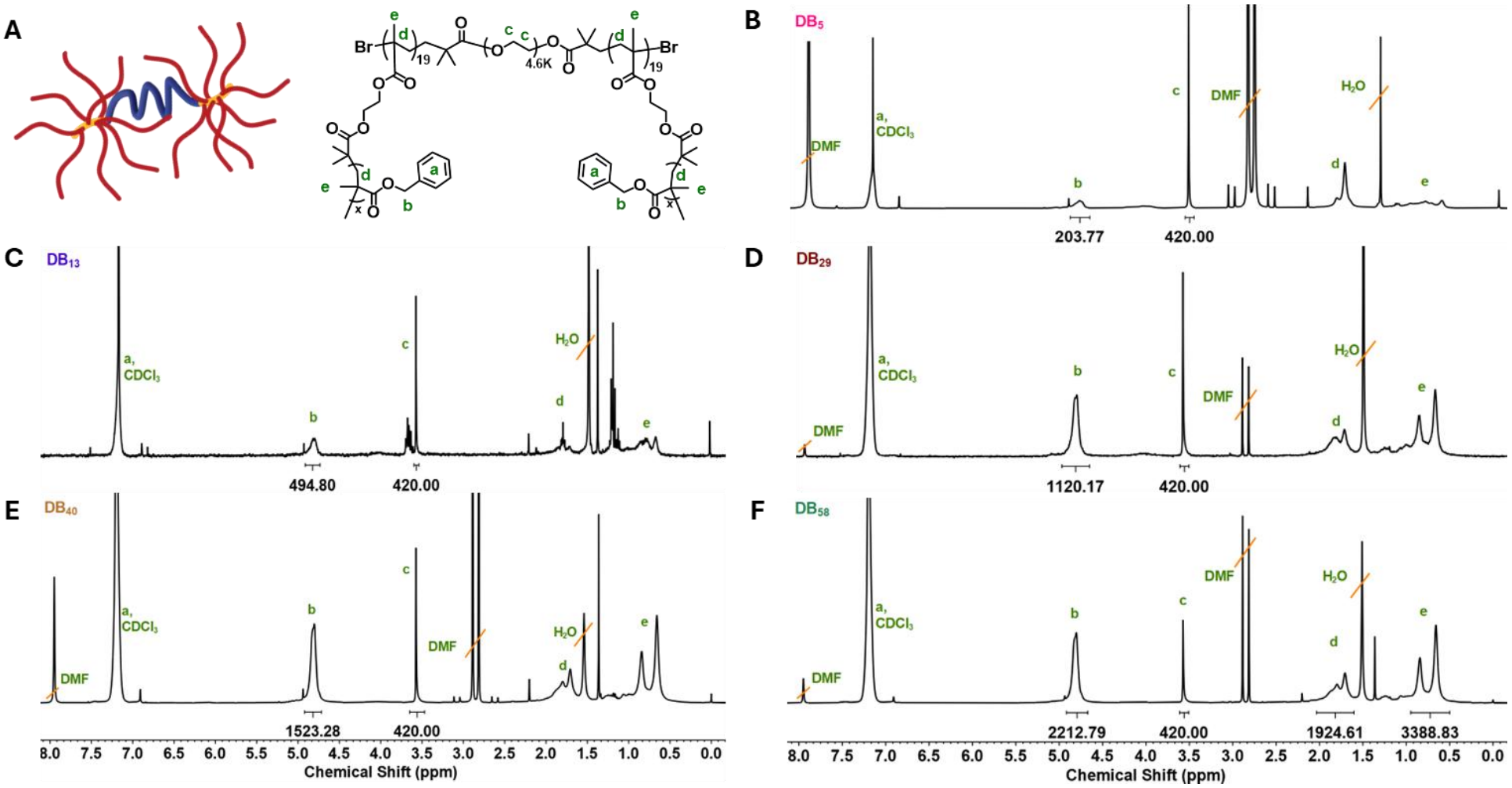

Figure 4.4. (A) Schematic Representation of Dumbbell Polymer and ^{1}H NMR of (PBIEM$_{19}$ -g-PBzMAx)-b-PEG-b-(PBIEM$_{19}$ -g-PBzMAx) (300 MHz, $CDCl_3$) δ 7.26 (a, Bzl), 4.87 (b, CH_2), 3.64 (c, CH_2CH_2), 1.82 (d, CH_2), 0.82 (e, CH_3) , (B) DB$_5$, (C) DB$_{13}$, (D) DB$_{29}$, (E) DB$_{40}$, and (F) DB$_{58}$

4.2 Effect of molecular polymer brush segment side chain length on self-assembly

To self-assemble the BBCPs, a solvent switch method was used, starting with a 2 mg/mL solution in DMF and their subsequent dialysis into deionised water as a coil-selective solvent. We used transmission electron microscopy (TEM) to survey the resulting assemblies (Figure 4.5) and dynamic light scattering (DLS) to estimate their hydrodynamic sizes (Figure S4.1A).

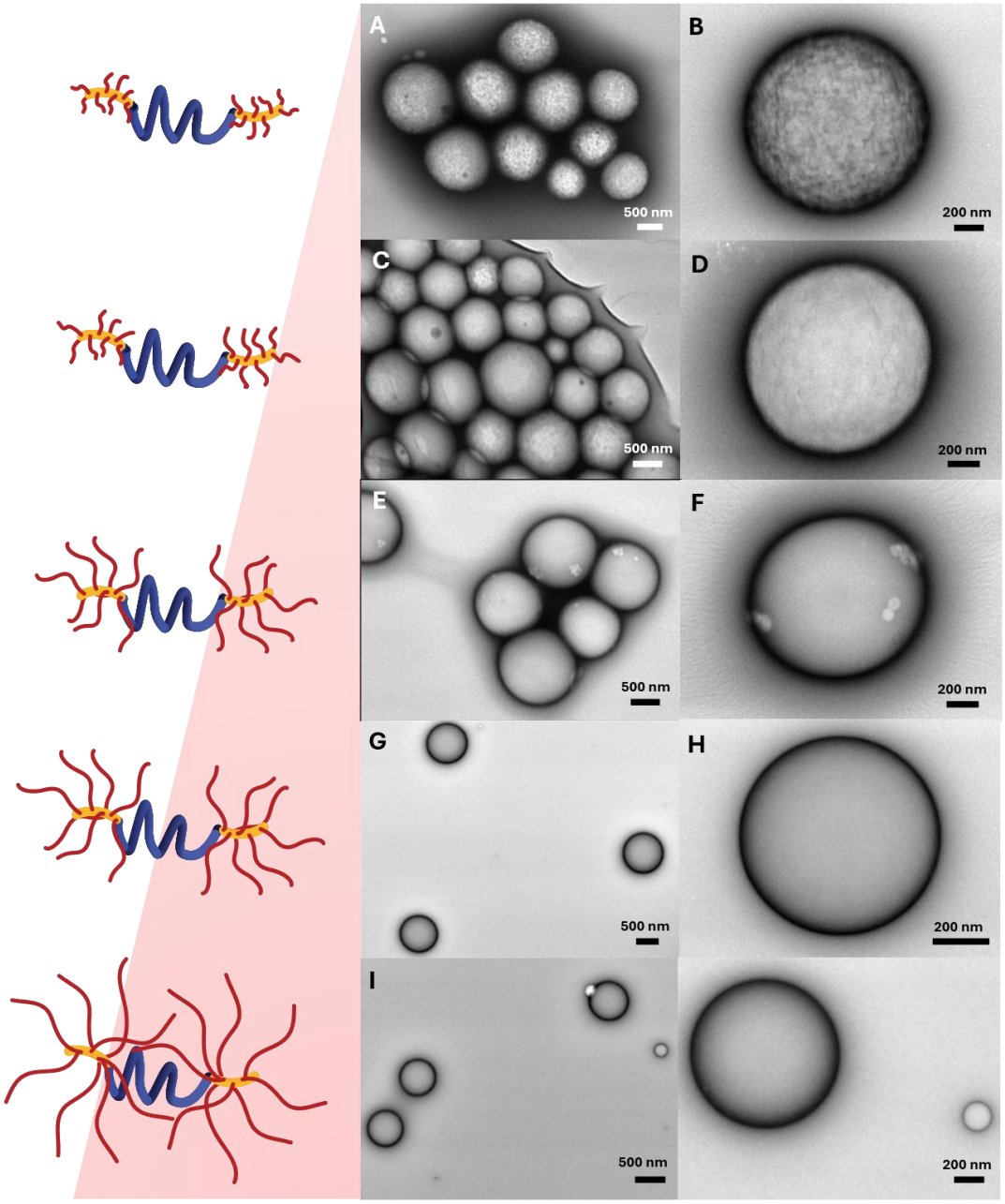

Figure 4.5. (left) Schematic representation of varying side chain lengths of BBCPs with TEM images of self-assemblies from (A,B) DB_5, (C,D) DB_{13}, (E,F) DB_{29}, (G,H) DB_{40}, (I,J) DB_{58} micrographs of negatively stained self-assembled BBCPs

The self-assembly of DB_5 resulted in spherical polymer particles with seemingly rough surface topology and diameters of beyond 1 μm in TEM (Figure 4.5.A & Figure 4.5.B). Encouraged by broad intensity peaks in dynamic light scattering (DLS) (Figure S4.1A), atomic force microscopy (AFM) was used as a complementary technique to look beyond large particles, confirming the presence of spherical particles with smaller diameters of ~50 nm (Figure 4.6). Extension of the side chains to give DB_{13} resulted in a maintenance of spherical particles with similar diameters as DB_5, with seemingly less indentation in the particle surface in TEM (Figure 4.5B and Figure 4.5.C). AFM analysis showed spherical particles ranging from ~100 – 200 nm in diameter (Figure 4.7). It is expected that at larger f_{coil}, the system maintains greater flexibility, allowing the rods to pack into a solvophobic core, with looped coronas. In a linear block terpolymer, this would present as flower-like micelles.[20] The shortest side chain lengths of 5 and 13 are not long enough to sufficiently long enough to achieve critical side chain repulsion for bottlebrush stiffening.[21] This is supported by theoretical simulations where short side chains do not significantly increase the comb diameter compared to linear polymers, thus maintaining an element of flexibility along the backbone.[22] However, reduced hydrophobic content in an amphiphile of this structure reduces enthalpic and entropic contributions in self-assembly processes.[23] This means that intermolecular forces driving micellisation is reduced, and some terpolymers may have only one rod block confined into the hydrophobic core, leading to unstable structures, and the potential toward bridging of micelles by dangling chains,[24] or aggregation.[25] Therefore, we postulate that the rough surface spherical particles from the self-assembly of DB_5 and DB_{13} form from the merging of multiple particles into large rough spherical multicomponent particles.

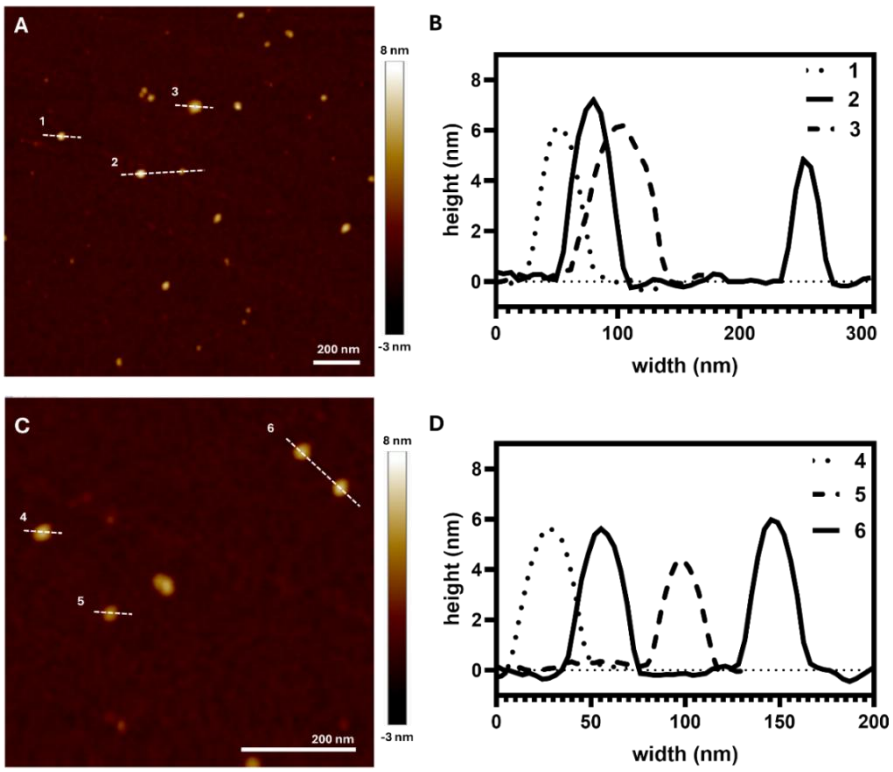

Figure 4.6. AFM of particles self-assembled from DB_5 (A, C) 2D Height map (B, D) Corresponding particle height

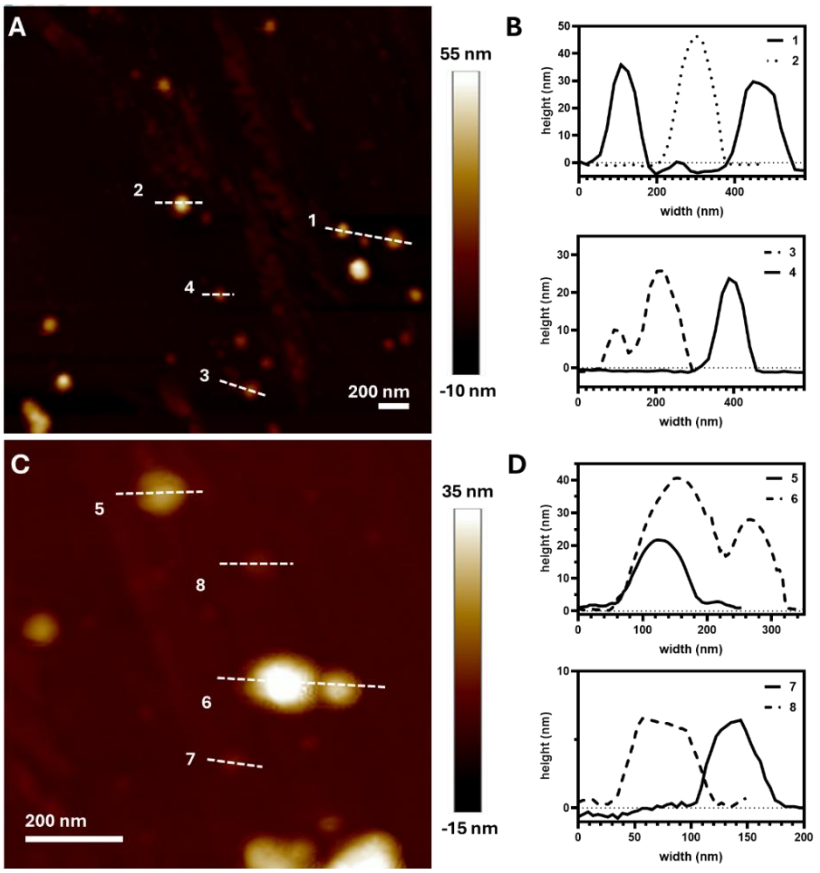

Figure 4.7. AFM of particles self-assembled from DB_{13} (A, C) 2D Height map (B, D) Corresponding particle height

At approximately double the side chain length, DB_{29}, this dumbbell also self-assembles into spherical particles, but with notably smoother surfaces by TEM (Figure 4.5E & 4.5.F). The microparticles show evidence of smaller spherical particles dried on top of them, seemingly as an artifact of the sample preparation process. The size of these particles (~50 nm diameter) corresponds to those observed in AFM with deflated heights of between ~ 8-70 nm (Figure 4.8). Large smooth particles are also observed in the self-assembly from DB_{40} (Figure 4.5G & 4.5.H) with smaller spherical particles with diameters ranging from ~150 – 300 nm observed by AFM (Figure 4.9). In both cases, the deflated height profiles by AFM exist across a range from ~10nm to beyond 25nm in height. The large variance in height profiles, combined with the absence of observed internal structures by TEM are likely to correspond to dense spherical particles.

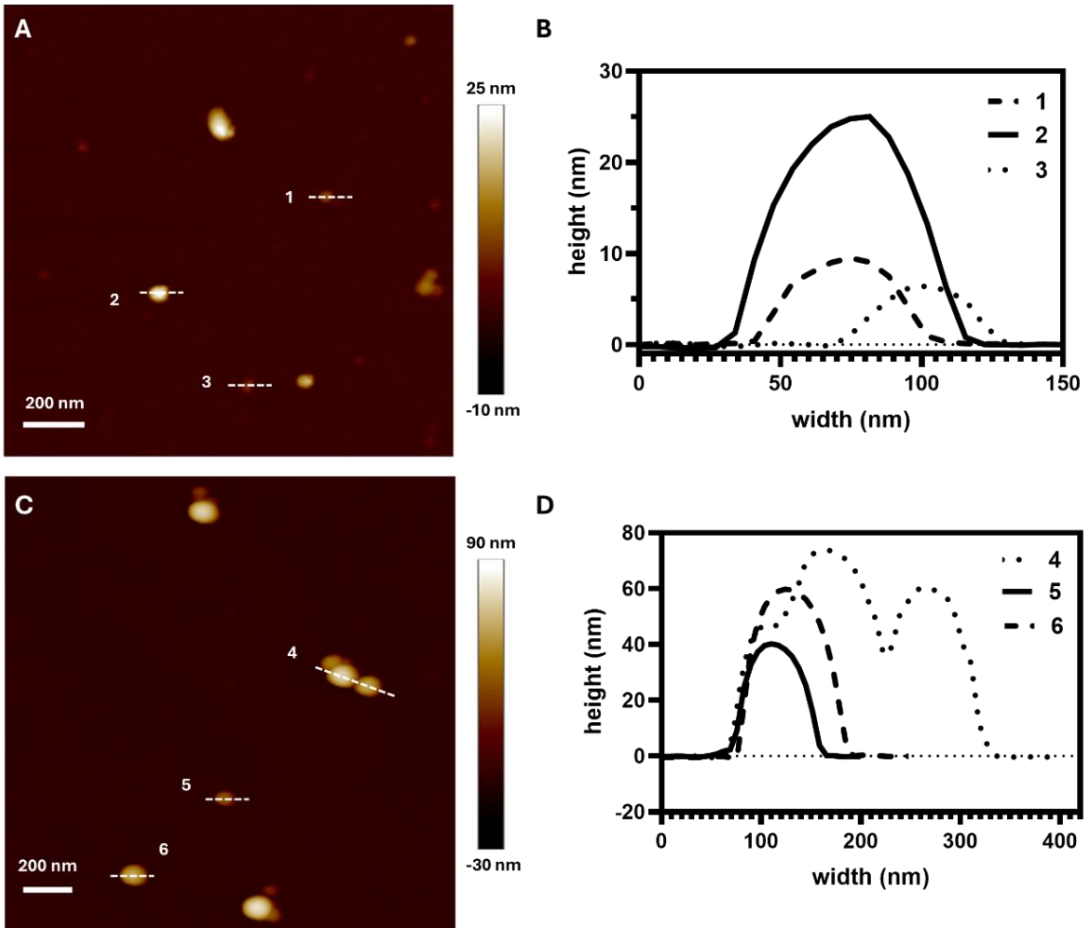

Figure 4.8. AFM of particles self-assembled from DB_{29} (A, C) 2D Height map (B, D) Corresponding particle height

The increased asymmetry of the block copolymers by side chain extension is represented by the sharp increase in the $f_{hydrophobic}$ from 0.52 – 0.74 in the shortest DBs to 0.86 and 0.9 in DB_{29} and DB_{40} respectively (Table 4.1). With side chain lengths now able to facilitate a bottlebrush regime,[26] the flanking rods are expected to be rigid in nature. The interaction between these rigid segments is expected to increase, lending toward dense polymer particles similar to those observed in the self-assembly of bottlebrush-linear block copolymers,[27] in Chapter II. Experimental data on the self-assembly of bottlebrush-linear-bottlebrush block copolymers remains limited, but simulation data confirms that at relatively larger coil lengths, spherical particles remain predominant.[28] Increasing rod lengths can make the phase transition from spherical to lamellar morphologies more accessible,[29] but this is limited at low polymer concentrations. These studies are limited by the rod segments modelling rigid crystalline behaviour instead of bottlebrush blocks, highlighting the novelty of this work.

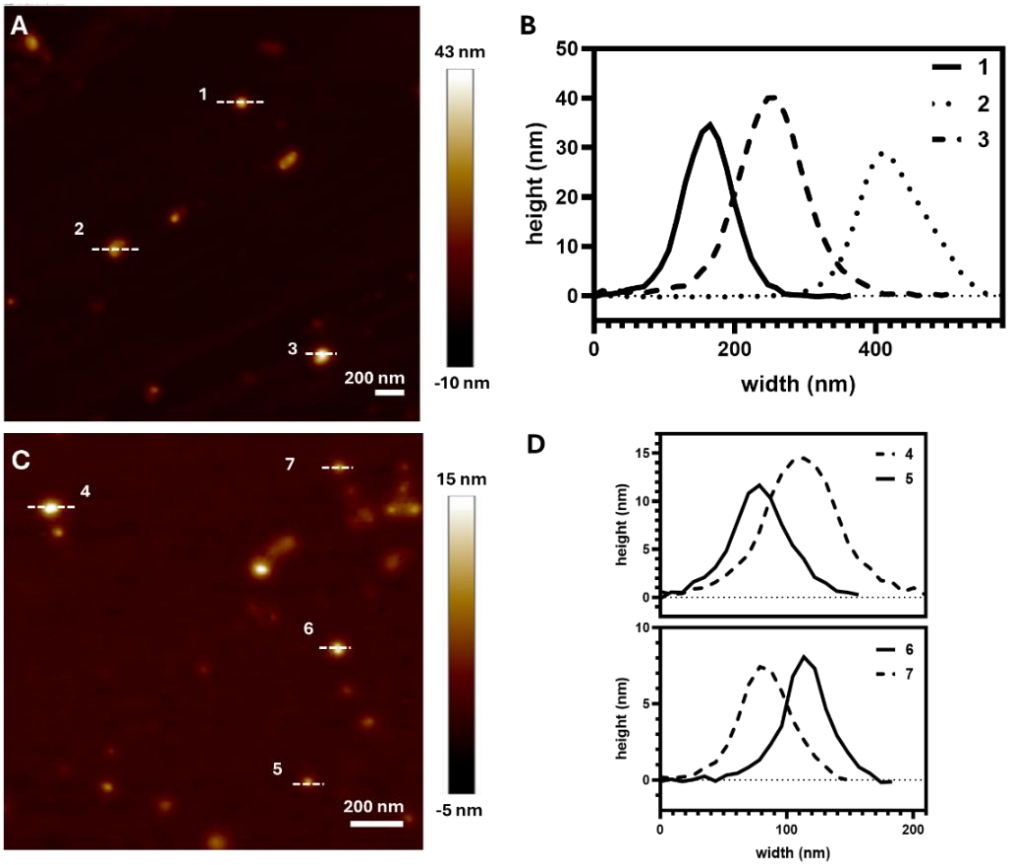

Figure 4.9. AFM of particles self-assembled from DB_{40} (A, C) 2D Height map (B, D) Corresponding particle height.

Extending to DB_{58} leads to a mixed morphology of large dense spherical nanoprecipitates with incidence of smaller flat assemblies verified by TEM (Figure 4.5.I & 4.5.J) and AFM (Figure 4.10). Having side chains of 58 repeat units is within the appropriate range to induce sufficient steric repulsion for brush rigidification and subsequent packing into planar structures.[10] Structurally, dumbbell architectures can be considered as two tadpoles attached by their coil. Therefore, we would expect that dumbbell polymers with analogous hydrophobic components to disc-forming tadpoles may also preferentially pack into discs. To this effect, DB_{29} maintains an appropriate hydrophilic hydrophobic ratio. However, in this case, with the hydrophilic coil being flanked by two rod segments results in a 'hairpin'[30] conformation as the coil is stretched upon space occupancy by water molecules.[31] Whilst we expected that shorter side chain lengths would allow sideways packing of the brush blocks to be more favourable and lend towards flat structures, it is likely that these side chain lengths are not long enough to achieve sufficient inter side chain repulsion induced rigidity.[32, 33] Instead, these dumbbells adopt conformations with higher surface curvature. Therefore, the intra- and inter-molecular rod-rod interactions play a significant role in morphology.

With DB_{58} exhibiting the largest $f_{\text{hydrophobic}}$ at approximately double that of disc forming tadpoles in Chapter II, the rod segments are expected to overwhelm the hydrophilic PEG coil leading to nanoprecipitates. Additionally, the locality of such large brush segments with respect to the connecting coil are not expected to pack into planar assemblies. As the approximate carbon–carbon length in polymethacrylates correlates to ~0.25 nm,[34] two adjacent rods with side chains of 58 repeat units would position the tethering points of the PEG coil at ~29 nm apart. The PEG coil in water is expected to extend (at maximum) to ~37 nm in length, with each monomer -(CH_2CH_2O)- unit approximately 0.35 nm long.[35] Simulation studies of end-tethered nanorods by Glotzer and coworkers suggest that at shorter tether or coil lengths, flat interfaces may be favoured as rod-rod interactions are thermodynamically favourable.[36]

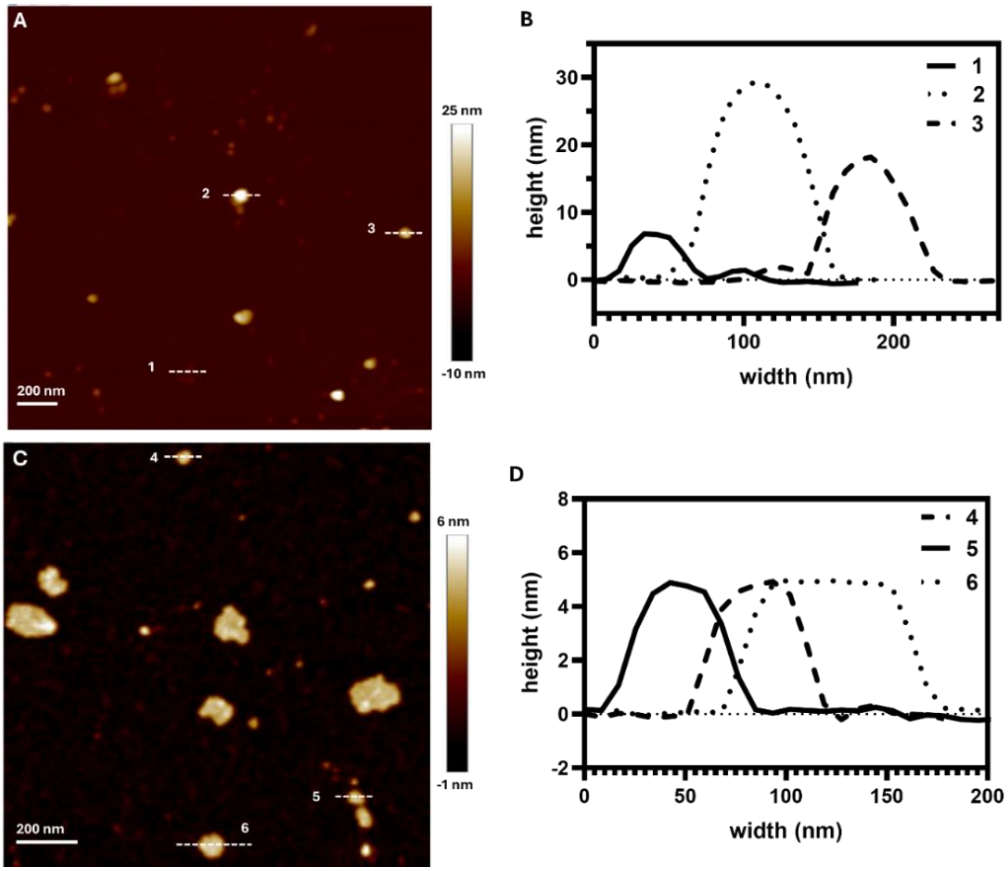

Figure 4.10. AFM of particles self-assembled from DB_{58} (A, C) 2D Height map (B, D) Corresponding particle height

Therefore, we expect that the incidence of planar assemblies is attributed to the interplay of both rigidification of the bottlebrush segments and the stretching of the tethering coil. However, the higher incidence of dense spherical aggregates suggests that DB_{58} may exist at a boundary of a window of disc formation. Whilst the coil can theoretically accommodate sideways rod packing, it is expected that the stretching effect on the coil in this conformation may be too large to be thermodynamically favourable. By increasing the PEG coil length between sufficiently rigidified bottlebrush segments, it is possible that discoidal assemblies may be better stabilised, however the hydrophobic and hydrophilic balance of the amphiphile will need to be considered to access discoidal particles exclusively.

4.3 Dumbbell and tadpole block copolymer co-assembly

Determining that DB_{58} maintains some propensity towards planar packing, we looked to investigate their co-assembly with disc forming building blocks. The co-assembly approach was utilised as a means of reducing the strain on the PEG coil to stabilise flat structures to access greater incidence of flat structures. DB_{58} was self-assembled with disc-forming $TP_{15\text{-}75}$ at 50 wt% of each polymer in a 2mg/mL DMF polymer solution against deionised water. $TP_{15\text{-}75}$, previously presented in Chapter II maintains a similar PEG coil with a molecular weight of 5000 g/mol. The connecting PBIEM of 15 repeat units has tethered PBzMA side chains of 75 repeat units long. Interestingly, when observed by AFM, the structures show structures with deflated heights of ~10 and 15 nm, with some incidence of stacked structures (Figure 4.11A-C). These heights correspond to multiples of 5nm, which corresponds to the deflated heights of the flat structures by the self-assembly of DB_{58} alone (Figure 4.10). The presence of a rim feature within the particles is inconsistent with discoidal particles, suggesting some internal structures. This is corroborated by TEM where membranous features around spherical particles is observed that seemingly differ to typical vesicular structures (Figure S4.2). Whilst the exact morphology remains inconclusive and requiring further investigation, co-assembly with a bottlebrush-linear diblock copolymer of similar chemistry dramatically alters packing behaviour. Acknowledging that the wt% of the dumbbell is relatively high, co-assembly was also investigated at 5 and 15wt% in a 2mg/mL solution. As the wt% of dumbbells is increased, the height maps by AFM suggest that particles tend to have taller feature heights (Figure 4.11). By height analysis, these heights increase by 5 nm increments, which corresponds to the height of a single brush section of the BBCPs, as previously described in Chapter II.[37] This suggests that there may be some stacking of particles. The reduction in the concentration of dumbbell polymers may reduce the likelihood of intermolecular rod-rod interactions in dumbbell polymers, positioning the self-assembly phase closer to discs as the dominant morphology from

the self-assembly of the tadpole polymer. Interestingly, the hydrodynamic size by DLS also increases with reduced wt% of dumbbells in the co-assembly, further supporting that stacked features may be concentration dependent (Figure S4.1B). Whilst it is possible that some of these may be an artifact of the drying process in sample preparation,[10] given the incidence, it is likely that this is a feature of the co-assembly process.

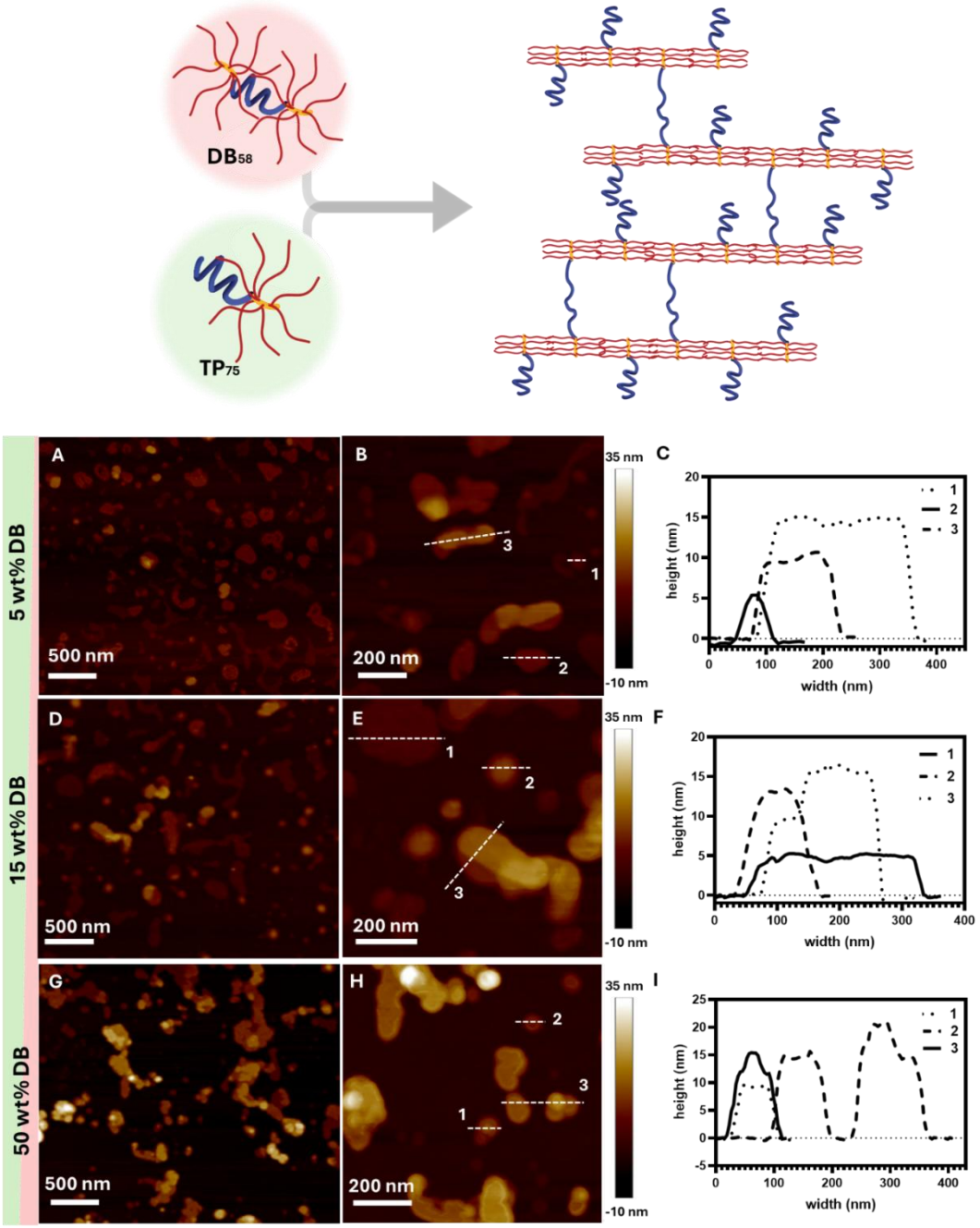

Figure 4.11. Schematic representation of suspected packing of bottlebrush-linear block copolymers in the co-assembly of $TP_{15\text{-}75}$ and DB_{58} (top) with AFM micrographs at (A-B) 5 wt%, (D-E) 15%, and (G-H) 50wt% with corresponding height maps for numbered particles (C) 5 wt%, (F) 15%, and (I) 50wt%.

As a secondary co-assembly study, $DB_{29,}$ with a similar hydrophobic to hydrophilic ratio to $TP_{15\text{-}75}$ was also co-assembled with the tadpole at 50 wt%. Despite having insufficiently long side chains to pack into planar structures alone, upon co-assembly, a network of flat structures of multiple heights with steps in 5 nm increments were observed by AFM (Figure 4.12), which corresponds to the height of a single brush section of the BBCPs. Therefore, height profiles of ~10 nm would correspond to the height of two particles linked, and ~15 nm would be representative of three particle heights. The high incidence of this in these samples indicates that dumbbell block copolymers could be acting as a cross-linker.[38] Interestingly, this stacking observed even at relatively high percentages of dumbbell polymer where one may expect intramolecular interactions to dominate and favour polymer aggregation. TEM confirmed the presence of flat particles in this sample.

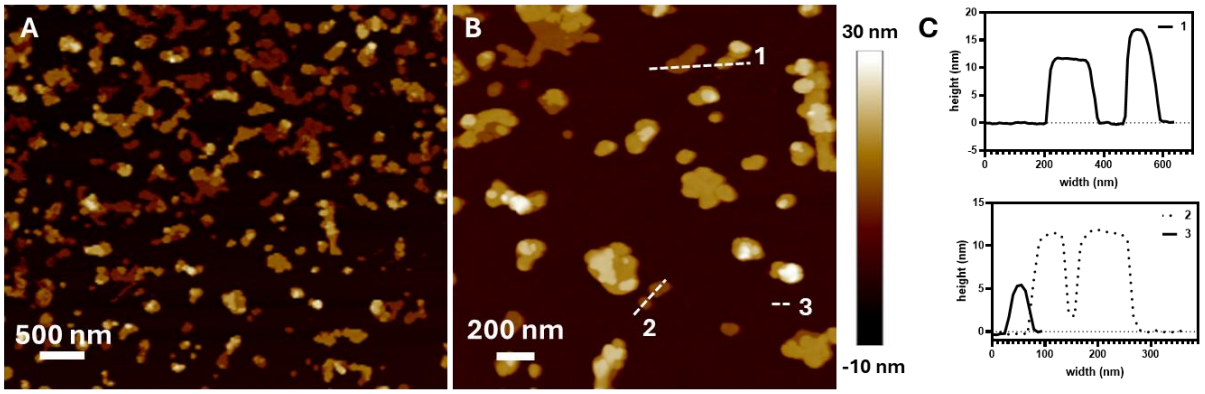

Figure 4.12. AFM micrographs of co-assembly of bottlebrush-linear block copolymers $TP_{15\text{-}75}$ and DB_{29} (A-B) at 50 wt% with (C) corresponding height maps

We postulate that the stacking effect observed in both samples is facilitated by the dumbbell polymers acting as cross-linkers with the bottlebrush segments self-assembling into different discs, being connected by the PEG coil. This has been observed between puck-like particles resulting in the formation of networks within a compound micelle.[38] Self-consistent field theory studies of crystalline rod-coil-cod systems have been investigated to understand packing behaviour in stacked lamella phases. It is shown that when the rod segments have a large diameter, the excess stretching on the coil results can force rearrangement of some rods to pack

head-to-head and reduce the spanning distance of the linear chains.[39] Where the tadpole structures would typically pack into discoidal features, the dumbbells intercalate and act as a 'bridge'. Where the rods are not considered too large, as in the case of DB_{29} there is expected to be a balance between hairpin folding with molecules maintaining themselves in single particles, and some extending across different phases.[39] Whilst we have observed that DB_{29} core-forming rods are not rigid enough to pack into flat structures alone (Figure 4.5E & F, Figure 4.8), we postulate that the tadpole structures can have a rigidifying effect on the core-forming segments of $DB_{29,}$ allowing them to span between structures and participate in lamella packing. Whilst this is a rudimentary claim requiring further investigation, understanding of bottlebrush-bottlebrush interactions may account for these observations, In the case of linear block copolymers, co-assembly of block copolymers of varying molecular weights result in morphologies where low MW polymers stretch, and high MW polymers compress to pack together.[40] Similar investigations were conducted using entirely bottlebrush building blocks of different MW into lamellar phases.[41] Whilst these studies show that extensive mismatch in molecular weight may interrupt co-assembly,[42] the asymmetry in the two polymer architectures as tadpoles and dumbbells can circumvent this by forming connected structures. Being chemically analogous polymers with side chains of the same chemistry, we can attribute the factors influencing the co-assembly process to be predominantly on packing behaviour.

Polymer networks are an important material for applications such as tissue engineering, elastomers, or those requiring high cargo-loading. Polymeric gels tend to form during incomplete phase separation where solvent is trapped between polymers. The incorporation of bottlebrush segments enables greater control over observed stiffness and softness through parameters such as grafting density, or alternating blocks of brush and linear segments.[43] Linear-*block*-brush-*block*-linear (LBL) polymers are predominantly employed in the formation of polymer networks and gels. Typically, either long hydrophilic linear segments are physically

cross-linked through entanglement, or bottlebrush segments are chemically cross-linked to form a network with high water holding capacity known as hydrogels.[44] However, this can typically only occur at high polymer content to force intermolecular interaction, compared to the 2 mg/ml polymer concentrations employed in this study. The presented system is not considered a gel, instead spontaneously forming networks of particles driven by the phase separation that occurs in typical amphiphilic polymer self-assembly. This is facilitated by the use of two chemically analogous but architecturally complementary building blocks, and their random spatial arrangement. However, considering that these networks do form at low polymer concentrations, we postulate that this system could be used to access gels or materials with viscoelastic properties for applications such as drug delivery, photonics and tissue engineering.

As the first report of co-assembly of two complex brush-linear block architectures with different packing behaviour, this represents an exciting landscape for further investigation and verification into the morphology and mechanism of stacked particles to inform design considerations to extend these architectures further. For example, stacked height profiles could be adjusted by changing bottlebrush backbone lengths. Alternatively, altering PEG coil lengths could reduce the density of particle networks toward other materials such as nanoparticle-hydrogel composites.[45]

5. Conclusion

Bottlebrush-linear-bottlebrush rod-coil-rod block copolymers represent a unique and underexplored architecture in self-assembly studies. By designing a polymer library via the grafting-from approach, this chapter develops a structure-property relationship between polymer architecture and self-assembled morphologies. Demonstrating morphological evolution from multicomponent particles to dense aggregates and some incidence of planar structures provides insight into how the side chain length of the bottlebrushes can influence the

stiffness contrast, hydrophobic content and subsequent conformation of the linear and rod segments in the self-assembly of these triblock terpolymers. Additionally, the observation of stacked planar structures in binary blends of tadpole and dumbbell structure presents opportunities to investigate how intermolecular brush-brush interactions can influence polymer conformations and morphologies. There is also scope to tune dumbbell block copolymers to be used as cross-linkers as they intercalate to form networks of particles or even gels at higher percentage polymer content. To assess these materials, rheological studies could be performed to further investigate the effects of intermolecular interactions on material properties for hydrogel applications. This work serves as a foundation to understand the self-assembly behaviour of previously underexplored bottlebrush-linear-bottlebrush architectures, highlighting how the unique nature of bottlebrush polymers can vastly change the packing parameter of building blocks when tethered by flexible linear coils. Future work into understanding the self-assembly mechanism of both block copolymer and binary blends of architecture both by experimental and theoretical modelling is required to verify and understand the potential of these complex polymer architectures. In this effort, the window for the fabrication towards anisotropic nanoparticles such as nanodiscs can be expanded by influencing the design of both polymer building-block and environmental conditions in the self-assembly process.

6. References

1. Verduzco, R.; Li, X.; Pesek, S. L.; Stein, G. E., Structure, function, self-assembly, and applications of bottlebrush copolymers. *Chemical Society Reviews* **2015,** *44* (8), 2405-2420.

2. Karayianni, M.; Pispas, S., Block copolymer solution self‐assembly: Recent advances, emerging trends, and applications. *Journal of Polymer Science* **2021,** *59* (17), 1874-1898.

3. Olsen, B. D.; Segalman, R. A., Self-assembly of rod–coil block copolymers. *Materials Science and Engineering: R: Reports* **2008,** *62* (2), 37-66.

4. Liu, C.-L.; Lin, C.-H.; Kuo, C.-C.; Lin, S.-T.; Chen, W.-C., Conjugated rod–coil block copolymers: Synthesis, morphology, photophysical properties, and stimuli-responsive applications. *Progress in Polymer Science* **2011,** *36* (5), 603-637.

5. Chen, C.-A.; Kao, T.-C.; Lin, S.-H.; Ho, C.-C.; Tung, S.-H.; Su, W.-F., Facile approach for rapid self-assembly of rod-coil block copolymers. *Polymer* **2018,** *139*, 20-25.

6. Peng, J.; Han, Y., Recent advances in conjugated polythiophene-based rod–rod block copolymers: From morphology control to optoelectronic applications. *Giant* **2020,** *4*, 100039.

7. Xu, F.; Zhang, J.; Zhang, P.; Luan, X.; Mai, Y., "Rod–coil" copolymers get self-assembled in solution. *Materials Chemistry Frontiers* **2019,** *3* (11), 2283-2307.

8. Wu, D.; Huang, Y.; Xu, F.; Mai, Y.; Yan, D., Recent advances in the solution self‐assembly of amphiphilic "rod‐coil" copolymers. *Journal of Polymer Science Part A: Polymer Chemistry* **2017,** *55* (9), 1459-1477.

9. Saha, D.; Witt, C. L.; Fatima, R.; Uchiyama, T.; Pande, V.; Song, D.-P.; Fei, H.-F.; Yavitt, B. M.; Watkins, J. J., Opportunities in Bottlebrush Block Copolymers for Advanced Materials. *ACS Nano* **2025,** *19* (2), 1884-1910.

10. Kerai, S. D.; Takano, S.; Zeng, P.; Müllner, M., Self-Assembly of Bottlebrush-Linear, Rod–Coil Copolymers into Discoidal Nanoparticles. *ACS Macro Letters* **2025**, 834-840.

11. Shi, Y.; Zhu, W.; Yao, D.; Long, M.; Peng, B.; Zhang, K.; Chen, Y., Disk-Like Micelles with a Highly Ordered Pattern from Molecular Bottlebrushes. *ACS Macro Lett.* **2014,** *3* (1), 70-73.

12. Xu, Z.; Lin, J.; Zhang, Q.; Wang, L.; Tian, X., Theoretical simulations of nanostructures self-assembled from copolymer systems. *Polymer Chemistry* **2016,** *7* (23), 3783-3811.

13. Chen, J.-Z.; Sun, Z.-Y.; Zhang, C.-X.; An, L.-J.; Tong, Z., Self-assembly of rod-coil-rod ABA-type triblock copolymers. *The Journal of Chemical Physics* **2008,** *128* (7), 074904.

14. Li, Y.; Jiang, T.; Lin, S.; Lin, J.; Cai, C.; Zhu, X., Hierarchical Nanostructures Self-Assembled from a Mixture System Containing Rod-Coil Block Copolymers and Rigid Homopolymers. *Scientific Reports* **2015,** *5* (1), 10137.

15. Otulakowski, Ł.; Lipowska-Kur, D.; Gadzinowski, M.; Slomkowski, S.; Basinska, T.; Forys, A.; Trzebicka, B., The Synthesis and Properties of Brush-Coil–Brush (Polyglycidol-g-polyglycidol)-b–

polystyrene–b-(polyglycidol-g-polyglycidol) Copolymers. *The Journal of Physical Chemistry B* **2025,** *129* (28), 7406-7419.

16. Jonikaite-Svegzdiene, J.; Kudresova, A.; Paukstis, S.; Skapas, M.; Makuska, R., Synthesis and self-assembly of polystyrene-based diblock and triblock coil–brush copolymers. *Polymer Chemistry* **2017,** *8* (36), 5621-5632.

17. Lebedeva, I. O.; Zhulina, E. B.; Borisov, O. V., Self-Assembly of Bottlebrush Block Copolymers in Selective Solvent: Micellar Structures. *Polymers* **2021,** *13* (9), 1351.

18. Zheng, Z.; Müllner, M.; Ling, J.; Müller, A. H. E., Surface Interactions Surpass Carbon–Carbon Bond: Understanding and Control of the Scission Behavior of Core–Shell Polymer Brushes on Surfaces. *ACS Nano* **2013,** *7* (3), 2284-2291.

19. Neugebauer, D.; Sumerlin, B. S.; Matyjaszewski, K.; Goodhart, B.; Sheiko, S. S., How dense are cylindrical brushes grafted from a multifunctional macroinitiator? *Polymer* **2004,** *45* (24), 8173-8179.

20. Balsara, N.; Tirrell, M.; Lodge, T., Micelle formation of BAB triblock copolymers in solvents that preferentially dissolve the A block. *Macromolecules* **1991,** *24* (8), 1975-1986.

21. Liberman, L.; Coughlin, M. L.; Weigand, S.; Edmund, J.; Bates, F. S.; Lodge, T. P., Impact of Side-Chain Length on the Self-Assembly of Linear-Bottlebrush Diblock Copolymers. *Macromolecules* **2022,** *55* (12), 4947-4955.

22. Elli, S.; Ganazzoli, F.; Timoshenko, E. G.; Kuznetsov, Y. A.; Connolly, R., Size and persistence length of molecular bottle-brushes by Monte Carlo simulations. *The Journal of Chemical Physics* **2004,** *120* (13), 6257-6267.

23. Kim, S. H.; Jo, W. H., A Monte Carlo simulation for the micellization of ABA- and BAB-type triblock copolymers in a selective solvent. II. Effects of the block composition. *The Journal of Chemical Physics* **2002,** *117* (18), 8565-8572.

24. Yuan, J.; Xu, Z.; Cheng, S.; Feng, L., The aggregation of polystyrene-b-poly(ethylene oxide)-b-polystyrene triblock copolymers in aqueous solution. *European Polymer Journal* **2002,** *38* (8), 1537-1546.

25. Omar, A. K.; Hanson, B.; Haws, R. T.; Hu, Z.; Vanden Bout, D. A.; Rossky, P. J.; Ganesan, V., Aggregation Behavior of Rod–Coil–Rod Triblock Copolymers in a Coil-Selective Solvent. *The Journal of Physical Chemistry B* **2015,** *119* (1), 330-337.

26. Zhulina, E. B.; Sheiko, S. S.; Borisov, O. V., Theoretical advances in molecular bottlebrushes and comblike (co)polymers: solutions, gels, and self-assembly. *Soft Matter* **2022,** *18* (46), 8714-8732.

27. Takano, S.; Nishimura, T.; Cheng, Y. T.; Müllner, M., Self-Assembly of Thioether-Based Diblock Copolymers: A Comparative Study of Linear and Bottlebrush Architectures. *Polymer Chemistry* **2025**.

28. Zhou, Y.; Song, S.; Long, X. P.; Zhang, C. Y.; Chen, Y. M., Dissipative Particle Dynamics Simulation on Self‐Assembly Behavior of Rod–Coil–Rod Triblock Copolymer in Solutions. *Macromolecular Theory and Simulations* **2014,** *23* (8), 490-499.

29. Toujani, C.; Padilla, L. A.; Alhraki, N.; Hur, S.-M.; Ramírez-Hernández, A., Self-assembly of rod–coil–rod block copolymers in a coil-selective solvent: coarse-grained simulation results. *Soft Matter* **2024,** *20* (14), 3131-3142.

30. Chen, X. L.; Jenekhe, S. A., Supramolecular Self-Assembly of Three-Dimensional Nanostructures and Microstructures: Microcapsules from Electroactive and Photoactive Rod−Coil−Rod Triblock Copolymers. *Macromolecules* **2000,** *33* (13), 4610-4612.

31. Huo, H.; Li, K.; Wang, Q.; Wu, C., Self-Assembly and Optical Property of Triblock Copolymers Made of Polystyrene and Oligo(p-phenyleneethynylene) in Different Mixtures of Toluene and Hexane. *Macromolecules* **2007,** *40* (18), 6692-6698.

32. Theodorakis, P. E.; Hsu, H.-P.; Paul, W.; Binder, K., Computer simulation of bottle-brush polymers with flexible backbone: Good solvent versus theta solvent conditions. *The Journal of Chemical Physics* **2011,** *135* (16), 164903.

33. Hou, W.; Wu, J.; Li, Z.; Zhang, Z.; Shi, Y.; Chen, Y., Efficient Synthesis and PISA Behavior of Molecular Bottlebrush Block Copolymers via a Grafting-From Strategy through RAFT Dispersion Polymerization. *Macromolecules* **2023,** *56* (3), 824-832.

34. Yoshikawa, C.; Sakakibara, K.; Nonsuwan, P.; Yamazaki, T.; Tsujii, Y., Nonbiofouling Coatings Using Bottlebrushes with Concentrated Polymer Brush Architecture. *Biomacromolecules* **2021,** *22* (6), 2505-2514.

35. Kenworthy, A. K.; Hristova, K.; Needham, D.; McIntosh, T. J., Range and magnitude of the steric pressure between bilayers containing phospholipids with covalently attached poly(ethylene glycol). *Biophysical Journal* **1995,** *68* (5), 1921-1936.

36. Horsch, M. A.; Zhang, Z.; Glotzer, S. C., Simulation studies of self-assembly of end-tethered nanorods in solution and role of rod aspect ratio and tether length. *The Journal of Chemical Physics* **2006,** *125* (18), 184903.

37. Kerai, S. D.; Takano, S.; Zeng, P.; Müllner, M., Self-Assembly of Bottlebrush-Linear, Rod–Coil Copolymers into Discoidal Nanoparticles. *ACS Macro Lett.* **2025,** *14* (6), 834-840.

38. Kim, T.-G.; Kim, C.; Park, J.-W., Redox-Responsive Self-Assembly of Amphiphilic Multiblock Rod–Coil Polymers. *Macromolecules* **2017,** *50* (20), 8185-8191.

39. Liu, F.; Sun, T.; Tang, P.; Zhang, H.; Qiu, F., Understanding chain folding morphology of semicrystalline polymers based on a rod–coil multiblock model. *Soft Matter* **2017,** *13* (44), 8250-8263.

40. Yamaguchi, D.; Hashimoto, T., A Phase Diagram for the Binary Blends of Nearly Symmetric Diblock Copolymers. 1. Parameter Space of Molecular Weight Ratio and Blend Composition. *Macromolecules* **2001,** *34* (18), 6495-6505.

41. Miyake, G. M.; Piunova, V. A.; Weitekamp, R. A.; Grubbs, R. H., Precisely Tunable Photonic Crystals From Rapidly Self‐Assembling Brush Block Copolymer Blends. *Angewandte Chemie International Edition* **2012,** *51* (45), 11246-11248.

42. Chen, X.; Song, D.-P.; Li, Y., Precisely Tunable Photonic Pigments via Interfacial Self-Assembly of Bottlebrush Block Copolymer Binary Blends. *Macromolecules* **2022,** *55* (17), 7438-7445.

43. Keith, A. N.; Vatankhah-Varnosfaderani, M.; Clair, C.; Fahimipour, F.; Dashtimoghadam, E.; Lallam, A.; Sztucki, M.; Ivanov, D. A.; Liang, H.; Dobrynin, A. V.; Sheiko, S. S., Bottlebrush Bridge between Soft Gels and Firm Tissues. *ACS Central Science* **2020,** *6* (3), 413-419.

44. Hu, K.; Mu, R.; Ma, Z.; Li, B., Bottlebrush Polymers: From Synthesis to Properties and Applications. *Macromol. Rapid Commun.* **2025,** *46* (16), 2500215.

45. Dannert, C.; Stokke, B. T.; Dias, R. S., Nanoparticle-Hydrogel Composites: From Molecular Interactions to Macroscopic Behavior. *Polymers* **2019,** *11* (2), 275.

7. Supporting Information

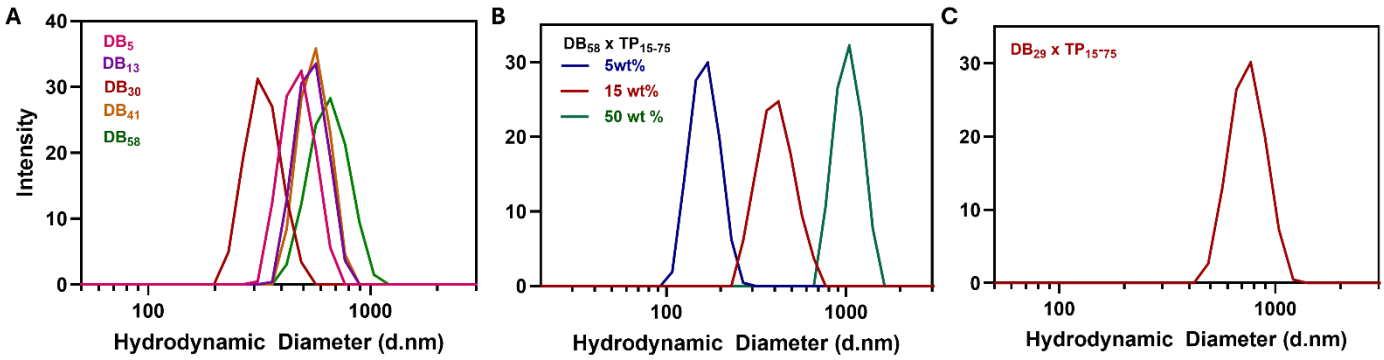

Figure S4.1. Hydrodynamic Diameter Intensity by DLS of (A) Self-Assembly of Dumbbells DB_5, DB_{13}, DB_{29}, DB_{40}, DB_{58} (B) Co-Assembly DB_{58} x $TP_{15\text{-}75}$ at 5 wt%, 15 wt% and 50wt% dumbbell (C) Co-Assembly of DB_{29} x $TP_{15\text{-}75}$ at 50 wt% dumbbell

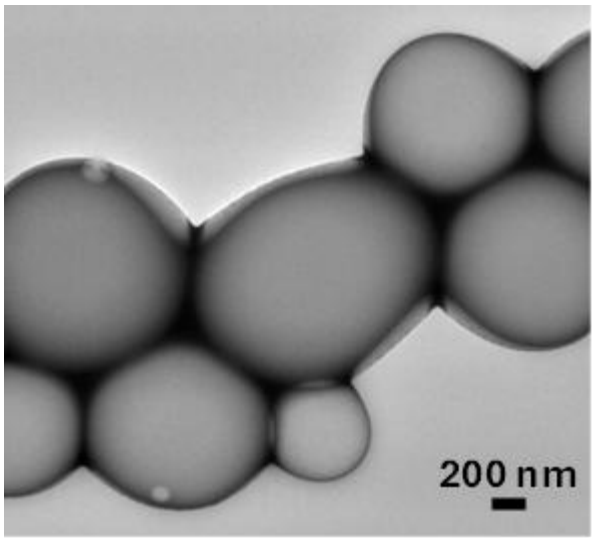

Figure S4.2. Negatively stained TEM micrograph of the Co-Assembly DB_{58} x $TP_{15\text{-}75}$ at 5 wt%

Chapter V : Conclusion and Outlook

This thesis begins to establish a foundational understanding of the structural and chemical requirements for molecular building blocks to access discoidal materials through self-assembly. While the field of polymer self-assembly has matured significantly in accessing spherical and cylindrical morphologies, the controlled formation of disc-like structures has remained an elusive target that requires fundamentally different design principles and assembly mechanisms. The formation of discoidal materials represents far more than simply another morphology to add to the catalogue of self-assembled structures. Discs occupy a unique position in the landscape of anisotropic particles, offering combinations of properties that cannot be achieved through spherical or cylindrical alternatives. The high surface area-to-volume ratio, the potential for preferential orientation and alignment in fluidic environments, and the distinctive surface interactions make discs exceptionally attractive targets for advanced applications. The current landscape of discoidal particles relies largely on top-down approaches where larger particles are processed into smaller components, through directed methods such as use of templates, or via kinetically driven processes such as crystallisation-driven self-assembly. This is owed to disc shapes being considered thermodynamically unfavourable in solution polymer self-assembly. However, the inclusion of bottlebrush segments in complex architectures proves to be an interesting avenue to circumvent these barriers and improve access to these lucrative morphologies.

The work presented here represents an important first step in deciphering the architectural requirements for disc formation in polymer systems. Through systematic investigation of molecular polymer brush – *block* – linear block copolymer 'tadpoles' in Chapter II of this thesis, we have begun to map the structural parameter space necessary for anisotropic disc formation. The central finding of this work is the identification of critical structural features that enable disc formation. The molecular polymer brush segment contrasted with the flexible linear polymer chain creates unique steric constraints that overcomes the energy bending

penalty, with the interplay between brush density, side chain length, and block composition creates a narrow but accessible window for disc morphology. Our investigations have revealed that side chain length represents a critical control parameter, with only specific ranges promoting disc formation. This sensitivity suggests a delicate balance of competing forces.

With these design principles in mind, Chapter III shows how chemically diverse tadpole structures can be co-assembled to extend functional nanoparticles. Through the inclusion of pH-sensitive poly(ethylene glycol)-*block*-[poly(3-azido-2-hydroxypropyl methacrylate)-*graft*-poly(ethyl ethoxylate)] (TP_{EE}) and inert poly(ethylene glycol)-*block*-[poly(2-(2-bromo isobutyryloxy)ethyl methacrylate)-*graft*-poly(benzyl methacrylate) (TP_{BzMA}) at different ratios, this chapter explores the effect of their co-assembly on particle formation and degradation upon pH treatment. Finding that the ratio of stimuli-responsive tadpoles directly correlates to their disassembly, with the potential of a 'shielding effect' where high Tg TP_{BzMA} may prevent the complete hydrolysation of TP_{EE} and subsequent disassembly of particles. This work provides proof-of-concept of how co-assembly can be used to access functional materials that can retain their structure, or be responsive to multiple stimuli, with their morphology tuned by the nature of the included building blocks.

Chapter IV investigated how extending architectural complexity of linear-bottlebrush diblock copolymers to bottlebrush-linear-bottlebrush 'dumbbell' systems can alter self-assembly behaviour to achieve higher order morphologies. By altering the locality of rigid blocks with respect to the linear segment, the bidirectional steric constraints saw morphological evolution from multicomponent particles to dense aggregates and some incidence of planar structures with increasing side chain lengths. To assess the effect on packing behaviour in a co-assembly system, these dumbbells in co-assembly approaches with bottlebrush-linear diblock copolymers shows potential for accessing networks of planar nanostructures.

Continuing from the findings reported, many aspects concerning polymeric building block design and self-assembly parameter can be explored in greater detail to expand the window to realise discoidal particles in a reliable manner.

1. Self-Assembly Investigations

The precise mechanistic details of how these structural parameters translate into anisotropic particles remain poorly understood, representing a significant gap in our fundamental knowledge of the direct self-assembly mechanism. The discovery of the structural window in Chapter II provides initial design rules for disc-forming systems, but there is large scope for many of these parameters to continue to be explored in systematic studies. Immediate extensions of the work described in this thesis could look to explore grafting density and glass transition temperature as structural and chemical design principles respectively. Delving more into directed self-assembly principles, solvent effects and processing conditions could also be investigated.

1.1 Grafting Density

It is well understood from Chapter II that inter side chain repulsion is necessary for core-segment stiffening in a tadpole building block. However, depending on the chemical composition of polymer backbones and side chains, the achievable grafting density can vary significantly. We expect that increasing grafting density will increase the window of disc realisation, quantitatively mapping this relationship out will improve accessibility of discoidal morphologies. More importantly, understanding the lower limit of grafting density that can still achieve discs is relevant to inform decisions on incorporating side chains with greater chemical versatility and bulkiness. This structure-property mapping will enable predictive design of disc-forming systems and could reveal optimal grafting densities for specific applications.

To achieve controlled grafting density variation, ring-opening metathesis polymerisation (ROMP) is a facile approach. Preliminary work involved designing macromonomers bearing norbornene end-functionality and varying their spatial arrangement with norbornene spacers in the polymer backbone, the grafting density of the bottlebrush segment can be systematically controlled up to 100%. To match the side brush length of core-forming segments, hydrophobic and stimuli-responsive macromonomers were polymerised to a target degree of polymerisation of ~40-50 repeat units. These macromonomers were polymerised from a synthesised norbornene-bromide bifunctional initiator, using ATRP to grow a methacrylate polymer chain. Two initiator variations were explored (Scheme 5.1), based on commercially available norbornene products. The macromonomers are summarised in Table 5.1 and Scheme 5.2.

Table 5.1. Characterisation data of norbornene functionalised macromonomers (MM)

Macromonomer	DP	[a] $M_{n,NMR}$	[b] $Đ_{SEC}$
poly(*tert*-butyl methacrylate)	51	7580	1.04
poly(2-*N*-(morpholino)ethyl methacrylate)	37	7700	1.08
polystyrene	32	3700	1.12

[a] Determined by ^{1}H NMR analysis, [b]Determined by SEC (M_w/M_n).

Scheme 5.1. Synthesis pathways of bifunctional initiators bearing norbornene and bromide groups for ROMP and ATRP respectively with different spacer moieties

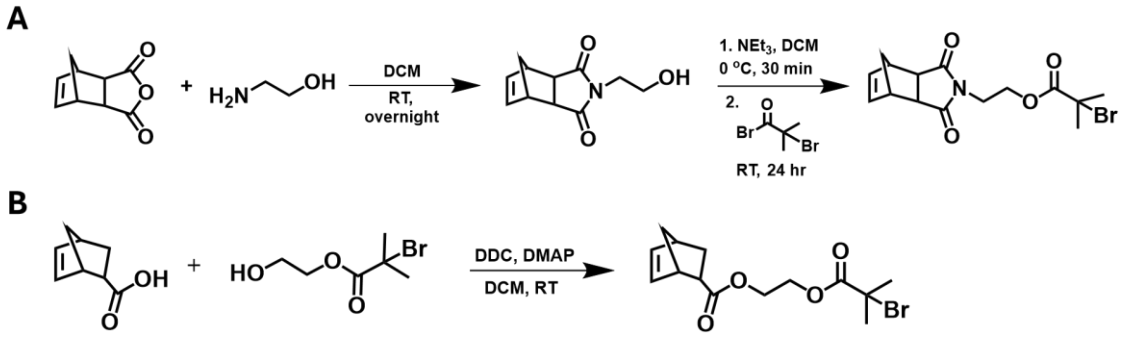

However, these ROMP homopolymerisations with each macromonomer have revealed significant kinetic limitations that must be addressed before systematic grafting density studies can proceed. ROMP is inherently designed to achieve complete conversion within minutes

under mild conditions, driven by highly active Grubbs catalysts and the substantial ring strain in norbornene. Despite moderate macromonomer molecular weights (DP 30-50), which should facilitate rapid polymerisation, kinetic profiles consistently show incomplete conversion even after extended reaction times. SEC analysis confirms polymerisation is occurring through leftward peak shifts and reduced macromonomer intensity, but the failure to achieve quantitative conversion creates critical purification challenges (Figure 5.2). In an effort to push reactions to higher conversion, monomer seeding has been attempted, whereby extra macromonomer was added periodically. However, this approach had seemingly little effect on reactivity, instead compromising polymerisation control evidenced by the broadening of the brush peak (Figure 5.2C) likely from the risk of introducing air to the system. Incomplete polymerisation means residual macromonomers cannot be easily separated from the brush products, compromising the purity required for reliable structure-property studies. Additionally, the extended reaction times necessary to approach completion led to progressive catalyst decomposition,[1, 2] among other unwanted side reactions, which erodes polymerisation control and broadens molecular weight distributions.

Scheme 5.2. Synthesis pathways of macromonomers using ATRP from norbornene-bromide bifunctional initiators (A) poly(*tert*-butyl methacrylate) (PtBMA) (B) poly(2-*N*-(morpholino)ethyl methacrylate) (PMEMA) (C) polystyrene (PS)

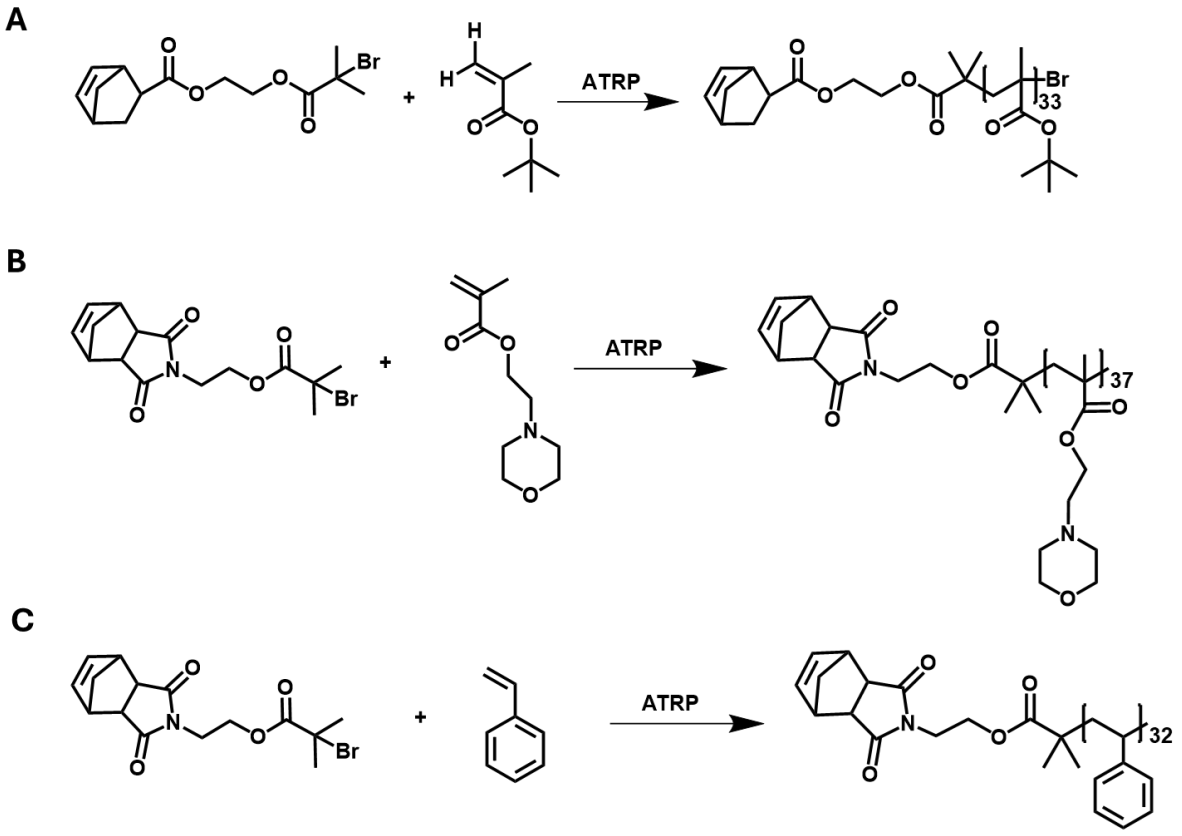

Optimisation efforts have systematically investigated variables known to affect ROMP kinetics, including norbornene isomer selection,[3] ruthenium catalyst variants, and solvent systems.[4] Despite these ongoing efforts, only marginal kinetic improvements have been observed to date. Other variations that can be explored include norbornene anchor modifications,[5] pH,[6] and ion strength.[6] Immediate future strategies will explore alternative macromonomer functionalisation approaches, such as omega-end rather than alpha-end norbornene attachment, and different spacer chemistries between the polymer chain and norbornene unit.

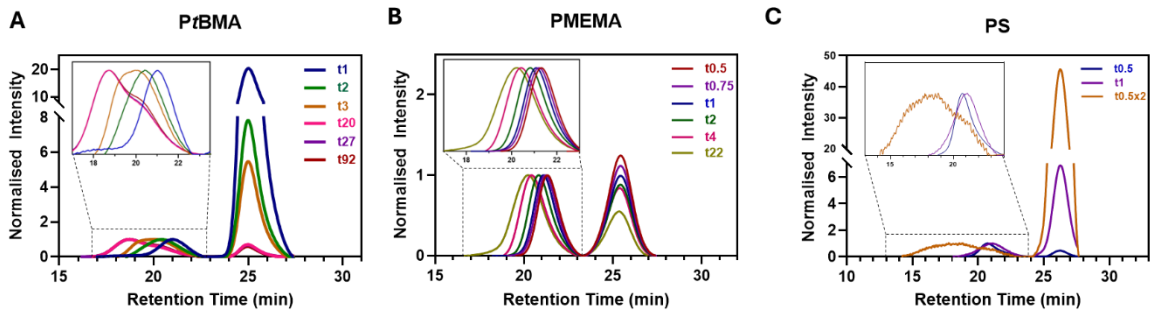

Figure 5.1. SEC analysis of ring-opening metathesis polymerisation kinetics of macromonomers normalised to 'brush' peak with insets zoomed in to 'brush' peak for (A) PtBMA (B) PMEMA and (C) PS

These kinetic limitations represent a critical bottleneck for the entire grafting density investigation. For meaningful structure-property relationships to be established, all brush components must be synthesised using the same controlled grafting approach to ensure comparability across the grafting density series. Furthermore, these ROMP-derived brushes will serve as precursors for subsequent PEG post-modification to achieve the target tadpole architecture. Until rapid, quantitative ROMP conversion is achieved, neither the systematic grafting density studies nor the multi-step tadpole synthesis can reliably proceed.

1.2 Glass Transition Temperature Effects

Despite evidence that both high-T_g and low-T_g systems can achieve discs, and work presented in this thesis on their co-assembly, there is no comparative study into their self-assembly. Comparison of chemically identical high-T_g versus low-T_g bottlebrush systems will illuminate how polymer dynamics can influence self-assembly mechanisms. Poly(methyl methacrylate) (PMMA) (T_g ~ 104 ℃)[7] and poly(methyl acrylate) (PMA) (T_g ~ 10 ℃)[8] are two polymers that are useful for this purpose, maintaining structural similarity, with vastly different T_g. Development of these materials is ongoing, influenced by disc-forming polymer tadpole dimensions elucidated in Chapter II. The successful synthesis and self-assembly of PEG_{114}-*b*-$PBIEM_{15}$-*graft*-PMMA attests to the universality of tadpole structures to achieve discs even

with differing chemistries. Upon the synthesis of a similar PEG_{114}-*block*-$PBIEM_{15}$-*graft*-PMA tadpole, comparison kinetic self-assembly investigations could reveal whether the disc formation mechanism changes fundamentally when chain mobility is restricted. This could uncover new pathways to controlling particle morphology and properties through processes such as thermal processing.

1.3 Solvent Effects and Processing Conditions

The influence of solvent quality and processing parameters on disc formation and final particle dimensions requires thorough investigation. In Chapter II, we showed that whilst the self-assembly of tadpoles from different solvents, namely DMF and THF, still achieved discoidal morphologies, a significant difference in diameter was observed. This suggests that solvent may have a larger role to play in the self-assembly mechanism. Future studies could examine how solvent switching rates, solvent selectivity gradients, and co-solvent systems affect both the kinetic profile of disc formation, but also the final particle dimension and characteristics. Understanding these processing-structure relationships will be crucial for scalable synthesis and could reveal routes to controlling disc size distributions and aspect ratios, whilst helping elucidate the underlying disc formation mechanism. These mechanistic and kinetic studies could incorporate *in situ* characterisation techniques, including time-resolved small-angle X-ray scattering (SAXS), small angle neutron scattering (SANS) and cryogenic transmission electron microscopy, to capture intermediate structures during self-assembly. Molecular dynamics simulations may also be a powerful tool to verify proposed mechanisms, whilst continuing to predict polymer packing behaviour in unexplored parameter spaces.

2. Functionalised Discoidal Particles

Adopting an application-based materials science approach, designing discoidal polymer nanoparticle systems specific to targeted applications without disrupting the fundamental assembly mechanism can be achieved. Immediate avenues that can be explored include:

2.1 Expanded Stimuli Response

While pH and UV responsiveness have been demonstrated in discs,[9, 10] the platform's versatility enables incorporation of diverse stimuli-responsive functionalities into core-forming blocks. Temperature-responsive, redox-active, ion-responsive, and enzymatically cleavable groups could create smart nanodiscs for targeted applications.

2.2 Functional Corona Engineering

Beyond core functionality, engineering responsive or functional corona-forming segments presents opportunities for creating multifunctional particles. Functionalised coronas could enable selective binding, catalysis, or environmental sensing while maintaining the advantageous disc morphology. This approach could enable the creation of particles with dual responsiveness.

2.3 Multi-Stimuli Responsive Systems

Advancing the co-assembly of polymerically diverse building blocks demonstrated in Chapter IV, a range of polymers with differing functionalities can be co-assembled into a multi-stimuli responsive system.

2.4 Biomimetic Systems

The structural similarity between synthetic nanodiscs and critical biological particles, particularly α-HDL,[11] presents unprecedented opportunities for biomimetic materials

development.[12, 13] Natural disc-shaped particles play crucial roles in biological systems, from cholesterol transport to membrane organisation, suggesting that synthetic disc-forming systems could access entirely new classes of bio-inspired functionality. The development of HDL mimetics using synthetic disc-forming polymers could revolutionise cardiovascular medicine, while other biomimetic applications could target platelet function, cell membrane interactions, or even viral particle mimicry.

3. Exploring Architectures

The architectural space for disc-forming polymers remains largely unexplored, presenting exciting opportunities for accessing new morphologies and hierarchical structures. Our current understanding is based primarily on relatively simple block copolymer architectures, starting from tadpoles, and beginning to explore dumbbell polymers, but more exotic designs could unlock entirely new assembly behaviours. Other architectures that could be investigated are:

3.1 Bottlebrush-Bottlebrush Block Copolymer Systems

Moving beyond linear-brush tadpole architectures, entirely bottlebrush block copolymer systems represent a compelling alternative route to disc formation that could offer unprecedented synthetic modularity through ROMP-based assembly. The potential for bottlebrush-bottlebrush architectures to achieve disc morphologies when sufficient asymmetry is maintained,[14] through fundamentally different mechanisms than those observed in conventional linear-brush systems represents an untapped research landscape.

To explore this architectural approach, poly(poly(ethylene glycol) methacrylate)$_{300}$ (PPEGMA$_{300}$) macromonomers have been synthesised as hydrophilic alternatives to the discrete PEG chains used in previous tadpole systems. The initial PPEGMA macromonomers were targeted at degrees of polymerisation of 15 and 30, corresponding to molecular weights of approximately 4,500 and 9,000 g/mol, respectively. These molecular weights were selected

as starting points comparable to the 5,000 g/mol PEG previously employed in linear tadpole systems, providing a baseline for direct architectural comparison. Notably, these PPEGMA macromonomers are intentionally shorter than or similar to the hydrophobic core-forming macromonomers (DP 30-50), establishing the asymmetric block architecture necessary for potential disc formation.

However, PPEGMA macromonomers exhibit the same problematic polymerisation kinetics observed with hydrophobic macromonomers (Figure 5.1), reinforcing the critical need for ROMP optimisation discussed previously. The poor kinetics appear to be a general challenge across all synthesised macromonomer types.

The bottlebrush-bottlebrush approach enables systematic exploration of multiple architectural variables simultaneously. Beyond the backbone length asymmetry established with these initial macromonomers, future work will investigate the effects of varying side chain lengths in both hydrophilic and hydrophobic segments, as well as overall molecular weight effects. This multi-parameter optimisation could reveal optimal windows for disc formation and potentially uncover entirely new morphological landscapes not accessible through linear-brush architectures.

Successfully implementing bottlebrush-bottlebrush systems could provide simplified synthetic routes to disc formation while maintaining the modularity advantages of ROMP-based assembly, making this architectural approach a promising complement to traditional linear tadpole strategies.

To this effort, we have synthesised poly(poly(ethylene glycol) methacrylate)$_{300}$ (PPEGMA$_{300}$) to be co-assembled with hydrophobic macromonomers presented previously. By design, these macromonomers are shorter than the core-forming macromonomers to lengths of 15 and 30, corresponding to 4500 and 9000 g/mol respectively. These macromonomers suffer from similar

poor polymerisation kinetics discussed with respect to hydrophobic macromonomers and require further optimisation. Beyond this, further work is required to explore block asymmetry in terms of backbone and side chain lengths, and molecular weight to find an optimal window where discs can be achieved. As an extension, new bottlebrush-bottlebrush block copolymer architectures could reveal simplified synthetic routes to disc formation or uncover entirely new morphological landscapes.

3.2 Multiblock and Hierarchical Architectures

The development of multiblock copolymers incorporating complex sequences of linear and bottlebrush segments as an extension of the work presented in Chapter IV presents possibilities for creating networks of anisotropic discoidal nanoparticles and accessing higher-order morphologies,[15] that have limited precedent in current materials science. With every addition of flexible and rigid blocks, the packing behaviour of polymers is expected to be distinctively different in selective solvents, potentially enabling hierarchical assembly towards materials with unprecedented combinations of properties.

The findings presented here establish disc formation as an exciting and largely untapped avenue for advancing the field of directed self-assembly. Pursuing entirely polymeric systems towards universal discoidal nanoparticles relevant to wide applications, bottlebrush-*alt*-linear block copolymers are well-positioned as building-blocks for bottom-up self-assembly. Whilst our understanding of the requirements for disc-forming building blocks remains rudimentary, the potential of simple bottlebrush-*block*-linear and bottlebrush-*block*-linear-*block*-bottlebrush systems presented in this thesis, combined with the unique properties and potential applications of discoidal materials suggests that this promising research landscape warrants significant future investigation.

4. References

1. Hong, S. H.; Wenzel, A. G.; Salguero, T. T.; Day, M. W.; Grubbs, R. H., Decomposition of Ruthenium Olefin Metathesis Catalysts. *Journal of the American Chemical Society* **2007,** *129* (25), 7961-7968.

2. Jawiczuk, M.; Marczyk, A.; Trzaskowski, B., Decomposition of Ruthenium Olefin Metathesis Catalyst. *Catalysts* **2020,** *10* (8), 887.

3. Troiano, R.; Carratù, M.; Pragliola, S.; Boccia, A. C.; Grisi, F., ROMP of norbornene and oxanorbornene derivatives with pendant fluorophore carbazole and coumarin groups. *European Polymer Journal* **2022,** *167*, 111065.

4. Blosch, S. E.; Alaboalirat, M.; Eades, C. B.; Scannelli, S. J.; Matson, J. B., Solvent Effects in Grafting-through Ring-Opening Metathesis Polymerization. *Macromolecules* **2022**.

5. Radzinski, S. C.; Foster, J. C.; Chapleski, R. C.; Troya, D.; Matson, J. B., Bottlebrush Polymer Synthesis by Ring-Opening Metathesis Polymerization: The Significance of the Anchor Group. *J. Am. Chem. Soc.* **2016,** *138* (22), 6998-7004.

6. Foster, J. C.; Grocott, M. C.; Arkinstall, L. A.; Varlas, S.; Redding, M. J.; Grayson, S. M.; O'Reilly, R. K., It is Better with Salt: Aqueous Ring-Opening Metathesis Polymerization at Neutral pH. *J. Am. Chem. Soc.* **2020,** *142* (32), 13878-13885.

7. Teng, H.; Koike, K.; Zhou, D.; Satoh, Z.; Koike, Y.; Okamoto, Y., High glass transition temperatures of poly(methyl methacrylate) prepared by free radical initiators. *Journal of Polymer Science Part A: Polymer Chemistry* **2009,** *47* (1), 315-317.

8. Kim, Y.-G.; Wichaita, W.; Thérien-Aubin, H., Influence of the Architecture of Soft Polymer-Functionalized Polymer Nanoparticles on Their Dynamics in Suspension. *Polymers* **2020,** *12* (8), 1844.

9. Zeng, H.; Liang, X.; Roberts, D. A.; Gillies, E. R.; Müllner, M., Self‐Assembly of Rod‐Coil Bottlebrush Copolymers into Degradable Nanodiscs with a UV‐Triggered Self‐Immolation Process. *Angewandte Chemie International Edition* **2024,** *63* (13).

10. Zeng, H.; Zeng, P.; Baek, J.; Kim, B. S.; Müllner, M., Self‐Assembly of Amorphous 2D Polymer Nanodiscs with Tuneable Size, pH‐Responsive Degradation and Controlled Drug Release. *Angewandte Chemie International Edition* **2025**.

11. Li, D.; Fawaz, M. V.; Morin, E. E.; Ming, R.; Sviridov, D.; Tang, J.; Ackermann, R.; Olsen, K.; Remaley, A. T.; Schwendeman, A., Effect of Synthetic High Density Lipoproteins Modification with Polyethylene Glycol on Pharmacokinetics and Pharmacodynamics. *Mol. Pharm.* **2018,** *15* (1), 83-96.

12. Dong, Y.; Tang, H.; Dai, H.; Zhao, H.; Wang, J., The application of nanodiscs in membrane protein drug discovery & development and drug delivery. *Frontiers in Chemistry* **2024,** *12*.

13. Mu, Q.; Deng, H.; An, X.; Liu, G.; Liu, C., Designing nanodiscs as versatile platforms for on-demand therapy. *Nanoscale* **2024,** *16* (5), 2220-2234.

14. Hou, W.; Wu, J.; Li, Z.; Zhang, Z.; Shi, Y.; Chen, Y., Efficient Synthesis and PISA Behavior of Molecular Bottlebrush Block Copolymers via a Grafting-From Strategy through RAFT Dispersion Polymerization. *Macromolecules* **2023,** *56* (3), 824-832.

15. Zhang, J.; Li, S.; Yin, Y.; Xiang, L.; Xu, F.; Mai, Y., One‐Dimensional Helical Nanostructures from the Hierarchical Self‐Assembly of an Achiral "Rod−Coil" Alternating Copolymer. *Macromolecular Rapid Communications* **2022,** *43* (21), 2200437.